

GEOLOGICA ULTRAIECTINA

Mededelingen van de
Faculteit Geowetenschappen

Universiteit Utrecht

Nr. 332

Compaction of granular carbonates under conditions relevant to diagenesis and fault sealing

Xiangmin Zhang

This thesis was partly accomplished with financial support from
Shell International Exploration and Production B.V.

This research was carried out at:
Experimental Rock Deformation (HPT) Laboratory
Faculty of Geosciences, Department of Earth Sciences
Utrecht University
Budapestlaan 4
3584 CD Utrecht
The Netherlands

www.geo.uu.nl

ISBN/EAN : 978-90-5744-193-6

**Compaction of granular carbonates
under conditions relevant to diagenesis and fault
sealing**

Compactie van granulaire carbonaten
onder de condities relevant voor diagenese
en voor afdichting van breuken
(met een samenvatting in het Nederlands)

Proefschrift

ter verkrijging van de graad van doctor aan de Universiteit Utrecht
op gezag van de rector magnificus, prof. dr. J.C. Stoof, ingevolge
het besluit van het college voor promoties in het openbaar te
verdedigen op maandag 29 november 2010
des middags te 4.15 uur

door

Xiangmin Zhang

geboren op 30 november 1965
te Yuanshi, China

Promotor: Prof. dr. C.J. Spiers

Members of the dissertation committee:

Prof. dr. M. R. Drury
Utrecht University, the Netherlands

Prof. dr. J.-P Gratier,
Université Joseph Fourier, France

Prof. dr. E. Tondi
University of Camerino, Italy

Prof. dr. Shengli Ma
China Earthquake Administration, China

Prof. dr. P. Baud
Laboratoire de Géophysique Experimentale
EOST Strasbourg, France

Table of Contents

Summary.....	1
1. Introduction.....	5
1.1 SCOPE OF THIS THESIS	5
1.2 PRESSURE SOLUTION IN CARBONATE ROCKS	6
1.2.1 Pressure solution microstructures in carbonate rocks	6
1.2.2 The effects of pressure solution in carbonate rocks	7
1.2.3 Effects of geological variables on pressure solution.....	9
1.3 THEORY OF PRESSURE SOLUTION	12
1.4 PREVIOUS EXPERIMENTAL WORK AND PROBLEM DEFINITION	15
1.5 AIMS AND APPROACHES OF THE PRESENT RESEARCH	16
1.6 REFERENCES	17
 2. Compaction experiments on wet calcite powder at room temperature: evidence for operation of intergranular pressure solution.....	 25
2.1 INTRODUCTION	25
2.2 EXPERIMENTAL METHOD	27
2.3 RESULTS	29
2.4 DISSCUSION	31
2.4.1 Deformation mechanisms in dry and decane-flooded samples	31
2.4.2 Deformation mechanisms in samples tested wet	31
2.4.3 Comparison of experimental data with intergranular pressure solution theory	32
2.5 CONCLUSIONS.....	36
2.6 REFERENCES	37
 3. Compaction of granular calcite by pressure solution at room temperature and effects of pore fluid chemistry	 41
3.1 INTRODUCTION	41
3.2 EXPERIMENTS	44
3.2.1 Starting material	44
3.2.2 Experimental apparatus and procedures	44
3.3. MECHANICAL RESULTS	46
3.3.1 Dry compaction and control experiments	46
3.3.2 Wet compaction	49
3.4 DISSCUSION	49

3.4.1 Deformation mechanisms in samples compacted dry and with chemically inert pore fluid	49
3.4.2 Deformation mechanisms in samples filled with solution	50
3.4.3 Experimental results vs. pressure solution theory	54
3.5 CONCLUSIONS.....	59
3.6 REFERENCES	59

4. Effects of phosphate ions on intergranular pressure solution in calcite – an experimental study..... 63

4.1 INTRODUCTION	63
4.2 EXPERIMENTAL METHOD	67
4.3 MECHANICAL RESULTS AND MICROSTRUCTURE	69
4.4 DISSCUSSION	70
4.4.1 Behaviour during dry compaction	70
4.4.2 Wet compaction behavior	73
4.4.3 Experiments vs. theory	75
4.4.4 Effect of phosphate ions on the rate of compaction.....	77
4.4.5 Implications	79
4.5 SUMMARY AND CONCLUSIONS.....	80
4.6 REFERENCES	81

5. Compaction creep of wet granular calcite by pressure solution at 28 to 150 °C 87

5.1 INTRODUCTION	87
5.2 EXPERIMENTAL METHOD	89
5.2.1 Samples and pore fluid preparation	89
5.2.2 Apparatus and calibration	90
5.2.3 Testing procedure	91
5.2.4 Data acquisition and processing	94
5.3 EXPERIMENTAL RESULTS	96
5.3.1 Mechanical data.....	96
5.3.2 Microstructural observations	97
5.3.3 Pore fluid analyses.....	98
5.4 DISSCUSSION	100
5.4.1 Deformation mechanisms	100
5.4.2 Comparison of IPS theory and experimental results	101
5.4.3 Synthesis: Deriving creep parameters for diffusion-controlled IPS in calcite	113
5.5 CONCLUSIONS.....	113
5.6 REFERENCES	116

6. Effects of pore fluid flow and chemistry on compaction creep of calcite by pressure solution at 150 °C.....	121
6.1 INTRODUCTION	121
6.2 EXPERIMENTAL METHOD	122
6.2.1 Starting materials and pore fluids	123
6.2.2 Experimental apparatus	123
6.2.3 Calibration and data acquisition	124
6.2.4 Testing procedure	126
6.3 EXPERIMENTAL RESULTS	126
6.4 DISSCUSION	135
6.4.1 Effects of flow- through on IPS strain rates: theoretical aspects	135
6.4.2 Ca^{2+} content of the pore fluid	138
6.4.3 Effects of the pore fluid salinity (NaCl)	139
6.4.4 Effects of Mg^{2+} and HPO_4^{2-}	142
6.5 Conclusions	143
6.6 REFERENCES	144
 7. Conclusions and suggestions for future research.....	 149
7.1 CONCLUSIONS.....	149
7.2 FUTURE RESEARCH	152
 Samenvatting	 155
 Acknowledgements	 161

Summary

Carbonate reservoir rocks contain more than 60% of the world's oil reserves and 40% of its gas reserves, and host many of the world's largest oil and gas fields. The evolution of the quality of such reservoirs, i.e. their porosity and permeability, is for a large part controlled by compaction due to pressure solution. As well as controlling reservoir quality, pressure solution compaction provides a driver for the migration of fluids in carbonate rocks over geological time. Together with processes such as clay smearing and cataclastic grain size reduction, pressure solution also forms an efficient mechanism of fault sealing in carbonate rocks. Moreover, during hydrocarbons production, and after injection of CO₂ into carbonate reservoirs for geological storage purposes, pressure solution may lead to vertical compaction creep and surface subsidence. Quantifying pressure solution compaction in carbonate rocks is therefore a subject of substantial practical and economic importance for hydrocarbons exploration and production, and for assessing the safety of geological storage of CO₂ in depleted carbonate reservoirs.

This thesis reports the results of an experimental study of pressure solution compaction of granular calcite aggregates, i.e. simulated carbonate reservoir rocks, under hydrocarbon reservoir conditions. Attention is focused on Intergranular Pressure Solution or IPS, i.e. stress-driven dissolution and precipitation occurring at the grain scale. The aims were to verify the operation of pressure solution by reproducing pressure solution microstructures, to determine the effects of variables such as stress, temperature, grain size, pore fluid chemistry and fluid flow on the rate of the process, and to reveal and quantify the rate limiting mechanism by comparison with theoretical models.

In **Chapter 1**, background information is given on pressure solution, as a major process of burial diagenesis in carbonate rocks. The widespread pressure solution features seen in carbonates in nature are reviewed, as are the effects of pressure solution on carbonate rock properties, such as porosity, and the influence of geological variables on pressure solution. Previous experimental work on pressure solution in carbonates is also reviewed and the main outstanding problems are identified. The aims of the present research are thus motivated in this chapter.

Chapter 2 reports 1-dimensional compaction experiments performed on fine-grained, pure calcite aggregates at low stresses (1-4 MPa) and at room temperature. A general procedure for compaction experiments suitable for investigations of pressure solution in carbonates was developed in these experiments. By applying a dry pre-compaction stress of 8 MPa, we obtained a reproducible starting porosity and could largely eliminate deformation mechanisms such as grain rearrangement, sliding and fracturing from subsequent compaction creep runs conducted under wet conditions. After dry pre-compaction at 8 MPa, samples were wet-compacted under “drained” conditions using pre-saturated solution as pore fluid. Control experiments, done either dry or with chemically inert pore fluid, showed negligible compaction at this stage. However, samples tested with saturated solution as pore fluid showed easily measurable compaction creep. The associated compaction strain rate decreased with increasing strain and increasing grain size, and increased with increasing applied stress. Addition of Mg²⁺ ions to the saturated pore fluid solution dramatically reduced compaction rates. By comparison with a theoretical model

for intergranular pressure solution in calcite, and noting that the presence of Mg^{2+} ions in solution is known to inhibit calcite precipitation and dissolution, the observed compaction behavior verified that intergranular pressure solution was the dominant compaction mechanism under our experimental conditions. The results also demonstrated that pressure solution compaction can start at shallow burial depths (just a few tens of meters) if other variables, especially pore fluid chemistry, are favorable.

Chapter 3 reports the results of 1-D compaction experiments performed on crushed limestones and pure granular calcite at room temperature and 1-4 MPa effective stress, using pore fluids ranging from saturated carbonate solution, with and without contaminant ions, to a variety of hydrocarbons. Once again, all samples were first pre-compacted dry at 8 MPa to obtain a well-controlled initial porosity and to eliminate purely mechanical compaction processes during testing at lower stresses. Compaction creep occurred only in samples filled with aqueous solutions, at strain rates of 10^{-6} – 10^{-9} s^{-1} . The measured strain rates increased with decreasing grain size and with increasing effective stress according to power laws with exponents of about -3 and 1 to 2 respectively. Moreover, the addition of dissolution and precipitation inhibitors (e.g. magnesium) to the pore fluid significantly decreased compaction rates of wet samples, indicating that creep must have involved calcite dissolution and precipitation. Pore fluid with salinity (NaCl) of 0.1-0.5 M increased the compaction strain rate compared to non-saline solutions, whereas no compaction was observed in samples filled with hydrocarbons. Samples made from natural oil-bearing limestone also showed far less compaction than oil-free samples. Interestingly, calcite aggregate initially filled with brine, and then flushed with hydrocarbons, compacted much more than samples that were first wetted with hydrocarbons and then flushed in the reverse order. When compared with theory, the experimental results suggest that the main deformation mechanism in our samples was pressure solution, and that diffusion is likely to be the rate controlling process in pure calcite systems. The results further imply that compaction and porosity/permeability evolution in natural carbonate rocks will depend strongly on pore fluid chemistry, as well as mechanical conditions. For example, pore fluids containing ions that act as calcite dissolution and precipitation inhibitors can preserve porosity in carbonate rocks. In addition, early entrapment of calcite-wetting hydrocarbons can strongly slow down or stop pressure solution compaction in carbonate reservoir rocks.

Having demonstrated the operation of IPS in wet calcite at room temperature in the preceding chapters, **Chapter 4** focuses on the effects of pore fluid phosphate ion concentration on 1-D compaction of fine-grained calcite powders by IPS at room temperature and applied axial stresses of 1-4 MPa. Phosphate was studied because of its importance as a biogenic constituent of sea and pore waters. Increasing the pore fluid phosphate concentration from 0 to 10^{-3} mol/l systematically reduced compaction strain rates by up to 2 orders of magnitude. The sensitivity of the compaction strain rate to phosphate concentration was the same as the sensitivity of calcite precipitation rates to the addition of phosphate ions reported in the literature, suggesting that the rate of IPS in phosphate-bearing samples was controlled by calcite precipitation on pore walls. The results imply that IPS and associated porosity/permeability reduction rates in calcite sediments may be strongly reduced when pore fluids are enriched in phosphates e. g. through high biological productivity or a seawater origin. Modeling of IPS related processes in carbonates must

therefore take into account the effects of pore fluid chemistry, specifically the inhibition of interfacial reactions by phosphate, as well as by cation impurities.

While Chapters 2, 3 and 4 deal with intergranular pressure solution at low stresses and temperatures corresponding to shallow burial depths, Chapters 5 and 6 consider compaction experiments under conditions of elevated stresses and temperatures – simulating deep diagenetic or mature reservoir conditions. **Chapter 5** documents 1-D compaction experiments carried out on crushed limestone, analytical grade calcite powder and superpure calcite powder at temperatures up to 150 °C, at 20- 47 MPa effective stress, under dry and wet (solution-flooded) conditions. Scanning Electronic Microscopy (SEM) revealed pressure solution microstructures such as sutured grain contacts, indentations, and overgrowth development in the wet-compacted samples. Dissolution pits and layers of precipitated calcite were also developed on the surfaces of cleaved crystals added to the powdered samples as microstructural reference crystals. These pits and precipitates clearly indicated the operation of pressure solution in our experiments. Substantial compaction creep strains were obtained in the wet compacted samples, whereas dry samples showed little or no creep and none of the mass transfer microstructures seen in wet samples. The compaction strain rates measured during wet tests systematically increased with increasing effective stress and decreasing grain size. Temperature had little effect on compaction strain rates between 28 and 150 °C. The effects of grain size, effective stress (changes) and starting material composition, together with the comparison between the experimental rate data and pressure solution modeling, suggest that the rate-limiting mechanisms were transitional between grain boundary diffusion-controlled IPS at low strains and precipitation-controlled IPS at higher strains. The experimentally derived value for the grain boundary diffusion product $D \times S$ (diffusion coefficient times effective thickness of grain boundary water film) for calcite during diffusion controlled pressure solution, falls between 2.98×10^{-18} and 3.73×10^{-19} m³/s at 150 °C, which is closely similar to that for many ionic salts under similar conditions.

In **Chapter 6**, compaction experiments on wet crushed limestone and analytical grade calcite powders, carried out at 150 °C and at effective stresses of 30 and 40 MPa are revisited, focusing on pore fluid chemical signatures for the dominant deformation mechanisms. The problem was approached by manipulate pore fluid composition using flow-through tests performed with fresh, calcite saturated solution, and by adding NaCl, Mg²⁺ or phosphate ions to the pore fluid mainly without flow-through. As concluded in Chapter 5, intergranular pressure solution was the dominant deformation mechanism under such conditions. Intermittent flow-through runs conducted using CaCO₃ saturated solution showed no effect on creep rate at low strain (<4-6%) but a major accelerate at high strains. Measurements of the Ca²⁺ concentration present in fluid samples collected from compacting samples in intermittent flow-through runs revealed a build up to high super-saturation of CaCO₃ during compaction under zero flow conditions, specially at high strains. Flow-through led to a drop in Ca²⁺ concentration. These data further support the inference that precipitation controlled the rate of IPS at high strains, as IPS theory predicts a significant super-saturation build up only for precipitation control.

Addition of NaCl to the pore fluid in a concentration of 0.5 M increased the creep rate of analytical grade calcite roughly in proportion to the enhancement of NaCl on calcite solubility –from IPS theory, this may reflect an acceleration of IPS via acceleration of grain

boundary diffusion control, at least at lower strains. Addition of Mg^{2+} and HPO_4^{2-} to the pore fluid, in concentration of 0.05 M and 0.001 M respectively, caused major retardation of compaction creep. Since the ions are known to retard dissolution and precipitation of calcite, their effects provide strong support for compaction being controlled by a dissolution-precipitation process such as IPS.

Integrating our mechanical, flow-through and chemical data, and taking into account our previous mechanical data reported in Chapter 5, points strongly to diffusion controlled IPS being the dominant deformation mechanism under closed system (zero flow) conditions at strains up to few percents, giving way to precipitation control at higher strains. Our (chemical) data suggest that this transition is due to accumulation of impurity in the pore fluids from samples or apparatus.

Since Mg^{2+} and phosphate ions are common in natural pore fluids, since they are known to retard dissolution and especially precipitation of calcite, it is likely that retarded precipitation will be the rate limiting step in IPS of carbonates in nature. This study implies that porosity in carbonate can be preserved in deep burial i.e. >4-5 km if the pore fluids are rich in calcite reaction inhibitors such as Mg^{2+} and phosphate ions. Fluid flow can accelerate pressure solution by change the rate limiting mechanism, this may happen in nature in forming stylolite and solution seams.

Chapter 7 summarizes the main conclusions of this thesis, and documents suggestions for future work that is needed.

1. Introduction

1.1 Scope of this thesis

Stress-driven dissolution-precipitation processes or “Pressure Solution” form a class of key deformation mechanisms operating in the upper and mid crust. These mechanisms manifest themselves in natural rocks at scales ranging from intergranular dissolution-precipitation features (μm to cm scale) to that of dissolution seams or “stylolite” and associated precipitation in veins (mm to m scale) (Bathurst, 1958). The elementary process of pressure solution, however, generally occurs at the grain scale (Figure 1.1). Intergranular Pressure Solution (IPS), i. e. pressure solution at the grain scale, is the principal mechanism of ductile creep deformation under diagenetic and low grade metamorphic conditions (Rutter, 1976, 1983; Paterson, 1973, 1995) and is likely to be a major factor controlling crustal fault strength, healing and slip behavior at depths in the range 3-15 km (Chester & Logan, 1986; Bos & Spiers, 2002; Gratier, et al. 2002, 2003; Gratier and Gueydan, 2007; Yashuhara et al. 2005; Niemeijer et al., 2008). It also plays an important role in the evolution of sedimentary basins (Ortoleva, 1994; Yang, 2000; Tuncay et al., 2000; Marcussen et al., 2010) and in controlling salt tectonic flow (Urai et al. 1986; Spiers and Carter, 1998; Urai and Spiers, 2007). The key role played by pressure solution in carbonates means that better understanding of the kinetics process of pressure solution is of great economical importance for hydrocarbon exploration and production (Scholle, 1977; Schmoker and Halley, 1982, Scholle and Halley, 1985; Scholle & Ulma-Scholle, 2003), reservoir characterization and modeling (Lucia, 2007; Ahr, 2008), geological storage of CO_2 (Renard et al., 2005; Le Guen et al., 2007, Liteanu & Spiers, 2009) and for research on fault slip dynamics and healing/sealing in carbonates (Vermilye and Scholz, 1998; Gratier et al., 2003, Gratier and Gueydan, 2007; Tondi, 2007; Verberne et al., 2010).

In particular, pressure solution is one of the most important diagenetic processes affecting carbonate reservoirs (Bathurst, 1958, 1975, 1993; Scholle & Halley, 1985; Moore, 2001; Lucia, 2007), - which contain more than 60% of the world’s oil and 40% of its gas reserves (SLB, 2007) and host many of the world’s giant oil and gas fields (Harris & Weber, 2006). Indeed, pressure solution is the main mechanism of compaction in carbonate sediments, since early cementation often precludes purely mechanical compaction (Croize et al. 2009), and it therefore plays a key role in controlling the evolution of porosity, permeability and reservoir quality (Schmoker & Halley, 1982; Schmoker, 1984; Brown, 1997; Bathurst, 1993; Moore, 2001; Ehrenberg et al. 2006; Lucia, 2007). Together with processes such as clay smearing and cataclastic grain size reduction, pressure solution is also an efficient mechanism of fault sealing, shear band sealing and compaction band sealing in both carbonate and clastic hydrocarbon reservoirs (Smith, 1966; Aydin, 2000; Tondi et al., 2006; Tondi, 2007). Compaction creep by pressure solution provides a drive for the migration of hydrocarbons and formation water from their source rocks (Moore, 1989; Chilingarian et al., 1992, 1996). It may also contribute to compaction creep of carbonate reservoirs and to surface subsidence associated with oil and gas production or with CO_2 storage in depleted carbonate reservoirs (Portier and Rochelle, 2005; Le Guen et al., 2007; Liteanu & Spiers, 2009). To date, however, the detailed mechanisms controlling

pressure solution in calcite have proven difficult to isolate from other deformation mechanisms, and the rates difficult to quantify in the form of constitutive laws.

This thesis reports the results of systematic experimental and microphysical modeling study of intergranular pressure solution in calcite aggregates i.e. simulated calcite rocks. The aim was to understand mechanisms and kinetics of intergranular pressure solution compaction in carbonate rocks under hydrocarbon reservoir conditions. To achieve this, compaction experiments were carried out to verify the operation of intergranular pressure solution, by reproducing intergranular pressure solution microstructures, to reveal and isolate the rate limiting mechanisms and to establish the effects of stress, temperature, grain size, pore fluid chemistry and fluid flow on the rate of the process. The constitutive parameters have been derived based on the experimental results and microphysical modeling. The results can be used for porosity evolution/basin modeling and reservoir quality prediction in hydrocarbon exploration and for reservoir characterization modeling in production in carbonate rocks and for geodynamic modeling in carbonate fault zones.

1.2 Pressure solution in carbonate rocks in nature

1.2.1 Pressure solution microstructures in carbonate rocks

Pressure solution has long been recognized from widespread dissolution and growth features preserved in carbonate rocks (Stockdale, 1922, 1926; Bathurst, 1958; Weyl, 1959). The most convincing (micro)structures for pressure solution are dissolution features that cut across ooids and fossils whose original shapes are known (Figure 1.2a)(Bathurst, 1958; Scholle and Ulma-Scholle, 2003). The sutured grain-to-grain contacts, indentations, truncations and overgrowths are generally accepted indicators of intergranular pressure solution and are widely developed in coarse-grained carbonate rocks such as grainstones and packstones (Bathurst, 1958, 1975, 1993; Heydari, 2001). Localized pressure solution seams with lateral extent of cm to m and a rough or “stylolitic” morphology are very common in carbonate rocks, especially, in fine grained mudstones and wackstones (Figure 1.2b)(Bathurst, 1958, 1975, 1993; Wanless, 1979; Moore, 1989, 2001; Renard et al., 2004; Brouste, et al., 2007). Stylolites are generally filled with a film or layer of insoluble residue consisting of clays etc, and differ from grain-to-grain sutured contacts only in scale (Bathurst, 1993). They transect the whole rock rather than isolated grains (Figure 1.2b, c). However, in coarse-grained limestones, intergranular pressure solution first occurs at sutured grain-to-grain contacts and then further propagates to form a stylolite crossing the whole rock normal to the maximum compressive stress (Petit and Mattauer, 1995; Moore, 1989, 2001; Renard et al., 2004). The basic process occurring at the advancing tip or front of a stylolite is therefore thought to involve IPS accelerated by stress concentration developed at the stylolite front (Fletcher and Pollard, 1981; Moore, 2001).

Other types of pressure solution features include “wispy seams” and “solution seams” (Koepnick, 1983; Moore, 2001; Renard et al., 2004). They are relatively smooth, undulating features that vary gently in the amplitudes and thickness of the insoluble remains (Moore, 2001). Solution cleavage seams, solution seams developed on shear fractures, and sealed pull-apart cracks are pressure solution features that developed in

connection with folding and faulting (Meike and Wenk, 1988; Stel and DeRuig, 1989; Peacock et al., 1998; Vermilye and Scholz, 1998; Petit et al., 1999; Gratier et al., 2003; Billi and Salvini, 2007; Tavani et al., 2010). In such cases, open fractures and pull-aparts are normally filled with cement sourced from pressure solution that has occurred in the nearby cleavage seams or shear fractures (Peacock et al., 1998; Gratier et al., 2003; Renard et al., 2004). Alongside intergranular pressure solution, these large scale features can also control the recovery of fault zone strength and the evolution of transport properties of both faults and fractured reservoirs (Canole et al., 1997; Watkinson and Ward, 2006, Tondi et al., 2006; Tondi, 2007).

The materials removed from grain-to-grain contacts or other dissolution sites such as stylolites or wispy/solution seams, are precipitated as cement either close to the dissolution sites or they are transported some distance, by diffusion or advective transport in the pore fluid phase, and then precipitated (Bathurst, 1975, 1993; Scholle et al., 1985; Heydari, 2000; Gratier et al., 2002; Ehrenberg et al., 2006, 2009). Typical microstructures by cementation related to pressure solution in carbonates include equant calcite spar and syntaxial overgrowths (Choquette and James, 1987; Scholle & Ulma-Scholle, 2003; Lucia, 1962, 2007). Porosity reduction during compaction by solution thus involves the effects of both deformation of the load supporting framework, by mass removal from grain contacts, plus cementation of the available pore space.

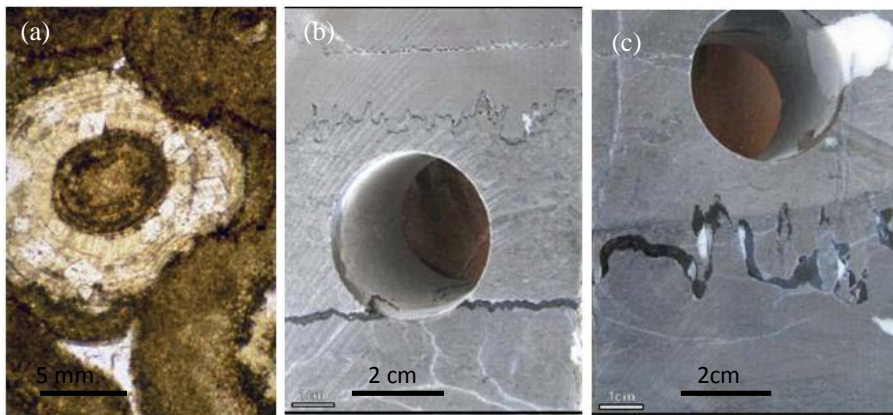


Figure 1.1. a) Grain to grain sutured contacts between ooidic grains indicating pressure solution in limestone reservoir rocks (from Scholle and Ulma-Scholle, 2003); b) and c) Stylolites developed in fine grained limestones seen in slabbed cores. Cylinder holes are places where

1.2.2 The effects of pressure solution on carbonate rocks

The term pressure solution compaction or “chemical compaction” was used in the petroleum literature to describe porosity loss which takes places by stress-driving dissolution-precipitation without the addition of new or allochthonous cement (Lloyd 1977). It has been convincingly shown that pressure solution is the principal diagenetic process responsible for transforming carbonate sediments to low porosity carbonate rocks (Bathurst, 1958, 1993; Moore and Druckman, 1981; Schmoker and Halley, 1982; Scholle &

Halley, 1985; Tada & Siever, 1989; Heydari, 2000; Eherenberg et al. 2006, 2007, 2009) upon burial beyond a few meters to a few tens of meters (Choquette and James, 1987; Croize et al. 2009). Modern carbonate deposits have a primary sedimentary porosity of 40-70% (Scholle et al. 1985; Croize et al., 2009) while ancient and deeply buried reservoirs have porosity typically less than 5% (Heydari, 2000; Scholle & Ulma-Scholle, 2003) (Figure 1.2). Mechanical compaction, prior to pressure solution during burial diagenesis, is achieved through grain re-organization, sliding and rotation, dewatering and minor grain breakage (Scholle, 1977; Shinn and Robbin, 1983; Scholle & Halley, 1985; Moore, 2001). The mechanical compaction is normally taken over by pressure solution once the grains form stable frameworks or cemented framework under shallow burial conditions (Scholle, 1971; Shinn and Robbin, 1983; Moore, 2001; Croize et al., 2009). Rittenhouse (1971) and Mitra and Beard (1980) showed that 25% is the minimum porosity mechanical compaction can achieve. Porosity reduction is impossible after forming a stable framework without deforming the grains themselves i.e. by grain crushing, pore collapse, plasticity or pressure solution (Wong and Baud, 1999; Croize et al., 2009). Under carbonate reservoir conditions, where stresses and temperatures are too low to promote grain crushing, pore collapse, plasticity or solid state diffusion, pressure solution is the most effective mechanism for diagenetic compaction, following the mechanical compaction phase at shallow depths. Pressure solution compaction and cementation can reduce the porosity of mechanically compacted sediments to porosities of 10-20%, in the case of carbonate reservoirs buried to 2-4 km depths (Eherenberg et al., 2004, 2006, 2007, 2009) and to 2-3% porosity in the case of ancient deeply buried limestones (Schmoer, 1983; Scholle and Ulma-Scholle, 2003). For example, in a study of deeply buried ooiditic grainstones of Upper Jurassic Smackover Formation of the northeastern Gulf of Mexico, USA, Heydari (2000) found that mechanical compaction reduced the initial sedimentary porosity of 40% sedimentary porosity to 27%, while pressure solution compaction caused a further drop to 12% porosity and cementation (precipitation) directly resulting from pressure solution reduced to finally ~ 5%.

As a result of both pressure solution deformation and removal of dissolved mass by advection, pressure solution can cause significant reduction of thickness in carbonate rocks. Compaction due to vertical deformation by pressure solution, of the type described above can produce significant vertical strains. Heydari (2000) reported a 28% thickness reduction by pressure solution in the Smackover grainstone. Bathurst (1993) pointed out that growth of stylolites in a vertical direction amounting to 20-35% thickness reduction is commonplace. In regions where laterally directed stress has been active such as Appalachians, the lateral shortening of beds due to the formation of vertical stylolites can greatly exceed the crustal shortening achieved by folding or other tectonic adjustment (Dunnington, 1967; Bathurst, 1993; Whitaker and Bartolomew, 1999). Such extreme shortening or vertical thinning are accompanied by large scale advection associated with migration of pore fluid on the scale of entire tectonic basins (Trurnit, 1968; Bathurst, 1993; Swennen et al., 2003).

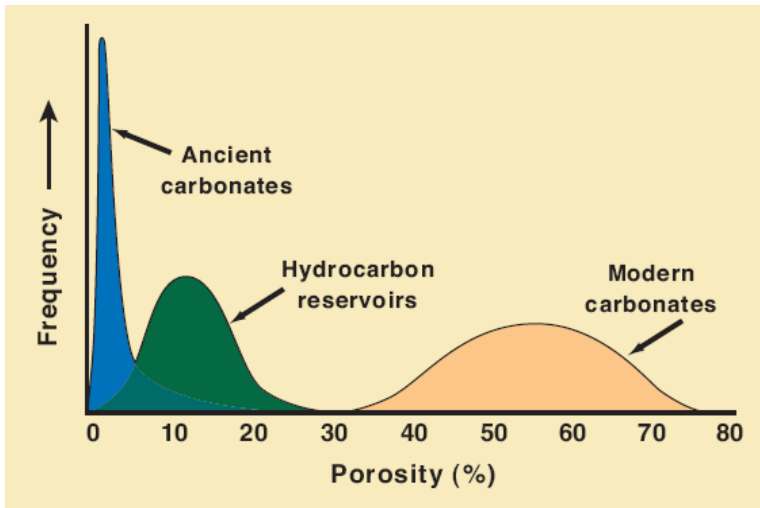


Figure 1.2. Porosity in modern carbonate sediments and in carbonate rocks (Scholle and Ulmar-Scholle, 2003).

Pressure solution compaction and cementation in fault zones, especial in the fault gouge- filled fault cores can recover the strength of fault zones (Gratier et al., 2002, 2003; Tondi et al., 2006; Tondi, 2007) and drastically alter their transport properties. Compaction and cementation of seismically active fault zones can control the seismic cycle via the effects of periodic re-strengthening and fluid pressure build up (Sleep, 1992; Hickman et al., 1995; Towend and Zoback, 2000; Faulkner, 2004). The sealing capacity of fault seals bounding hydrocarbon reservoirs, and its evolution after fault motion can also be determined by pressure solution (Renard, et al. 2000).

1.2.3 Effects of geological variables on pressure solution

In many carbonate rocks, especial from young sedimentary basins in passive margins which did not experience uplift, deep burial diagenesis took place in a chemically semi-closed system (Moore, 2003; Schomer & Halley, 1982; Scholle, 1983; Haydria, 2000; Croize et al., 2009). Hence the effects of geological variables such as stress, pore fluid pressure, and temperature on (the rate of) pressure solution can be examined by studying the porosity versus burial depth curves (Schmoker and Halley, 1982; Halley and Schomer, 1983; Scholle and Halley, 1985; Eherenberg, 1993, Ehrenberg and Nadeau, 2005; Ehrenberg, 2006; Ehrenberg et al., 2009). Moreover, the effects of one geological variable, such as stress, pore fluid pressure, temperature, age, grain size, or pore fluid chemistry can be studied by comparing the porosities of carbonate rocks taken from environments where other variables took similar values (Coogan, 1970; Schmoker, 1984; Oswald et al., 1996; Ehrenberg et al., 2009).

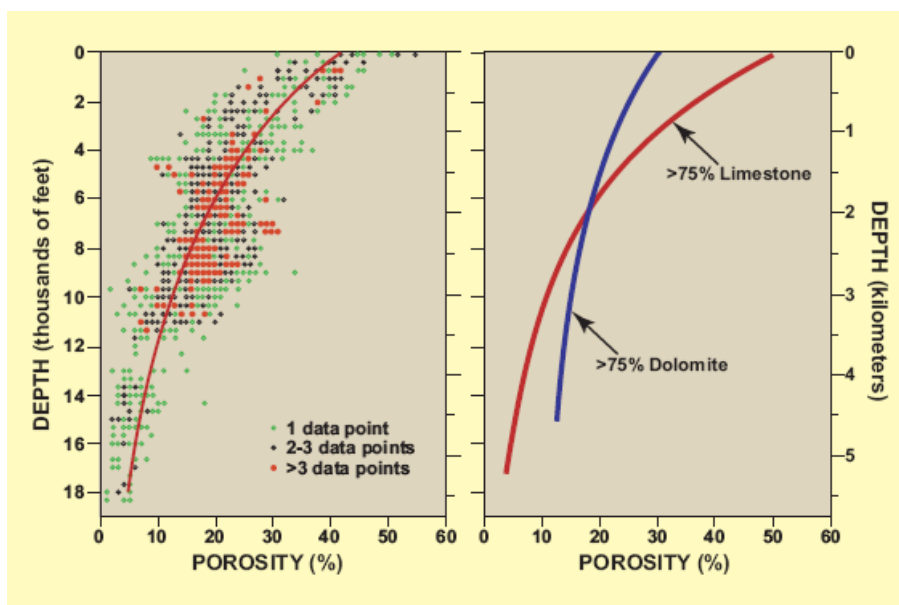


Figure 1.3. Porosity curves vs. depth in carbonate rocks. The dominate mechanism of porosity loss is pressure solution in a chemically semi-closed system (from Schmoker and Halley, 1982; Scholle, 1983, Scholle & Ulma-Scholle, 2003).

The general relation between porosity and burial depth for carbonate rocks has been studied by several authors (Schmoker and Halley, 1982; Halley and Schmoker, 1983; Scholmer et al., 1985; Scholle & Halley, 1985) (Figure 1.3) in USA and in Europe. More recently, numerous studies have been carried out in carbonate reservoirs in Middle East and North Sea by Ehrenberg and co-workers (Ehrenberg, 2004, 2006; Ehrenberg and Nadeau, 2005; Ehrenberg et al., 2006, 2007, 2009). Both shallow and deep marine carbonate strata show continuous loss of porosity with depth, indicating that porosity reducing processes act continuously from near the surface to depths in excess 4 km (Scholle & Halley, 1985). This demonstrates that the burial depth with attendant lithostatic load is one of the most critical factors determining the onset and ultimate efficiency of pressure solution compaction (Brown, 1997; Moore, 2001).

Observations of the minimum burial depth needed to start pressure solution in carbonates suggest depths from as shallow as few meters to few tens of meters (Bathurst, 1975; Mayers and Hill, 1983; Croize et al., 2009) to as deep as 600-1000 m (Dunnington, 1967; Buxton and Sibley, 1981; Sallerm 1984). The normally observed transition from mechanical compaction to pressure solution occurs between 250-400 m (Beall and Fischer, 1969; Moore, 2001). From these observations, one can calculate the minimum effective stress needed to start pressure solution at about room temperature. These observations indicate minimum effective stress of 1-8 MPa but also indicate that many other factors influence pressure solution besides depth alone.

The effect of temperature on the rate (degree) of pressure solution in carbonate is controversial (Lucia 2007). On the one hand, Schmoker (1984) has generated a compelling

case for subsurface porosity loss depending exponentially on temperature and linearly on time and hence operating as a function of thermal maturity in the basin of deposition. Taking the porosity-depth relationships of a number of carbonate sequences from separate basins with different thermal histories, Schmoker plotted porosity versus the calculated thermal maturity (TTI) and described the data using a power function of the form of $\phi = a(TTI)^b$ and indicated that the coefficient a is a petrological parameter and the exponent b is nearly constant for carbonate rocks from different locations. He believed that the exponent b represents the rate limiting step in pressure solution compaction that is, diffusive solution film transport from the site of dissolution to the site of precipitation. Recent study on Finnmark and Khuff platform carbonate by Ehrenberg (2006) supported Schmoker's work. On the other hand, Lockridge and Scholle (1978) could detect no difference in the porosity–depth curves for chalks between North America and the North Sea, even though the geothermal gradients in the North Sea are 1.5 to 2 times higher than encountered in North America.

The effects of grain size on pressure solution can be studied by measuring the porosity of different limestone types, (e. g. grainstone vs. mudstone, wackstone or chalk) which have experienced the same burial history. Schmoker and Halley (1982) and Halley and Schmoker (1983) compared the porosity vs. depth curves for different carbonate and found that chalks lose their porosity more rapidly than shallow water limestones, due to their fine grain size and pure composition. Heydari (2000) also found that fine grained limestones experience a high degree of pressure solution compared to coarse grained oolitic grainstones. Brown (1997) found that the grain size plays a role in pressure solution – porosity preserved in grain supported pores and destroyed in lime-mud (matrix) supported carbonate rocks.

Pore fluid chemistry also seems to play a significant role in controlling the degree and rate of pressure solution in carbonate rocks. Compared with carbonate rocks saturated with Mg-rich sea water, carbonate saturated with low Mg pore fluids show enhanced pressure solution (Neugebauer, 1873, 1974; Scholle, 1997). Hydrocarbons can retard the pressure solution process in carbonate reservoirs. Oswald et al. (1995, 1996) reported a pronounced decrease in porosity and reservoir thickness moving away from the crests of producing anticlines of the Thamama Group carbonate reservoirs in Abu Dhabi, U.A.E.. Pressure solution was identified to be the major process by which reservoir quality was degraded, reducing porosities from 25% in crestal areas to only 10% off structure. Pore fluids during burial controlled the degree of pressure solution, with stylolites preferentially forming in the water leg and inhibited in the oil leg (Oswald et al. 1996).

Aside from pore fluid chemistry, flow through can play a key role in controlling the transport of materials dissolved by pressure solution of carbonates to the place of precipitation. As pointed out by Bathurst (1993), diffusion is a slow process and bulk transport of solvent and solute together by advective fluid flow can often be important. Coupled with fluid expulsion, pressure solution can result in CaCO_3 dissolution in fine grained beds and precipitation in coarse grained beds (Heydari, 2000).

Finally, pore fluid overpressure can reduce the effective stress and slow down or even stop pressure solution. The high porosity seen in chalks at a depth of 3000 m in the Ekofisk oil field, North Sea has been attributed to the inhibition of pressure solution by overpressure (Scholle, 1977, 1983; Feazel and Schatzinger, 1985) and by the presence of

preferentially wetting hydrocarbons (Scholle, 1983). Insoluble organic material and clay mineral are evident to promote the intergranular pressure solution and especially for stylolite in reservoir rocks (Brown, 1997; Wely, 1959; Ehrenberg et al., 2004, 2007, 2009).

1.3 Theory of Intergranular Pressure Solution (IPS)

The theory of Intergranular Pressure Solution, which is the basic process controlling both creep by pressure solution and the development of stylolites, has been concisely described by Spiers, Zhang and co-workers (Spiers et al. 2004). The approach adopted by these authors will be followed here. It is well established that the thermodynamic driving force for IPS in a chemically closed system (no long range transport in the pore fluid phase) is provided by stress-induced gradients in chemical potential of the solid around individual grains (Paterson, 1973; Rutter, 1976, 1983; Raj, 1982; Lehner, 1990, 1995, Shimizu, 1995; Gal and Nur, 1998,). In the case of a stressed granular aggregate in which the pores are grain boundaries contain a solution phase, the normal component of molar chemical potential of the solid at the margins of a representative portion of grain boundary can be written as

$$\mu_{gb} \approx f^s + \sigma_n \Omega^s \quad (1.1)$$

where f^s is the Helmholtz free energy and Ω^s the molar volume of the solid at the margin of the grain boundary zone, and where σ_n (in Pa) is the compressive normal stress acting across the grain-to-grain contact element. This expression applies regardless of internal grain boundary structure and can be obtained from either a non-equilibrium (Lehner 1990) or equilibrium (Paterson 1973) thermodynamic approach to the problem, even though the latter is not strictly valid (Lehner and Balaible, 1984; Lehner, 1990). On pore walls, the potential of the solid at any point follows from Gibbs' condition of equilibrium between a stressed solid and its solution (Gibbs 1906; Lehner 1990; Heidug 1991, 1995). Neglecting interfacial energy effects, this is given

$$\mu_p \approx f^s + P_f \Omega^s \quad (1.2)$$

where f^s and Ω^s represent the free energy and the molecular volume of the solid at its surface, and P_f is the pore fluid pressure. Neglecting small gradients in f^s within the solid grains, differences in stress between grain contacts and free pore walls, thus lead to a potential drop

$$\Delta\mu_n = (\sigma_n - P_f) \Omega^s \quad (1.3)$$

Making use of the standard relation between the chemical potential (μ) of a dissolved solid and its concentration (C) in an ideal solution

$$\mu = \mu_0 + RT \ln \frac{C}{C_0} \quad (1.4)$$

it is easily shown that such potential drops ($\Delta\mu_n$) between source and sink sites correspond to a difference in solubility of the solid (ΔC) such that

$$\Delta\mu_n = RT \ln \frac{C_s + \Delta C}{C_s} = RT \left(\exp \frac{\sigma_n \Omega}{RT} - 1 \right) \approx RT \frac{\Delta C}{C_0} \quad (1.5)$$

Here R is the gas constant, T is absolute temperature, ΔC (in m^3/m^3) is the enhancement of the solubility of the solid at the source site relative to the sink site, and C_s (in m^3/m^3) is the solubility of the solid at the sink, which will in general be almost equal to the solubility (C_0) of the solid grains under purely hydrostatic reference conditions (pressure in solid and fluid = P_f). The approximation on the far right hand side of (1.5) applies when stress-induced solubility differences are small ($\Delta C/C_s \ll 1$), i.e. when stresses are relatively low (Rutter, 1976).

It is the above differences in chemical potential and solubility around grain boundaries, and between grain contact boundaries and pores walls, that lead to dissolution-precipitation transport and hence to pressure solution creep. In a dense aggregate under closed system conditions, gradients in normal stress and hence μ_{gb} , around grains will produce deviatoric deformation. In a porous aggregate, the potential drop $(\sigma_n - P_f)\Omega^s$ between points within loaded grain boundaries and free pore walls will additionally lead to compaction.

Under closed-system condition, the grain scale potential drops ($\Delta\mu_n$) developed in a stressed monomineralic rock provide the driving force for the three serial processes involved in pressure solution, namely dissolution within highly stressed grain contacts, diffusion through the grain boundary fluid, and precipitation at low stress boundaries or on pore walls (Raj, 1982; Rutter, 1983). Since they are serial, the slowest of these processes will control the deformation rate under steady state conditions (Raj & Chyung, 1981; Raj, 1982; Rutter 1983; Lehner, 1990). In deriving models for each rate-limiting process, it can therefore be assumed that all of the driving force ($\Delta\mu_n$) is taken up in driving the rate-controlling process in question, with the driving force needed for the other two processes (and for pore diffusion) being negligible (Raj, 1982; Lehner, 1990; De Meer & Spiers, 1995, 1997).

To derive creep models for rate control by each of the three potentially rate limiting steps, it is thus necessary to establish a relation between the rate of the individual processes of dissolution, diffusion, and precipitation and the stress-dependent driving force ($\Delta\mu_n$). For dissolution and precipitation controlled pressure solution creep, linear dissolution and precipitation reaction rate equations resembling those characterizing crystal growth and dissolution are usually assumed (e.g. Raj, 1982; Lehner 1990, 1995; Renard et al. 1999; Van Noort et al., 2008). These take the form

$$V_s = k_s \Omega^s \frac{\Delta\mu_n}{RT} \quad (1.6a)$$

$$V_p = k_p \Omega^s \frac{\Delta\mu_n}{RT} \quad (1.6b)$$

where V_s and V_p , are the velocities of dissolution and precipitation (in $\text{m}\cdot\text{s}^{-1}$), and where k_s and k_p are the respective reaction rate coefficients for dissolution at grain boundaries and precipitation at grain boundaries and/or pore walls. Note that the use of (1.6a) and (1.6b) assumes that the dissolution/precipitation process within grain boundaries and at pore walls is similar to that across a normal solid-liquid interface. For diffusion controlled pressure solution, the process rate is related to the diffusion flux in the grain boundary fluid given by Fick's first law written

$$J_{gb} = -\left(\frac{DC\Omega^s}{RT}\right)\nabla\mu_{gb} \quad (1.7)$$

(Spiers and Schutjens, 1990). Here D ($\text{m}^2\cdot\text{s}^{-1}$) is the grain boundary diffusion coefficient, R is the gas constant, T is the absolute temperature, and C is the solubility of the solute in the grain boundary fluid (in m^3/m^3). For the closed-system case, these relations can be coupled with (1.2) or (1.3), with expressions linking σ_n to the applied stress, and with the laws of mass and/or energy conservation to produce constitutive equations for (in m^3/m^3) creep by intergranular pressure solution creep.

Numerous authors (Rutter, 1976; Raj, 1982; Lehner, 1990; Spiers and Schutjens, 1990; Shimizu, 1995; Mullis, 1991; 1993) have published theoretically derived rate equations obtained along these lines, for both deviatoric and compaction creep under closed system conditions. All of these models lead to essentially identical results, differing only in the geometric terms describing the influence of grain packing and porosity. Here we will illustrate these results for the case of compaction creep by intergranular pressure solution (e.g. isotropic stress in Figure 4). For both uniaxial and isostatic compaction creep of a regular pack of spherical grains, the constitutive equations obtained take the form

$$\dot{\varepsilon}_s = k_s \frac{\left[\exp\left(\frac{B\sigma_e\Omega}{RT}\right) - 1\right]}{d} f_s(\phi_0, e_v) \quad \text{for dissolution control} \quad (1.8)$$

$$\dot{\varepsilon}_d = DCS \frac{\left[\exp\left(\frac{B\sigma_e\Omega}{RT}\right) - 1\right]}{d^3} f_d(\phi_0, e_v) \quad \text{for diffusion control} \quad (1.9)$$

$$\dot{\varepsilon}_p = k_p \frac{\left[\exp\left(\frac{B\sigma_e\Omega}{RT}\right) - 1\right]}{d} f_p(\phi_0, e_v) \quad \text{for precipitation control} \quad (1.10)$$

(Lehner, 1990; Spiers and Schutjens, 1990; DeMeer and Spiers, 1995; 1997; Renard et al., 1999; Niemeijer et al., 2002). Here $\dot{\varepsilon}_x$, represents volumetric strain rate (s^{-1}) for the cases of dissolution, diffusion or precipitation control (subscript $x = s, d, p$), σ_e is the applied

effective axial stress or isostatic pressure (in Pa), d is the grain size (in m), S is the average thickness of the grain boundary fluid phase (in m), and the $f_x(\phi)$ are dimensionless functions of porosity (ϕ) that account for changes in grain contact area, transport path length and pore wall area during compaction.

In an open system, where mass can be removed or added through diffusive or advective transport via the pore fluid phase, the fluid may be supersaturated or under-saturated with respect to the pore walls due to the control by the long range transport process. Under such conditions, the driving force for transport from stressed grain contacts to neighboring pores, hence for pressure solution creep, becomes equal to the potential difference, $\Delta\mu_{open}$ between the solid within the contacts (at μ_{gb}) and the solute (at μ_s) in the adjacent pore fluid (Lehner, 1995). For small under-saturations ($\Delta S/C_0$) of the pore fluid with respect to pore walls $\mu_s = \mu_p - RT \cdot \Delta S/C_0$ and $\Delta\mu_{open} = (\mu_{gb} - \mu_s) = \Delta\mu_n + RT \Delta S/C_0$ (Lehner, 1995). Using this expression for driving force in deriving constitutive relations for compaction by pressure solution leads to a set of equations identical to (1.8), (1.9) and (1.10), but where $\sigma_e \Omega^s$ is replaced by $Y = (\sigma_e \Omega^s + RT \cdot \Delta S/BC_0)$, for the open system case. Thus pressure solution creep is accelerated when the pore fluid is under-saturated ($\Delta S > 0$), retarded when it is super-saturated ($\Delta S < 0$), and stopped when $Y \leq 0$ (Lehner, 1995; De Meer and Spiers, 1997).

1.4 Previous experimental work and problem definition

Relative to the abundant literature on field studies of pressure solution in carbonate rocks, experimental work is sparse. Baker et al. (1980) carried out compaction experiments intended to activate intergranular pressure solution in deep sea carbonate sediments (i.e. low magnesium calcite), crushed Iceland spar and reagent-grade calcite powder at 25-100 MPa effective pressure and 22-180 °C, for 1 to 10 days. Significant porosity reduction to values as low as 9.9% occurred in 10 days. However, as high stresses and temperatures were used, the contribution from deformation mechanisms other than intergranular pressure solution, i. e. grain scale brittle behavior or plasticity is unknown. Uniaxial compaction experiments carried out under chemically closed system conditions by Shinn and Robbin (1983) at room temperature, a fluid pressure of 0.1 MPa and applied effective stresses from 6.5 to 95 MPa, on cores of modern carbonate sediments, resulted in features such as incipient stylolites and truncated fossils, indicating the operation of pressure solution. However, the kinetics and rate control process could not be determined. Dewers & Muhari (2000) reported a combination of cataclastic deformation and intergranular pressure solution in compaction experiments on powdered Iceland spar. Triaxial deformation experiments performed on chalk by Hellmann et al. (2002) also showed that pressure solution was probably operating under their experimental conditions, i. e. in a closed system at 21-100 °C, 4 MPa differential effective stress and pore pressures up to 0.3 MPa. However, the strain rates attained were too low to be used for quantitative studies. Recent work by Liteanu & Spiers (2009) and Liteanu (2009) on compaction of granular calcite at 80 °C showed that while pressure solution is definitely operative, especially in the presence of super-critical CO₂, grain failure due to subcritical crack growth is important in coarser grained samples (i.e. >100 μm) and in the presence of NaCl in the pore fluid. Even with

substantial amounts of creep data it proved difficult to isolate IPS, to identify the rate controlling process and to obtain a constitutive law.

It is clear to the above that one of the main problems with compaction experiments on pressure solution in carbonates is to isolate the compaction strain rate due to IPS as opposed to other mechanisms (Raj 1982; Tada & Siever 1989). It has not been successfully isolated and quantified via lab experiments with the exception of the work by Liteanu & Sipers (2009), the effects of key variables such as grain size, effective stress, temperature and pore fluid chemistry have generally not been investigated in a systematic way, with the result that little insight exists into the likely rate-controlling processes or associated rate-determining (constitutive) parameters. For progress in modeling the time dependent compaction of carbonate, porosity-permeability reduction, and the creep response of carbonate reservoir to hydrocarbon production, better data are essential.

1.5 Aims and approaches of the present research

Based on the above, the principal aims of this research are to obtain a better quantitative understanding of the compaction behavior of calcite aggregate by intergranular pressure solution and to constrain the effects of the controlling variables on the rate and rate controlling process of IPS in carbonate reservoir rocks. The specific aims are:

- 1). To develop a test procedure for compaction of wet calcite aggregates which minimizing the role of deformation mechanisms other than intergranular pressure solution.
- 2). To verify the operation of intergranular pressure solution in compaction experiments on granular calcite relevant to conditions ranging from shallow burial (low effective stress and low temperature) to typical reservoir (hydrothermal) conditions (20-47 MPa effective stresses and up to 150 °C).
- 3). To quantify the effects of major variables, namely the stress, temperature, grain size and pore fluid chemistry, expected to control the rate of IPS and porosity reduction rates in carbonate reservoir rocks and fault gouge under upper crustal conditions.
- 4). To determine and to constrain the rate limiting step of intergranular pressure solution in carbonate rocks under upper crustal conditions. .
- 5). To derive constitute parameters for intergranular pressure solution in carbonate rocks and for fault gouge, to enable future modeling of their compaction behavior in site.

The main approach used to achieve the above aims was to carry out compaction experiments under conditions simulating depth up to ~3-4 km. The experimental results were compared with microphysical models. The compacted samples were examined by SEM to obtain microstructural evidence of the operative deformation mechanism. Since IPS involves coupling of mechanical deformation, chemical reaction and mass transfer through a fluid phase, the effects of pore fluid composition and the flow through were used to gain new information on the rate controlling processes. This was done by manipulating the pore fluid chemistry i. e. by adding reaction inhibitors and observing the compaction response. Comparison of theoretical microphysical modeling with the IPS compaction data is the main approach to quantify the IPS variables and deriving constitutive parameters and rate law.

1.6 References

- Ahr, W.M, (2008), *Geology of Carbonate Reservoirs –the identification, description, and characterization of hydrocarbon reservoirs in carbonate rocks*, John Wiley & Sons, INC, publication, P277.
- Baker, P. A., M. Kastner, J.D. Byerlee, D.A. Lockner (1980), Pressure solution and hydrothermal recrystallization of carbonate sediments — An experimental study, *Marine Geology* 38, 185-203.
- Bathurst, R. G. C. (1958), Diagenetic fabrics in some British Dinantian limestones. *Liverpool and Manchester Geology* 2, 1-36.
- Bathurst, R. G. C., (1975), Carbonate sediments and their diagenesis, *Development in Sedimentary*. 12, 2nd edition, Elsevier, Amsterdam, New York, 658 pp.
- Bathurst, R. G. C., (1984), The integration of pressure solution with mechanical compaction and cementation. In: *Stylolite and associated phenomena relevance to hydrocarbon reservoirs*. Abu Dhabi National Reserv. Res. Found. Spec. Pub., 41-55
- Bathurst, R.G.C., (1987), Diagenetically enhanced bedding in argillaceous platform limestone: stratified cementation and selective compaction: *Sedimentology* 34, 749-778.
- Bathurst, R. G. C., (1993), Microfabrics in carbonate diagenesis, a critical look at forty years in research, in R. Rezak, and D. I. Lavoie, eds., *Carbonate Microfabrics*: New York, Springer-Verlag, 3-14.
- Billi A., and F. Salvini (2007), Fault-related solution cleavage in exposed carbonate reservoir rocks in the southern Apennines, Italy, *Journal of Petroleum Geology* 24, 147-169.
- Bolas, H. M. N., C. Hermanrud, T. A. Schutter, and G. M. G. Teige (2008), Stress-insensitive chemical compaction responsible for high overpressures in deep buried north sea chalk? *Marine and Petroleum Geology* 25, 565-587.
- Bos B. and C. J. Spiers (2002), Frictional-viscous flow of phyllosilicate-bearing fault rock: Microphysical model and implications for crustal strength profiles. *J. Geophys. Res.* 107, B2, 10.1029/2001JB000301.
- Breesch, L., R., Swennen, B., Dewever, A., Mezini (2007), Deposition and diagenesis of carbonate conglomerates in the Kremenara anticline, Albania: a paragenetic time marker in the Albanian foreland fold-and-thrust belt, *Sedimentology* 54, 483-496.
- Brouste, A. F. Renard, J.P. Gratier, J. Schmittbuhl (2007), Variety of stylolites morphologies and statistical characterization of the amount of heterogeneities in the rock, *J. Struct. Geol.* 29, 422-434.
- Brown, A., (1984), Empirical relation between carbonate porosity and thermal maturity: an approach to regional porosity prediction: Discussion. *AAPG Bulletin* 69, 2024-2028.
- Brown, A. (1997), Porosity variation in Carbonates as a function of depth: Mississippian Madison Group, Williston Basin, in Kupecz, J. A., Gluyas, J. G and Bloch, S (editors), Reservoir quality prediction in sandstone and carbonates, *AAPG Memoir* 69, 29-45.
- Budd, D. A. (2002), The relative role of compaction and early cementation in the destruction of permeability in carbonate grainstones: a case study from the paleogene of west-central florida, USA, *J. Sediment. Res.* 72, 116-128.

- Caminatti, M., J. L. Dias, and B. Wolf (2009), From turbidites to carbonates: Breaking paradigms in deep water, in *Offshore Technology Conference*, Houston, Texas, doi: 10.4043/20124-MS.
- Canole, P., F. Odonne, and M. Polve (1997), Heterogeneous strain associated with normal faulting: evidence of mass transfer by pressure solution associated with fault displacement, *Tectonophysics* 283, 129-143.
- Carrio-Schaffhauser E., P. Gaviglio (1990), Pressure solution and cementation stimulated by faulting in limestones, *J. Struct. Geol.* 12, 987-994.
- Chester, F. M. and J. M. Logan (1986), Implications for mechanical properties of brittle faults from observations of the Punchbowl fault zone, California, *Pure and Appl. Geophys.* 124, 79-106.
- Chilingarian, G. V., S. J. Mazzulo, and H. H., Rieke (1992), Carbonate Reservoir Characterization: a Geologic-Engineering Analysis, Part I, *Developments in Petroleum Science* 30, Elsevier, Amsterdam.
- Chilingarian, G. V., S. J. Mazzulo, and H. H. Rieke (1996), Carbonate Reservoir Characterization: a Geologic-Engineering Analysis, Part II, *Developments in Petroleum Science* 44, Elsevier, Amsterdam.
- Choquette, p. W., and L.C. Pray (1970), Geologic nomenclature and classification of porosity in sedimentary carbonates: *AAPG Bulletin* 54, 207-250.
- Choquette, P. W., and N. P. James (1987), Diagenesis #12: Diagenesis in limestones 1-3. The deep burial environment. *Geosci. Can.* 14, 3-35.
- Coogan, A. H., (1970), Measurements of compaction in oolitic grainstone, *J. Sediment. Res.* 40, 921-929.
- Croize, D., S. N. Ehrenberg, K. Bjorlykke, F. Renard, and J. Jahren (2009), Petrophysical properties of bioclastic platform carbonates: Implications for porosity controls during burial, *Marine and Petroleum Geology*, in press, doi: 10.1016/j.marpetgeo.2009.11.008.
- Dunham, R. J., 1962, Classification of carbonate rocks according to their depositional texture, in W. E. Ham, ed., *Classification of carbonate rocks*, Tulsa, OK, *AAPG Memoir* 1, 108-121.
- Ehrenberg, S. N. (2004), Factors controlling porosity in the upper carboniferous-lower Permian carbonate strata of Barents Sea, *AAPG Bulletin* 88, 1653-1676.
- Ehrenberg, S. N., and P. H. Nadeau (2005), Sandstone vs. Carbonate petroleum reservoirs: a global perspective on porosity-depth and porosity-permeability relationships, *AAPG Bulletin* 89, 435-445.
- Ehrenberg, S. N., G. P. Eberli, M. Keramati and A. Moallemi (2006), Permeability-porosity relationships in interbedded limestone-dolostone reservoirs, *AAPG Bulletin* 90, 91-114.
- Ehrenberg, S. N. (2006), porosity destruction in carbonate platforms, *Journal of petroleum Geology* 29, 41-52, doi: 10.1111/j.1747-5457.2006.00041.x.
- Ehrenberg, S. N., P. H. Nadeau and A. A. M. Aqrabi (2007), A comparison of Khuff and Arab reservoir potential throughout the Middle East, *AAPG Bulletin* 91, 275-286; DOI: 10.1306/09140606054.
- Ehrenberg S. N., P. H. Nadeau and O. Steen (2009), Petroleum reservoir porosity versus depth: Influence of geological age, *AAPG Bulletin* 93, 1281 – 1296.

- Faulkner, D. R., (2004), A model for the variation in permeability of clay-bearing fault gouge with depth in the brittle crust, *Geophys. Res. Lett.* 31, L19611. Doi: 10.1029/2004GL020736.
- Feazel, C. T. and R. A., Schatzinger (1985), Prevention of carbonate cementation in petroleum reservoirs. In: N. Schneidemann and P. M. Harris (Eds.), Carbonate cements. *SEPM Spec. Pub.* 36, 97-106.
- Fletcher, R. C., and D. D. Pollard (1981), Anticrack model for pressure solution surfaces, *Geology* 9, 419-424.
- Flügel, E., (2004), *Micro Facies of Carbonate Rocks-Aanalysis, Interpretation and Application*. Springer, P996
- Fuerten, F., Pierre-Yves F. Robin, and M. Schweinberger (2002), Finite element modelling of the evolution of pressure solution cleavage, *J. Struct. Geol.* 24, 1055-1064.
- Gratier J.P., P. Favreau, F. Renard, and E. Pili (2002), Fluid pressure evolution during the earthquake cycle controlled by fluid flow and pressure solution crack sealing, *Earth Planets and Space* 54, 1139-1146.
- Gratier J.P., P. Favreau, F. Renard (2003), Modeling fluid transfer along Californian faults when integrating pressure solution crack sealing and compaction process, *J. Geophys. Res.* 108 (B2) 28-52.
- Gratier, J.P., L. Muquet, R. Hassani, and F. Renard (2005), Experimental microstylolites in quartz and modeled application to natural stylolitic structures, *J. Struct. Geol.* 27, 89-100.
- Gratier, J.P., and F. Gueydan (2007), Deformation in the presence of fluids and mineral reactions: effect of fracturing and fluid-rocks interaction on seismic cycle, in : *Tectonic Faults, agent of change on a dynamic earth*, edited by M.R. Handy, G. Hirth, N. Hovius, Dahlem Workshop, The MIT Press, Cambridge, Mass., USA. 319-356.
- Greene, G. W., K. Kristiansen, E. E. Meyer, J. R. Boles, J. N. Israelachvili (2009), Role of electrochemical reactions in pressure solution, *Geochimica et Cosmochimica Acta*, 73(10), 2862-2874.
- Halley, R. B., and J. W. Schmoker (1983), High porosity Cenozoic carbonate rocks of south Florida: progressive loss of porosity with depth: *AAPG Bulletin* 67, 191-200.
- Hellmann, R., P. Gaviglio, P. J. N. Renders, J.-P. Gratier, S. Békri, and P. Adler (2002), Experimental pressure solution compaction of chalk in aqueous solutions. Part 2. Deformation examined by SEM, porosimetry, synthetic permeability, and X-ray computerized tomography. In *Water-Rock Interactions, Ore Deposits, and Environmental Geochemistry: A tribute to David A. Crerar* (R. Hellmann and S.A. Wood, eds.), Geochemical Society, pp. 153-178.
- Hellmann, R., P. J. N. Renders, J.-P. Gratier and R. Guiguet (2002), Experimental pressure solution compaction of chalk in aqueous solutions. Part 1. Deformation behavior and chemistry. In *Water-Rock Interactions, Ore Deposits, and Environmental Geochemistry: A tribute to David A. Crerar* (R. Hellmann and S.A. Wood, eds.), Geochemical Society, pp. 129-152.
- Heydari, E., (2000), Porosity Loss, Fluid Flow, and Mass Transfer in Limestone Reservoirs: Application to the Upper Jurassic Smackover Formation, Mississippi, *AAPG Bulletin* 84, 100-118; DOI: 10.1306/C9EBCD79-1735-11D7-8645000102C1865D.

- Hickman S. H., R. Sibson and R. Bruhn (1995), Introduction to special section: mechanical involvement of fluid in faulting. *J. Geophys. Res.* 100, 12831-12840.
- Houseknecht, D. W. and L. A. Hathon (1987), Petrographic constraints on models of intergranular pressure solution in quartzose sandstones, *Applied Geochemistry* 2, 507-521.
- Koepnick, R. B., (1983), Distribution and vertical permeability of stylolites within a Lower Cretaceous carbonate reservoir, Abu Dhabi, United Arab Emirates, Stylolites and Associated Phenomena Relevance to Hydrocarbon Reservoir, *Abu Dhabi, U. A.E., Abu Dhabi Reservoir Research Foundation Special Publication*, 261-278.
- Le Guen Y., F. Renard, R. Hellmann, E. Brosse, M. Collombet, D. Tisserand, J. P. Gratier, (2007), Enhanced deformation of limestone and sandstone in the presence of high PCO₂ fluids. *J. Geophys. Res.* 112, B05421, doi :10.1029/2006JB004637.
- Liteanu, E. and C. J. Spiers (2009). Influence of pore fluid salt content on compaction creep of calcite aggregates in the presence of supercritical CO₂. *Chem. Geol.* 265, 134-147. doi:10.1016/i.chemgeo.2008.12.010.
- Lockridge, J. P., and P. A. Scholle (1978), Niobrara gas in eastern Colorado and northwestern Kansas: *Rocky Mountain Assoc. Geol.* 1978 Symp., p. 35-49.
- Lucia, F. J., (2007), *Carbonate Reservoir Characterization- An Integrated Approach*, Second Edition, Springer. P336.
- Lydzba, D., S. Pietruszczak, J. F. Shao (2007), Intergranular pressure solution in chalk: a multiscale approach, *Computers and Geotechnics* 34, 291-305.
- Marcussen, O., J. I. Faleide, J. Jahren, and K. Bjorlykke (2010), Mudstone compaction curves in basin modelling: a study of mesozoic and Cenozoic sediments in the northern north sea, *Basin Research* 22, 324-340, doi: 10.1111/j.1365-2117.2009.00430-x.
- Marone, C., J. E. Vidale, and W. L. Ellsworth (1995), Fault healing inferred from time dependent variations in source properties of repeating earthquakes, *Geophys. Res. Lett.* 22, 3095-3098, doi: 10.1029/95GL03076.
- McClay, (1977), Pressure solution and Coble creep in rocks and minerals: a review, *J. Geol. Soc.* 134, 57-70. DOI:10.1144/gsjgs.134.1.0057.
- Meike, A., H.-R. Wenk (1988), A TEM study of microstructures associated with solution cleavage in limestone, *Tectonophysics*, 14 (1-2), 137-148.
- Mitra, S., and W. C. Bear (1980), Theoretical models of porosity reduction by pressure solution for well-sorted sandstones: *J. Sediment. Petrol.* 50, 1347-1360.
- Moore, C. H., and Druckman (1981), Burial diagenesis and porosity evolution, upper Jurassic Smackover, Arkansas and Louisiana, *AAPG Bulletin*, 65, 597-628.
- Moore, C. H., (1989), Carbonate Diagenesis and Porosity, *Developments in Sedimentology*, 46, Elsevier, Amsterdam.
- Moore, C. H., and E. Heydari, 1993, Burial diagenesis and hydrocarbon migration in platform limestones: a conceptual model based on the Upper Jurassic of Gulf Coast of USA, in A. D. Horbury, and A.G. Robinson, eds., *Diagenesis and basin development: Studies in Geology* 36, Tulsa, Oklahoma, AAPG, 213-229.
- Moore, C. H., (2001), Carbonate Reservoirs-Porosity evolution and diagenesis in a sequence stratigraphic framework, *Developments in Sedimentology* 55, Elsevier, Amsterdam.

- Harris, P. M., and L. J. Weber (2006), Giant hydrocarbon reservoirs of the world: from rocks to reservoir characterization and modeling: *AAPG Memoir 88/SEPM Special Publication*.
- Nicholson C., M. J. Kamerling, C. C. Sorlien, T. Hopps, and J. P. Gratier (2007), Subsidence, compaction and gravity-sliding : implication for 3D geometry dynamic rupture and seismic hazard of active basin-bounding faults in southern California, *Bull. Seis. Soc. Am.* 97, 1607-1620.
- Niemeijer, A. R., C. J. Spiers, and B. Bos (2002), Compaction creep of quartz sand at 400-600 C: Experimental evidence for dissolution-controlled pressure solution, *Earth Planet. Sci. Lett.* 195, 261-275.
- Niemeijer, A., C. Marone and , D. Elsworth (2008), Healing of simulated fault gouges aided by pressure solution: results from rock analogue experiments, *J. Geophys. Res.* 113, doi: 10.1029/2007JB005376.
- Ortoleva, P. J. (1994), Basin compartments and seal, *AAPG Memoir 61*
- Oswald, E. J, Mueller, H. W., Goff, D. F., H., Al-Habshi, Al-Matroushi, S., (1995), Controls on porosity evolution in Thamama group carbonate reservoirs in *Abu Dhabi, U.A.E. SPE Middle East*.
- Oswald, E. J., D. F. Goff and H. W. Mueller, (1996), Compaction Controls on Porosity in Thamama Group Carbonate Reservoirs in Abu Dhabi, *AAPG Bulletin* 80, DOI:10.1306/522B37EF-1727-11D7-8645000102C1865D.
- Paterson M. S. (1973) Thermodynamics and its geological applications. *Rev. Geophys.* 11, 355-389.
- Paterson M. S. (1995) A theory for granular flow accommodated by material transfer via an intergranular fluid. *Tectonophysics*, 245, 135-152.
- Peacock, D.C.P., Q. J. Fisher, E. J. M. Willemse, and A. Aydin (1998), The relationship between faults and pressure solution seams in carbonate rocks and the implications for fluid flow, *Geol. Soc. Lond. Spec. Pub.* 147, 105-115.
- Person, M., L. P. Baumgartner, B. Bos, J. A. D. Connolly, J. P. Gratier, F. Gueydan, S. A. Miller, C. L. Rosenberg, J. L. Urai, B. W. D. Yardley (2007), Fluids, Geochemical cycles and mass transport in fault zones, in : *Tectonics faults : agents of change on a dynamic earth*, edited by M.R. Handy, G. Hirth, N. Hovius, Dahlem Workshop, The MIT Press, Cambridge, Mass., USA. 403-426.
- Petit, J. P. and M. Mattauer, (1995), Palaeostress superimposition deduced from mesoscale structures in limestone: the Matelles exposure, Languedoc, France, *J. Struct. Geol.* 17, 245-256.
- Petit, J. P., C. A. J. Wibberley and G. Ruiz, (1999), 'Crack-seal', slip: a new fault valve mechanism? *J. Struct. Geol.* 21, 1199-1207.
- Pili E., F. Poitrasson, and J. P. Gratier (2002), Carbon-oxygen isotope and trace element constraints on how fluids percolate faulted limestones from the San Andreas Fault system: partitioning of fluid sources and pathways, *Chem. Geol.* 190, 231-250.
- Renard F., Park A., P. Ortoleva, and J. P. Gratier (1999), A transitional pressure solution model. *Tectonophysics* 312, 97-115.
- Renard, F., J. Schmittbuhl, JP Gratier, P. Meakin, E. Merino (2004), The three-dimensional morphology of stylolites : roughness analysis and possible genetic implicatoins, *J. Geophys. Res* 109 (B3) 73.

- Renard, F., E. Gundersen, R. Hellemann, M. Collombet, and Y. LeGuen (2005), Numerical modeling of the effect of carbon dioxide sequestration on the rate of pressure solution creep in limestone: Preliminary results, *Oil Gas Sci. Technol.-Rev. IFP* 60, 381-399.
- Rittenhouse, G., (1971), Pore-space reduction by solution and cementation: *AAPG Bulletin* 55, 80-91.
- Rutter E. H. (1976), The kinetics of rock deformation by pressure solution. *Philos. Trans. R. Soc. London* 283, 203-219.
- Rutter EH. (1983), Pressure solution in nature, theory and experiment. *J. Geol. Soc. Lond.* 140,725-40.
- Scholle, P. A., (1971), Diagenesis of deep-water carbonate turbidites, Upper Cretaceous Monte Antola Flysch, Northern Apenines, Italy, *J. Sediment. Petrol.* 41, 233-250.
- Schmoker,, J. W., and R. B. Halley, (1982), Carbonate porosity vs. depth: a predictable relation for south Florida: *AAPG Bulletin* 66, 2561-2570.
- Schmoker, J. W., (1984), Empirical relation between carbonate and thermal maturity: an approach to regional porosity prediction: *AAPG Bulletin* 68, 1697-1703.
- Schmoker, J. W., K. Krystinik, and R. Hally (1985), Selected characteristics of limestone and dolomite reservoirs in the United States: *AAPG Bulletin* 69, 733-741.
- Scholle, P. A., (1977), Chalk diagenesis and its relation to petroleum exploration: oil from chalks, a modern miracle? *AAPG Bulletin* 61, 982-1009.
- Scholle, P. A., and R. B. Halley (1985), Burial diagenesis: out of sight, out of mind. In: N. Schneidermann and P. M. Harris (Eds.), Carbonate Cements. *SEPM Spec. Pub.* 36, 309-334.
- Scholle, P. A., D. S. Ulma-Scholle (2003), A Color guide to the Petrography of Carbonate Rocks: Grains, Texture,porosity and Diagenesis, *AAPG Memoir* 77, Oklahoma, USA, AAPG, 470P.
- Schulmberg, (2007), Carbonate- a tough but worthwhile Challenge, *Oil Review Middle East* 6
http://www.slb.com/~media/Files/industry_challenges/carbonates/industry_articles/200712_orme_carbonates.ashx.
- Shinn, E. A., and D. M. Robbin (1983), Mechanical and chemical compaction in fine-grained shallow-water limestones, *J. Sediment. Petrol.* 53, 595-618.
- Sleep, N. H., and M. L. Blanpied (1992), Creep, compaction and the weak rheology of major faults, *Nature* 359, 687-692, doi: 10.1038/359687a0.
- Smith D. A. (1966) Theoretical considerations of sealing and non-sealing faults. *AAPG Bulletin* 50, 363-374.
- Spiers, C. J. and N. L. Carter (1998), Microphysics of rocksalt flow in nature. Forth Conference on the Mechanical behaviour of Salt, The Pennsylvania State University, June 17 and 18, 1996, *Trans Tech Publication Series on Rock and Soil Mechanics*, 22, 115-128.
- Stel. H., M. J. De Ruig (1989), Opposite vergence of a kink fold and pressure solution cleavage, southeast Spain: a study of the relation between paleostress and fold kinematics, *Tectonophysics* 165, 117-124.
- Stockdale, B. P. (1922), Stylolite: their nature and origin, *Indiana Univ. Studies*, 2, 1-97.
- Stockdale, B. P. (1926), The stratigraphic significance of solution in rocks. *J. Geol.* 34, 399-414.

- Swennen, R., Ferket, H., Benchilla, L., Roure, F., Ellam, R. and SUBTRAP-team (2003). Fluid flow and diagenesis in carbonate dominated Foreland Fold and Thrust Belts: petrographic inferences from field studies of late-diagenetic fabrics from Albania, Belgium, Canada, Mexico and Pakistan. *Journal of Geochemical Exploration*, 78-79, 481-485.
- Tavani, S., F. Storti, J. A. Muñoz (2010), Scaling relationships between strata bound pressure solution cleavage spacing and layer thickness in a folded carbonate multilayer of the Northern Apennines (Italy), *J. Struct. Geol.*, 32 (3), 278-287.
- Tondi E, M. Antonellini, A. Aydin, L. Marchegiani and G. Cello (2006), The role of deformation bands, stylolites and sheared stylolites in fault development in carbonate grainstones of the Majella Mountain, Italy, *J. Struct. Geol.* 28, 376-391.
- Tondi E., (2007), Nucleation, development and petrophysical properties of faults in carbonate grainstones: Evidence from the San Vito Lo Capo peninsula (Sicily, Italy), *J. Struct. Geol.* 29, 614-628.
- Towend, J and M. D. Zoback, (2000), How faulting keeps the crust strong, *Geology* 28, 399-402. Doi: 10.1130/0091-7613(2000)28<39.
- Tuncay, K., A. Park and P. Ortoleva (2000), Sedimentary basin deformation: an incremental stress approach, *Tectonophysics* 323,77-104 .
- Urai, J. L., C. J.Spiers, H. Zwart & G. S. Lister (1986), Weakening of rock salt by water during long-term creep, *Nature* 324, 554-557.
- Urai, J. L., & C. J. Spiers (2007), The effect of grain boundary water on deformation mechanisms and rheology of rocksalt during long term deformation. In: *Proc. 6th Conference on the Mechanical Behavior of Salt, Understanding of THMC Processes in Salt* (eds, M. Wallner, K. Lux, W. Minkley, H. Hardy Jr.), Hannover, Germany: 149-158.
- Van Noort , R. H., H. J. M. Visser, and C. J. Spiers (2008), Influence of grain boundary structure on dissolution controlled pressure solution and retarding effects of grain boundary healing, *J. Geophys. Res.* 113, doi: 10.1029/2007JB005223.
- Van Noort , R. H., and C. J. Spiers (2009), Knetics effects of microscale plasticity at grain boundaries during pressure solution, *J. Geophys. Res.* 114, doi: 10.1029/2008/2008JB005634.
- Vermilye, J. M., and C. Scholz (1998), The process zone: A microstructural view of fault growth, *J. Geophys. Res.* 103, B6, 12,223-12,237.
- Verwer, K., G. Eberli, G. Baechle, and R. Weger (2010), Effect of carbonate pore structure on dynamic shear moduli, *Geophysics*, 75, E1-E8.
- Verberne, B. A., C. He, and C. J. Spiers (2010), Frictional properties of sedimentary rocks and natural fault gouge from the Longmenshan Fault Zone, Sichuan, China. *Bull. Seis. Soc. Am.* (in press).
- Wall, B. R. G., R. Girbacea, A. Mesonjesi and A. Aydin (2006), Evolution of fracture and fault-controlled fluid path in carbonates of the Albanides fold-thrust belt, *AAPG Bulletin*, 90, 1227-1249, DOI: 10.1306/03280604014.
- Wanless, H. R., (1979), Limestone response to stress: Pressure solution and dolomitization, *J. Sediment. Petrol.* 49, 437-462.

- Watkinson1, A. J. and E. M. G. Ward (2006), Reactivation of pressure-solution seams by a strike-slip fault-sequential, dilational jog formation and fluid flow, *AAPG Bulletin* 90, 1187-1200, DOI: 10.1306/03060604088.
- Whitaker, A. E., and M. J. Bartolomew (1999), Layer parallel shortening: a mechanism for determining deformation timing at the junction of the central and southern Appalachians, *Am. J. Sci.* 299, 238-254.
- Wong, T. F. and P. Baud (1999), Mechanical Compaction of Porous Sandstone, *Oil Gas Sci. Technol. - Rev. IFP*, 54, 715-727. DOI: 10.2516/ogst:1999061
- Yang, X. S. (2000), Pressure solution in sedimentary basins: effect of temperature gradient, *Earth Planet. Sci. Lett.* 176, 233-243.
- Yasuhara, H., Derek Elsworth, Amir Polak (2004), Compaction and diagenesis of sandstones - the role of pressure solution, *Elsevier Geo-Engineering Book Series*, 2, 733-738.
- Yasuhara, H., C. Marone and D. Elsworth (2005), Fault zone restrengthening and frictional healing: the role of pressure solution. *J. Geophys. Res.* 110, B06310,doi:10.1029/2004JB003327.
- Yasuhara, H., and D. Elsworth (2008), Compaction of rock fracture moderated by competing roles of stress corrosion and pressure solution, *Pure Appl. Geophys.* 165, 1289-1306, doi: 10.1007/s00024-008-0356-2.
- Zubtsov, S. F. Renard, J.-P. Gratier, R. Guiguet, D. K. Dysthe, V. Y. Traskine (2004), Experimental pressure solution creep of polymineralic aggregates, *Tectonophysics* 385, 45-57.

2. Compaction experiments on wet calcite powder at room temperature: evidence for operation of intergranular pressure solution

This chapter is based on the paper published as: Zhang, X., J. Salemans, C. J. Peach and C. J. Spiers (2002), Compaction experiments on wet calcite powder at room temperature: evidence for operation of intergranular pressure solution, Geological society special publication no. 200, Geological Society of London, 20-30.

Abstract

Dead weight uniaxial compaction creep experiments have been carried out on fine-grained, super-pure calcite ($<74\text{ }\mu\text{m}$) at room temperature and applied effective stresses of 1-4 MPa. All samples were pre-compacted dry at a stress of 8 MPa, for 30 minutes, to obtain a well-controlled initial porosity. The samples were then wet-compacted under “drained” conditions with pre-saturated solution as pore fluid. Control experiments, which were done either dry or with chemically inert pore fluid, showed negligible compaction. However, samples tested with saturated solution as pore fluid showed easily measurable compaction creep. The compaction strain rate decreased with increasing strain, increasing grain size, and increased with increasing applied stress. Addition of Mg^{2+} ions to the saturated solution dramatically inhibited compaction. From the literature, Mg^{2+} ions are known to inhibit the calcite precipitation. By comparison with a theoretical model for intergranular pressure solution in calcite, the observed mechanical behavior and the way that compaction responds to the pore fluid chemistry suggest that intergranular pressure solution was the mechanism of the deformation under our experimental conditions.

2.1 Introduction

Intergranular Pressure Solution (IPS) is an effective mechanism of deformation and porosity and permeability reduction in both sedimentary and fault rocks under diagenetic and low grade metamorphic conditions (Sorby, 1863; Weyl, 1959; Durney, 1972; Rutter, 1976, 1983; Tada & Siever, 1989; De Meer & Spiers, 1999). Both in silicate and carbonate rocks, evidence of intergranular pressure solution is widespread (Heald, 1956; Bathurst, 1958; Burger, 1975; Cox & Withford, 1987; Houseknecht, 1987, 1988), and there is widespread interest in quantifying the rate of the process in these rock materials (Rutter, 1976, 1983; Dewers & Hajash, 1995; De Meer & Spiers, 1999), notably in relation to hydrocarbons exploration and production research (Carozzi & Bergen, 1987; Heydari, 2000).

Much work has accordingly been done on the theoretical modeling of the intergranular pressure solution rate in two-component solid-liquid systems. In most of these models, grain boundaries are considered to contain fluid in some interconnected form which cannot be squeezed out, i. e. in a strongly adsorbed thin film (Weyl, 1959; Rutter, 1976, 1983;

Robin, 1978; Hickman & Evans, 1991, 1995) or in a micro-scale island-channel network containing free fluid (Elliot, 1973; Raj, 1982; Lehner, 1990, 1995; Spiers & Schutjens, 1990). When there is no long range transport of solid into or out of the system, the mechanism is believed to involve dissolution of material at grain contacts under high mean normal stress (high chemical potential), diffusion through the intergranular and pore fluid phase, and precipitation at interfaces under low mean normal stress (low chemical potential). As these processes operate in series under such conditions, the slowest step will be rate controlling at steady state (Raj, 1982; Lehner, 1990; De Meer & Spiers, 1999). Despite the ambiguities of the details of the grain boundary structure, the main variables influencing intergranular pressure solution are well known. These are: grain size, effective stress, temperature, mineralogy, and pore fluid chemistry (Tada & Sievers, 1989; Rutter, 1983; De Meer & Spiers, 1999). While the existing models for creep by intergranular pressure solution can be reasonably applied to two component systems such as NaCl plus saturated solution, the rate controlling parameters such as reaction rate or grain boundary diffusion coefficients are not well known. Moreover, existing models have not been adapted for complex reaction mechanisms such as those involved in calcite dissolution/precipitation.

Numerous experimental investigations have been conducted in attempt to demonstrate the operation of IPS in the laboratory, to identify the detailed mechanism and to quantify the rate of the process. These experiments employ either single crystal contacts or fine-grained polycrystalline aggregate plus saturated solution. When single crystals are used, the cleaved or polished surfaces are usually indented with a knife-edge piston (Tada & Sieve, 1986; Gratier, 1993), or else the crystal is pressed against another crystal or glass (Hickman & Evans, 1991, 1992, 1995; Schutjens & Spiers, 1999; De Meer & Spiers, 2001). In some single crystal experiments, a regular hole is machined in the crystal to observe free surface dissolution occurring when the crystal is loaded (Sprunt & Nur, 1977; Den Brok & Morel, 2001). The main advantage of single crystal experiments is that one obtains a well-controlled contact area and that the normal stress and displacement across the contact can be calculated or measured. In addition, because the contact is relatively big, it is possible to directly observe the dynamic evolution of the contacts under the optical microscope (Hickman & Evans, 1991, 1992, 1995; Schutjens & Spiers, 1999).

However, single crystal/contact experiments are only feasible for very soluble minerals such as NaCl, KCl and NaNO₃ (Hickman & Evans, 1991; Gratier, 1993; Schutjens & Spiers, 1999). For the less soluble rock forming minerals, the process is so slow that one does not expect to observe any contact dissolution in reasonable times (Rutter, 1976, 1983). In this case, fine-grained polycrystalline aggregates are normally used, and compaction experiments are employed since these amplify the effect of intergranular pressure solution process (Spiers & Schutjens, 1990). Unfortunately, compaction creep experiments performed on wet quartz sand under effective stresses up to several tens of MPa and temperatures up to 400 °C have met with limited success in this respect. In such experiments, limited or ambiguous microstructural evidence for IPS has generally been found (De Boer *et al.*, 1977) and the mechanical data are mostly inconsistent or insufficient to compare with models for IPS as the rate-controlling mechanism (Renton *et al.*, 1969; De Boer *et al.*, 1977; Cox & Paterson, 1991; Schutjens, 1991; Dewers & Hajash, 1995; Rutter & Wanten, 2000). Baker *et al.* (1980) carried out intergranular pressure solution

experiments on deep sea carbonate (i.e. low magnesium calcite), Iceland spar and reagent-grade calcite powder at 25-100 MPa effective pressure and 22-180 °C, for 1 to 10 days. Significant porosity reduction to values as low as 9.9% occurred in 10 days. However, as high stresses and temperatures were used, the contribution from deformation mechanisms other than intergranular pressure solution is unknown. Recent work of Dewers & Muhari (2000) also suggests a mixture of cataclastic deformation and intergranular pressure solution in compaction experiments on Iceland spar. Thus the mechanism and kinetics of intergranular pressure solution in calcite remain poorly understood. Indeed there is little or no proof for its operation under lab conditions.

The aim of this study is to determine if intergranular pressure solution operates in wet granular calcite compacted at low applied stress and at room temperature, placing emphasis on differentiating intergranular pressure solution from other possible deformation mechanisms. As many authors have pointed out before (Raj, 1982; Tada & Siever, 1989), one of the main problems of compaction experiments for intergranular pressure solution is to distinguish the compaction strain rate due to intergranular pressure solution from effects of contact asperity removal, grain re-orientation, intergranular sliding, grain cracking and plastic deformation mechanisms. To minimize such effects in our experiments, all samples were subjected to initial dry loading (pre-compaction) at higher stress (8 MPa) than the test stresses (1-4 MPa). We used very fine-grained calcite powder ($<74\text{ }\mu\text{m}$) in order to favour intergranular pressure solution and investigated effects of Mg^{2+} ions in solution, since Mg^{2+} ions can inhibit precipitation of calcite (Reddy & Wang, 1980; Davis *et al.*, 2000).

2.2 Experimental method

The test materials used in this study were super-pure granular calcite (Merck 99.95% pure) with an average grain size of $15\text{ }\mu\text{m}$ ($5\text{--}30\text{ }\mu\text{m}$), plus high purity calcite single crystals (Iceland spar) crushed and mechanically sieved into grain size fractions of 28-37, 37-45, 45-63, 63-74 μm . Chemical analysis showed that the crystal used contained impurities of magnitude of ppm. The super pure Merck calcite grains have a rhombohedral shape. Pre-saturated solutions were prepared for each experimental run by adding excess test material (same grain size fraction as tested sample) to distilled water and stirring for 48 hours. Pore fluid Mg^{2+} concentration was varied by adding controlled amounts of $\text{MgCl}_2 \cdot 6\text{H}_2\text{O}$ to the solution at the last stage of stirring.

The experiments were performed using the dead-weight compaction set-up, illustrated in Figure 2.1 (see also De Meer & Spiers, 1997). The detailed sample assembly is shown in Figure 2.1b. A glass capillary tube with inner diameter of 2.1 mm, mounted in the brass base is used as a “pressure vessel” in this set up. Two stainless steel pistons are used to load the samples. Paper filters were placed between the sample and pistons to prevent grains penetrating or jamming between the pistons and the glass tube. An acoustic emission receiver was installed in the brass base close to the bottom piston, to detect any grain cracking or brittle deformation. The acoustic emission (AE) transducer was connected via a preamplifier to a band-pass filter with further amplification before discrimination of events using an adjustable-threshold comparator. The total gain was 60dB and the frequency band limited to between 100 kHz and 1 MHz, with a -36dB per octave roll-off characteristic,

above and below the band. The resonant frequency of the transducer, a PZT ceramic filter element, was 1-2 MHz. Individual events triggered a 200 ms monostable pulse stretcher (to eliminate ring-down counts and overlapping events), before accumulation by a digital computer-based counter and logging program. For maximum sensitivity, the trigger level, for event discrimination, was set just above the background electrical noise level. Signal to noise ratios for typical events were around 12 dB, as seen on a digital storage oscilloscope (Gould 840), and triggering by all significant events occurred, provided they were separated more than 200 ms, the time of the monostable pulse stretcher blanking circuit.

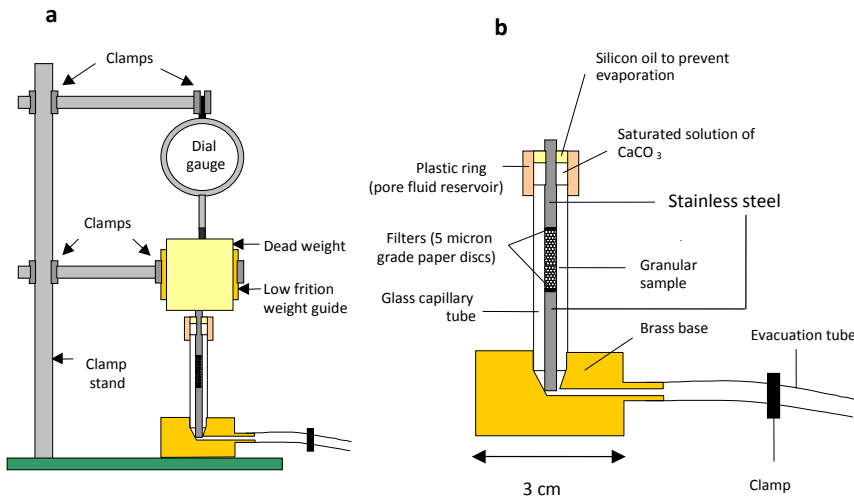


Figure 2.1. Experimental apparatus. (a). Compaction apparatus; (b). Details of the sample assembly.

After loading into the apparatus, 60 mg samples were first pre-compacted for 30 minutes under dry conditions at an applied axial stress (σ_c) of 8 MPa. The aim was to obtain a well-controlled ‘starting aggregate’ with reproducible porosity, and to eliminate intergranular rearrangements during later compaction. The samples were then unloaded and the length (taken as the initial length) of the samples was measured using a travelling microscope. The porosity of the dry loaded samples was calculated from the initial length of the sample, the weight of the sample and the density of calcite (2710 kg/m^3). These values were $50 \pm 1.5\%$. A plastic ring was then placed around the top of the capillary tube to form a reservoir for the fluid, and an evacuation tube was attached to the fluid outlet of the brass-base (see Figure 2.1b). In doing this, all joints were sealed with silicone grease to prevent evaporation.

After dry compaction, wet testing was carried out at applied axial stresses of 1-4 MPa. The required load was first set by adding different weights to the upper piston. The dial gauge was then brought into position (Figure 2.1) and set to zero. Fluid was subsequently added via the fluid reservoir (see Figure 2.1b), and drawn through the sample into the brass base, using the evacuation tube. From the moment the sample was wetted (<30 seconds),

creep of the sample was monitored as a function of time for up to 25 days, by reading the dial gauge. During creep, the system was sealed to reduce evaporation by clamping the evacuation pipe, and by putting a drop of silicone oil on top of the saturated solution in the upper reservoir ring. The wet experiments were all carried out in the “drained” condition, so the applied stress was the effective stress. Note that in addition to the wet experiments performed using saturated CaCO_3 solution, a number of control experiments were also performed both dry and adding decane ($\text{C}_{10}\text{H}_{22}$) instead of saturated solution. Both the saturated solution phase and decane were observed to penetrate the samples rapidly, even without applying a vacuum, thus demonstrating that both fluids wet the calcite powder. In separate tests on cleaved calcite fragments, the wetting angle of decane on calcite was assessed relative to water and found to be significantly lower.

The apparatus (Figure 2.1) and method described allowed strains to be measured with an accuracy of $\sim 10^{-4}$. Runs performed without a sample showed that room temperature variation ($\pm 2^\circ\text{C}$) effects on the dial gauge reading were negligible. This is believed to be because the thermal expansion of the clamp stand counteracted the temperature effects on the dial gauge, dead weight, pistons and brass base (Figure 2.1a). The apparatus enabled us to measure strains with a relative error of 1-5%. Strain rates were calculated as a function of strain and time, using the three-point central difference method. The relative errors in strain rate are estimated to be 1% to 10% at rate values of 10^{-7} to 10^{-9} s^{-1} respectively. Wall friction was measured in a series of experiments whereby the load transmitted through the sample was measured using a balance. This method showed that, in the wet and decane flooded samples, frictional forces were generally less than 10 % of the applied load.

2.3 Results

Thirteen experiments were successfully performed. The pre-compaction stage at an axial stress of 8 MPa under dry conditions resulted in more or less instantaneous or time-independent compaction of the samples by a few percent (2-5%). Acoustic emission events were recorded only at the very beginning of the initial dry loading. No acoustic emissions were picked up in the subsequent wet stage of the experiments. Viewing the difficulties of picking up acoustic emission signals in calcite (Wong, pers. comm.), we draw no further inference from this result. Control experiments in which samples were tested either dry or flooded with decane ($\text{C}_{10}\text{H}_{22}$, similar viscosity to water) showed hardly any creep (Figure 2.2). Wet samples deformed surprisingly rapidly. Representative creep curves obtained for the wet samples are shown for different applied stresses in Figure 2.2a and for different grain sizes in Figure 2.2b. Note that compaction is enhanced by increasing the applied stress and by decreasing grain size. When Mg^{2+} was present in the pore fluid, compaction of the sample was strongly and systematically inhibited depending on Mg^{2+} concentration (Figure 2.3). Since the compaction strains are small, one does not expect to see microstructural evidence of IPS in the wet compacted samples, therefore no microstructural observations were attempted.

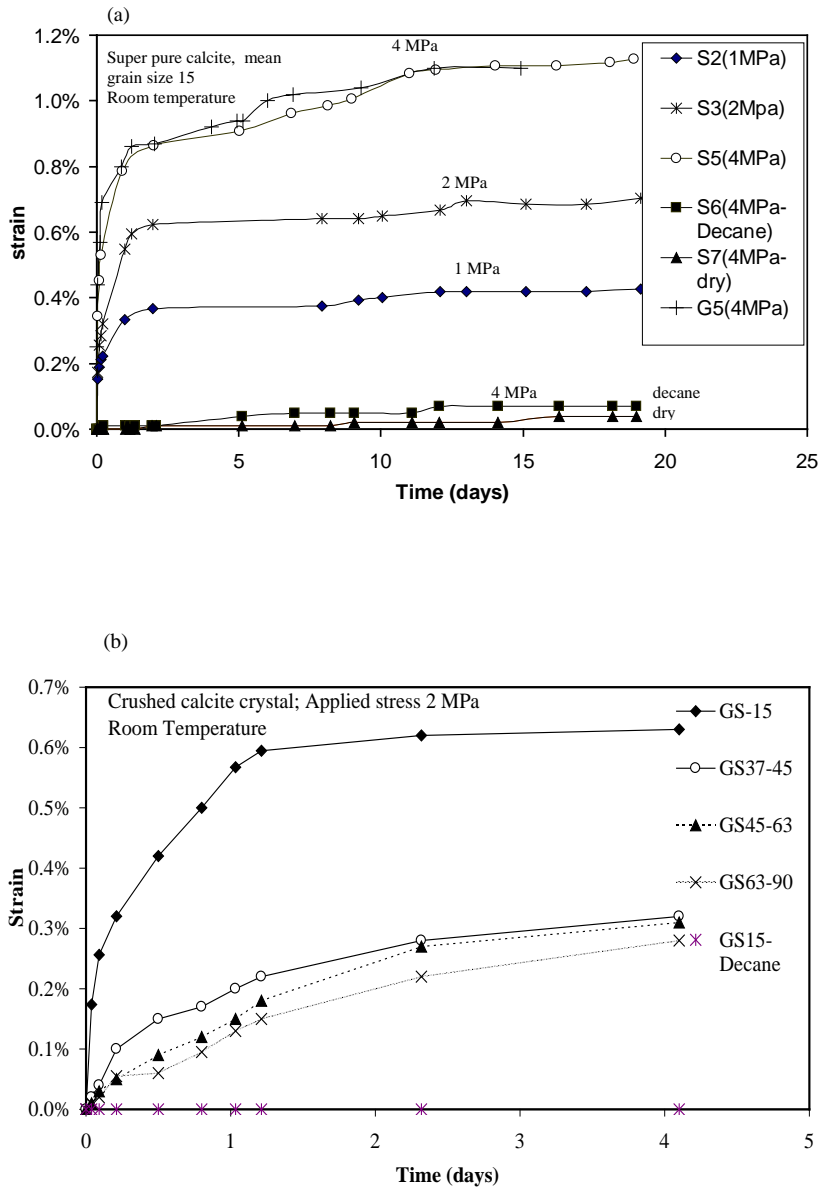


Figure 2.2. Compaction creep curves for (a) different applied stresses and (b) different grain sizes.

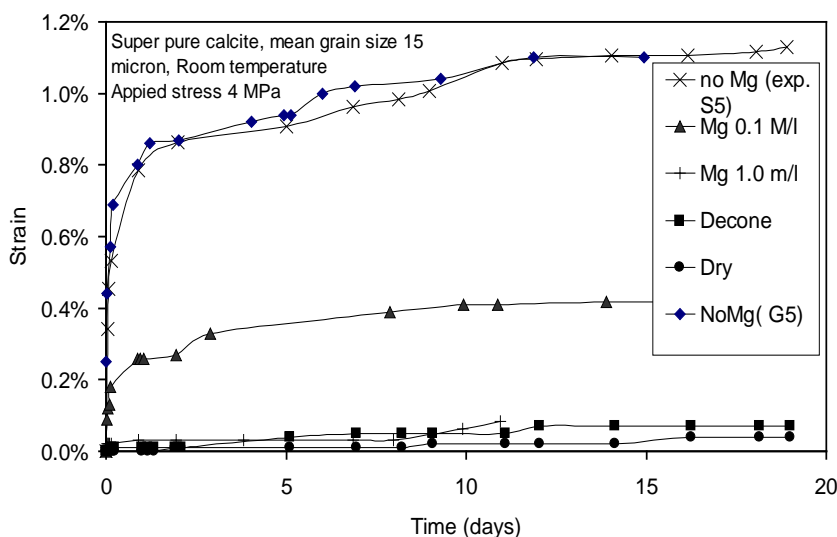


Figure 2.3. Comparison of compaction behavior of dry samples, samples flooded with inert fluid (decane), wet samples (containing saturated solution), and samples filled with solution containing Mg^{2+} .

2.4 Discussion

2.4.1 Deformation mechanisms in dry and decane-flooded samples

Pre-compaction under dry conditions, at an axial stress of 8 MPa, caused a few percent of instantaneous strains. This compaction is presumably mainly due to grain re-orientation, intergranular sliding and grain cracking. Small amounts instantaneous strain are probably also caused by crystal plastic deformation as well as an elastic contribution. When samples were reloaded dry, at lower axial stress (1-4 MPa) (control experiments), almost no instantaneous compaction or compaction creep could be measured. The decane-flooded samples showed similar behavior. We therefore infer that dry pre-compaction produced an aggregate which was "locked" against deformation at lower stress (dry or flooded with decane) and that creep by conventional dislocation mechanisms was negligible in our experiments at stress of 1-4 MPa.

2.4.2 Deformation mechanisms in samples tested wet

Unlike the dry and decane-flooded samples, the samples tested wet under the same experimental conditions, showed significant compaction. The behavior of the decane-flooded samples suggests that the initially dry compacted or "locked" aggregate cannot be "unlocked" merely by reduction of friction or by physical surface (energy) effects at grain

contacts through the addition of a fluid. Because our experimental conditions do not favour solid state plastic deformation (Rutter, 1976) and since no creep occurred in dry compaction, the creep mechanism operating in the wet samples must be a fluid-enhanced deformation mechanism. Given the observed effects of stress and grain size on compaction strain rates, intergranular pressure solution accompanied by intergranular sliding accommodation, is the most obvious candidate. If intergranular pressure solution was indeed the rate controlling deformation mechanism, compaction rate should be influenced by manipulation of any of the serial process of dissolution, diffusion and precipitation, e.g. by adding chemical reaction inhibitors or enhancers to slow down or speed up dissolution or precipitation. From the literature, it is well known that Mg^{2+} ions in concentrations larger than $10^{-3} \text{ mol}\cdot\text{l}^{-1}$ can significantly inhibit calcite precipitation (Reddy, 1977; Mucci & Morse, 1983), while concentrations less than $2\times 10^{-4} \text{ mol}\cdot\text{l}^{-1}$ have no big effects. Our experimental results showed that Mg^{2+} with concentrations of 0.1 and $1 \text{ mol}\cdot\text{l}^{-1}$ in the pore fluid drastically slowed down the compaction of our calcite samples. This finding suggests that deformation of the wet samples must involve processes of precipitation and dissolution, supporting our inference of IPS.

Another fluid-enhanced deformation mechanism which might have operated under our experimental conditions is subcritical cracking by a stress corrosion mechanism (Atkinson, 1982, 1984). Subcritical cracking can potentially cause grain and/or grain contact failure at low stresses, if water is present in the sample, thus producing time-dependent compaction creep. The effect of Mg^{2+} in inhibiting compaction suggests that dissolution and precipitation of calcite are involved, e.g. through intergranular pressure solution. However, if subcritical cracking in calcite is through dissolution of calcite at the crack tips, as suggested by Atkinson (1984), we cannot rule out the possibility that creep deformation in our wet sample is caused by subcritical cracking. On the other hand, the dependence of the compaction strain rate on grain size is expected to be different for subcritical cracking than for intergranular pressure solution. Finer grain size tends to promote intergranular pressure solution (Rutter, 1976; De Meer & Spiers, 1999) whereas it tends to inhibit grain cracking (Zhang *et al.*, 1990; Brzesowsky, 1995). In addition, the strain rate dependence on applied stress for IPS is very different from the stress corrosion crack growth velocity dependence on applied stress (Atkinson & Meredith, 1989). In the following section, we compare the effects of strain, grain size and applied stress on our measured compaction strain rates with theoretical predictions of intergranular pressure solution models.

2.4.3 Comparison of experimental data with intergranular pressure solution theory

Intergranular pressure solution theory (De Meer & Spiers, 1999) predicts that the compaction strain rate of a porous aggregate increases as a function of decreasing grain size and increasing applied effective stress (Raj, 1982; Spiers & Schutjens, 1991). The strain rate is also predicted to decrease with increasing volumetric strain (Spiers and Brzesowsky, 1993). Following De Meer & Spiers (1999), for low stress and small volumetric strains (up to 15-20%), the general forms of the theoretical IPS creep equations for hydrostatic or uniaxial compaction of a simple cubic grain pack of spherical grains are:

Parameters/function	Expression/ values	Sources
K_s	$R_s = k_s(1 - Q_s)$ $k_s = k_s^0 \exp(-Q_s/RT)$ $Q_s = 33 \text{ kJ/mol}$	Reddy & Wang, 1980 Inskeep and Bloom, 1985 Busenberg & Plummer 1986
K_d	$D = 1 \times 10^{-10} \text{ at } T = 25^\circ \text{C}$ $D = D_0 \exp(-Q_d/RT)$ $Q_s = 15 \text{ kJ/mol}$	Nakashima, 1995
K_p	$R_p = k_p(Q_p - 1)$ $k_p = k_p^0 \exp(-Q_p/RT)$ $k_p = 1.61 \times 10^{-11} \text{ m} \cdot \text{s}^{-1} \text{ at } T = 25^\circ \text{C}$ $Q_s = 46 \text{ kJ/mol}$	Reddy & Wang, 1980 Inskeep and Bloom, 1985
Solubility production ($\text{mol}^2 \text{l}^{-2}$)	$10^{-8.4}$	Reddy & Wang 1980
$\Omega \text{ (m}^3 \text{mol}^{-1}\text{)}$	3.6934×10^{-5}	
$R \text{ (Jmol}^{-1} \text{K}^{-1}\text{)}$	8.314	
$T \text{ (K)}$	294	

Table 2.1 Parameter values used in the theoretical model of IPS for calcite.

$$\dot{\varepsilon} = AK_s \frac{\sigma_e^n}{d} f_s(e_v) \quad \text{dissolution control} \quad (2.1)$$

$$\dot{\varepsilon} = BK_d \frac{\sigma_e}{d^3} f_d(e_v) \quad \text{diffusion control} \quad (2.2)$$

$$\dot{\varepsilon} = CK_p \frac{\sigma_e^m}{d} f_p(e_v) \quad \text{precipitation control} \quad (2.3)$$

Here $\dot{\varepsilon}$ represents volumetric strain rate (defined as $\dot{\varepsilon} = -\dot{v}/v$, with v being instantaneous volume), A , B , and C are constants related to the packing of the granular aggregate, K_s and K_p incorporate temperature-dependent dissolution and precipitation rate coefficients, K_d is a temperature-dependent term incorporating the product of grain boundary diffusivity, solid solubility and average grain boundary fluid thickness, σ_e is the applied effective stress, d is the grain size, and e_v is the volumetric compaction strain (Spiers & Schutjens, 1990; De Meer & Spiers, 1999). The exponents n and m respectively represent the order of the dissolution or precipitation velocity vs. driving force relation.

Figure 2.4 shows a log-log plot of strain rate vs. strain, constructed for the experimental data of Figure 2.2a. The measured strain rates decrease first steadily and then rapidly with increasing strain. Note that the experimental strain rates decrease with strain very rapidly.

The theoretical models of intergranular pressure solution (equations (2.1)-(2.3)) predict that strain rate is inversely proportional to grain size for interfacial reaction controlled IPS, compared with an inverse cubic relation for diffusion controlled IPS. Turning to our experimental results, Figure 2.5 shows a log-log plot of strain rate against grain size for fixed volumetric strains. This was constructed using the rate data obtained from the 2 MPa experiments on the crushed calcite crystal material with different grain sizes (Figure 2.2b). The slopes of the data set fall in the range of 1-3, with 1-2 for coarse grains and 2-3 for finer grains. It is therefore not clear which intergranular pressure solution mechanism might control the compaction rate from the grain size dependence alone. However, it is clear that compaction is faster in the finer grained samples. This is important because it is consistent with IPS but makes it unlikely that creep is caused by grain cracking. In the latter case, strain rate is expected to increase with increasing grain size (Zhang *et al.* 1990; Brzesowsky 1995).

In a log-log plot of strain rate against stress, theory predicts that diffusion controlled intergranular pressure solution will show a slope of $n=1$ and that interfacial reaction controlled intergranular pressure solution will show a n -value which depends on the kinetics of reaction. From the crystal growth literature, the precipitation rate of calcite is quadratically dependent on the degree of super-saturation or driving force (Reddy 1977; Reddy & Wang 1980, see Table 2.1). Figure 2.6 shows a comparison of our experimental data from Figure 2.2a versus the theoretical dependence of strain rate on stress. The slope of our experimental data is about 2, which is roughly consistent with the theoretical prediction for reaction or diffusion controlled IPS. The stress sensitivity itself cannot be used for distinguish the rate limiting mechanisms of IPS also. However, the stress corrosion crack growth velocity depends on stress in a highly non-linear way, with a power law stress exponent larger than 10 (Atkinson 1984; Atkinson & Meredith 1989).

On the basis of the above, we infer that compaction in our wet experiments probably did occur by IPS (accompanied by inter-grain sliding) and that precipitation was most likely rate controlling. The poor agreement between our experimental results and our precipitation controlled IPS model, regarding the dependence of strain rate on strain (Figure 2.4), could be due to the fact that the model assumes a spherical grain shape whereas our calcite powders consisted of rough grains. An additional reason for discrepancies between theory and the experimental results could lie in the assumption of the model that IPS involves a series of strain-dependent steady state with no transient effects (e.g. transients associated with changes in pore fluid composition). For added confidence, our inference that precipitation controlled IPS is probably the controlling mechanism in the present experiments should be tested in future by carrying out flow through experiments following the approach of De Meer & Spiers (1997).

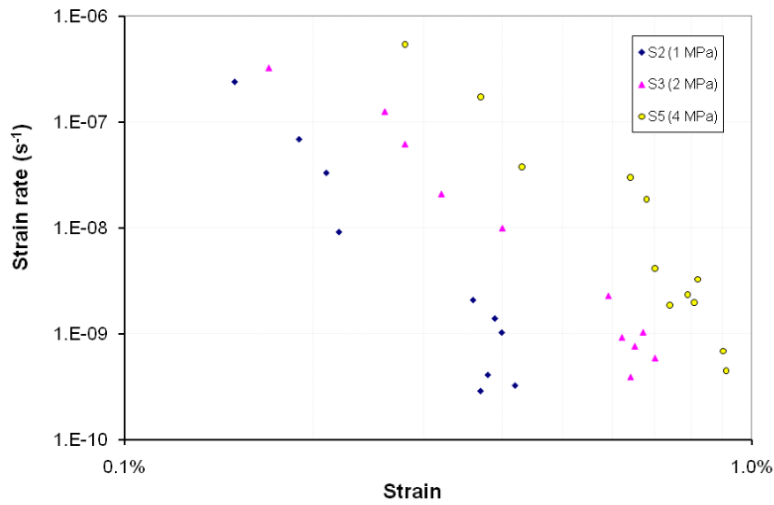


Figure 2.4. Plots of strain rate versus strain for samples indicated in Figure 2.2a.

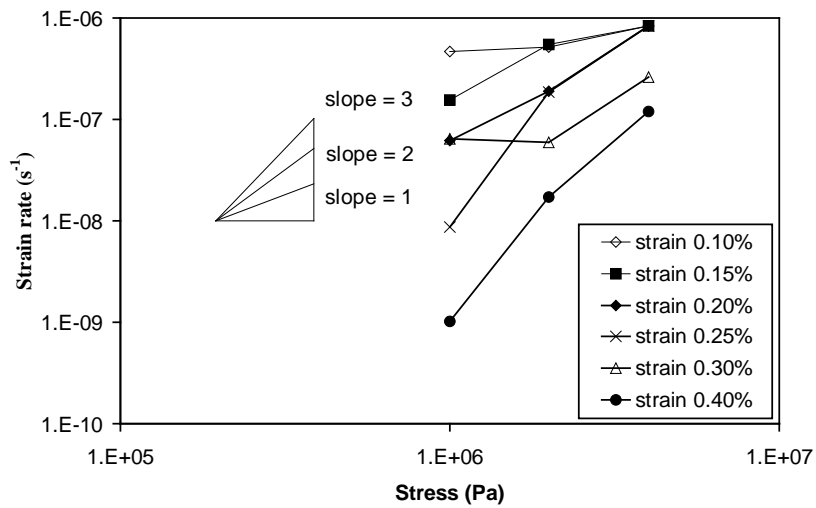


Figure 2.5. Log-log plot of strain rate vs. stress for data of in Figure 2.2a.

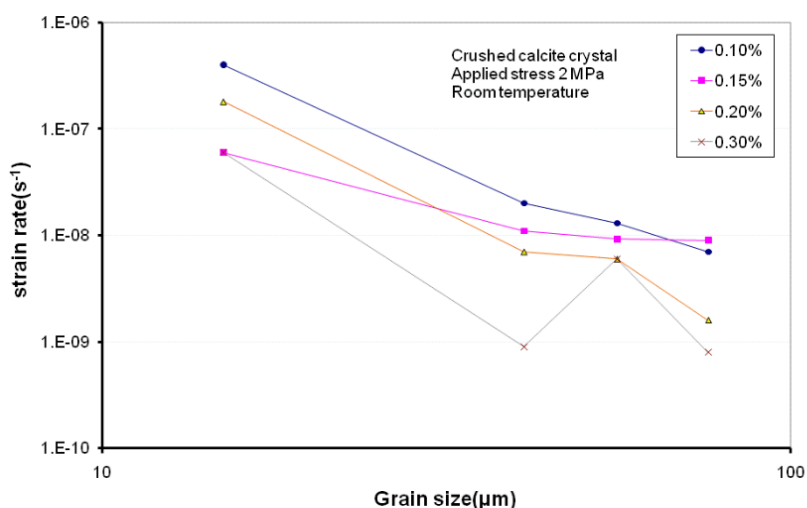


Figure 2.6. Strain rate dependence on grain size.

The fact that we seem to have obtained intergranular pressure solution in the lab suggests that the same process should operate under comparable conditions in nature, for example during carbonate diagenesis and fault sealing under shallow, low temperature conditions. Since Mg^{2+} is always present in significant concentration in carbonate pore waters (Collins 1975), the effects of Mg^{2+} which we have observed may be very important in controlling the rate of intergranular pressure solution in natural situations. However, until we can confirm and better qualify the rate controlling process (notably the effect of porosity), we make no attempt to estimate rates of intergranular pressure solution in calcite rocks in nature.

2.5 Conclusions

We have carried out 1-D, dead-weight compaction creep experiments on calcite powder at room temperature. After pre-compaction at a stress of 8 MPa, the samples showed no further compaction when reloaded dry, or flooded with inert fluid (decane) at lower stresses (1-4 MPa). This suggests that grain re-orientation, intergranular sliding and coupled plastic deformation do not proceed under dry conditions or in the presence of an inert fluid, after pre-compaction. However, samples tested with calcite saturated solution showed significant time-dependent compaction creep. The compaction rate decreased rapidly with increasing volumetric strain. It increased with the applied stress squared and was inversely related to grain size to the power of 1 to 3. The behaviour of the wet versus the dry and decane-flooded samples demonstrated that wet deformation was certainly a fluid-enhanced process. Adding Mg^{2+} into the saturated solution drastically slowed down the creep of compaction. This effect of Mg^{2+} ions, a well-known inhibitor of calcite precipitation, suggests that

deformation of the wet samples involved some kind of dissolution/precipitation process. The two candidate deformation mechanisms are intergranular pressure solution and stress corrosion cracking. The observed grain size, and stress dependence contradicts expectations for creep via stress corrosion cracking. However, the mechanical behaviour of the wet samples, that is the dependence of strain rate on applied stress and grain size, is broadly consistent with intergranular pressure solution model. We infer that intergranular pressure solution was probably the main deformation in our wet experiments. However, further experimental work is needed to quantitatively characterize the process.

2.6 References

- Atkinson, B. K. (1982), Subcritical crack propagation in rocks: theory, experimental results and application. *J. Struct. Geol.* 4, 41-56.
- Atkinson, B. K. (1984), Subcritical crack growth in geological materials. *J. Geophys. Res.* 89, 4077-4114.
- Atkinson, B. K. & P. G. Meredith (1989), The theory of subcritical crack growth with applications to minerals and rocks. In: Atkinson B. K. (eds) *Fracture Mechanics of Rock*. Academic Press London, 111-166.
- Baker, P. A., M. Kastner, J. D. Byerlee and D. A. Lockner (1980), Intergranular pressure solution and hydrothermal recrystallization of carbonate sediments- an experimental study. *Marine Geology* 38, 185-203.
- Bathurst, R. G. C. 1958. Diagenetic fabrics in some British Dinantian limestones. *Liverpool and Manchester Geology* 2, 1-36.
- Brzesowsky, R. H. (1995), Micromechanics of sand grain failure and sand compaction. PhD dissertation, Utrecht University, Netherlands, *Geologica Ultraiectina*, 133.
- Burger, H. R. (1975), "Pressure solution" or indentation?: Comment and reply. *Geology* 3, 292-293.
- Busenberg, E., and L. N. Plummer (1986), A comparative study of dissolution and crystal growth kinetics of calcite and aragonite. *U.S Geol. Surv. Bull.* 1578. 139-168.
- Carozzi, A. V. & D. Von Bergen (1987), Stylolitic porosity in carbonate: a critical factor for deep hydrocarbon production. *Journal of Petroleum Geology* 10, 267-282.
- Collins, A. G. (1975), Geochemistry of oilfield water, *Development in Petroleum Sciences* I, Elsevier Science, 142-143.
- Cox, M. A. & S. J. L. Withford (1987), Stylolites in the Caballos Novaculite, west Texas. *Geology* 15, 439-442.
- Cox, S. F. & M. S. Paterson (1991), Experimental dissolution-precipitation creep in quartz aggregate at high temperature. *Geophys. Res. Lett.* 18, 1401-1404.
- Davis, K. J., P. M. Dove & J. J. De Yoreo (2000), The role of Mg^{2+} as an impurity in calcite growth. *Science* 290, 1134-1137.
- De Boer, R. B., P. J. C. Nagtegaal & E. M. Duyvis (1977), Intergranular pressure solution experiments on quartz sand. *Geochimica et Cosmochimica Acta*, 41, 257-264.
- De Meer, S. & C. J. Spiers (1997), Uniaxial compaction creep of wet gypsum aggregates. *J. Geophys. Res.* 102, 875-891.

- De Meer, S. & C. J. Spiers (1999), On mechanisms and kinetics of creep by intergranular pressure solution. In: Jamtveit, B. & Meakin, P. (eds) *Growth Dissolution and Pattern Formation Geo-systems*. Kluwer Academic Publishers. Dordrecht, The Netherlands, 345-366.
- De Meer, S. & C. J. Spiers (2001), Diffusive properties of wetted grain contacts undergoing active intergranular pressure solution, *Abstract of Deformation Mechanisms, Rheology & Tectonics*, Noordwijkerhout, The Netherlands, April 2-4, 2001, p113.
- Den Brok, S. W. J. & J. Morel (2001), The effects of elastic strain on the microstructure of free surface of stressed minerals in contact with an aqueous solution. *Geophys. Res. Lett.* 28, 603-606.
- Dewers, T. & A. Hajash (1995), Rate law for water-assisted compaction and stress-induced water-rock interaction in sandstones, *J. Geophys. Res.* 100, 13,093-13,112.
- Dewers, T. & S. Muhari (2000), Transition from plastic to viscous flow in aggregate granular creep, *Abstract of EOS Trans.* AGU, 81
- Durney, D. W. (1972), Solution transfer, an important geological deformation mechanism. *Nature* 235, 315-317.
- Elliot, D. (1973), Diffusion flow laws in metamorphic rocks. *Bulletin Geol. Soc. Am.* 84, 2645-2664.
- Gratier, J. P. (1993), Experimental intergranular pressure solution of halite by an indenter technique. *Geophys. Res. Lett.* 20, 1647-1650.
- Heald, M. T. (1956), Cementation of Simpton and St. Peter sandstones in parts of Oklahoma, Arkansas, and Missouri. *J. of Geol.* 64, 16-30.
- Heydari, F. (2000), Porosity loss, fluid flow, and mass transfer in limestone reservoirs: Application to the upper Jurassic Smackover formation, Mississippi. *AAPG Bulletin*, 84, 100-118.
- Hickman, S.H. & B. Evans (1991), Experimental pressure solution in halite: the effect of grain/interphase boundary structure. *J. Geol. Soc. Lond.* 148, 549-560.
- Hickman, S. H. & B. Evans (1992), Growth of the grain contacts in halite by solution-transfer: implication for diagenesis, lithification and strength recovery. In: Evans, B. & Wong, T. F. (eds), *Fault Mechanics and Transport Properties of Rocks*. Academic press, San Diego, USA, 253-280.
- Hickman, S. H. & B. Evans (1995), Kinetics of intergranular pressure solution at halite-silica interfaces and intergranular clay films. *J. Geophys. Res.* 100, 13,113-13,132.
- Houseknecht, D. W. (1987), Assessing the relative importance of compaction processes and cementation to reduction of porosity in sandstones. *AAPG Bulletin* 71, 633-642.
- Houseknecht, D. W. (1988), Intergranular pressure solution in four quartzose sandstones. *J. Sediment. Petrol.* 58, 228-246.
- Inskeep, W. P., and P. R. Bloom (1985), An evaluation of rate equations for calcite precipitation kinetics at $p\text{CO}_2$ less than 0.01 atm and pH greater than 8, *Geochim. Cosmochim. Acta*, 9, 2165-2180
- Lehner, F.K. (1990), Thermodynamics of rock deformation by intergranular pressure solution. In: Barber, D.J. & Meredith, P.G. (eds) *Deformation Processes in Minerals, Ceramics and Rocks*. Unwin Hyman, London, 296-333.
- Lehner, F.K. (1995), A model for intergranular pressure solution in open systems. *Tectonophysics* 245, 153-170.

- Mucci, F. & J. W. Morse (1983), The incorporation of Mg^{2+} and Sr^{2+} into calcite overgrowths: influence of growth rate and solution composition. *Geochimica et Cosmochimica Acta* 47, 217-233.
- Raj, R. (1982), Creep in polycrystalline aggregates by matter transport through a liquid phase. *J. Geophys. Res.* 87, 4731-4739.
- Reddy, M. M. (1977), Crystallization of calcium carbonate in the presence of trace concentrations of phosphorous-containing anions, *J. Cryst. Growth* 41, 287-295.
- Reddy, M.M. & K. K. Wang (1980), Crystallization of calcium carbonate in the presence of metal ions. I. Inhibition of magnesium ion at pH 8.8 and 25 °C. *J. Cryst. Growth*, 50, 470-480.
- Renton, J. J., M. T. Heald & C. B. Cecil (1969), Experimental investigation of pressure solution of quartz. *J. Sediment. Petrol.* 39, 1107-1117.
- Robin, P. F. (1978), Intergranular pressure solution at grain-to grain contacts. *Geochimica et Cosmochimica Acta* 42, 1383-1389.
- Rutter, E. H. (1976), The kinetics of rock deformation by intergranular pressure solution. *Philos. Trans. R. Soc. Lond.* A282, 257-291.
- Rutter, E. H. (1983), Intergranular pressure solution in nature, theory and experiment. *J. Geol. Soc. Lond.* 140, 725-740.
- Rutter, E. H. & P. H. Wanten (2000), Experimental study of the compaction of phyllosilicate-bearing sand at elevated temperature and with controlled pore water pressure. *J. Sediment. Res.* 70, 107-116.
- Schutjens, P. M. T. M. (1991), Experimental compaction of quartz sands at low effective stress and temperature conditions. *J. Geol. Soc. Lond.* 148, 527-539.
- Schutjens, P. M. T. M. & C. J. Spiers (1999), Intergranular pressure solution in NaCl: grain-to-grain contact experiments under the optical microscope. *Oil Gas Sci. Technol.* 54, 729-750.
- Sorby, H. C. (1863), On the direct correlation of mechanical and chemical forces. *Proceedings of the Royal Society, London*, 12, 583-600.
- Spiers, C. J. & R. H. Brzesowsky (1993), Densification of wet granular salt: Theory versus experiment. In: Kakihana, H., Hardy, H. R. Jr., Hoshi, T. & Toyokura, K. (eds), *Seventh Symposium on Salt*. Vol I. Elsevier, Amsterdam, 83-92.
- Spiers, C. J. & P. M. T. M. Schutjens (1990), Densification of crystalline aggregates by fluid-phase diffusional creep. In: Barber, D. J. & Meredith, P.G. (eds) *Deformation Processes in Minerals, Ceramics and Rocks*. Unwin Hyman, London, 334-353.
- Sprunt, E. S. & A. Nur (1977), Experimental study of the effects of stress on solution rate. *J. Geophys. Res.* 82, 3013-3022.
- Tada, T. & R. Siever (1986), Experimental knife-edge intergranular pressure solution of halite. *Geochimica et Cosmochimica Acta* 50, 29-36.
- Tada, R. & R. Siever (1989), Intergranular pressure solution during diagenesis. *Annual Review of Earth and Planet Sciences* 17, 89-118.
- Weyl, P. K. (1959). Intergranular pressure solution and force of crystallization - a phenomenological theory. *J. Geophys. Res.* 64, 2001-2025.
- Wiechers, H. N. S., P. Sturrock & G. V. R. Marais (1975), Calcium carbonate crystallization kinetics. *Water Research* 9, 835-845.

Zhang, J., T. F. Wong & D. M. Davis (1990), Micromechanics of pressure-induced grain crushing in porous rocks. *J. Geophys. Res.* 95, 341-352.

3. Compaction of granular calcite by pressure solution at room temperature and effects of pore fluid chemistry

This chapter was published as: Zhang, X and C.J. Spiers (2005), Compaction of granular calcite by pressure solution at room temperature and effects of pore fluid chemistry, International Journal of Rock Mechanics and Mining Sciences, 42, 950-960.

Abstract

Pressure solution is an efficient compaction mechanism leading to porosity/permeability reduction in both clastic and carbonate rocks. We performed compaction experiments on crushed limestone and granular calcite at room temperature and 1-4 MPa effective stress using various pore fluids. By applying a dry pre-compaction at 8 MPa, we could largely eliminate deformation mechanisms such as grain rearrangement, sliding and fracturing from runs employing a pore fluid. Compaction creep occurred only in samples filled with a saturated carbonate solution, in contrast to those filled with chemically inert fluids, at $\dot{\epsilon} = 10^{-6} \sim 10^{-9} \text{ s}^{-1}$. The measured strain rates increased with decreasing grain size and with increasing effective stress according to power laws with exponents of about 3 and 1-2 respectively. Samples made from naturally oil-contaminated limestone showed far less compaction than oil-free samples. Addition of dissolution and precipitation inhibitors (magnesium and phosphate ions) to the pore fluid significantly decreased compaction rates of wet samples, indicating that creep must have involved calcite dissolution/precipitation. Pore fluid with a salinity (NaCl) of 0.1-0.5 mole/l increased the compaction strain rate compared to non-saline solutions. The experimental results suggest the main deformation mechanism in calcite under our experimental conditions was pressure solution and that diffusion is likely to be the rate controlling process in pure solution system. They imply that compaction and porosity/permeability evolution in natural carbonate rocks depend strongly on pore fluid chemistry, as well as mechanical conditions.

3.1 Introduction

The compaction behaviour of sediments and sedimentary rocks plays a determining role in controlling processes such as diagenetic densification, porosity/permeability evolution in sedimentary basins over geological time and the response of reservoir formation to hydrocarbon production. The principal deformation mechanism responsible for compaction in sedimentary materials are intergranular/particulate sliding, grain fracture, grain plasticity and intergranular dissolution-precipitation process or pressure solution (Evans et al., 1999). In the absence of other mechanisms, intergranular sliding is unable to produce large compaction strains, as it will soon lead to the development of a locked aggregate. Further deformation requires the grain themselves to deform (Fischmeister et al., 1982). Under upper crustal conditions, compaction by mechanism such as fracture or plasticity of clay rich particles is expected to depend largely on stress and to be relatively independent of

time (Evans et al., 1999; Fischmeister et al., 1982). By contrast, dissolution-precipitation processes are expected to produce time dependent compaction creep and it is therefore these mechanisms that are of more interest when considering compaction of sediments and sedimentary and fault rocks over geological time periods. The role of mechanism played by pressure solution in the compaction of sedimentary rocks is evident by widespread microstructures reported in the literatures. These include sutured grain contacts, grain truncation, indentation, overgrowth and stylolite et al. (Bathurst, 1958; Tada and Siever, 1989; Spiers and Schutjens, 1990; Railsback, 2002). Such processes may also be important mechanisms of compaction creep in clastic and carbonate reservoir after hydrocarbon production, if in-situ temperatures are high enough.

Despite the perceived importance of pressure solution mechanism, they remain poorly understood, at least from the kinetic viewpoint. It is well established that pressure solution is a water-assisted physico-chemical process driven by effective stress induced chemical potential and achieved through a three step process of dissolution of solid minerals at grain contacts, diffusion of solutes along the grain boundaries and precipitation at free pore walls in a chemically closed system (Lehner, 1990; Rutter, 1983; Renard et al., 1997; Paterson, 1995). The slowest of the three serial processes controls the overall deformation. The structure of the interface between two grains is crucial because it is a medium of dissolution and diffusion of minerals. Two models of grain contact structures have been proposed, namely thin film and “island & channel” model (Figure 3.1). In the thin film model, the grain contacts are assumed to consist of a thin water film trapped inside contacts and cannot be squeezed out by applied stress (Rutter, 1983). The “island & channel” model assumes that the interface possess a dynamically roughening contacts of islands and channels penetrated by water (Spiers and Schutjens, 1990; Lehner, 1990). In both models, water in between the grain contacts is important to dissolve solid minerals and to transport material out of the contact areas. In natural conditions, pressure solution may only occur where water is present and inhibited where dry or other fluids such as hydrocarbons filled. The specific rate controlling processes are not well known and are not quantified, principally because their slow nature makes them hard to study in the lab.

From microstructural/petrographic studies it is clear that pressure solution is particularly important in carbonate reservoirs, forming a major mechanism of diagenesis, compaction, deformation and stylolite formation. Some weak experimental evidence of pressure solution in carbonate rocks has been reported recently (Hellmann et al., 2002; Zhang et al., 2002). Nonetheless, it has not been successfully isolated and quantified via lab experiments, and likely effects of pore fluid chemistry and of hydrocarbons on the progress of the process have received little or no attention. For progress in modelling the time dependent compaction of carbonate, porosity-permeability reduction, and the creep response of carbonate reservoir to hydrocarbon production, better data are essential.

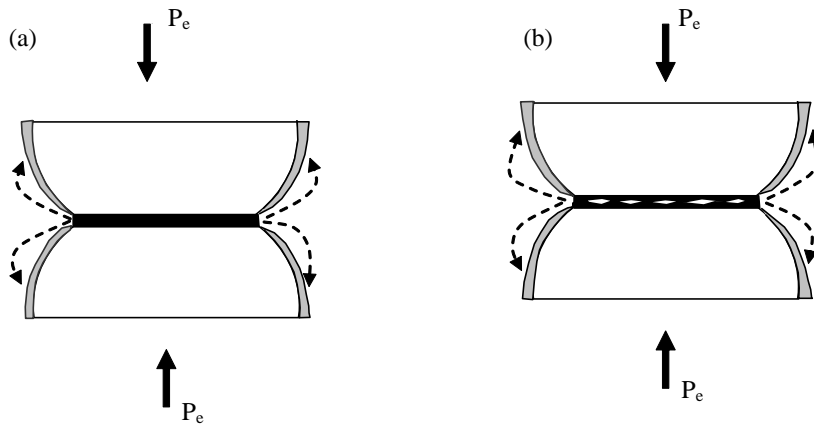


Figure 3.1. Models of intergranular pressure solution. Materials are dissolved at stressed grain contacts and transported via grain boundary with structure of (a) thin film of water or (b) dynamic “island & channel”. Precipitation occurs at the free pore walls. As a result, intergranular pressure solution leads to compaction of bulk rock and decrease of porosity and permeability.

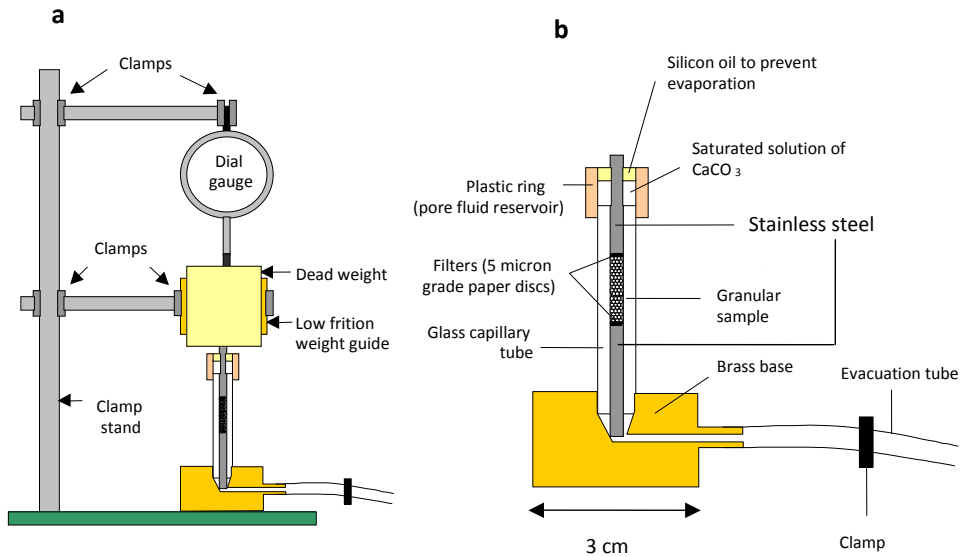


Figure 3.2. Micro-odometer used in present experiments. a) Apparatus and loading frame; b) details of compaction cell and sample assembly.

In this study, we investigate experimentally the compaction behaviour of granular calcite under condition favouring pressure solution while specifically minimizing the effects of other mechanisms. We systematically investigate the effects of grain size (and distribution) and stress on compaction behaviour and compare our results with theoretical models for pressure solution. In addition, we test the effects of fluid compositions such as magnesium, phosphate ions and salinity (NaCl). The experiments were carried out, using the small-scale compaction apparatus, on the crushed limestone and super pure calcite samples filled with various pore fluids. Our experimental results show that the compaction strain rates in calcite are sensitive to grain size (distribution) and applied stress. The dissolved ions of magnesium and phosphate, as well as the hydrocarbons in the pore fluid slow down the compaction rates. However, salinity is found to promote the compaction at range 0.1-0.5 mole/l.

3.2 Experiments

3.2.1 Starting material

Two kinds of material were used for the experiments, namely high purity CaCO_3 (Suprapur, Merck 99.95%) and crushed limestone obtained from a producing oilfield. The pure calcite had an average grain size of about 15 μm and a range of 2-45 μm . XRF analysis of oil-free samples of the limestone showed that it consisted of weight 96% calcite with impurities of SiO_2 , Al_2O_3 , MgO , MnO and P_2O_5 . Naturally oil-contaminated, but otherwise identical limestone was used in some experiments for comparison. The limestones were crushed and either mechanically sieved into grain size fractions of 22 ± 10 , 37 ± 8 , 41 ± 4 , 54 ± 9 , 76 ± 13 and 82 ± 8 μm or gravity separated into fractions of 3 ± 3 and 5 ± 4 μm . Grain size analysis of crushed limestone and pure calcite using a Malvern particle sizer and microscope checking showed that their individual fractions had a near normal distribution.

Carbonate saturated pore fluids were made by adding excess test material to deionized water and stirring for 48-96 hours. Previous work has shown that chemical equilibrium between the solid and solution is reached within the time interval (Svensson and Dreybrodt, 1992; Eisenlohr et al., 1999). Pore fluid salinity (NaCl), as well as magnesium and phosphate ion concentrations were varied by adding NaCl, $\text{MgCl}_2\cdot 6\text{H}_2\text{O}$, or Na_2HPO_4 in appropriate amounts at the end of solution preparation. A range of hydrocarbons, namely hexane (C_6H_{14}), decane ($\text{C}_{10}\text{H}_{22}$), cyclohexane (C_6H_{12}) and toluene (C_7H_8), as well as silicone oil and alcohol, was also used as pore fluids, for comparison and control experiments.

3.2.2 Experimental apparatus and procedures

The experiments were performed using the small-scale 1-D compaction cell or micro-oedometer shown in Figure 3.2 (DeMeer and Spiers, 1997; Zhang et al., 2002). This allows compaction experiments to be performed on small samples of fine-grained material, which is difficult to provide in large quantities. This has been extensively used in recent studies of

pressure solution (DenBrok et al., 1999; DeMeer and Spiers, 1997, 1999; Zhang et al., 2002). Each experiment was set up as follows. The glass capillary tube, with diameter of 2.1 mm, was first inserted into the brass base and the lower piston and paper filter were lowered into it. About 0.05-0.06 grams of pre-weighed granular sample material were then funnelled into the tube on top of the paper filter disc. A second paper filter disc and the upper piston were then inserted onto the sample. The assembly was then placed on the test frame and dead-weight loaded (Figure 3.2a).

All samples were first pre-compacted dry for 30 minutes at an applied stress of 8 MPa. Dry pre-compaction was performed to obtain an approximately constant initial porosity and a reproducible 'locked state' in the aggregate, prior to "wet" testing. Control experiments at 1-8 MPa showed that dry pre-compaction for 30 minutes at 8 MPa was needed to achieve a reproducible locked state, independently of sample material and grain size. After dry pre-compaction, the sample was unloaded, and its length was measured using a travelling microscope (accuracy 0.01mm). This is referred to as the initial length (l_0). The corresponding initial porosity (ϕ_0) was calculated using this initial length measurement. A plastic ring was then placed around the top of the capillary tube to form a reservoir for the pore fluid, and an evacuation tube was attached to the fluid outlet of the brass-base (see Figure 3.2). In both cases, the joints were sealed with silicone grease to prevent evaporation.

The main body of fluid-added experiments was carried out at applied stresses of 1-4 MPa. These were performed by adding different dead-weights to the upper piston after dry pre-compaction and initial length measurement. In each experiment, the dial gauge was then placed on top of the chosen dead weight, and set to zero. The chosen pore fluid was subsequently added to the fluid reservoir (see Figure 3.2b), and then drawn through the sample using the evacuation tube. From the moment that the sample was completely wetted, vertical compaction was monitored, as a function of time for a period up to 3-20 days, by reading the dial gauge (see Figure 3.2a). The system was sealed against evaporation by clamping the evacuation pipe, and by adding a droplet of silicone oil to the top of the pore fluid reservoir.

The apparatus (Figure 3.2) and method described allowed strains to be measured with an accuracy of $\sim 10^{-4}$. Strain rates were calculated as a function of strain and time, using the three-point central difference method. The relative errors in strain rate thus obtained are estimated to be 1% to 10%, at rate values of 10^{-7} to 10^{-9} s^{-1} respectively. Wall friction was measured in a series of experiments whereby the load transmitted through the sample was measured using a balance. These showed that, in fluid-flooded samples, frictional forces were low and typically $< 5\%$ of the applied axial force.

Exp. ID	Dry Pre-compaction stress /duration	Fluid	Initial porosity (ϕ_0)	Grain size (μm)	Applied stress wet/duration	Final strain (%)
S1	2 MPa/15 min	silicone oil	45.2	0-28	2 MPa/2 days	6.0
S2	4 MPa/20 min	silicone oil	43.1	0-28	2 MPa/6 days	0.3
S3	3 MPa/20 min	silicone oil	44.4	0-28	2 MPa/12 days	4.3
S4	2 MPa/20 min	silicone oil	44.9	0-28	3 MPa/11 days	5.3
S5	8 MPa/30 min	silicone oil	38.5	0-28	2 MPa/3 days	0.0
S6	8 MPa/30 min	silicone oil	38.9	0-28	4 MPa/6 days	0.1
A1	4 MPa/15 min	alcohol	42.1	0-28	2 MPa/5 days	0.4
A2	4 MPa/15 min	alcohol	41.6	0-28	2 MPa/4 days	3.5
A3	3 MPa/15 min	alcohol	42.5	0-28	4 MPa/11 days	5.1
A4	4.6 MPa/24 hrs	alcohol	40.8	0-28	2 MPa/2 days	0.1
A5	8 MPa/30 min	alcohol	38.9	0-28	2 MPa/3 days	0.0
A6	8 MPa/30 min	alcohol	39.8	16-28	4 MPa/6 days	0.0
D1	4 MPa/20 min	n-Decan	44.3	0-28	2 MPa/4 days	2.3
D2	4 MPa/20 min	n-Decan	42.2	0-28	2 MPa/11 days	0.2
D3	3 MPa/20 min	n-Decan	41.7	0-28	3 MPa/4 days	4.7
D4	2 MPa/15 min	n-Decan	47.2	0-28	2 MPa/13 days	4.1
D5	8 MPa/30min	n-Decan	46.7	37-45	2 MPa/10 days	0.0
D6	8 MPa/30min	n-Decan	38.3	0-28	2 MPa/7 days	0.0
D7	8 MPa/30 min	n-Decan	38.8	28-37	4 MPa/6 days	0.0
d-1	4 MPa/30 min	dry	43.6	0-28	4 MPa/5 days	0.0
d-2	8 MPa/30 min	dry	39.2	0-28	4 MPa/5 days	0.0

Table 3.1. List of control experiments. A dry pre-compaction at 8 MPa for 30 minutes

3.3 Mechanical results

3.3.1 Dry compaction and control experiments

In this study, dry pre-compaction experiments were performed on sample materials to determine the stresses and times needed to produce a reproducible locked state (porosity) prior to wet testing. Dry pre-compaction at stresses of 4-8 MPa and room temperature resulted in instantaneous compaction of a few percent strains. Control experiments were performed on samples either dry or filled with chemical inert fluid at lower stresses. Table 3.1 lists the results of control experiments performed on crushed limestone. It is clear from Table 3.1, that dry pre-compaction at a stress of 8 MPa for 30 minutes is needed to avoid time-independent compaction in samples subsequently loaded at lower stresses (1-4 MPa), either dry or filled with chemically inactive fluids (silicone oil, alcohol, decane, other hydrocarbons). No time-dependent compaction (compaction creep) was observed in any of

the control samples tested dry or with chemically inactive/inert pore fluid when a pre-compaction applied at 8 MPa. Similar results were obtained for the pure samples filled with various hydrocarbons as shown in Figure 3.3.

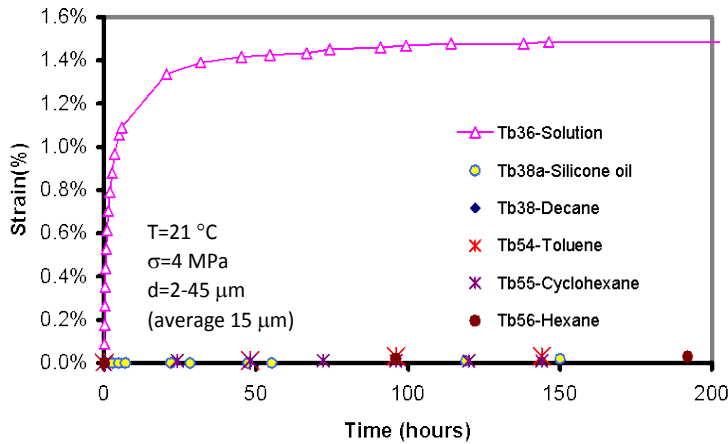


Figure 3.3. Effect of different hydrocarbon pore fluids on compaction of super pure calcite samples. Grain size 2-45 μm (average grain size 15 μm), applied stress 2 MPa, room temperature.

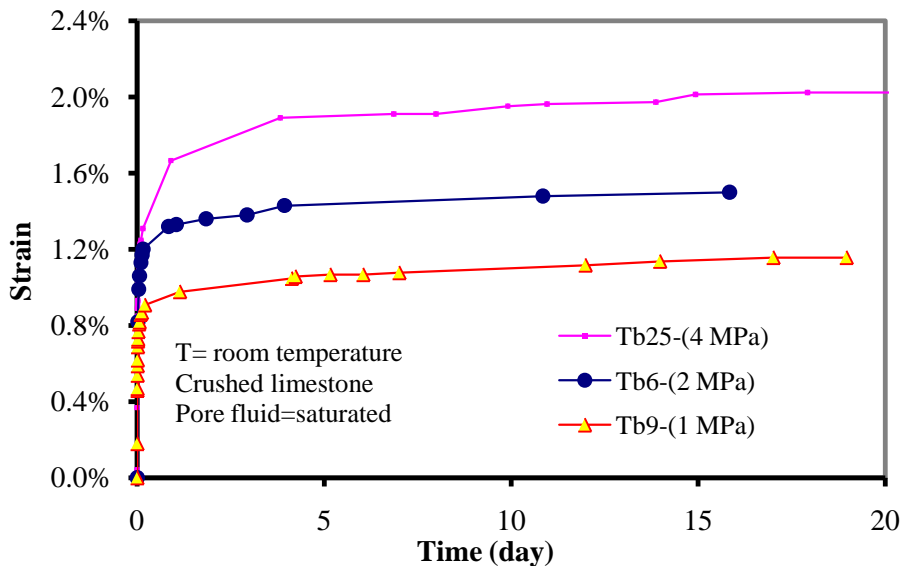


Figure 3.4. Effects of applied stress on volumetric compaction strain for crushed clean limestone samples with a grain size $3 \pm 3 \mu\text{m}$ flooded with CaCO_3 solution. Experiments carried out at applied stresses of 1, 2, and 4 MPa, room temperature.

Exp. ID	Material	Grain size(μm)	Stress (MPa)	Solution	Initial porosity (%)	Final strains (%)
Tb1	crushed limestone	41 \pm 4	2	Saturated CaCO_3	47.40	0.63
Tb2	crushed limestone	54 \pm 9	2	Saturated CaCO_3	44.23	0.49
Tb3	crushed limestone	76 \pm 13	2	Saturated CaCO_3	46.65	0.56
Tb4	crushed limestone	82 \pm 8	2	Saturated CaCO_3	47.30	0.16
Tb5	crushed limestone	41 \pm 4	2	Decane	46.47	0.00
Tb6	crushed limestone	3 \pm 3	2	saturated CaCO_3	41.85	1.50
Tb7	crushed limestone	5 \pm 4	2	Saturated CaCO_3	39.06	1.63
Tb8	crushed limestone	22 \pm 10	2	Saturated CaCO_3	46.50	1.17
Tb8b	crushed limestone	68 \pm 6	2	Saturated CaCO_3	46.85	0.81
Tb8c	crushed limestone	68 \pm 22	2	Saturated CaCO_3	47.25	1.04
Tb9	crushed limestone	3 \pm 3	1	Saturated CaCO_3	43.38	1.16
Tb10	crushed limestone	5 \pm 4	1	Saturated CaCO_3	39.72	0.97
Tb11	crushed limestone	5 \pm 4	2	Decane	39.49	0.00
Tb25	crushed limestone	3 \pm 3	4	Saturated CaCO_3	43.36	2.04
Tb36	pure calcite	2-45	4	Saturated CaCO_3	50.9	1.5
Tb38	pure calcite	2-45	4	Decane	52.2	0.03
Tb38a	pure calcite	2-45	4	Silicone oil	50.6	0
Tb40	pure calcite	2-45	4	Saturated CaCO_3	49.6	1.52
Tb46	crushed limestone	37 \pm 9	4	Saturated CaCO_3	48.34	0.74
Tb47	crushed limestone (oil contaminated)	37 \pm 9	4	Saturated soltion made from oil contaminated sample	44.7	0.08
Tb54	pure calcite	2-45	4	Tolueen	47	0
Tb55	pure calcite	2-45	4	Cyclohexaan	48.39	0
Tb56	pure calcite	2-45	4	Hexaan	49	0
Tb59	pure calcite	2-45	4	Hexaan	46.78	0
Tb60	pure calcite	2-45	4	Solution-Decone	50.6	1.25
Tb61	pure calcite	2-45	4	Decone-solution	49.44	0.34
Tb29	pure calcite	2-45	4	Solution- 10^{-3} Mg^{2+}	50.93	0.90
Tb51	pure calcite	2-45	4	Solution- 10^{-4} PO_4	50.7	0.58
Tb52	pure calcite	2-45	4	Solution- 10^{-3} PO_4	51.7	0.23
Tb20	pure calcite	2-28	4	Soluton-no NaCl	50.01	0.92
Tb41	pure calcite	2-28	4	Soluton-0.1NaCl	48.9	0.89
Tb42	pure calcite	2-28	4	Solution-0.5NaCl	49.6	0.92

Table 3.2. List of compaction experiments carried out in this study.

The compactions in samples filled with chemically inert fluids such as silicone oil, alcohol, decane, and other kinds of hydrocarbons only occur in samples with dry pre-compaction at stresses lower than 8 MPa. In these samples, filling inert fluid did “un-lock” the grains when reloaded and showed compaction strains. Note that the two samples reloaded dry at 4 MPa, either pre-compacted at 4 or 8 MPa, showed no compactions (Table 3.1). Note also in Table 3.1, the porosities of samples treated at 8 MPa dry are relatively uniform and much lower than those treated with lower stresses (2-4 MPa). Experiments showed that samples with wider grain size distributions such as used mainly for control experiments (0-28 μm) are the most difficult to “lock up”. Nevertheless, with pre-compaction at 8 MPa, all samples achieved a well controlled “locked up” state.

3.3.2 Wet compaction

In contrast to samples flooded with inert fluid, solution-filled samples showed clear evidence for compaction creep. Table 3.2 lists all the experiments done. Figures 3.4 & 3.5 show the effects of applied stress and grain size respectively on volumetric strain for clean crushed limestone tested with saturated carbonate solution. Towards higher applied stresses and finer grain size, the samples attained larger strains under otherwise identical conditions. Figure 3.6 shows a comparison of compaction behaviour obtained for samples made from crushed clean vs. oil-contaminated limestone. Both materials were wetted by the pore fluid solution. Note that crushed clean limestone compacted significantly more than oil-contaminated limestone. Figure 3.7 shows the effects of displacing saturated pore fluid solution with decane and vice versa. Displacing the saturated solution phase by decane reduces the rate and amount of creep but does not stop it. Decane flooded sample shows little or no creep and only starts to creep when decane is displaced by adding solution phase. Figure 8 shows the effects of adding magnesium and phosphate ions to the pore fluid on the compaction behaviour of super pure calcite. With a Mg-concentration of 0.01mole/l and phosphate concentrations of 0.0001-0.001mole/l, the sample compaction creep decreases significantly compared to additive-free samples. Salinity (NaCl concentration) in the range of 0.1 to 0.5 mole/l in the pore fluid has promoted compaction creep as shown in Figure 3.9.

3.4. Discussion

3.4.1 Deformation mechanisms in samples compacted dry and with chemically inert pore fluid

It is well-established in materials science that when subjected to compactional loading, most-granular materials undergo an initial stage of densification dominated by instantaneous grain rearrangement and microfracture until the aggregate “locks up”. Following initial locking, dry aggregates densify by solid-state deformation of individual grains coupled with intergranular sliding (Fischmeister et al. 1982, Spiers and Schutjens, 1990). In the “locked up” state, intergranular sliding and rearrangement cannot proceed

without deformation of the grains themselves. Therefore, it is solid-state deformation mechanisms that generally control densification beyond initial loading.

The initial dry pre-compaction were most likely due to the grain rearrangement, grain re-orientation and intergranular sliding. Due to the low applied stresses, intragranular plastic deformation is not likely to be important though minor plasticity or deformation twinning cannot be ruled out (De Bresser et al., 2002).

The compactions in some samples (not properly treated in dry pre-compaction) filled with inert fluids (Table 3.1), could be most likely caused by fluid-assisted grain re-arrangement & sliding for fluids reduce the frictions of grain contacts. In addition to reduce grain contact frictions, fluids (chemically inert) can also change the interfacial properties of grains (solid-fluid contacts vs. solid-air contacts). This change could be important for microfracture/grain cracking under certain stress conditions. However, it was not the case for our experiments, because the inert fluids did not promote any compactions in samples treated by dry pre-compaction at 8 MPa. The well “locked up” state of samples treated at 8 MPa dry with respect to subsequent reloading at lower stresses (1-4 MPa) is crucial for obtaining reliable mechanical data of solution assisted compaction.

3.4.2 Deformation mechanisms in samples filled with solution

In contrast to samples filled with inert fluids, samples filled with aqueous solution showed time-dependent compaction when loaded at stresses of 1-4 MPa. Note that all samples compacted with solution were subjected to 8 MPa dry pre-compaction treatment for 30 minutes. As we have discussed in above section, this treatment resulted in a well “locked up” state of grains with respect to stresses in the range 1-4 MPa. Moreover, we have shown that the “locked up” state cannot be unlocked by adding inert pore fluids. Since the viscosities and other physical properties of inert fluids such as decane and alcohol are similar to those of water, the physical effects of water addition (like friction reduction at grain contacts) should be the same as inert fluid i. e. contributing no compaction strain. This implies that the creep effects obtained by adding aqueous solution to our samples must be chemical in origin. In other words, the creep of initially “locked up” aggregates in presence of aqueous solution must have involved water-assisted deformation of individual grains.

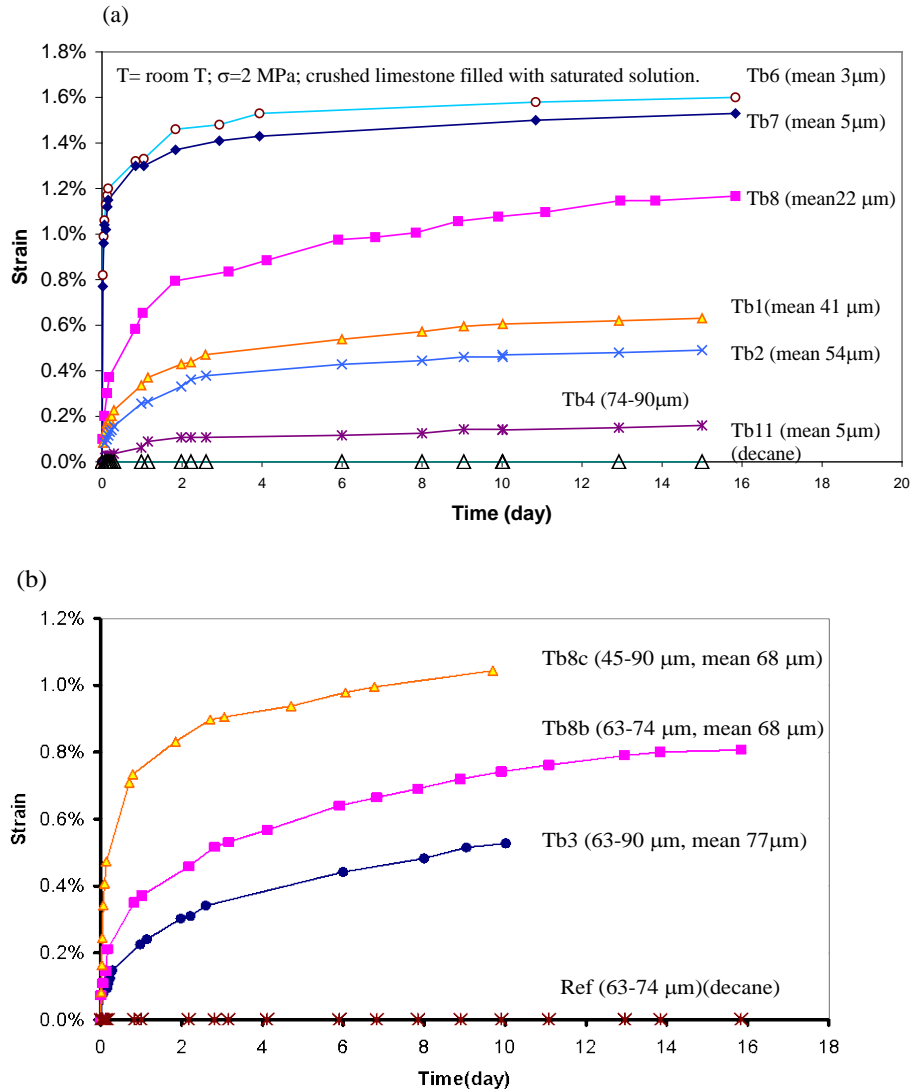


Figure 3.5. Effects of mean grain size in μm (a) and grain size distribution width at constant mean grain size (b) on compaction strain in samples flooded with saturated CaCO_3 solution. Results of compaction experiments on crushed clean limestone samples at an applied stress of 2 MPa and room temperature. Note that compaction is sensitive to both mean grain size and grain size distribution (Tb8b vs. Tb8c), with a finer grain size and a wider distribution producing more compaction strain.

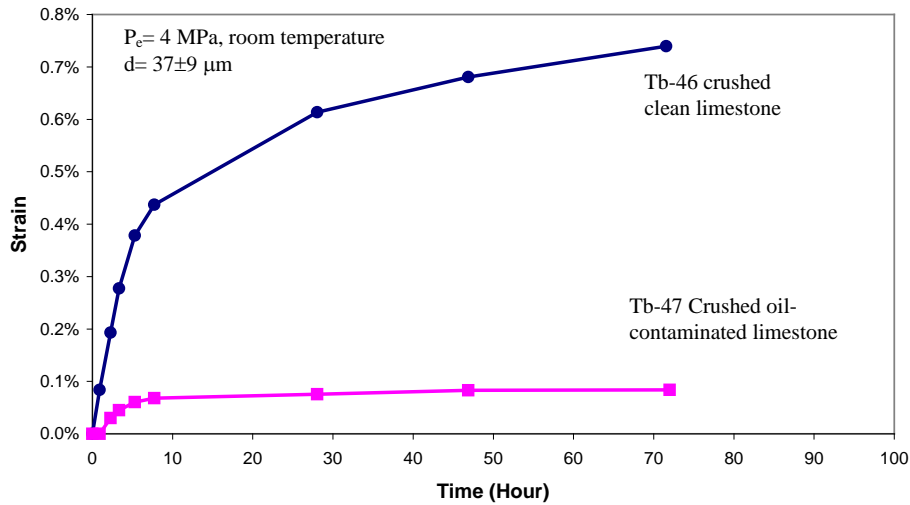


Figure 3.6. Comparison of behaviour shown by samples made from clean vs. oil-contaminated limestone powders. Material: crushed limestone with grain size $37 \pm 9 \mu\text{m}$. Conditions: applied stress 4 MPa, room temperature. Solutions were made from corresponding test materials.

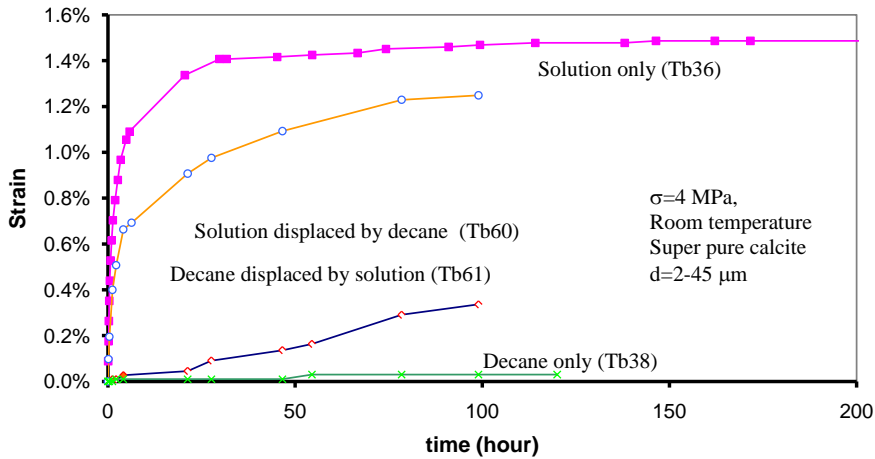


Figure 3.7. Effects of displacement of saturated solution by decane on the compaction creep of super pure calcite samples with grain size of 2-45 μm (average grain size 15 μm) at applied stress of 2 MPa and room temperature.

Compaction of carbonate at room temperature

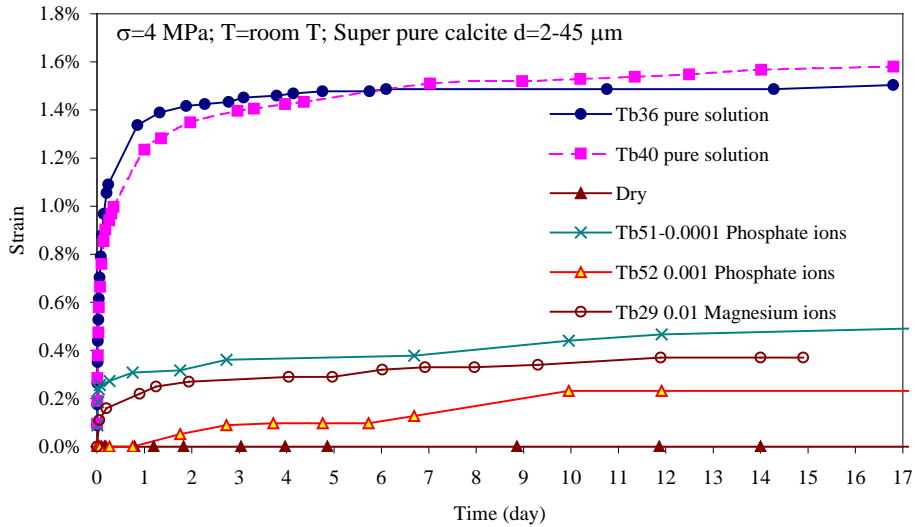


Figure 3.8. Effects of added $\text{MgCl}_2 \cdot 6\text{H}_2\text{O}$ and Na_2HPO_4 on compaction of wet granular calcite. Note the reduced compaction compared with samples filled saturated CaCO_3 solution under the same experimental conditions. Super pure samples with grain size fraction of 2-28 μm (average grain size 15 μm), room temperature, applied stress 4 MPa.

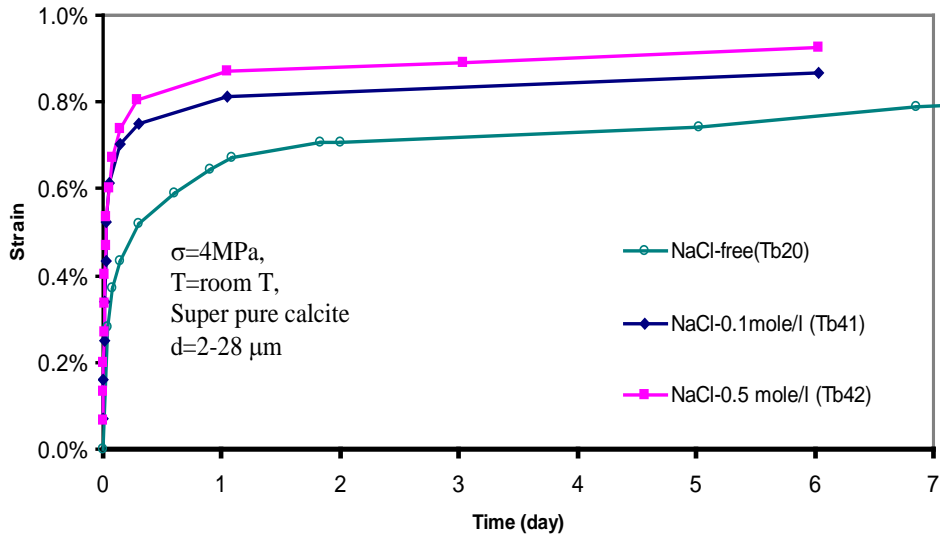


Figure 3.9. Effects of pore fluid salinity on compaction of super pure calcite with a grain size of 2-28 μm (average grain size 15 μm). Applied stress 2 MPa, room temperature, pore fluid is saturated solution with respect to granular starting materials.

There are several candidate mechanisms for “water-assisted” deformation, under our experimental conditions (room temperature, low stress). The first candidate is water-assisted grain crushing, caused by a reduction in interfacial energy of solid phase (grains) with respect to air-filled or inert fluid filled samples. Although we have shown that a switch from air-filled samples (dry) to samples flooded with chemically inert fluid (decane, alcohol, silicone oil) produce no difference in compaction behaviour, we cannot completely rule out the possibility that equilibrium crack growth at grain contacts (Griffith cracking) is easier in water than in air, decane, alcohol, or silicone oil. However, previous studies showed that grain crushing is easier in coarser-grained samples (Zhang et al., 1990; Cuss et al., 2003). The theoretically predicted stress for grain crushed of carbonate rocks is a function of porosity and grain size (Zhang et al., 1990). Taking the values of porosity and grain size of our samples, the predicted stresses (>10 MPa) are much higher than those of our experimental stresses. Hence grain crushing is not likely to have been important. The second candidate deformation mechanism is water-assisted stress corrosion (critical crack growth). However, the stress corrosion crack growth velocity depends on stress in a high non-linear way, with power law stress exponent value >8 (Atkinson and Meredith, 1989). As we will see in the follow section the stress dependence in our experiments is much less than 8. Our experimental results showed that more strains achieved in finer-grained samples. In addition, the observed effects of magnesium and phosphate on compaction creep suggest that the operative mechanism of water-assisted deformation in solution filled samples could have involved calcite dissolution and precipitation. This points to the third candidate-mechanism, namely pressure solution, in which dissolution and precipitation of mineral are known to be involved. The effects of grain size and stress on the observed rates of compaction are close to theoretical prediction. Hence pressure solution remains the dominant deformation mechanism in our experiments.

3.4.3 Experimental results vs. pressure solution theory

We now compare the experimentally observed effects of grain size, applied stress and pore fluid chemistry on compaction rate with those predicted by pressure solution theory. For uniaxial compaction creep of a granular aggregate flooded with saturated solution, with some assumptions such as negligible surface energy et al, and at small strains (<20%)(DeMeer & Spiers, 1999), the pressure solution constitutive equations obtained from theory (Raj, 1982; Spiers and Schutjens, 1990; DeMeer and Spiers, 1997, 1999) can be written.

$$\dot{\epsilon} = K_s \frac{\sigma_e^n}{df_s(\phi)} \quad \text{for dissolution control} \quad (3.1)$$

$$\dot{\epsilon} = K_d \frac{\sigma_e}{d^3 f_d(\phi)} \quad \text{for diffusion control} \quad (3.2)$$

$$\dot{\epsilon} = K_p \frac{\sigma_e^m}{df_p(\phi)} \quad \text{for precipitation control} \quad (3.3)$$

Here $\dot{\epsilon}$ is volumetric strain rate, K_s and K_p incorporate temperature-dependent dissolution and precipitation rate coefficients, K_d is a temperature-dependent term incorporating the grain boundary diffusivity and width, σ_e is applied effective stress, d is grain size, and ϕ is porosity and n , m are exponential constants depending dissolution and precipitation reaction orders, $f(\phi)$ is function of porosity. In all cases, the compaction strain rates are inversely related to the grain size either linearly (dissolution, precipitation control) or according to a power law. This is in contrast to the brittle deformation such as grain crushing failure, where compaction rate is positive related to the grain size (Brzesowsky, 1995; Chuhan, et al., 2002).

Effects of applied stress

From the data on crushed limestone presented in Figure 3.4, it is clear that compaction strain increases with increasing applied stress. Figure 3.10 is a plot of log strain rates vs. log applied stress, at fixed strains, derived from the data of Figure 3.4. The slopes are about 1-2, which is consistent with our previously reported results for samples of super pure calcite (Zhang et al., 2002). This dependence of strain rate on applied stress (1-2) is also consistent with the hypothesis that deformation in our compaction tests is dominated by pressure solution, since values of 1-3 are predicted by pressure solution theory, depending whether pressure solution is controlled by diffusion ($\dot{\epsilon} \propto \sigma_e$) or by dissolution/precipitation ($\dot{\epsilon} \propto \sigma_e^{2-3}$) (DeMeer and Spiers, 1997). Since the stress corrosion at crack velocity is much strongly dependent on stress (is >8 , in limestone) (Atkinson and Meredith, 1989), this mechanism is unlikely to have been the dominate one.

Effects of grain size and grain size distribution

From Figure 3.5, we can see clearly that the experimentally determined strain rates are inversely related to grain size. More strains were obtained in finer samples than in coarser ones within the same test period. At constant strain, strain rates are larger for finer-grained samples under the same applied stress. Figure 3.11 shows a log-log plot of strain rate vs. grain size for crushed limestone at various constant strains. The slope of the data for individual strains in Figure 3.11 is about 3, implying a inverse power law dependence of strain rate on grain size. The dependence of strain rate on grain size is close to predicted by pressure solution theory, suggesting that it is more likely to be diffusion controlled (slope=3 vs. 1). At the same time, it must be recognized that grain size distribution, as well as the mean grain size, also plays a role in determining pressure solution rates (Ter Heege, et al., 2004). As shown in Figure 3.5b, samples with widely distributed grain size fractions but similar mean grain size creep faster than those with narrowly distributed grain size. This effect may be due to effect of grain size packing and spacing distribution on porosity, on sliding, or on the volume-averaged effects of pressure solution (or other active mechanisms).

Rate dependence on pore fluid chemistry

a). Effects of different hydrocarbons

In contrast to the samples filled with aqueous solution phase, samples filled with hydrocarbons as pore fluid, showed little or no compaction, proving that wet compaction involved some kind of chemically related process, such as pressure solution, and that no such processes occur in the presence of hydrocarbons. In addition, two compaction experiments were carried out using clean and oil-bearing limestone samples to investigate the effects of natural hydrocarbon contamination on creep in samples with added solution. As the contaminated sample reached much lower strains under the same experimental conditions, it is evident that natural oil inhibits wet compaction. This could be caused by the different wetting abilities of hydrocarbons and water on the calcite surface. Taylor et al. showed that hydrocarbons can be more easily wet the calcite surface than water (Taylor et al., 2000).

The effects of water and decane in the fluid displacement experiments (Figure 3.6) suggest the wetting of the grain boundaries by water was necessary for compaction creep under our experimental conditions, also indicating the active creep mechanism was water-assisted pressure solution.

b) Effects of Magnesium and phosphate ions in the pore fluid

The effects of Magnesium and phosphate ions on calcite precipitation have been extensively studied in the geochemical literatures (Reddy and Wang, 1980; Dove and Hochella, 1993; Reddy, 1977). These studies show that the presence of dissolved magnesium and phosphate in the solution inhibits the calcite precipitation significantly. Some studies also show that magnesium and phosphate ions inhibit calcite dissolution (Berner and Morse, 1974). Our compaction experiments performed using calcite saturated pore fluid with added $MgCl_2$ and Na_2HPO_4 also show major retardation effects of magnesium and phosphate on compaction strain rate (see Figure 3.8). The observed reduction of compaction creep rate by these calcite precipitation/dissolution inhibitors suggests that creep in calcite must involve calcite precipitation and dissolution. This strongly supports our hypothesis that the deformation mechanism in the solution-filled sample was pressure solution. In natural sea water and pore fluid, magnesium and phosphate are common ions, hence pore fluid chemistry can be expected to play a major role in controlling the deformation and compaction of calcite rocks under conditions favouring pressure solution.

c) Effects of pore fluid salinity

Salinity, i. e. NaCl contents, is also a very important aspect of the pore fluid chemistry which influences the solubility of calcite and the kinetics of calcite dissolution and precipitation (Morse and Mucci, 1980; Mucci, 1983). Ellis (1963) found that increasing pore fluid salinity increases the solubility of calcite, at temperature up to 300 °C. Mucci (1983) also found that NaCl concentrations in the range of 0-0.78 mole/l increase calcite solubility.

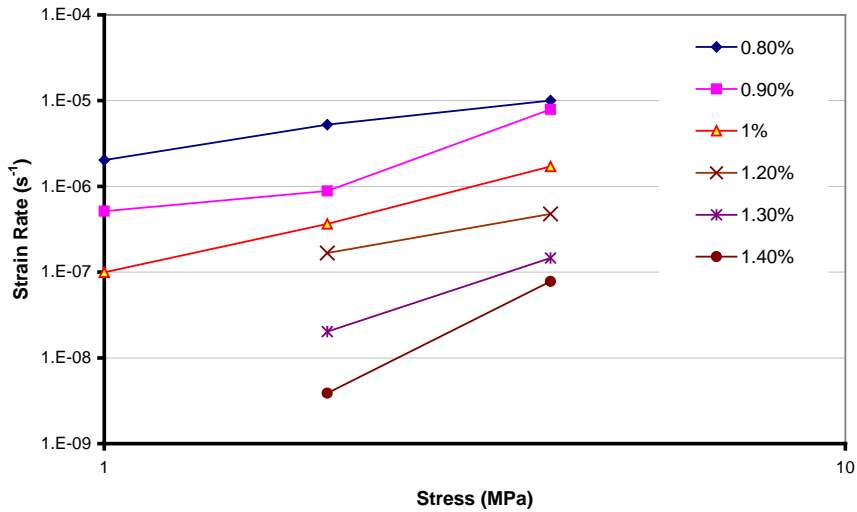


Figure 3.10. Log-log plot of strain rate vs. applied stress at fixed strains using data presented in Figure 3.4.

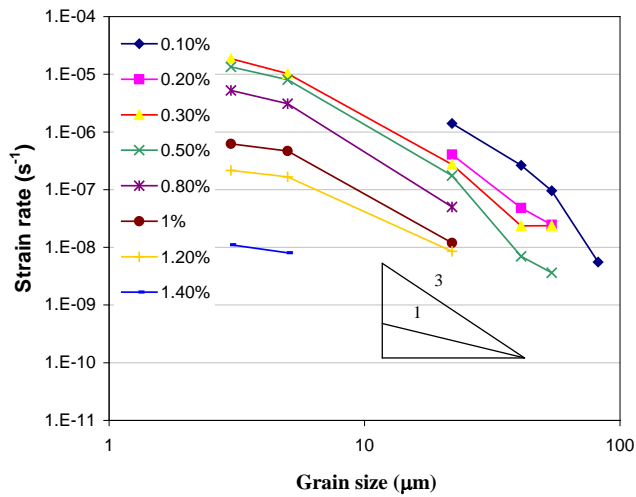


Figure 3.11. Log-log plot of strain rate vs. grain size at fixed strains using data presented in Figure 3.5a.

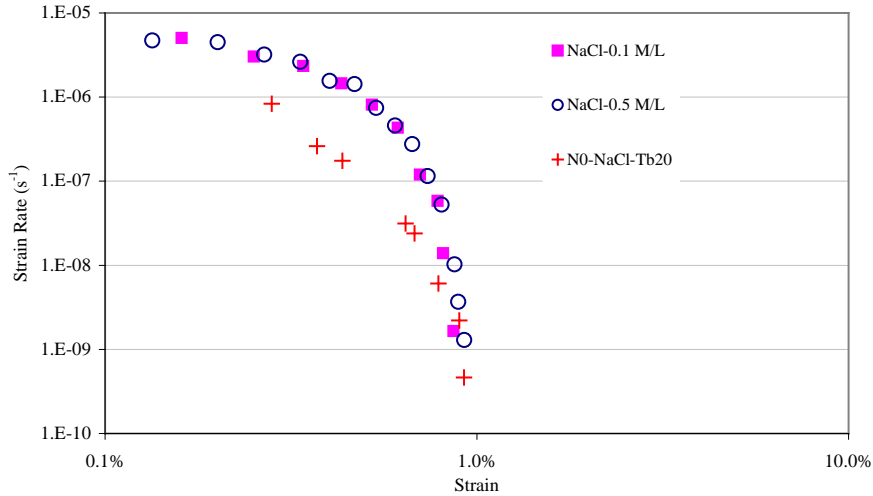


Figure 3.12. Log-log plot of strain rate vs. strain for compaction of samples filled with different salinity (error bars close to the size of the data symbols). Note samples with salinity of 0.1-0.5 mole/l promote compaction compared to salinity free ones.

The effects of salinity on calcite solubility can be expected to increase the diffusion controlled pressure solution (Equ(2)). In addition, the salinity of pore fluid is a potential factor that could influence pressure solution through effects on the grain boundary fluid film thickness (Renard and Ortoleva, 1997) hence speeding up diffusion process. Figure 3.12 shows a plot of log strain rate vs. log strain derived from Figure 3.9. The samples with salinity of 0.1 to 0.5 mole/l show an increase in compaction strain rates compared to salinity-free samples ($\dot{\epsilon}_{saline} \approx 3\dot{\epsilon}_{solution}$). On the other hand, the presence of NaCl inhibits the calcite precipitation (Zhong and Mucci, 1989). The effects of NaCl on the observed strain rates of calcite suggest that the rate controlling step in the pressure solution of calcite in the pore fluid system is diffusion controlled. Hellmann et al (2002) obtained similar results in their compaction experiments on chalk with salinity of 0.5 mole/l. They also concluded that pressure solution was active in their experiments.

In summary, pressure solution is the main mechanism in our experiments. In the pure fluid system, the rate limiting step of pressure solution in calcite is probably diffusion controlled. The measured pressure solution strain rates of fine-grained calcite from our experiments are from 10^{-6} to 10^{-9} s $^{-1}$ at room temperature and 1-4 MPa. Pore fluid plays a great role in controlling the rates. Hence compaction behaviours as well as the porosity/permeability evolution in natural carbonate rocks strongly depend on the pore fluid chemistry i. e. the calcite reaction inhibitors as well as the mechanical conditions.

3.5 Conclusions

The following conclusions can be drawn from this study:

- 1). Compaction creep occurs only in the samples filled with saturated carbonate solution. The compaction rate of wet calcite increases with decreasing grain size according to an inverse power law with an exponent of 3. In addition, samples with a wider grain size distribution compact faster than those with same mean grain size but with a narrower distribution. The dependence of compaction strain rates on stress can be described by a power law with $\dot{\epsilon} \propto \sigma^n$ with $n=1-2$.
- 2). Intergranular pressure solution is the dominant compaction mechanism at room temperature and stresses of 1-4 MPa in crushed limestone and super pure calcite samples with grain size of 3-90 μm loaded in the presence of saturated CaCO_3 solution. Compaction occurs at strain rates of 10^{-6} to 10^{-9} s^{-1} under these conditions.
- 3). Salinity ranging of 0.1-0.5 mole/l increases the compaction rate in 3 times compared to salinity free sample.
- 4). The compaction strain rates in calcite can be significantly slowed down or stopped by addition of magnesium or phosphate ions to the pore fluid in the orders of 10^{-4} – 10^{-2} mole/l.
- 5). Compaction of granular calcite by pressure solution is strongly inhibited by the presence of hydrocarbons that wet the grain surfaces.

3.6 References

- Atkinson B. K, and P. G. Meredith (1989), The theory of subcritical crack growth with applications to minerals and rocks. In: Atkinson B. K. (eds) *Fracture Mechanics of Rock*. Academic Press London, p. 111-66.
- Bathurst R.G. C. (1958), Diagenetic fabrics in some British Dinantian limestones. *Liverpool and Manchester Geology* 2, 11-36.
- Berner R. A. and J. W. Morse (1974), Dissolution kinetics of calcium carbonate in sea water IV. Theory of calcite dissolution. *Am. J. Sci.* 274, 108-34.
- Brzesowsky R. H. (1995), Micromechanics of sand grain failure and sand compaction. *Geologica Ultraiectina* 133, Utrecht Netherlands: Utrecht University.
- Chuhan F., A., A. Kjeldstad, K. Bjorlykke, K. Hoeg (2002), Porosity loss in sand by grain crushing-experimental evidence and relevance to reservoir quality. *Marine and Petroleum Geology* 19, 39-53.
- Cuss R. J., E. H. Rutter and R. F. Holloway (2003), The application of critical state soil mechanics to the mechanical behaviour of porous sandstones, *Int. J. Rock. Mech. Min. Sci.* 40, 847-62.
- De Bresser J. H. P., B. Evans and J. Renner (2002), On estimating the strength of calcite rocks under natural conditions, in: S. DeMeer, M. R. Drury, J. H. de Bresser, G. M. Pennock, (Eds), *Deformation Mechanisms, Rheology and Tectonics: Current Status and Future Perspectives*, *Geol. Soc. Lond. Spec. Pub.* 200; 309-29.

- DeMeer S., and C. J. Spiers (1997), Uniaxial compaction creep of wet gypsum aggregates. *J. Geophys. Res.* 102, 875-91.
- DeMeer S. and C. J. Spiers (1999), Mechanisms and kinetics of creep by intergranular pressure solution. in: B. Jamtveit, P. Meakin (Eds.), *Growth, Dissolution and Pattern Formation in Geosystems*, Kluwer Academic Publishers, Dordrecht, 345-63.
- DenBrok B., M. Zahid and C. Passchier (1999), Pressure solution compaction of sodium chlorate and implications for pressure solution in NaCl. *Tectonophysics* 307, 297-312.
- Dove P. M, and M. F. Hochella (1993), Calcite precipitation mechanisms and inhibition by orthophosphate: In situ observations by Scanning Force Microscopy, *Geochimica et Cosmochimica Acta* 57, 705-14.
- Eisenlohr L, K. Meteva, F. Gabrovsek and W. Dreybrodt (1999), The inhibiting action of intrinsic impurities in natural calcium carbonate minerals to their dissolution kinetics in aqueous H₂O-CO₂ solutions. *Geochimica et Cosmochimica Acta* 63, 989-1002.
- Ellis A. J. (1963), The solubility of calcite in sodium chloride solutions at high temperatures. *Am. J. Sci.* 261, 259-67.
- Evans B., Y. Bernabe and W. Zhu (1999), Evolution of pore structure and permeability of rocks in laboratory experiments. in "Growth, Dissolution and Pattern Formation in Geosystem", B. Jamteit and P. Meakin (eds.). Kluwer Academic Publishers, Netherland, p. 327-44
- Fischmeister H. F, E. Artz, L. R. Olssen (1982), Particle deformation and sliding during compression of spherical powders: a study by quantitative metallurgy. *Powder Metall.* 21, 179-87.
- Hellmann R. P. J., N. Renders, J. P. Gratier and R. Guiguet (2002), Experimental pressure solution compaction of chalk in aqueous solutions Part 1, Deformation behavior and chemistry, in: Hellmann RPJ, Wood SA, Water-Rock Interaction, Ore Deposits, and Environmental Geochemistry: A Tribute to David A. Crerar, *The Geochemical Society, Special Publication* 7, 129-52.
- Lehner F. K. (1990), Thermal dynamics of rock deformation by pressure solution. in: D. Barber, P. Meredith (Eds.), *Deformation Processes in Minerals, Ceramics and Rocks*, Unwin Hyman, London, 296-33.
- Morse J. W., A. Mucci and F. J. Millero (1980), The solubility of calcite and aragonite in seawater of 35‰ salinity at 25 °C and atmospheric pressure. *Geochimica et Cosmochimica* 44, 85-94.
- Mucci A. (1983), The solubility of calcite and aragonite in seawater at various salinities, temperatures, and one atmosphere total pressure, *Am. J. Sci.* 283, 780-99.
- Paterson, M. S. (1995), A theory for granular flow accommodate by material transfer via an intergranular fluid, *Tectonophysics* 280, 257-66.
- Railsback L. B. (2002), *An Atlas of Pressure Dissolution Features*, <http://www.gly.uga.edu/railsback/PDFindex1.html>.
- Raj R. (1982), Creep in polycrystalline aggregates by matter transport through a liquid phase. *J. Geophys. Res.* 87, 4731-39.
- Reddy MM. (1977), Crystallization of calcium carbonate in the presence of trace concentrations of phosphorous –containing anions. I inhibition by phosphate and glycerophosphate ions at pH 8.8 and 25 C. *J. Cryst. Growth* 41, 287-95.

- Reddy M. M, and K. K. Wang (1980), Crystallization of calcium carbonate in the presence of metal ions. I. Inhibition of magnesium ion at pH 8.8 and 250C. *J. Cryst. Growth* 50, 470-80.
- Renard F, and P. Ortoleva (1997), Water films at grain contacts: Debye-Hückel, osmotic model of stress, salinity, and mineralogy dependence. *Geochimica et Cosmochimica* 61, 1963-70.
- Renard F, P. Ortoleva and J. P. Gratier (1997), Pressure solution in sandstones: influences of clays and dependence on temperature and stress. *Tectonophysics* 280, 257-66.
- Rutter E. H. (1983), Pressure solution in nature, theory and experiment. *J. Geol. Soc. Lond.* 140, 725-40.
- Spiers C. J., and P. M. T. M. Schutjens (1990), Densification of crystalline aggregates by fluid-phase diffusional creep. In: Barber, DJ. and Meredith, PG. (eds.). *Deformation processes in minerals, ceramics and rocks*. Cambridge University Press. 334-53.
- Svensson U, and W. Dreybrodt (1992), Dissolution kinetics of natural calcite minerals in CO₂-water system approaching equilibrium. *Chem. Geol.* 100, 129-45.
- Tada R, and R. Siever (1989), Intergranular pressure solution during diagenesis. *Ann. Rev. Earth and Planet Sci.* 17, 89-118.
- Taylor S.C., C. Hall, and W.D. Hoff (2000), Wilson MA. Partial wetting in capillary liquid absorption by limestones, *J. Collo. Interface Sci.* 224, 351-357.
- Ter Heege, J. H., J. H. P. De Bresser, and C. J. Spiers (2004), Composite flow laws for crystalline materials with log-normally distributed grain size: theory and application to olivine. *J. Struct. Geol.* 26, 1693-1705,
- Zhang X, J. Salemans, C. J. Peach, C. J. Spiers (2002), Compaction experiments on wet calcite powder at room temperature: evidence for operation of intergranular pressure solution, in: S. de Meer, M. R. Drury, J. H. de Bresser, G. M. Pennock, (Eds), *Deformation Mechanisms, Rheology and Tectonics: Current Status and Future Perspectives*, *Geol. Soc. Lond. Spec. Pub.* 200, 29-39.
- Zhang J, Wong T. F., and D. M. Davis (1990), Micromechanics of pressure-induced grain crushing in porous rocks, *J. Geophys. Res.* 95, 341-52.
- Zhong S. and A. Mucci (1989), Calcite and aragonite precipitation from sea water solutions of various salinities: Precipitation rates and overgrowth compositions, *Chem. Geol.* 78, 283-299.

4. Effects of phosphate ions on intergranular pressure solution in calcite – an experimental study

This chapter was published as: Zhang, X and C.J. Spiers (2005), Effects of phosphate ions on intergranular pressure solution in calcite – an experimental study. Geochimica et Cosmochimica Acta, 69, 5681-5691. doi:10.1016/j.gca.2005.08.006.

Abstract

Intergranular Pressure Solution (IPS) is a coupled chemical-mechanical process of widespread importance during diagenesis and low temperature deformation of sedimentary rocks. Laboratory experiments on IPS in halite, quartz and calcite have largely concentrated on the mechanical aspects of the process. In this study, we report the effects of pore fluid chemistry, specifically varying phosphate ion concentration, on the mechanical compaction by IPS of fine-grained calcite powders at room temperature and 1-4 MPa applied effective stress. Phosphate was investigated because of its importance as a biogenic constituent of sea and pore waters. Increasing the pore fluid phosphate concentration from 0 to 10^{-3} mol/l systematically reduced compaction strain rates by up to 2 orders of magnitude. The sensitivity of the compaction strain rate to phosphate concentration was the same as the sensitivity of calcite precipitation rates to the addition of phosphate ions reported in the literature, suggesting that the rate of IPS in phosphate-bearing samples was controlled by calcite precipitation on pore walls. The results imply that IPS and associated porosity/permeability reduction rates in calcite sediments may be strongly reduced when pore fluids are enriched in phosphates e. g. through high biological productivity or a seawater origin. Future modelling of IPS related processes in carbonates must therefore take into account the effects of pore fluid chemistry, specifically the inhibition of interfacial reactions.

4.1 Introduction

Aside from the direct mechanical effects of pore fluid pressure on the brittle/frictional and poroelastic behaviour of rocks (Hubbert and Rubey, 1959; Byerlee, 1993; Sibson, 1994; Wang, 2000), pore fluid plays a crucial chemical role in controlling time-dependent rock compaction and deformation. One of the most important mechanisms of fluid-rock interaction in upper crustal environments, is Intergranular Pressure Solution (IPS) (Weyl, 1959; Paterson, 1973, 1995; Rutter, 1976, 1983; Raj and Chyung, 1981; Raj, 1982; Spiers and Schutjens, 1990; Spiers et al., 1990; Lehner, 1990, 1995; Dewers and Hajash, 1995; Hickman et al., 1995; Renard et al., 1997; De Meer and Spiers, 1999; Dysthe et al., 2002a, 2002b; Gunderson et al., 2002; Spiers et al., 2004). Intergranular pressure solution is possible in wet rock systems where grain-to-grain contacts are penetrated by water in thin film form or in a non-equilibrium island-channel network (Rutter, 1983; Lehner, 1990, 1995; denBrok and Morel, 2001; Revil, 2001). It is a coupled chemical-mechanical process

involving dissolution of solid within stressed grain contacts, diffusion through the grain boundary fluid into the pores, followed by removal of the dissolved material through long range transport or by precipitation on low stress interfaces and free pore walls (Spiers et al., 2004). In a chemically open, two component, fluid-rock system in which long range advective or diffusive transport occurs, the thermodynamic driving force for compaction by IPS is given

$$\Delta\mu = (\sigma_n - P_f)\Omega + RT\Delta C / C_0 \quad (4.1)$$

as discussed by Lehner (1995) and Spiers et al. (2004). Here, $\Delta\mu$ is the chemical potential difference between the solid phase within stressed grain contacts and dissolved solid present in the open pore fluid, σ_n is the normal stress acting across grain contacts, P_f is the pore fluid pressure, Ω is the molar volume of the solid, ΔC is the under-saturation of the pore fluid (under-saturation taken positive) with respect to the solubility (C_0) of the solid under hydrostatic reference conditions (P_f , T), R is the gas constant, and T is temperature (K). Given a positive driving force ($\Delta\mu > 0$), the rate of IPS and hence of deformation is controlled by the serial kinetic processes of dissolution and diffusion from grain contacts to pores (Lehner, 1995; Spiers et al., 2004). In a chemically closed system (no long range advective/diffusive transport of dissolved solid), equation (4.1) reduces to

$$\Delta\mu = (\sigma_n - P_f)\Omega \quad (4.2)$$

where $\Delta\mu$ now represents the potential difference between the stressed solid within grain boundaries and that at free pore walls (Lehner, 1995; Spiers et al. 2004). Under steady-state conditions, the rate of compaction by IPS is now controlled by the kinetics of dissolution at grain contacts, diffusion through the grain boundary fluid phase and precipitation on pore walls, with the slowest step being rate limiting (Lehner, 1995; De Meer and Spiers, 1997, 1999; Spiers et al., 2004). The driving force is partitioned among the three serial processes, such that the slowest process (rate-limiting) consumes the bulk of the available potential and is thus the principal dissipative process (Raj, 1982; Lehner, 1995).

Alongside purely mechanical processes of grain breakage and rearrangement (Chester et al., 2004), IPS is an important mechanism of compaction, diagenetic lithification and porosity/permeability reduction in sedimentary rocks (Weyl, 1959; Durney, 1972; Tada and Siever, 1989; Aydin, 2000). It is an effective mechanism of both strength recovery and creep in active fault zones (Hickman et al., 1995; Karner et al., 1997; Bos and Spiers, 2002a, 2002b; Nakatani and Schultz, 2004) and a widespread mechanism of deformation under low temperature metamorphic conditions (Elliot, 1973; Rutter, 1976, 1983; Stöckhert et al., 1999). Together with processes such as clay smearing and cataclastic grain size reduction, IPS is also an efficient mechanism of fault sealing, shear band sealing and compaction band sealing in hydrocarbon reservoirs (Smith, 1966; Aydin, 2000). In carbonate rocks, intergranular pressure solution and localized pressure solution seams or stylolites are particularly widespread and important in controlling porosity/permeability evolution and fluid transport (Bathurst, 1958; Leythaeuser et al., 1995; Heydari, 2000).

Moreover, recent work by Leythaeuser et al (1995) has shown that pressure solution within stylolites may play a crucial role in the concentration of organic materials and the generation of hydrocarbons. Realistic modelling of processes such as diagenetic compaction, petroleum generation, fault sealing and other mass transport processes in carbonate sediments accordingly requires quantitative data on the process and kinetics of intergranular pressure solution in calcite, and on the influence of (bio) geochemical environment.

In an attempt to provide such data, laboratory investigations of pressure solution in carbonates have aimed at reproducing the IPS microstructures widely seen in nature and at understanding the processes and the parameters governing the rate of the process. Baker et al. (1980) carried out compaction experiments on deep sea sediments (i.e. low magnesium calcite), crushed Iceland spar and reagent-grade calcite powder at 25-100 MPa effective stress, pore fluid pressures of 15-50 MPa and temperatures 22-180 °C, for 1 to 10 days. Significant porosity reduction was obtained in 10 days in their experiments. Uniaxial compaction experiments carried out under chemically closed system conditions by Shinn and Robbin (1983) at room temperature, a fluid pressure of 0.1 MPa and applied effective stresses from 6.5 to 95 MPa, on cores of modern carbonate sediments, resulted in features such as incipient stylolites and truncated fossils, indicating the operation of pressure solution. These authors used a pore fluid consisting of marine pore water. High quality triaxial deformation experiments performed on chalk by Hellmann et al. (2002) also showed that pressure solution was probably operating under their experimental conditions, in a closed system at 20-100 °C, 4 MPa differential effective stress and pore pressure <0.3 MPa. In this case, the pore fluids were pure water and saline fluid (0.5 M NaCl +0.05 M MgSO₄·7H₂O).

Though many of the above experimental studies exhibited clear evidence for IPS and related processes, none allowed the (very low) rate of IPS to be systematically quantified, nor were sufficient data obtained to allow comparison with IPS models or identification of the rate controlling mechanism. More recent compaction creep experiments, performed by ourselves on wet, fine-grained calcite at 22 °C and 1-4 MPa effective stress (Zhang et al., 2002; Zhang and Spiers, 2005), yielded measurable compaction rates (10^{-6} - 10^{-10} s⁻¹) plus a systematic dependence of creep rate on stress, grain size and pore fluid composition (Mg²⁺ content) that broadly resembles the predictions of IPS theory. Effects of pore fluid chemistry have also been investigated in some of the aforementioned studies (Hellmann et al., 2002). However, the results produced to date are of preliminary nature only and much remains unknown, notably regarding the rate controlling process of IPS in calcite and the influence of (bio)-geochemical conditions. Recent experimental work on the diffusion of ions in thin aqueous films (De Meer et al., 2002; Alcanter et al., 2003; Spiers et al., 2004), as well as molecular dynamic simulations (Dysthe et al., 2002b), indicates that the diffusion coefficient (D) in thin intergranular films during IPS is not strongly reduced as proposed by Rutter (1976, 1983) but is similar to, or perhaps one order of magnitude lower than that in bulk solution (see also Renard et al., 1997; Revil, 2001). Provided intergranular fluid film are at least 1 nm in thickness (S), which is the minimum value generally assumed (Renard et al. 1997), this implies that interfacial reactions may control rates of IPS in calcite rocks, since precipitation and dissolution reaction rates are strongly retarded by common pore fluid ions like phosphate and magnesium (Reddy, 1977; Dove and Hochella, 1993; Davis et

al., 2000; Spiers et al., 2004). Pore fluid chemistry can accordingly be expected to play a major role in determining the rate controlling mechanism of IPS in natural carbonate systems.

The purpose of this study is to investigate experimentally the effects of pore fluid chemistry on the mechanical compaction behaviour of granular calcite under conditions where our previous work (Zhang et al., 2002; Zhang and Spiers, 2005) suggests that IPS is the dominant deformation mechanism. Our broad aim is two-fold: 1) to better constrain the likely rate controlling process of IPS through observing the effects of pore fluid additives, and 2) to gain insight into the magnitude of the effects of geologically important pore fluid impurities. We chose dissolved phosphate as our pore fluid impurity since it is a well-known calcite precipitation and dissolution inhibitor (Reddy, 1977; Meyer, 1984; Dove and Hochella, 1993; Jonasson et al., 1996; Katsifaras and Spanos, 1999; Plant and House, 2002), and so theoretically should slow down intergranular pressure solution. In addition, biogenic phosphate ions are a principal constituent of seawater and many upper crustal pore fluids. We show that increasing the phosphate ion concentration from 10^{-6} to 10^{-3} mol/l systematically and drastically reduces compaction strain rates in calcite, suggesting major effects of pore fluid phosphate concentrations on carbonate compaction and diagenesis rates in nature.

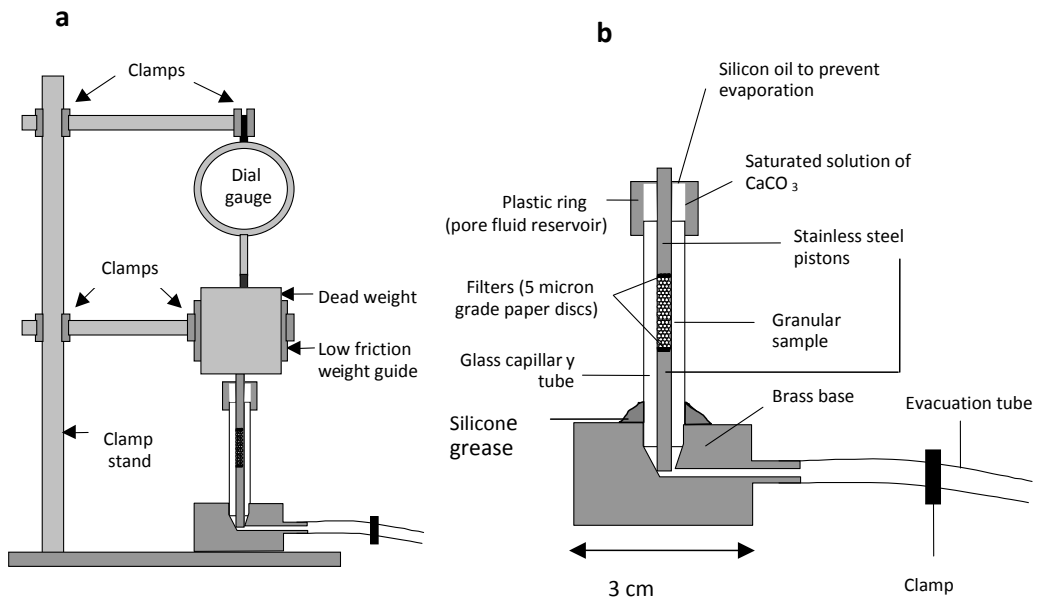


Figure 4.1. a) Compaction apparatus set up. b) Details of sample assembly.

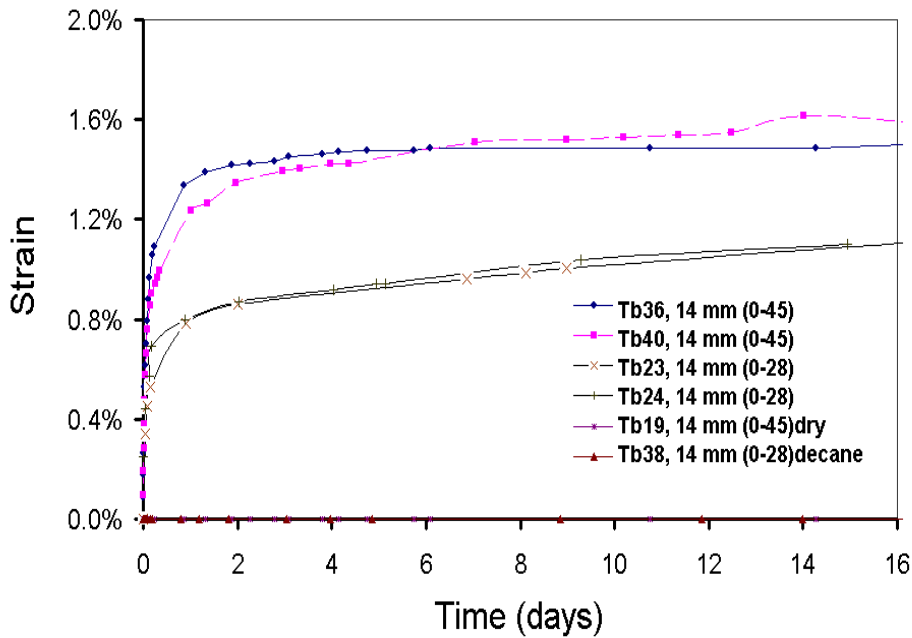


Figure 4.2. Compaction creep curves for super pure calcite samples loaded at applied stress (σ_c) of 4 MPa at room temperature. Samples loaded dry (Tb19) or with decane as pore fluid (Tb38) show no creep. Samples flooded with pre-saturated solution with no added phosphate (Tb36, 40, 23, 24) show significant compaction creep, with identical samples yielding closely reproducible behaviour (Tb36/40, Tb23/24). Note that while the average grain size (gs) of all of the wet tested samples represented here is $\sim 14 \mu\text{m}$, those with the wider grain size distribution or range (Tb36, 40: 0-45 μm) compacted more than those with a narrower distribution (Tb23, 24: 0-28 μm).

4.2 Experimental method

The test materials used in this study were super pure granular calcite (Merck 99.95% pure) with an average grain size of $15 \mu\text{m}$ (0-45 μm), and reagent grade granular calcite (Merck 99% pure) with an average grain size of $14 \mu\text{m}$ (0-28 μm). The main impurities in the reagent grade calcite were $\text{Sr} < 0.1\%$, $\text{Na} < 0.2\%$ and $\text{Mg} < 0.05\%$. It was necessary to use these two sources of calcite to obtain appropriate grain size fractions. The reagent grade material (0-28 μm , mean $14 \mu\text{m}$) was used without further treatment. The super pure samples were sieved into a fraction of 0-28 μm which was further separated into fractions of 6 ± 2 , 12 ± 4 , and $22 \pm 6 \mu\text{m}$ by sedimentation from suspension in deionized water. Unsieved

samples with an accordingly wide grain size distribution (0-45 μm , mean 15 μm) were also used. Grain size distributions were measured using a Malvern particle sizer and checked by SEM observation. More than 80% (weight) of the sieved and separated grain fractions fell within the expected ranges. Pre-saturated pore fluid solutions were prepared for each wet compaction experiment by adding excess calcite test material (same grain size fraction as the sample to be compacted) to deionized water and stirring for 48 hours at room temperature following the equilibration data presented by Sjöberg and Richard (1983). Pore fluids containing phosphate ion concentrations ranging from 10^{-6} to 10^{-3} mol/l were prepared by adding Na_2HPO_4 in varying amounts to the pre-saturated carbonate solution (cf. Reddy, 1977). No attempt was made to control the partial pressure of CO_2 during preparation or experiment. The calculated pH value in the phosphate-free CaCO_3 saturated solution is 8.27.

The experiments were performed using dead-weight compaction set-ups of the type illustrated in Figure 4.1a (De Meer et al., 1995; Zhang et al., 2002; Zhang and Spiers, 2005). Five such set-ups were used in parallel. The detailed sample assembly is showed in Fig 1b. A high precision dial gauge is used to measure upper piston displacement and hence sample compaction.

In all experiments, granular calcite samples of about 40 mg were first pre-compacted for 30 minutes under dry conditions at an applied axial stress (σ_e) of 8 MPa. The aim here was to obtain a well-controlled ‘starting aggregate’ with reproducible porosity and to eliminate purely physical grain rearrangement and brittle/plastic deformation effects during subsequent wet compaction at lower stresses. The samples were then unloaded and their length (taken as the initial length) was measured using a travelling microscope. The porosity of the pre-compacted samples (the initial porosity in Table 4.1) was calculated from the initial length, the weight of the sample and the density of calcite. Note that reagent grade samples showed porosities of $54.24 \pm 1.11\%$, whereas the super pure samples showed values of $49.09 \pm 1.93\%$.

After dry compaction, wet testing was carried out at applied axial stresses (σ_e) of 1-4 MPa. Details on the experimental procedure and accuracy of measurements can be found in Zhang and Spiers (2005). Note that the pore fluid pressure was maintained 1 atm in all wet experiments via the pore fluid reservoir (Figure 4.1b), so that the applied axial stresses (σ_e) are effective stresses in the rock mechanics sense. In each experiment, we recorded displacement vs. time data to construct compaction strain (e_v) versus time curves, and to determine how the compaction strain rate ($\dot{\epsilon}$) depended on stress, grain size and phosphate concentration. In this paper, strain is defined as the volumetric strain $e_v = -\Delta v / v_0$ where Δv is the total volume change of the sample at any instant and v_0 is the initial volume. Compaction strain rate is defined as $\dot{\epsilon} = -\dot{v} / v$, where $\dot{v} = dv / dt$ and v is the instantaneous volume of the sample.

ID	Material	Mean grain size(μm)	Pore fluid phase	Phosphate content mol/l	Applied stress (σ_c)	Initial porosity (%)	Final strain (%)
Tb19	Super pure	~14	Dry		4	51.8	0
Tb20	Super pure	~14	CaCO ₃ Solution	0	4	50.01	0.92
Tb21	Super pure	~14	CaCO ₃ Solution	0	1	49.8	0.42
Tb22	Super pure	~14	CaCO ₃ Solution	0	2	50.6	0.7
Tb23	Super pure	~14	CaCO ₃ Solution	0	3	50.9	1.13
Tb24	Super pure	~14	CaCO ₃ Solution	0	4	49.5	1.1
Tb36	Super pure	~14	CaCO ₃ Solution	0	4	50.9	1.5
Tb38	Super pure	~14	Decane		4	52.2	0
Tb40	Super pure	~14	CaCO ₃ Solution	0	4	49.6	1.5
Tb51	Super pure	~14	CaCO ₃ Solution	10 ⁻⁴	4	50.7	0.58
Tb52	Super pure	~14	CaCO ₃ Solution	10 ⁻³	4	51.7	0.23
Tb66	Super pure	12 \pm 4	Decane		4	46.7	0
Tb67	Super pure	~14	CaCO ₃ Solution	0	4	50.4	0.84
Tb69	Super pure	6 \pm 2	CaCO ₃ Solution	0	4	45.96	1.48
Tb70	Super pure	12 \pm 4	CaCO ₃ Solution	0	4	46.96	1.19
Tb71	Super pure	22 \pm 6	CaCO ₃ Solution	0	4	50.77	0.92
Tb78	Super pure	12 \pm 4	CaCO ₃ Solution	0	4	47.46	1.08
Tb79	Super pure	12 \pm 4	CaCO ₃ Solution	10 ⁻⁶	4	48.7	1.04
Tb80	Super pure	12 \pm 4	CaCO ₃ Solution	10 ⁻⁵	4	48	0.58
Tb81	Super pure	12 \pm 4	CaCO ₃ Solution	10 ⁻⁴	4	47.8	0.4
Tb82	Super pure	12 \pm 4	CaCO ₃ Solution	10 ⁻³	4	47.6	0.28
Tb88	Reagent	~14	CaCO ₃ Solution	0	4	53.68	2.81
Tb89	Reagent	~14	CaCO ₃ Solution	10 ⁻⁶	4	54.16	2.7
Tb90	Reagent	~14	CaCO ₃ Solution	10 ⁻⁵	4	54.87	2.39
Tb91	Reagent	~14	CaCO ₃ Solution	10 ⁻⁴	4	52.8	1.68
Tb92	Reagent	~14	CaCO ₃ Solution	10 ⁻³	4	54.85	0.8
Tb93	Reagent	~14	CaCO ₃ Solution	0	4	52.7	2.7
Tb94	Reagent	~14	CaCO ₃ Solution	10 ⁻⁶	4	56	2.57
Tb95	Reagent	~14	CaCO ₃ Solution	10 ⁻⁵	4	54.7	2.19
Tb96	Reagent	~14	CaCO ₃ Solution	10 ⁻⁴	4	53.26	1.93
Tb97	Reagent	~14	CaCO ₃ Solution	10 ⁻³	4	55.4	1.18
Tb98	Reagent	~14	Decane		4	53.2	0.05

Table 4.1. List of experiments.

4.3 Mechanical results and microstructure

All 32 experiments performed in this study are listed in Table 4.1. Dry pre-compaction at 8 MPa produced a few percent of instantaneous strain in all cases. Samples subsequently loaded at 1-4 MPa and then flooded with chemically inert decane, or loaded dry, showed no

measurable compaction creep (Figure 4.2, Figure 4.3a). However, those flooded with pre-saturated CaCO_3 solutions typically compacted by 0.5-1.5 % within 2-14 days, as illustrated in Figure 4.2 and Figure 4.3. Figure 4.2 shows results for super pure calcite samples, with roughly the same mean grain size (14 μm) but different grain size distributions (range 0-45 μm vs. 0-28 μm) that were tested under otherwise identical conditions, i. e. wet with no phosphate ions in solution. It is clear from these data that wet samples with the same grain size distribution yield reproducible compaction creep curves. However, the samples with the narrower grain size distribution compacted significantly less than those with wider distribution. Figure 4.3a shows the compaction creep curves obtained for super pure calcite samples with grain size fractions of 6 ± 2 , 12 ± 4 , and 22 ± 6 μm , tested in the presence of saturated CaCO_3 solution, again with no added phosphate. For these samples, the strain rates at fixed strains, and the total strains achieved, increase systematically with decreasing grain size. Figure 4.3b shows the effect of applied stress on strain rate at fixed strains, and on total strains achieved, for super pure material with a grain size of 12 ± 4 μm . The data clearly demonstrate a direct relationship.

Compaction curves obtained for the reagent grade and super pure calcite samples tested with pore fluid phosphate concentrations varying from zero through 10^{-6} to 10^{-3} mol/l of added Na_2HPO_4 are presented in Figure 4.4a and 4.4b. For both materials, the compaction rates at fixed strains (approx. i.e. fixed aggregate structure), and the total strains achieved, decrease systematically with increasing concentration of phosphate ions in the pore fluid, though all other experimental conditions are identical. Note that the reagent grade samples compacted to larger strains than the super pure calcite samples, possibly reflecting the higher initial porosities of the reagent grade samples ($54.24\pm 1.11\%$ vs. $49.09\pm 1.93\%$) and/or their wider grain size distribution.

The overall microstructure of wet compacted samples, of dry compacted samples and of samples compacted with decane, is similar. All show a porous, granular microstructure consisting of aggregate rhombohedral grains (Figure 4.5) with the grain size of the parent powder. Crushes are rare. Some grain corners in the wet (phosphate-free) samples do appear truncated, suggesting possible mass removal (Figure 4.5). These features were not seen in other samples.

4.4 Discussion

4.4.1 Behaviour during dry compaction

Pre-compaction under dry conditions, at an axial stress of 8 MPa, caused a few percent (2-3%) instantaneous strains. This presumably involves grain rearrangement, and intergranular sliding, micro-cataclasis (grain contact crushing/granulation), and minor crystal plastic deformation, or twinning, as well as an elastic contribution (see also Zhang et al., 2002; Zhang and Spiers, 2005). When samples were re-loaded dry at the lower axial stress of 1-4 MPa, almost no instantaneous compaction or compaction creep were measured. The decane-flooded samples showed similar behaviour. We therefore infer that dry pre-compaction produced an aggregate which was “locked” against deformation at lower stress, under both dry and decane-flooded conditions, and that time-dependent creep

by intracrystalline plasticity (De Bresser et al., 2002) or subcritical crack growth mechanisms (Atkinson, 1982, 1984; Atkinson and Meredith 1989) was negligible in dry and decane flooded experiments at 4 MPa stress.

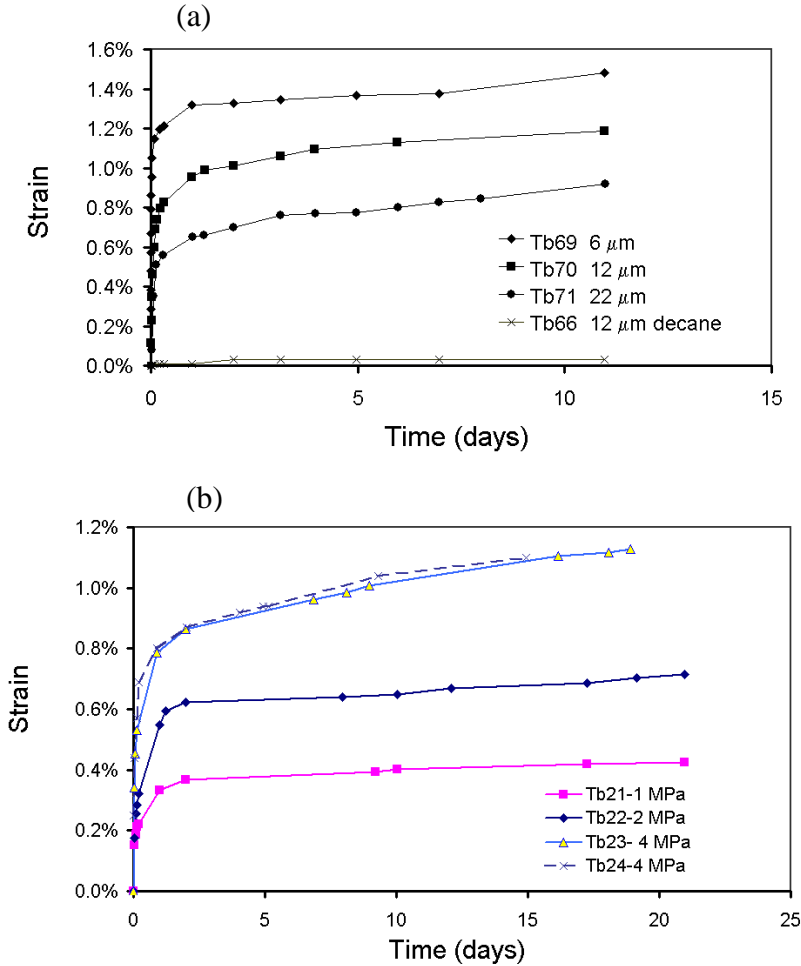


Figure 4.3. Compaction creep curves for super pure calcite samples tested at room temperature using pre-saturated solution as pore fluid, with no added phosphate. Data for decane-flooded sample shown for comparison. a) Effect of mean grain size of several fractions. Applied effective stress $\sigma_e = 4$ MPa. Note the increase in compaction with decreasing grain size. b) Effect of applied stress on compaction of samples with a mean grain size of 14 μm.

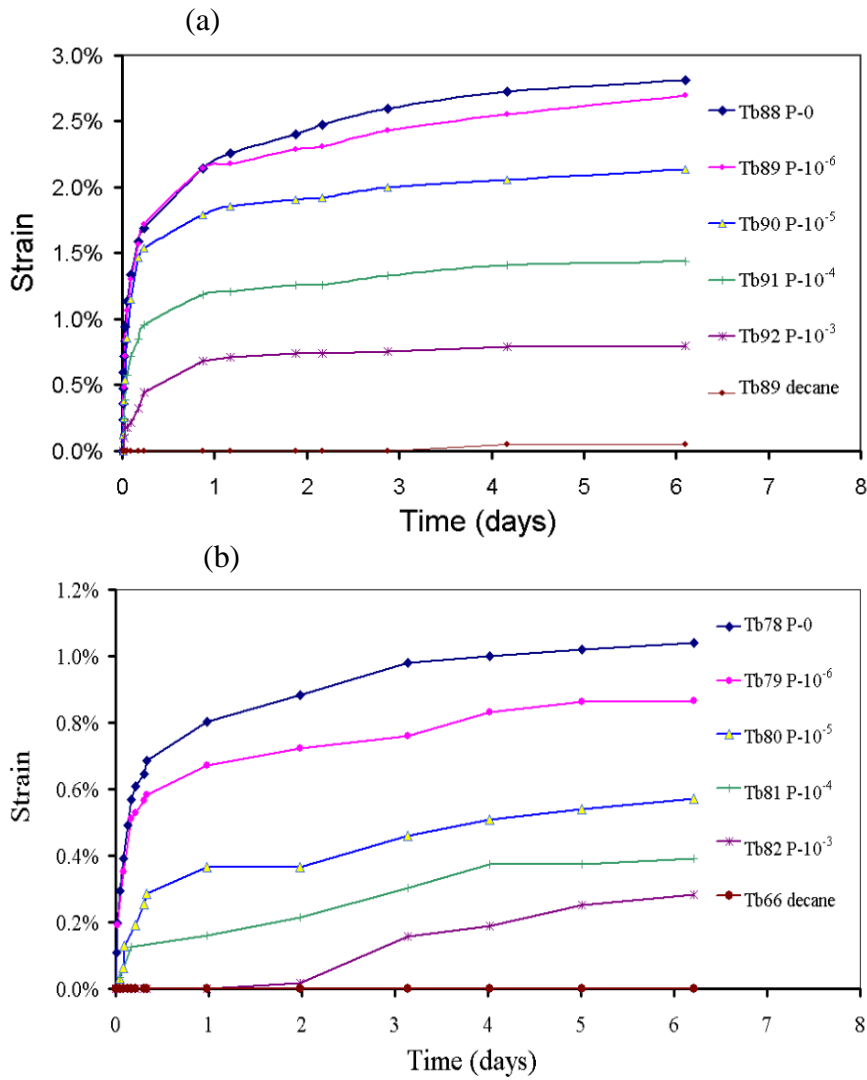


Figure 4.4. Effects of pore fluid phosphate concentration (added Na_2HPO_4) on compaction creep of reagent grade and super pure calcite samples. a) Reagent grade samples with mean grain size $\sim 14 \mu\text{m}$. b) Super pure calcite samples with grain size $12 \pm 4 \mu\text{m}$. In both cases, phosphate concentrations in the calcite-saturated pore fluid phase are shown in units of mol/l. Experimental conditions: $\sigma_c = 4$ MPa, room temperature. Data for decane-flooded samples are shown for comparison.

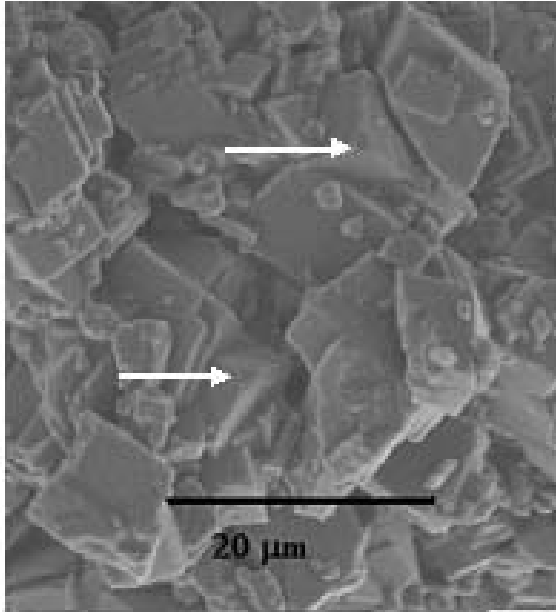


Figure 4.5. SEM micrograph showing the fracture surface of wet compacted super pure sample (Tb36) with no added phosphate ions in the pore fluid. Some of the grain corners show truncated features suggesting possible mass removal.

4.4.2 Wet compaction behavior

Unlike the dry and decane-flooded samples, samples tested wet with no phosphate ions showed significant compaction. The behavior of the decane-flooded samples demonstrates that the initially dry, pre-compacted or “locked” aggregate cannot be “unlocked” by purely physical effects related to the addition of a fluid (e.g. surface energy or intergranular lubrication effects) that might facilitate intergranular sliding. Since our experimental conditions do not favour solid-state plastic deformation in calcite (Rutter, 1983; De Bresser et al., 2002) and since no creep occurred in our dry or decane flooded samples, solid-state creep processes can be eliminated. The creep mechanism operating in our wet samples must therefore be a water- or solution-enhanced deformation mechanism. Given the observed effects of grain size and stress on compaction behavior, which are qualitatively consistent with the predictions of IPS theory (Rutter, 1983; Lehner, 1990, 1995; De Meer and Spiers, 1999), plus the grain contact truncation features illustrated in Figure 4.5, IPS accompanied by intergranular sliding accommodation is the most likely candidate (Zhang and Spiers, 2005). Note that no other mechanism of low temperature deformation shows similar effects

of fluid addition and grain size (e. g. Barber, 1990). If IPS is the dominant deformation mechanism, the compaction rate should be influenced by adding solute species that are known to slow down or speed up the dissolution or precipitation reaction. The fact that compaction is indeed inhibited by adding phosphate ions to the pore fluid in our wet experiments thus suggests that wet compaction must have involved processes of dissolution, diffusion and precipitation, supporting our inference of IPS with accommodation by intergranular sliding.

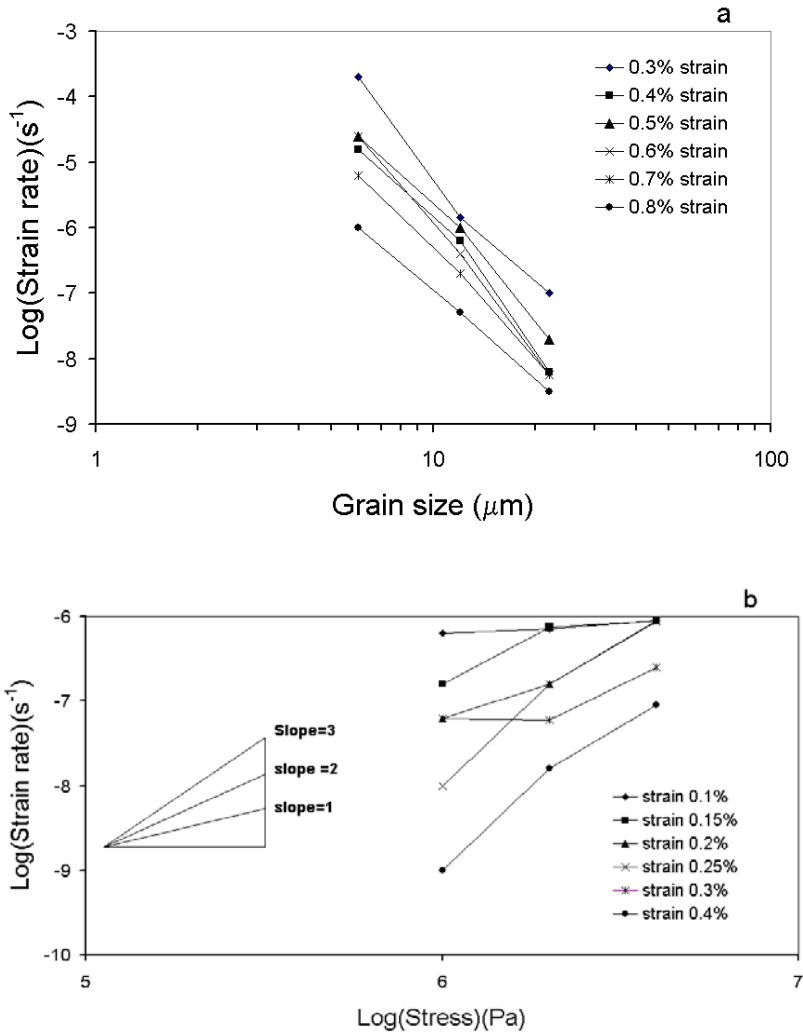


Figure 4.6. Log-log plots showing the effects of a) grain size and b) applied stress on the compaction strain rate obtained from experiments on super pure calcite samples with no added phosphate. Data derived from compaction curves given in Figure 4.3 by computing strain rate at fixed values of volumetric strain (%). Applied stress in 4.6a is 4 MPa; Grain size in 4.6b is 14 μm .

Another fluid-enhanced deformation mechanism which might have operated in our wet experiments is subcritical cracking by a stress corrosion mechanism (Atkinson 1982, 1984). Subcritical cracking can potentially cause grain and/or grain-contact failure (crushing) at low stresses, if water is present in the sample, thus producing time-dependent compaction creep. The effect of phosphate ions in inhibiting compaction suggests that dissolution and precipitation of calcite are involved, e.g. through intergranular pressure solution. However, if subcritical cracking in calcite involves similar interfacial reactions at crack tips, as suggested by Atkinson (1984), we cannot rule out the possibility that creep in our wet samples was caused by subcritical cracking. On the other hand, finer grain size tends to promote intergranular pressure solution (Rutter, 1983; De Meer and Spiers, 1999)(Figure 4.3a) whereas it tends to slow down creep by grain cracking (Zhang et al., 1990). Moreover, acoustic emission (AE) measurements performed in selected runs (see also Zhang et al., 2002) showed no evidence for brittle deformation in wet samples. Hence, IPS with intergranular sliding accommodation remains the most likely process responsible for creep of our wet samples.

4.4.3 Experiments vs. theory

It is well established that IPS is a coupled chemical-mechanical process driven by stress and achieved (in a chemically closed system) through the serial processes of dissolution at highly stressed grain contacts, diffusion of material out of the grain contact through a solution film or microscale channel network, and precipitation on pore walls (Rutter, 1976, 1983; Raj and Chyung, 1981; Raj 1982; Lehner, 1990, 1995; De Meer and Spiers, 1999; Spiers et al., 2004). In a chemically closed system, such as in our experiments, the slowest of these three processes controls the total strain rate, at steady state. Following previous work (see De Meer and Spiers 1995, 1999; Niemeijer et al., 2002), the theoretical IPS creep equations for uniaxial (or hydrostatic) compaction of a pack of spherical grains at low stress can be written:

$$\dot{\epsilon}_s = A_s k_s \frac{\sigma_e^n}{d} f_s(\phi) \quad \text{for dissolution control} \quad (4.3)$$

$$\dot{\epsilon}_d = A_d k_d \frac{\sigma_e}{d^3} f_d(\phi) \quad \text{for diffusion control} \quad (4.4)$$

$$\dot{\epsilon}_p = A_p k_p \frac{\sigma_e^m}{d} f_p(\phi) \quad \text{for precipitation control} \quad (4.5)$$

Here $\dot{\epsilon}_x$ represents volumetric strain rate as defined previously. A_s , A_d , and A_p are constants embodying geometric factors related to the packing of the granular aggregate and to loading geometry, k_s and k_p are temperature-dependent dissolution and precipitation reaction rate coefficients, k_d is a temperature-dependent term incorporating the product of

grain boundary diffusivity (D), solid solubility (C) and average grain boundary fluid thickness (S), σ_e is the applied effective stress, d is grain size, and ϕ is porosity. The exponents n and m respectively represent the order of the dissolution or precipitation velocity vs. driving force relation for the corresponding interfacial reactions, and thus typically take values of 1-3 depending on reaction mechanism (De Meer and Spiers 1999; Niemeijer et al., 2002). The $f_x(\phi)$ are porosity-dependent functions that describe the effects of changing aggregate geometry during compaction, leading to decreasing strain rates with decreasing porosity (or increasing strain). Note that for low strains (<15%), the porosity dependence of $\dot{\epsilon}$ embodied by $f(\phi)$ can be represented as $f(\phi) \propto \frac{1}{e_v^q}$, where e_v is

volumetric strain and where $q=1$ for dissolution control and 2 for diffusion and precipitation control (De Meer and Spiers, 1999).

From equations (4.3) to (4.5), it is clear that IPS strain rates in a chemically closed system are predicted to be inversely proportional to grain size to the power of 1 for interfacial reaction control and 3 for diffusion control. The compaction creep curves of Figure 4.3, obtained for super pure samples flooded with saturated CaCO_3 solution without added phosphate, show that both decreasing grain size and increasing applied stress promote compaction. To compare our results with the theoretical equations (4.3-4.5), we have used the data presented in Figure 4.3 to construct log-log plots showing the dependence of compaction strain rate on grain size and stress (Figure 4.6), at specific values of strain (hence at roughly constant porosity). From Figure 4.6a, it is evident that although the observed dependence of strain rate on grain size is broadly in agreement with pressure solution theory, the sensitivity (i. e. the slope of the data sets in Figure 4.6a) is larger (4-5) than the theoretical predictions of 1 or 3 (equations 4.3-4.5). The high sensitivity of strain rate to grain size seen in Figure 4.6a (slope of 4-5) more closely resembles the diffusion controlled IPS model (slope 3) than the reaction-controlled models (slope 1). However, we have seen from the data of Figure 4.2 that grain size distribution width has a strong effect on strain rate, with wider distribution promoting faster creep. This might easily influence the apparent sensitivity of strain rate to mean grain size seen in Figure 4.6a, particularly if distribution width systematically changes with mean grain size. Such an effect of grain size distribution width has recently been predicted on theoretical grounds for strongly grain-size-sensitive creep processes (Ter Heege et al., 2004), but has yet to be rigorously incorporated into IPS models. Note however that the high sensitivity of strain rate to grain size seen in our experiments on phosphate-free samples could also reflect variations in initial porosity and grain packing from sample to sample. Clearly, more work is needed to ascertain the possible role of effects of grain size distribution and initial porosity.

Referring to Figure 4.6b, the rather low sensitivity of strain rate to stress (slope =1-3) is broadly consistent with pressure solution theory predicted slope 1-3, as opposed to expectation for plastic deformation mechanism whereby the stress sensitivity in calcite at room temperature is expected to be $\gg 3$. However, the strong variability in slope seen in our strain rate versus stress data (Figure 4.6b) makes it difficult to relate our data to any specific IPS model, such as reaction versus diffusion control. Again, the lack of precise agreement between experiment and theory may reflect variations in grain size distribution

and/or initial porosity from sample to sample. We are unable, then, on the basis of a comparison between theory and experiment, to obtain a good enough match to assess the rate controlling process of the proposed mechanism of IPS in the samples compacted without phosphate in the pore fluid.

4.4.4 Effect of phosphate ions on the rate of compaction

From the theory of pressure solution (equations 4.3-4.5), it is evident that IPS strain rates will tend to be influenced by pore fluid chemistry when interfacial reactions are rate-limiting, because such reactions are generally very sensitive to impurities in solution (Reddy, 1977; Meyer, 1984; Dove and Hochella, 1993; Jonasson et al., 1996; Katsifaras and Spanos, 1999; Davis et al., 2000; Plant and House, 2002). If one could decrease the kinetic coefficients k_s or k_p in equations 4.3 or 4.5, by adding a reaction inhibitor to the pore fluid solution phase, one of the interfacial reactions (precipitation/dissolution) must eventually become rate limiting. The strain rate will then become proportional to the controlling kinetic coefficient. Thus the dependence of measured strain rate on the concentration of reaction inhibitor can potentially reveal a) if IPS is operating and b) which kinetic process is the rate-limiting step.

Phosphate ions are one of the most important and well-studied inhibitors for calcite precipitation (Reddy, 1977; Meyer, 1984; Dove and Hochella, 1993; Jonasson et al. 1996; Katsifaras and Spanos, 1999; Plant and House, 2002). Many authors (Reddy, 1977; Meyer, 1984; Dove and Hochella, 1993; Plant and House, 2002) have inferred that retardation of calcite growth by phosphate-bearing ions involves blockage of crystal growth sites (i. e. the atomic scale attachment sites) on the calcite surface. Reddy (1977) studied the effects of phosphate on the precipitation of calcite, and found that phosphate ions in a concentration of only 2×10^{-6} mol/l of added Na_2HPO_4 could decrease the precipitation rate by a factor of 2. His experimental data fit a simple Langmuir model for adsorption of phosphate onto the calcite surface. The general equation obtained by Reddy (1997) for the effect of phosphate on k_p can be written as

$$\frac{k_0}{k_0 - k_p} = 1 + \frac{k_2}{k_1 C_{phosp}} \quad (4.6a)$$

or

$$\frac{k_p}{k_0} = \frac{a}{a + C_{phosp}} \quad (4.6b)$$

where k_0 (in $\text{mol} \cdot \text{m}^{-2} \cdot \text{s}^{-1}$) is the crystal growth rate coefficient in the absence of phosphate, k_p is now the precipitation rate coefficient in the presence of phosphate, k_1 and k_2 are the

adsorption and desorption rate constants for phosphate ions, C_{phosp} (in mol/l) is the concentration of phosphate ions added to the pore fluid (in the form of Na_2HPO_4), and $a=k_2/k_1=1.9\times 10^{-6}$ mol/l (Reddy, 1977). Meyer (1984) obtained closely similar results for the inhibition of phosphate on calcite precipitation as Reddy (1977).

In all of our experiments where phosphate ions were added, compaction was retarded compared to the phosphate-free samples, as shown in Figure 4.4. The effect of adding a phosphate concentration of 10^{-6} mol/l to pure solution was to reduce compaction rate at a given strain by a factor of ~ 2 , as observed by Reddy 1977 for the calcite precipitation reaction. Figure 4.7 shows the dependence of strain rate on strain for samples containing phosphate concentrations from 10^{-6} to 10^{-3} mol/l in the pore fluid, as derived from the compaction curves of Figure 4.4. These data have been used to construct a plot showing the effect of phosphate concentration on strain rate at constant volumetric strain. The results are shown in Figure 4.8, where the strain rate ($\dot{\epsilon}$) measured for phosphate bearing samples is normalized to the strain rate ($\dot{\epsilon}_0$) measured for phosphate-free control samples. Note that at a fixed strain, all similar samples have roughly the same grain-pore structure, as their initial porosity is nearly the same. The data thus show that an increase in phosphate concentration from 10^{-6} to 10^{-3} mol/l causes a decrease in creep rate of around 2 orders of magnitude, in both super pure and reagent grade calcite samples. If IPS is the dominant deformation mechanism, equations 3-5 then imply that the parameters $k_d=DCS$, k_p , or k_s must have been influenced by phosphate concentration. The diffusion product ($k_d=DCS$) is not likely to be strongly dependent on the phosphate concentration in the pore fluid, because the diffusion coefficients of all involved ions (Ca^{2+} , CO_3^{2-} , HPO_3^{2-} and PO_4^{3-} etc.) are all close in water. Calculations performed using MINEQL show that the solubility of calcite in the presence of phosphate does decrease slightly (i. e. by 10-15%). This is too small an effect to explain the present results. However, the precipitation rate coefficient (k_p), is known to depend on phosphate concentration as specified in Equation (4.6). Added to Figure 4.8 is a curve showing the decrease of precipitation rate coefficient with phosphate concentration as expressed by equation (4.6b) due to Reddy (1977). The similarity in the effect of phosphate concentration on the normalized strain rate ($\dot{\epsilon}/\dot{\epsilon}_0$) and the normalized precipitation coefficient (k_p/k_0) is striking. With reference to equations (4.5 and 4.6b), this suggests that compaction of our phosphate-bearing samples may have occurred by precipitation limited IPS. It is well known in the literature that phosphate in solution can also inhibit dissolution of calcite by blocking active attachment sites (Berner and Morse, 1974; Walter and Hanor, 1979; Sabbides and Koutsoukos, 1993; Alkattan et al., 2002). Unfortunately, there are no quantitative data on phosphate inhibition of calcite dissolution in the literature at our pH (pH=8.27) conditions, although Alkattan et al. (2002) have reported an effect at pH ≤ 2 . Our experiments cannot therefore discriminate whether the reduction of compaction rates is caused by inhibition of precipitation or dissolution, though some kind of interfacial reaction control seems likely.

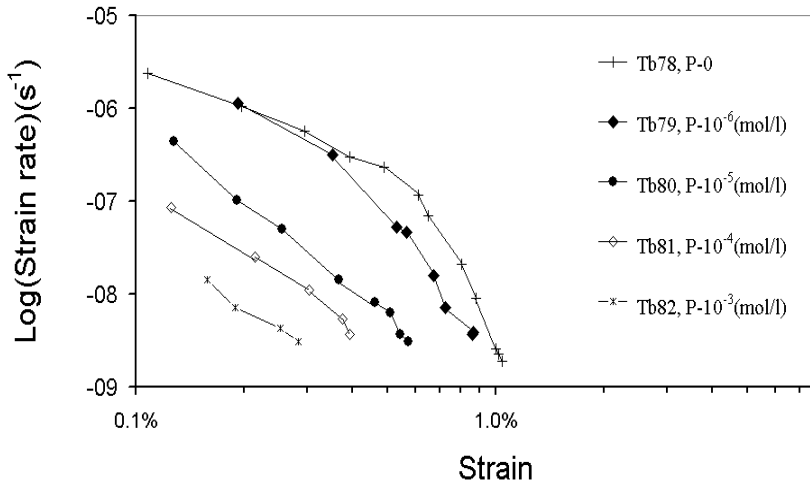


Figure 4.7. Log-log plot of compaction strain rate vs. strain for super pure calcite compacted wet with the added phosphate concentrations shown. The data are derived from those shown in Figure 4b. Note the retarding effect of phosphate on strain rates compared at fixed strains.

4.4.5 Implications

As we have inferred above, the compaction behaviour of calcite in our experiments was probably dominated by intergranular pressure solution. The fact that strain rates decreased with increasing phosphate concentration in the pore fluid, in the same way as the rate coefficient for calcite precipitation, suggests that the rate controlling step of IPS of calcite with phosphate in the pore fluid may be calcite precipitation. Coupling equations (4.5) and (4.6) accordingly offers a basis for constructing a precipitation controlled IPS compaction 'law' for calcite with varying phosphate content in the pore fluid solution. However, the lack of quantitative data on the effect of phosphate on calcite dissolution rate, makes it at present impossible to judge if a dissolution controlled law would be more appropriate. In addition, the rate limiting step of IPS in our samples flooded with pure CaCO_3 solution, and possible effects of grain size distribution width and initial porosity, remain unclear. The strong grain size dependence of strain rate might even imply diffusion control in samples with zero phosphate ions in the pore fluid.

Clearly then, further studies still need to be done to fully understand IPS in calcite, to constrain the rate limiting steps and to obtain a mechanism-based rate law for compaction and deformation of calcite by IPS. However, this study does show that IPS in calcite is strongly retarded by low concentrations of phosphate ions in the pore fluid and is probably precipitation- or perhaps dissolution-controlled under these conditions. A similar retarding effect of Mg^{2+} ions was observed in our previous compaction work on calcite (Zhang et al., 2002; Zhang and Spiers, 2005). In nature, the phosphate content of pore fluids is related to biological productivity and organic reactions occurring in the pore fluid or pore fluid source

region (Föllmi, 1996). It therefore seems likely that IPS in calcite will be relatively rapid in environments where the pore fluid is meteoric or organic poor, and much slower where the pore fluid is derived from seawater or is phosphate rich due to organic reactions or biological activity. Accordingly hydrocarbon maturation may also influence the process. Clearly, numerical modeling of the process of IPS and coupled fluid-mass transport in carbonate rocks at different scales must ultimately take into account such effects of pore fluid chemistry, if realistic results are to be obtained. Interestingly, recent studies on quartz sediments point to interface reaction control of IPS in experiment and nature and hence a likely role of pore fluid impurities (Spiers et al., 2004). In particular, precipitation has recently been inferred to be the likely rate controlling step for the case of quartz in sedimentary basins by Walderhaug and co-workers (Bjorkum et al., 1998; Lander and Walderhaug, 1999; Walderhaug, 2000).

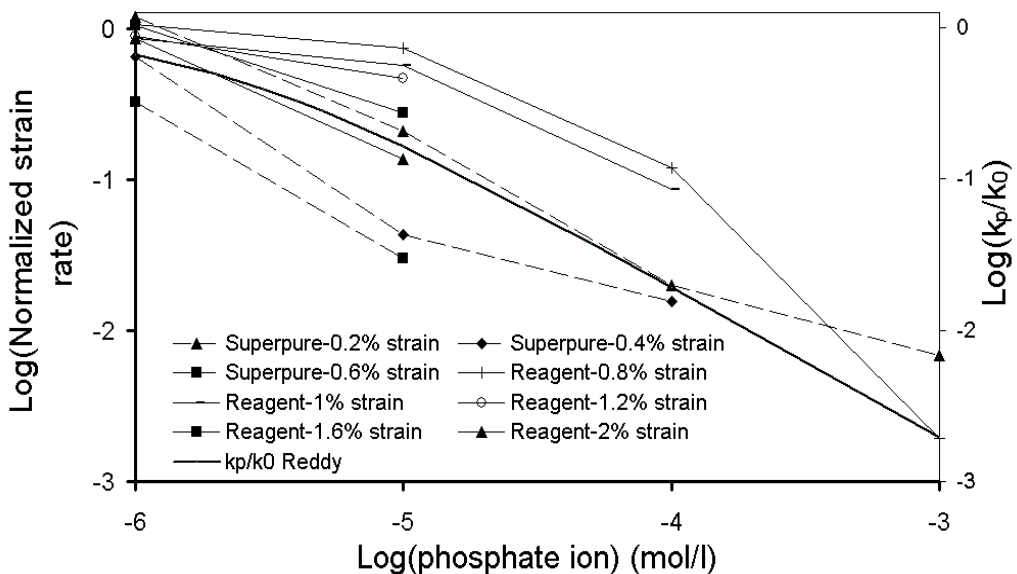


Figure 4.8. Log-log plot showing normalized compaction strain rate versus phosphate concentration for samples compacted wet with Na_2HPO_4 added to the pore fluid. The strain rate ($\dot{\epsilon}$) is normalized with respect to the value ($\dot{\epsilon}_0$) measured at zero phosphate content for super pure (Tb 78) and reagent grade calcite samples (Tb88). Applied stress 4 MPa; The effect of phosphate content on the normalized precipitation rate coefficient (k_p/k_0) for calcite found by Reddy (1977) is shown for comparison (heavy line).

4.5 Summary and conclusions

Uniaxial compaction creep experiments have been carried out on fine-grained calcite powders at applied stress of 1–4 MPa, at room temperature, and with various phosphate ion concentrations in the pore fluid from zero through 10^{-6} to 10^{-3} mol/l. The following main conclusions can be drawn.

1) Measurable rates of time-dependent compaction occur in wet, fine-grained material under the experimental conditions employed. On the basis of the main effects and trends seen in our mechanical data (effect of fluid, grain size and stress), the dominant mechanism of deformation is inferred to be intergranular pressure solution with associated intergranular sliding.

2) An increase in phosphate concentration in the pore fluid from 0 to 10^{-6} mol/l decreases IPS strain rates by a factor of ~ 2 . Further increase in concentration from 10^{-6} to 10^{-3} mol/l decreases IPS strain rates by an additional 2 orders of magnitude. This reduction in strain rate is similar to the reduction in the calcite precipitation reaction rate caused by adding phosphate ions, suggesting that precipitation on pore walls is the rate limiting step in samples tested using a phosphate-bearing pore fluid. Note however, that dissolution reaction control cannot be eliminated. The rate controlling process in phosphate free samples remains unclear, as the observed compaction behaviour does not exactly match theoretical models for either diffusion or reaction controlled IPS. Some of these discrepancies between theory and experiment may reflect effects of grain size distribution width and initial porosity not accounted for in existing models. Further work is needed to shed light on this.

3) Our results imply that IPS and associated porosity reduction rates in calcite sediments may be strongly reduced when pore fluids are enriched in phosphates as a result of high biological productivity or a seawater origin. Such effects may strongly influence the progress of diagenetic porosity/permeability as well as fluid and hydrocarbon migration in carbonate sediments.

4) The present data offer a starting point for developing a constitutive model for compaction of calcite by IPS in the presence of phosphate ions, but more data are needed to confirm the rate controlling process, as indicated under (2) above.

5) Interactions between pore fluid chemistry and mechanical compaction processes such as IPS can potentially reveal details of deformation mechanisms such as the rate limiting steps of pressure solution and hence deserve more attention in future research.

4.6 References

- Alcantar N., J. Israelachvili and J. Boles (2003), Forces and ionic transport between mica surfaces: implications for pressure solution. *Geochim. Cosmochim Acta* 67, 1289-1304.
- Alkattan M., E. H. Oelkers, J. L. Dandurand and J. Schott (2002), An experimental study of calcite dissolution rates at acidic conditions and 25 °C in the presence of Na_3PO_3 and MgCl_2 . *Chem. Geol.* 190, 291-302.
- Atkinson B. K. (1982), Subcritical crack propagation in rocks: theory, experimental results and application. *J. Struct. Geol.* 4, 41-56.
- Atkinson B. K. (1984), Subcritical crack growth in geological materials. *J. Geophys. Res.* 89, 4077-4114.
- Atkinson B. K. and P. G. Meredith (1989), The theory of subcritical crack growth with applications to minerals and rocks. In: Atkinson B. K. (eds) *Fracture Mechanics of Rock*. Academic Press London, 111-166.

- Aydin A. (2000), Fractures, faults, a hydrocarbon entrapment, migration and flow. *Marine and Petroleum Geology* 17, 797-814.
- Baker P. A., M.Kastner, J. D. Byerlee and Lockner D. A. (1980), Pressure solution and hydrothermal recrystallization of carbonate sediments- an experimental study. *Marine Geology* 38, 185-203.
- Barber D. J. (1990), Regimes of plastic deformation - processes and microstructures: an overview.- In: BARBER, D.J., MEREDITH, P.G.: *Deformation processes in Minerals, Ceramics and rocks*, Unwin Hyman, London, 138-178.
- Bathurst R.G. C. (1958), Diagenetic fabrics in some British Dinantian limestones. *Liverpool and Manchester Geology* 2, 11-36.
- Berner R. A., and J. W. Morse (1974), Dissolution kinetics of calcium carbonate in sea water IV. Theory of calcite dissolution. *Am. J. Sci.* 274, 108-134.
- Bjorkum P.A., E. H. Oelkers and P. H. Nadeau (1998), Porosity prediction in quartzose sandstones as a function of time, temperature, depth, stylolite frequency, and hydrocarbon saturation. *AAPG Bulletin* 82, 637-648.
- Bos B. and C. J. Spiers (2002), Fluid-assisted healing processes in simulated, gouge-bearing faults: Insights from experiments on rock-analogue material. *Pure and Appl. Geophys.* 159, 2537-2566.
- Bos B. and C. J. Spiers (2002), Frictional-viscous flow of phyllosilicate-bearing fault rock: Microphysical model and implications for crustal strength profiles. *J. Geophys. Res.* 107, B2, 10.1029/2001JB000301.
- Byerlee J. L. (1993), Model for episodic flow of high pressure water in fault zones before earthquakes. *Geology* 21, 303-306.
- Chester J. S., S. C. Lenz, F. M. Chester, and R. A. Lang (2004), Mechanisms of compaction of quartz sand at diagenetic conditions. *Earth and Planet. Sci. Lett.* 220, 435-451.
- Davis K. J., P. M. Dove and J. J. Yoreo (2000), The role of Mg^{2+} as an impurity in calcite growth. *Science* 290, 1134-1137.
- DeBresser J. H. P., B. Evans and J. Renner (2002), On estimating the strength of calcite rocks under natural conditions, in: S. De Meer, M. R. Drury, J. H. de Bresser, G. M. Pennock, (Eds), *Deformation Mechanisms, Rheology and Tectonics: Current Status and Future Perspectives*, Geological Society, London, Special Publications, 200, 309-329.
- De Meer S. and C. J. Spiers (1995), Creep of wet gypsum aggregates under hydrostatic loading conditions. *Tectonophysics* 245, 171-184.
- De Meer S. and C. J. Spiers (1997), Uniaxial compaction creep of wet gypsum aggregates. *J. Geophys. Res.* 102, 875-891.
- De Meer S. and C. J. Spiers (1999), Mechanisms and kinetics of creep by intergranular pressure solution. in: B. Jamtveit, P. Meakin (Eds.), *Growth, Dissolution and Pattern Formation in Geosystems*, Kluwer Academic Publishers, Dordrecht, 345-363.
- De Meer S., C. J. Spiers, C. J. Peach and T. Watanabe (2002), Diffusive properties of fluid-filled grain boundaries measured electrically during active pressure solution. *Earth and Planet. Sci. Lett.* 200, 147-157.

- De Meer, S., C. J. Spiers, and S. Nakashima (2005), Structure and diffusive properties of fluid-filled grain boundaries: An in-situ study using infrared (micro) spectroscopy, *Earth and Planet. Sci. Lett.* 232, 403-414. Doi:10.1016/j.epsl.2004.12.030.
- DenBrok S. W. J. and J. Morel (2001), The effects of elastic strain on the microstructure of free surface of stressed minerals in contact with an aqueous solution. *Geophys. Res. Lett.* 28, 603-606.
- Dewers T and A. Hajash (1995), Rate law for water-assisted compaction and stress-induced water-rock interaction in sandstones. *J. Geophys. Res.* 100, B7, 13,093-13,112.
- Dove P. M. and M. F. Hochella (1993), Calcite precipitation mechanisms and inhibition by orthophosphate: In situ observations by Scanning Force Microscopy. *Geochim. Cosmochim Acta* 57, 705-714.
- Durney D. W. (1972), Solution transfer, an important geological deformation mechanism. *Nature* 235, 315-317.
- Dysthe D. K., Y. Podladchikov, F. Renard, J. Feder and B. amtveit, (2002), Universal Scaling in transient creep. *Phys. Rev. Lett.* 89, 246102(1)-(4).
- Dysthe D. K., F. Renard, F. Porcheron and B. Rousseau (2002), Fluid in mineral interfaces- molecular simulations of structue and diffusion. *Geophys. Res. Lett.* 29, 13(1)-13(4).
- Elliot D. (1973), Diffusion flow laws in metamorphic rocks. *Bull. Geol. Soc. Am.* 84, 2645-2664.
- Föllmi K. B. (1996), The phosphorus cycle, phosphogenesis and marine phosphate-rich deposits. *Earth Science Reviews* 40, 55-124
- Gundersen E., D. Dysthe, F. Renard, K. Bjørlykke and B. Jamtveit (2002), Numerical modelling of pressure solution in sandstone, rate-limiting processes and the effect of clays, in: S. de Meer, M.R. Drury, J.H.P. de Bresser and G.M. Pennock (Eds), Deformation Mechanisms, Rheology and Tectonics: Current Status and Future Perspectives, *Geol. Soc. London, Spec. Publ.*, 200, 41-60.
- Hellmann R., P. J. N. Renders, J. P. Gratier and R. Guiguet (2002), Experimental pressure solution compaction of chalk in aqueous solutions Part 1, Deformation behavior and chemistry, in: R. Hellmann, S. A. Wood, Water-Rock Interaction, Ore Deposits, and Environmental Geochemistry: A Tribute to David A. Crerar, *The Geochemical Society, Special Publication* 7, 129-152.
- Hickman S. H., R. Sibson and R. Bruhn (1995), Introduction to special section: mechanical involvement of fluid in faulting. *J. Geophys. Res.* 100, 12831-12840.
- Hubbert M. K. and W. W. Rubey (1959), Role of fluid pressure in mechanics of overthrust faulting. *Bull. Geol. Soc. Am.* 70, 115-166.
- Heydari, E. (2000), Porosity loss, fluid flow, and mass transfer in limestone reservoirs: application to the upper Jurassic Smackover Formation, Mississippi. *AAPG Bulletin* 84, 100-118.
- Jonasson R. G., K. Rispler, B. Wiwchar, W. D. Gunter (1996), Effect of phosphate inhibitors on calcite nucleation kinetics as a function of temperature using light scattering in an autoclave. *Chem. Geol.* 132, 215-225.
- Karner S. L., C. Marone and B. Evans (1997), Laboratory study of fault healing and lithification in simulated fault gouge under hydrothermal conditions. *Tectonophysics* 277, 41-55.

- Katsifaras A. and N. Spanos (1999), Effect of inorganic phosphate ions on the spontaneous precipitation of vaterite and on the transformation of vaterite to calcite. *J. Cryst. Growth*, 204, 183-190.
- Lander R. H., O. Walderhaug (1999), Predicting porosity through simulating sandstone compaction and quartz cementation. *AAPG Bulletin* 83, 433-449.
- Lehner F. K. (1990), Thermodynamics of rock deformation by pressure solution, in: D. Barber, P. Meredith (Eds), *Deformation Processes in Minerals, Ceramics and Rocks*, Unwin Hyman, London, 296-333.
- Lehner F. K. (1995), A model for intergranular pressure solution in open systems. *Tectonophysics* 245, 153-170.
- Leythaeuser D., O. Borromeo, F. Mosca, R. di Primio, M. Radke, R. G. Schaefer (1995), Pressure solution in carbonate source rocks and its control on petroleum generation and migration. *Marine and Petroleum Geology* 12, 717-733.
- Meyer H. J. (1984), The influence of impurities on the growth rate of calcite. *J. Cryst. Growth* 66, 639-646.
- Nakatani M., and C. H. Scholz (2004), Frictional healing of quartz gouge under hydrothermal conditions: 1. Experimental evidence for solution transfer healing mechanism. *J. Geophys. Res.* 109, doi: 10.1029/2001JB001522.
- Niemeijer A. R., C. J. Spiers and B. Bos (2002), Compaction creep of quartz sand at 400–600°C: experimental evidence for dissolution-controlled pressure solution. *Earth and Planet. Sci. Lett.* 195, 261-275.
- Paterson M. S. (1973), Thermodynamics and its geological applications. *Rev. Geophys.* 11, 355-389.
- Paterson M. S. (1995), A theory for granular flow accommodated by material transfer via an intergranular fluid. *Tectonophysics* 245, 135-152.
- Plant L. J. and W. A. House (2002), Precipitation of calcite in the presence of inorganic phosphate. *Colloids and Surfaces A: Physicochemical and Engineering Aspects* 203, 43-153.
- Raj R. and C. K. Chyung (1981), Solution-precipitation creep in glass ceramics. *Acta Metall.*, 29, 19-166.
- Raj R. (1982), Creep in polycrystalline aggregates by matter transport through a liquid phase. *J. Geophys. Res.* 87, B6, 4731-4739.
- Reddy M. M. (1977), Crystallization of calcium carbonate in the presence of trace concentrations of phosphorous –containing anions. I inhibition by phosphate and glycerophosphate ions at pH 8.8 and 25 °C. *J. Cryst. Growth* 41, 287-295.
- Renard F., P. Ortoleva and J. P. Gratier (1997), Pressure solution in sandstones: influence of clays and dependence on temperature and stress. *Tectonophysics* 280, 257-266.
- Revil A. (2001), Pervasive pressure solution transfer in a quartz sand. *J. Geophys. Res.* 106, B5, 8665-8686.
- Rutter E. H. (1976), The kinetics of rock deformation by pressure solution. *Philos. Trans. R. Soc. London* 283, 203-219.
- Rutter E. H. (1983), Pressure solution in nature, theory and experiment. *J. Geol. Soc. Lond.* 140, 725-740.
- Sabbides G. and P. G. Koutsoukos (1993), The crystallization of calcium carbonate in artificial seawater; role of the substrate. *J. Cryst. Growth* 133,13-22.

- Shinn E. A. and D. M. Robbin (1983), Mechanical and Chemical compaction in fine-grained shallow water limestones. *J. Sedimen. Petrol.* 53, 595-618.
- Sibson R. H. (1994), Crustal stress, faulting, and fluid flow. In: *Geofluids: Origin, Migration and Evolution of Fluid in Sedimentary Basins* (Eds. J. Parnell). *Spec. Publ. Geol. Soc. Lond.* 78, 69-84.
- Sjoberg E. L. and D. T. Rickard (1983), Temperature dependence of calcite dissolution kinetics between 1 and 62 °C at pH 2.7 to 8.4 in aqueous solution. *Geochim. Cosmochim. Acta* 48, 485-493.
- Smith D. A. (1966), Theoretical considerations of sealing and non-sealing faults. *AAPG Bulletin* 50, 363-374.
- Spiers C. J. and P. M. T. M. Schutjens (1990), Densification of crystalline aggregates by fluid-phase diffusional creep. In: Barber, D. J. and Meredith, P.G. (eds) *Deformation Processes in Minerals, Ceramics and Rocks*. Unwin Hyman, London, 334-353.
- Spiers C. J., P. M. T. M. Schutjens, R. H. Brzesowsky, C. J. Peach, J. L. Liezenberg and H. J. Zwart (1990), Experimental determination of constitutive parameters governing creep of rocksalt by pressure solution, in: R.J. Knipe, E.H. Rutter (Eds), *Deformation Mechanisms, Rheology and Tectonics, Geol. Soc., London, Spec. Publ.*, 54, 215-227.
- Spiers C. J. and R. H. Brzesowsky (1993), Densification behaviour of wet granular salt: theory vs. experiment, in: *Seventh Symp. On Salt*, vol I., pp. 83-92.
- Spiers C. J., S. De Meer, A. R. Niemeijer and X. Zhang (2004), Kinetics of rock deformation by pressure solution and the role of thin aqueous films, In: Nakashima, S., Spiers, C. J., Mercury, L., Fenter, P. A., Hochella, M. F., (eds) *Physicochemistry of water in geological and biological systems*, Universal Academy Press, INC, Tokyo, Japan, 129-158.
- Stöckhert B., M. Wachmann, M. Küster and S. Bimmerman (1999), Low effective viscosity during high pressure metamorphism due to dissolution precipitation creep; the record of HP-LT metamorphic carbonates and siliciclastic rocks from Crete. *Tectonophysics* 303, 299-319.
- Tada R. and R. Siever (1989), Intergranular pressure solution during diagenesis. *Ann. Rev. Earth Planet. Science* 17, 89-118.
- TerHeege J. H., J. H. P. DeBresser and C. J. Spiers (2004), Composite flow laws for crystalline materials with log-normally distributed grain size: theory and application to olivine. *J. Struct. Geol.* 26, 1693-1705.
- Walderhaug O. (2000), Modeling quartz cementation and porosity in Middle Jurassic Brent Group sandstones of the Kvitebjorn field, Northern North Sea. *AAPG Bulletin* 84, 1325-1339.
- Walter L. M. and J. S. Hanor (1979), Effect of orthophosphate on the dissolution kinetics of biogenic magnesian calcites. *Geochim. Cosmochim. Acta* 43, 1377-1385.
- Wang H. F., (2000), *Theory of linear poroelasticity with applications to geomechanics and hydrology*, Princeton University Press, 340 pp.
- Weyl P. K. (1959), Pressure solution and the force of crystallization – a phenomenological theory. *J. Geophys. Res.* 64, 2001-2025.
- Zhang J., T. F. Wong and D. M. Davis (1990), Micromechanics of pressure-induced grain crushing in porous rocks. *J. Geophys. Res.* 95, 341-352.

- Zhang X., J. Salemans, C. J. Peach and C. J. Spiers (2002), Compaction experiments on wet calcite powder at room temperature: evidence for operation of intergranular pressure solution, in: S. De Meer, M. R. Drury, J. H. de Bresser, G. M. Pennock, (Eds), *Deformation Mechanisms, Rheology and Tectononics: Current Status and Future Perspectives*. *Geol. Soc, London, Spec. Publ.*, 200, 29-39.
- Zhang X. and C. J. Spiers (2005), Compaction of granular calcite by pressure solution at room temperature and effects of pore fluid chemistry. *Int. J. Rock. Mech. Min. Sci.*, 42, 950-960. doi:10.1016/j.ijrmms.2005.05.017.

5. Compaction creep of wet granular calcite by pressure solution at 28 to 150 °C

This chapter was published as: Zhang, X., C. J. Spiers and C. J. Peach (2010), Compaction creep of wet granular calcite by pressure solution at 28 to 150 °C, J. Geophys. Res. 115, doi:10.1029/2008JB005853.

Abstract

Uniaxial compaction experiments have been carried out on wet calcite powders prepared from crushed limestone, analytical grade calcite, and superpure calcite. The tests were performed at 28 °C–150 °C, effective stresses of 20–47 MPa, and a pore pressure of 20 MPa, using presaturated CaCO₃ solution as the pore fluid. Sample grain sizes ranged from 12 to 86 μm. The aim was to determine if creep occurs by intergranular pressure solution (IPS) under these conditions and to identify the rate-controlling process. The wet samples showed significant creep, while dry and oil-flooded samples did not. Wet samples were also characterized by microstructures such as sutured grain contacts, grain indentations, and overgrowths, suggesting the operation of IPS. The behavior of the wet samples at low strains (<4–5%) agreed well with the predictions of standard models for diffusion-controlled pressure solution. However, at higher strains (5–10%), creep slowed down compared with the model predictions. Transient flow-through tests performed in this regime led to an acceleration of creep, consistent with models for precipitation-controlled IPS, and demonstrated an increase in the impurity content of the pore fluid toward higher strains. Since some of these impurities (notably Mg²⁺) retard precipitation in calcite, we suggest that creep occurred by diffusion-controlled IPS at low strain, giving way to precipitation control at larger strains as impurities accumulated. Fitting of the diffusion-controlled IPS model to the low strain data yielded values of the grain boundary diffusion product DS in calcite of $\sim 10^{-19} \text{ m}^3 \text{ s}^{-1}$ at 150 °C.

5.1 Introduction

Intergranular Pressure Solution (IPS) has long been recognized as an important mechanism of compaction and deformation under upper and mid crustal conditions (Weyl, 1959; Durney, 1972). Compaction by IPS is achieved by stress-driven dissolution of material from grain contacts that comprise the load-bearing framework of the aggregate. The dissolved material is transported out of the contacts by diffusion through a fluid film or a micro-scale channel network at the grain boundary, and then precipitated on the pore walls or removed from the system by long-range advection or diffusion (Lehner, 1990, 1995; Renard et al., 1997, 2000, 2005; Zubtsov et al., 2005). In this way, IPS plays a key role in the reduction of porosity and permeability of rocks under diagenetic and low-grade metamorphic conditions, exerting important controls on the quality of hydrocarbon reservoirs, on the sealing capacity of reservoir-bounding faults and on the evolution of the

strength properties of fault zones (Bos and Spiers, 2002). In seismogenic fault zones, ongoing compaction by IPS may lead to the formation of sealed compartments in which the pore fluid pressure increases until fault rupture recurs, thus controlling the seismic cycle (Caine et al., 1996; Renard et al., 2000; Gratier et al., 2002). Similarly, the compaction of basin sediments and gouge-filled fault zones by IPS can determine the evolution of fluid pressure and fluid flow on the basin scale (Miller et al., 1999; Yang, 2000; Gratier et al., 2003; Tuncay and Ortoleva, 2004).

Accepted microstructural evidence for IPS includes (1) mass removal (i.e., dissolution) features at grain-to-grain contacts, such as interpenetrating indentations, sutured contacts, or truncation of grains and (2) precipitation features such as idiomorphic overgrowth or new grain growth on pore walls (Rutter, 1976, 1983). Such microstructures are widely found in carbonate and sandstone rocks, often in association with evidence for grain scale microfracturing and cracking healing (Renard et al., 2000; Gratier et al., 2003). However, evidence for IPS and localized zones of pressure solution, such as stylolites, is perhaps most common in carbonate rocks (Bathurst, 1958; Tada and Siever, 1989; Renard et al., 2004). About 60% of the world's oil and 40% of its gas reserves are found in carbonate reservoirs (http://www.slb.com/services/industry_challenges/carbonates.aspx). Obtaining a thorough understanding of the process and rate of IPS in calcite under upper crustal conditions therefore forms a challenge of major interest for modeling porosity-permeability evolution and distribution in reservoir and fault zone carbonates. A brief review of previous laboratory investigations of pressure solution in carbonate rocks is presented by Zhang and Spiers (2005a, 2005b). The mechanical data reported to date (e.g., Hellmann et al., 2002; Zhang et al., 2002; Zhang and Spiers, 2005a, 2005b; Renard et al., 2005; Zubtsov et al., 2005; Zhang et al., 2009) all indicate the operation of IPS in calcite at temperatures of 20 °C–30 °C and effective stresses of 1–50 MPa. However, the process is slow, so that only small strains are achieved and clear microstructural evidence for IPS is lacking. Recent studies also point to a significant role of microcracking alongside IPS, depending on pore fluid salinity and the partial pressure of CO₂ (Liteanu and Spiers, 2009). In addition, the effects of key variables such as grain size, effective stress, and temperature have generally not been investigated in a systematic way, with the result that little insight exists into the likely rate-controlling processes or associated rate-determining (constitutive) parameters.

The aim of the present study was to perform long-term (i.e., relatively high strain) compaction creep experiments on granular calcite in which the operation of pressure solution could be verified by microstructural observations and the effects of the key controlling variables could be more systematically investigated and the likely rate-controlling processes clarified. To this end, uniaxial compaction experiments were carried out on granular calcite aggregates of controlled mean particle size (12–82 μm) at a temperature of 150 °C, effective axial stresses in the range of 20–47 MPa, and a pore fluid pressure of 20 MPa. In this paper, effective axial stress is defined as the applied axial stress minus the pore fluid pressure. The pore fluid used consisted of water presaturated with calcium carbonate at the test temperature. Two experiments were carried out by stepping the temperature up and down, in the ranges of 100 °C to 150 °C and 150 °C to 28 °C, respectively. We employed high-precision displacement measurements and corrections for thermal fluctuations that enabled compaction strain rates down to 10^{-9} s^{-1} to be measured within 5%. Our experimental procedure was designed to minimize any contribution of

mechanical grain rearrangement and microfracturing to creep by precompacting the samples at a fixed stress (50 MPa) in excess of the stresses used in subsequent creep testing. Careful control experiments were also carried out using chemically inert pore fluids and lab-dry samples to discriminate between purely mechanical and chemical compaction. Our results suggest that IPS was indeed the dominant compaction mechanism in our wet experiments, showing transitional behavior between grain boundary diffusion- and precipitation-controlled kinetics.

5.2 Experimental method

The experiments consisted of uniaxial or 1-D compaction creep tests conducted at effective axial stresses (σ_e) in the range of 20–47 MPa, a pore fluid pressure (P_f) of 20 MPa, and temperatures (T) in the range of 28 °C–150 °C, though mainly at 150 °C. Constant stress, stress-stepping, and temperature-stepping methods were used. In this type of experiment, provided friction at the sample/vessel interface is low, lateral stresses are determined by the applied effective stress (σ_e), the mechanical properties of the sample, and the condition of zero lateral displacement at the sample wall. The stress state experienced by the sample thus resembles that expected in a simply buried sedimentary pile when the maximum principal stress is vertical.

5.2.1 Samples and pore fluid preparation

Most of the experiments reported in this study were performed on calcite powder obtained by milling a hydrocarbon-free, high-purity limestone, kindly provided by Shell International Exploration and Production from an oil field in South America. X-ray fluorescence spectrometry coupled with X-ray diffraction analysis showed that the limestone consisted of 96 wt % calcite, with the main impurities being SiO_2 , MgO , and Al_2O_3 , reflecting a few percent of clay minerals and quartz as well as around 1% of magnesium probably in solid solution in the calcite. The limestone was characterized by a dense, finely crystalline microstructure with a grain size of 2–30 μm and a porosity of 1–2%. The limestone was crushed in a ball mill and separated into particle size (d) fractions of 12 ± 4 , 22 ± 6 , 37 ± 8 , and 82 ± 8 μm by means of sieving and gravity setting in a deionized water column (for samples with particle size finer than 30 μm). The particle size distributions of the separated powders were measured using a Malvern, laser diffraction, particle size analyzer and checked by optical and scanning electron microscope (SEM) analysis. For all samples, more than 80 wt % of the grains fell in the ranges specified above. The individual particles were mainly monocrystalline at sizes below ~ 15 μm and polycrystalline above ~ 30 μm . Henceforth, except where otherwise indicated, we use the terms grain size and particle size interchangeably to refer to the free particle size of our calcite fractions.

Besides the natural limestone, we also used Merck analytical grade and Merck superpure grade calcite powders as samples. The Merck analytical grade powder has a purity of 99% calcite, with main impurities being Sr, Na, and Mg. Its particle size, based on SEM observations, is between 1 and 40 μm with a mean value of 14 μm (determined by a

linear intercept analysis of SEM micrographs). The Merck superpure calcite is microstructurally similar and has a purity of 99.95%. A particle size fraction of $12 \pm 4 \mu\text{m}$ was separated from both Merck materials by gravity setting for comparison with the same-sized fraction prepared from the natural limestone. Most particles in this range were monocrystalline.

Saturated solutions were made from the various particle size fractions to serve as pore fluids specific for each solid sample tested. The solutions were made by adding excess sample powder to deionized water and stirring for at least 48 h at ambient laboratory conditions. It is well established in the literature that chemical equilibrium is reached within 48 h in the $\text{CaCO}_3\text{-H}_2\text{O-CO}_2$ system under such conditions (Sjöberg and Rickard, 1984; Pokrovsky and Schott, 2002; Liteanu and Spiers, 2009). In taking such solutions to the elevated pressure and temperature conditions used in our experiments, the solutions become slightly supersaturated with calcite but re-equilibrate relatively quickly (Duan and Li, 2008).

5.2.2 Apparatus and calibration

Our compaction experiments were conducted using a servo-controlled Instron 8562 materials testing machine, equipped with a 100 kN load cell, to apply axial load to a 1-D piston-cylinder compaction vessel with an inner diameter of 20 mm (Figure 5.1). The compaction vessel and loading pistons are constructed from Monel K-500, a corrosion resistant Ni-Cu-Al-Fe alloy as described by Schutjens (1991). Sealing of the pistons is achieved by means of viton O-rings. Both upper and lower pistons are tipped with porous Monel filters to prevent sample particles from entering the piston bores.

During experimentation, axial force applied to the piston is measured externally using the Instron Load Cell (accuracy 0.1%). The position of the Instron loading ram is measured using a Linear Variable Differential Transformer (LVDT) located in the drive unit of the testing machine (internal LVDT). To measure sample compaction accurately, a Sangamo precision LVDT (resolution $0.1 \mu\text{m}$) was mounted on the top of the pressure vessel to measure the relative displacement between top piston and vessel (Figure 5.1). Sample temperature was measured using a K-type thermocouple, located in a blind hole in the vessel wall near the sample. Sample temperature was controlled within 0.2°C using a Eurotherm controller, plus K-type thermocouples located in the furnace windings. Calibration experiments showed that temperature gradients along and across the sample are negligible. This is due to the much smaller size of the sample compared to the furnace and vessel. Pore fluid pressure was measured using a high precision (0.02 MPa) pressure transducer and was kept constant at 20 ± 0.2 MPa during heating, cooling and loading, using a gas/liquid pressure separator buffered on the gas side by a large-volume reservoir containing nitrogen.

Pre-test calibration runs showed the seal friction on the upper (moving) piston to be typically $< 1\%$ of the applied force. The stiffness of the apparatus was calibrated before each experiment, by means of “empty runs” performed without a sample under the same experimental conditions as the subsequent compaction test. The load vs. position data thus obtained for the internal Instron LVDT was used to correct the machine distortion in

computing initial sample length. The load vs. displacement data measured by the Sangamo LVDT was used for the correction of sample shortening data recorded using this sensor.

When compaction rates were very low ($\leq 10^{-8} \text{ s}^{-1}$), the effects of temperature variation in the laboratory on the thermal expansion and contraction of the machine needed to be taken into account to obtain sufficient accuracy in measuring strain rate (error <5%). To allow correction for such thermal fluctuations, the temperature of the metal spacer above the top piston (see Figure 5.1) was measured using a K-type thermocouple and continuously logged. Blank runs carried out with an incompressible dummy sample (hard steel), under typical experimental conditions (e.g. $T=150 \text{ °C}$; $P_f=20\text{MPa}$; $\sigma_e=30 \text{ MPa}$), enabled displacement caused by ambient temperature fluctuations, and by deliberate change of sample temperature, to be accurately calibrated against apparatus and sample temperature and thus corrected for.

5.2.3 Testing procedure

In setting up each experiment, the bottom piston and pressure vessel were assembled first, spraying the bore of the vessel with boron nitride or graphite to reduce friction at the sample and vessel interface. Approximately 6 grams of calcite powder were then funneled into the vessel and flattened gently by inserting the top piston to form a sample with length/diameter aspect ratio of 1:1. The top piston was then removed and 3 or 4 fragments cleaved from a calcite single crystal (measuring $1\text{mm} \times 2\text{mm} \times 0.5\text{mm}$) were funneled into the vessel, scattering them on top of the powdered calcite sample. These were added to serve as microstructural reference crystals to demonstrate pitting by IPS, if active. The thermocouples and furnace were then mounted onto the vessel and the top piston inserted until it touched the sample. The entire assembly was then located in the Instron loading frame. Finally, the Sangamo LVDT and associated spacer/insulator assembly were installed on the upper piston, and the pore fluid control system was connected to the upper piston (Figure 5.1).

In each run, the sample was first subjected to a dry pre-compaction phase at an applied axial stress of 50 MPa, at room temperature, for 60 minutes. This was done to create a standardized microstructure unable to undergo purely mechanical intergranular rearrangement at lower stresses (i. e. to produce a “locked” aggregate - following De Meer & Spiers, 1997; Zhang & Spiers, 2005a). After dry compaction, the sample was unloaded to a stress of 20.5 MPa. The sample was subsequently evacuated for 30 minutes then filled with saturated CaCO_3 solution. The pore fluid pressure was then increased to 20 MPa, maintaining a small effective stress ($< 0.5 \text{ MPa}$) on the sample. During subsequent heating, the pore fluid pressure was kept constant at this value by the gas buffer system. Sample temperature was reached in about 12 hours. However, a total period of 15-20 hours was allowed in order to establish full thermal and chemical equilibrium. This choice was based on the geochemical literature (Sjöberg and Rickard, 1984; Pokrovsky and Schott, 2002; Duan and Li, 2008), which shows that equilibration can be expected within 10–20 h under our experimental conditions (100 °C – 150 °C), resulting in an increase in sample mass of $< 0.01\%$.

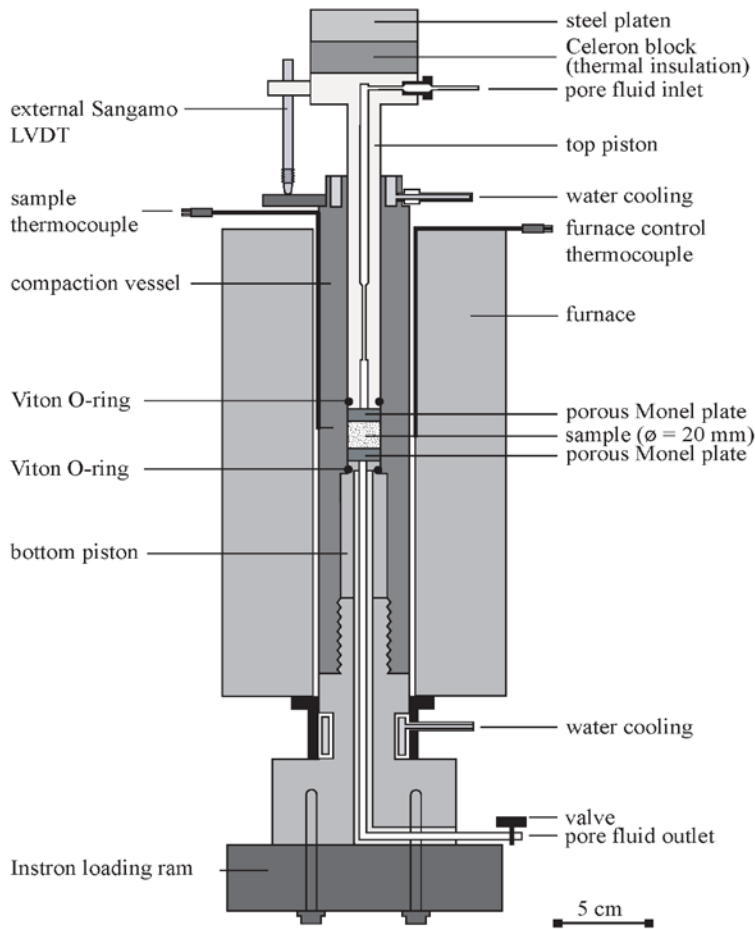


Figure 5.1. Schematic diagram illustrating the experimental set up.

After heating and equilibration, the desired effective stress (20–47 MPa) was applied using the Instron loading frame, the applied force linearly over a period of about one minute. Compaction creep tests were conducted using constant stress, stress-stepping and temperature-stepping modes, making use of pre-determined loading paths programmed into the Instron control system. Individual creep experiments lasted from 7 to 40 days. Intermittent flow-through tests were carried out at different stages of the selected compaction experiments by carefully opening the needle valve in the down-stream part of the pore fluid system (Figure 5.1), thus generating a small pore fluid pressure difference (0.02–0.1 MPa) across the sample. These intermittent flow-through tests were performed to allow sampling of the pore fluid and evaluation of change in composition during compaction. Flow-through also provides a method of recognizing when IPS is controlled by

the kinetics of precipitation on pore walls, as theory predicts that it is only in this case that creep by IPS is accelerated by flushing with fresh pore fluid (DeMeer & Spiers, 1997).

Experiments were terminated by switching off the furnace and allowing the apparatus to cool to room temperature, while simultaneously then reducing the effective axial stress to 1-2 MPa. The pore fluid pressure was then reduced from 20 MPa to zero, while the remaining axial stress was completely removed. This procedure was adopted to avoid loading the sample beyond the maximum effective stress used during the creep stage of the experiment, while maintaining a positive effective stress. The sample was subsequently flushed, in-situ, with compressed air to expel the pore fluid. The vessel was then removed from the Instron and the sample was carefully pressed out. The recovered sample was immediately oven-dried, weighed and its thickness measured using a micrometer. All samples compacted in the presence of aqueous solution were always intact and well-indurated. Weight loss of the sample due to either solution phase transport transfer effects handling damage was normally less than 0.2%. The cleaved crystals were then detached from the surface of the sample and prepared for SEM observation. Finally, the compacted

ID	Sample Material and Grain Size (μm)	Pore Fluid	T ($^{\circ}\text{C}$)	P_f (MPa)	σ_e (MPa)	Experiment Type	Initial Porosity ϕ_0 (%)	Final Strain (%)	Duration (hours)
Mdry	Lst (37 \pm 8)	Lab air	150	0.1	30	Constant stress	27.00	0.50	100
M0	Lst (37 \pm 8)	Silicone oil	150	20	30	Constant stress	28.00	0.60	400
M1	Lst (37 \pm 8)	CaCO ₃ Soln	150	20	30, 20, 30, 40	Stress stepping	26.79	6.90	590
M2	Lst (37 \pm 8)	CaCO ₃ Soln	150	20	20, 25, 30, 35	Stress stepping	27.57	6.48	425
M3	Lst (37 \pm 8)	CaCO ₃ Soln	150	20	20, 25, 30, 35	Stress stepping	25.03	1.67	400
M5	Lst (37 \pm 8)	CaCO ₃ Soln	100, 130, 150	20	30	Temperature Stepping	29.30	6.34	926
M8	Lst (82 \pm 8)	CaCO ₃ Soln	150	20	30, 40	Stress stepping	27.76	6.57	578
M9	Lst (22 \pm 6)	CaCO ₃ Soln	150, 28	20	30, 40	Stress stepping	31.49	9.40	405
M11	Lst (12 \pm 4)	CaCO ₃ Soln	150	20	30	Intermittent flow-through	27.60	6.86	192
M13	Analytical calcite (12 \pm 4)	CaCO ₃ Soln	150	20	30	Intermittent flow-through	34.50	9.65	160
M18	Super pure (12 \pm 4)	CaCO ₃ Soln	150	20	30	Constant stress	33.90	10.48	152

Table 5.1. List of the 1-dimensional compaction experiments reported in this study. All samples were subjected to initial dry compaction at 50 MPa at room temperature to achieve a standard starting microstructure. An exception was sample M3 which was pre-compacted at 50 MPa effective stress under wet conditions for half an hour. Lst: crushed limestone samples. Soln: solution.

sample was impregnated with a low viscosity epoxy resin and polished sections were made for SEM study.

Besides the experiments performed using aqueous pore fluid, as described above (referred to as “wet” tests), a range of control experiments were carried out on both dry sample (i. e. samples containing lab air) and on samples containing chemically inert silicone oil as a pore fluid. Typical experimental conditions of 150 °C and 30 MPa effective stress were used for these tests, following an identical procedure to that used in the wet tests.

5.2.4 Data acquisition and processing

During each experiment, data signals representing Instron position (internal LVDT), applied force, pore fluid pressure, sample temperature, and Sangamo LVDT position were computer logged and recorded on a chart recorder as a backup. The logging frequency was 0.1 to 0.002 Hz, depending on the compaction rate. In processing the logged data, the moment at which the desired effective stress was reached was defined as the start of each creep experiment, and the corresponding length (l_0) and porosity (ϕ_0) of the sample at that time were taken as the initial values. The position recorded by the Sangamo LVDT at this moment was taken as the point of zero creep displacement. By defining the starting point of the experiment in this way, we excluded elastic and other time-independent strains from our creep data.

To obtain the porosity of each sample at any instant, we used the relation: $\phi = (V_t - V_s)/V_t = (\pi r^2 l - w/\rho)/\pi r^2 l$, where ϕ is porosity, V_s and V_t are the volume of the solid particles and the bulk sample (respectively), w is the mass of the sample, ρ is the density of pure calcite (2710 kg/m³), r is the radius of the pressure vessel, and l is the instantaneous length of the sample (as determined from the Instron LVDT position corrected for machine distortion). Volumetric strain, which is identical to axial strain in the present uniaxial compaction geometry, was calculated using the engineering definition $e_v = \Delta l/l_0$, where l_0 is the initial sample length and Δl is the total sample shortening determined using the Sangamo LVDT. The volumetric strain rate at any instant was calculated using the definition $\dot{e}_v = \dot{l}/l$, whereby the shorting rate $\dot{l} = -dl/dt$ was approximated from the Sangamo LVDT data set on a pointwise basis using a three-point central difference method. Note that in a system where solid mass is conserved, as demonstrated in the present experiments (within 0.2%), the volumetric strain e_v can be expressed as $e_v = (\phi_0 - \phi)/(1 - \phi_0)$. Normalized porosity is used in this study for comparison of different tests and is related to volumetric strain by $\phi/\phi_0 = (1 - e_v/\phi_0)/(1 - e_v)$.

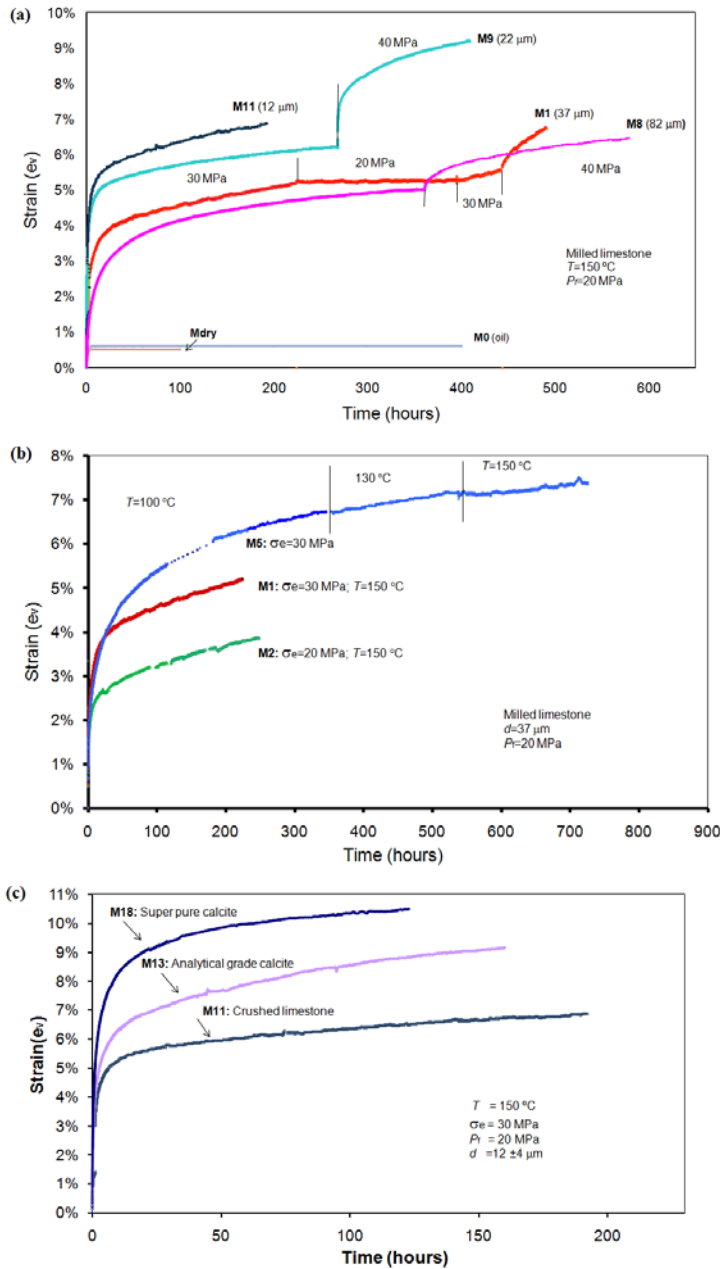


Figure 5.2. Typical compaction creep curves obtained for wet samples. **a).** Compaction creep curves for crushed limestone samples with different grain size (μm). Experimental conditions: $P_f=20$ MPa, $\sigma_e=20, 30$ and 40 MPa, $T=150$ °C. Stress increments or stress indicated. Note also the slope of the curve becomes much steeper for fine-grained sample when stress is stepped up (M9 vs. M8). **b).** Creep curves for crushed limestone with grain size of 37 ± 8 μm at different temperatures and effective stresses. **c).** Creep curves for crushed limestone, analytical grade and super-pure calcite. Grain size 12 ± 4 μm . Conditions: $T=150$ °C, $\sigma_e=30$ MPa, $P_f=20$ MPa.

5.3 Experimental Results

All experiments carried out in this study are listed in Table 5.1, along with data on the initial porosity of the samples (ϕ_0) at the start of the creep stage, the duration of the creep stage, and the final strains (e_v) achieved.

5.3.1 Mechanical data

The precompaction stage of our experiments resulted in 10–15% instantaneous compaction strain and a porosity of $\sim 31 \pm 4\%$. The initial porosity at the start of creep (ϕ_0) was $27.8 \pm 2.1\%$ for the crushed limestone samples and $34.2 \pm 0.3\%$ for the Merck samples. Samples tested dry or flooded with chemically inert silicone oil showed only minor creep ($<0.6\%$), mainly in the first few hours after loading (Figure 5.2a, Table 5.1). In contrast, wet samples showed significant creep, accumulating strains of up to 4–10% over several days (Figure 5.2, Table 5.1). All compaction curves for wet samples show similar features: fast compaction at the beginning of the experiment followed by a phase of continuously decreasing strain rate. When the applied stress was stepped up, faster compaction was measured (Figure 5.2a). When the effective stress was stepped down, compaction slowed or halted (Figure 5.2a). Broadly speaking, faster creep rates and larger creep strains were obtained in experiments and steps characterized by higher effective stress and by finer particle size (Figures 2a and 2b). Effects of temperature on compaction rate appeared to be minor (see temperature stepping test M5, Figure 5.2b). Significantly, under the same experimental conditions, samples of higher purity showed higher compaction strain rates when compared at fixed strains and achieved larger strains at fixed times (Figure 5.2c), though the initial porosity was also higher in the pure samples ($\sim 34\%$) than in the crushed limestone samples ($\sim 27\%$). There was no enhancement of strain rate at low flow-through rates. However, experiments in which intermittent flow-through of the pore fluid was allowed with high flow-through rate (M11, M13, see Table 5.1) showed transient acceleration of creep at higher strains (lower normalized porosity), seen as a minor excursion in the strain versus time curves (Figure 5.2c).

Typical strain rate versus strain data derived from Figure 5.2 for samples compacted at fixed stress (30 MPa) and temperature (150 °C) are shown in Figure 5.3. All samples show a steady decrease in strain rate with increasing strain up to strains of ~ 4 –6%, at which point most exhibit a sharper decrease in strain rate, which then flattens off to produce a z-shaped “kink” in the curves (Figures 3a and 3b). Intermittent flow-through tests performed beyond this kink led to transient increases in strain rate of about one order of magnitude (Figure 5.3a) when using high flow rates. However, bursts of flow-through applied at small strain well before the kink had no influence on strain rate (Figure 5.3a).

5.3.2 Microstructural observations

All wet-compacted samples remained indurated and fully intact when extracted from the deformation apparatus, so that mechanical corruption of the microstructure is unlikely. The microstructure of intact portions of our dry-compacted control sample (Mdry) was found to be characterized by irregular, rough-surfaced mono- and polycrystalline particles displaying mostly sharp point contacts or open, porous grain contacts (Figure 5.4a). Intragranular microcracks are common. In contrast, wet-compacted samples show a high proportion of tightly interlocking or sutured grain contacts, as well as occasional indented contacts (Figures 4b and 4c). These are interpreted to be evidence of varying amounts of

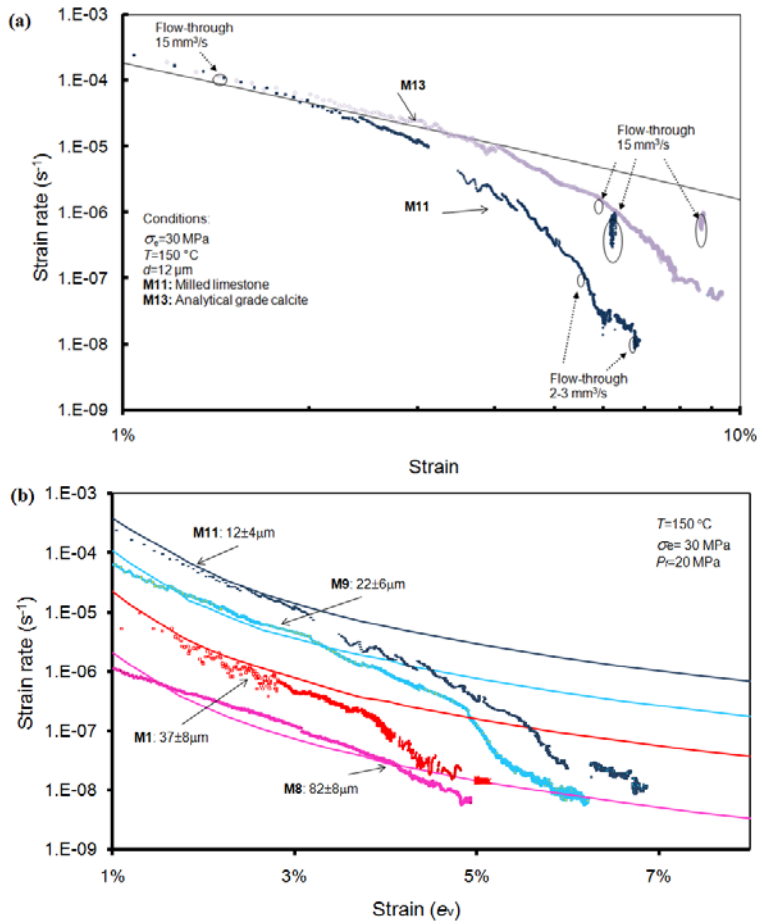


Figure 5.3. (a) Log-log plots of strain rate versus strain for samples M11 and M13 compacted at 30 MPa effective stress and 150°C with intermittent flow-through at various strains. (b) Semi-log plots of strain rate versus strain for samples M1, M8, M9, and M11. The strain rates increase systematically with decrease of grain sizes. Solid lines represent the model for DS in Table 5.2 ($DS = 5.98 \times 10^{-19} \text{ m}^3 \text{ s}^{-1}$ at 150 °C and with initial porosity of 30%).

contact dissolution. Small, idiomorphic crystals observed on pore walls (Figure 5.4d) are interpreted to represent overgrowths. Such overgrowths are less evident than grain contacts dissolution features. Neither was observed in samples compacted dry or using silicone oil as pore fluid.

The reference calcite crystals added to the powdered samples revealed a remarkable range of microstructural features. The cleaved surfaces of the reference crystals are originally smooth and show no visible imperfections in the SEM, suggesting they are flat within a few hundred nanometers (Figure 5.5a). However, the reference crystals recovered from wet-compacted samples show widespread pit-like microstructures, 1–30 μm in diameter, developed on the cleaved surfaces (Figure 5.5b). Moreover, larger dissolution pits are observed on crystals extracted from samples with coarser grain size. No such pits are seen on reference crystals extracted from dry samples. The pits are accordingly believed to mark the indentation points of sample grains into the reference crystal surfaces as a result of IPS. In detail, the individual pits consist of clusters of smaller ones, indicating a high degree of irregularity and roughness of the inferred dissolution surface (Figure 5.5b). Twins are often developed in the cleaved surface of the reference crystals and are always overprinted by dissolution pits. Interestingly, the cleaved surfaces of the reference crystals extracted from the Merck analytical grade and superpure samples were much more extensively indented than those removed from the experiments on limestone samples, suggesting a correlation with the higher strains attained in the purer Merck samples (Table 5.1). Figure 5.5c shows the detailed structure of a dissolution pit developed in a crystal added to analytical grade sample M13. The floor of the pit shows a rough structure with amplitude of the order of at least 10–100 nm. The edge of the pit is surrounded by steps and terraces, which presumably represent dissolution or growth sites. Growth layers can clearly be seen to have formed around or adjacent to some dissolution pits (Figure 5.5d).

5.3.3 Pore fluid analyses

The fluid samples extracted from experiments M11 and M13 during the intermittent periods of flow-through imposed in these experiments (see Figure 5.3a) were analyzed using inductively coupled plasma mass spectrometry. To obtain a representative pore fluid of the compacting material, fluids were carefully collected at the very beginning of each the flow-through tests. The Ca^{2+} and Mg^{2+} of the measured pore fluids are shown in Table 5.3. It is clear that the Ca^{2+} were built up at higher strains. The Mg^{2+} concentrations are also measured higher at higher strains.

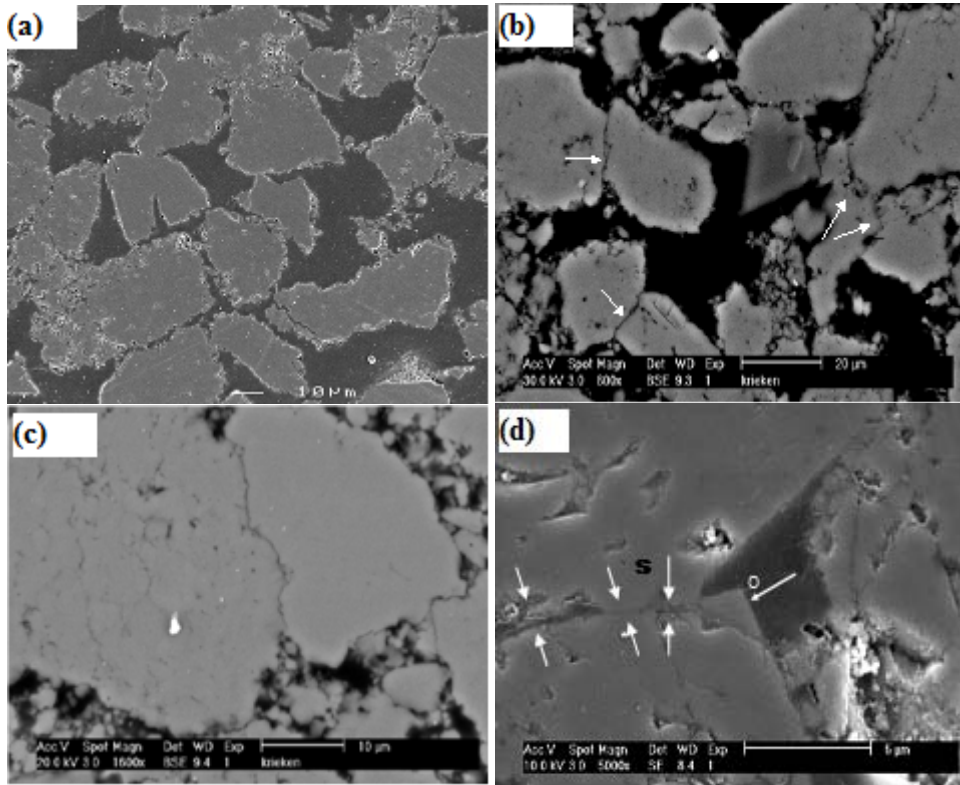


Figure 5.4. Microstructures of the compacted samples revealed by SEM analysis of polished sections. Images produced using backscatter electron mode or secondary electron imaging. (a) Micrograph of dry-compacted sample (Mdry). Crushed limestone of grain size $37 \pm 8 \mu\text{m}$. Experimental conditions: $\sigma_e = 30 \text{ MPa}$, $T = 150 \text{ }^\circ\text{C}$. Note the high-porosity, rough surface grains, point contacts, and porous grain contact zones and intragranular fractures. Similar microstructures were observed in the dry and oil-bearing control experiments. (b) Microstructure typical of wet-compacted samples, showing increased proportion of well-developed, interlocking grain contacts. Crushed limestone of grain size $37 \pm 8 \mu\text{m}$ (sample M2). Experimental conditions: $\sigma_e = 30 \text{ MPa}$, $T = 150 \text{ }^\circ\text{C}$. (c) Sutured grain contact typical of those developed in wet-compacted samples: crushed limestone of grain size $37 \pm 8 \mu\text{m}$ (sample M2). Experimental conditions: $\sigma_e = 30 \text{ MPa}$, $T = 150 \text{ }^\circ\text{C}$. (d) Interpreted overgrowth (O) on a pore wall in wet-compacted sample M2, adjacent to a tightly interlocking and sutured grain contact (S). Crushed limestone of grain size $37 \pm 8 \mu\text{m}$. Experimental conditions: $\sigma_e = 30 \text{ MPa}$, $T = 150 \text{ }^\circ\text{C}$.

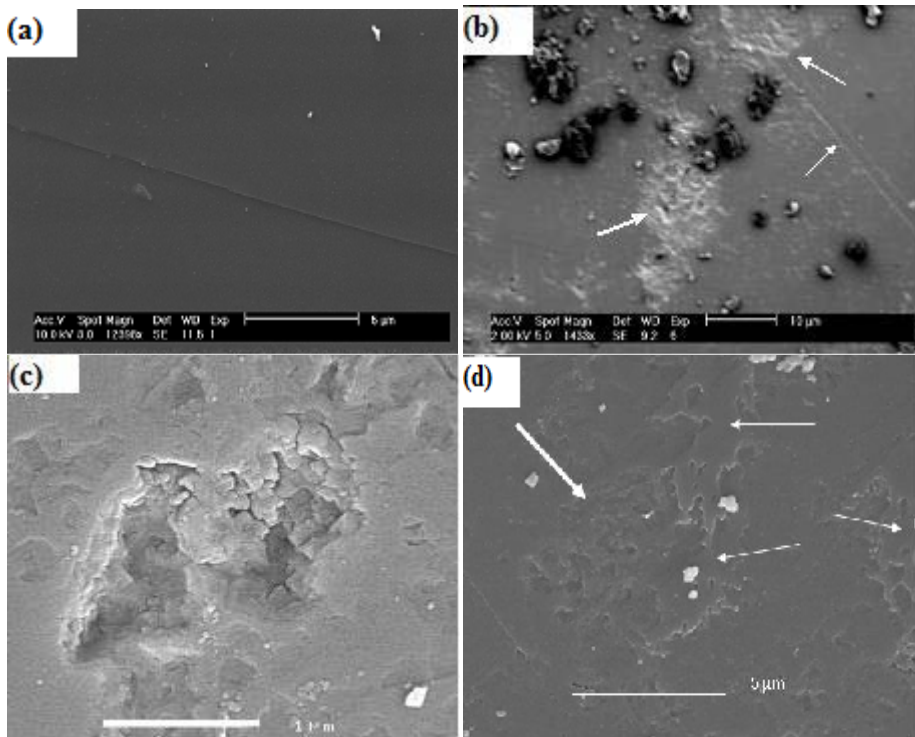


Figure 5.5. Secondary electron SEM images showing microstructures developed on the surfaces of reference calcite crystals added to the powered samples. (a) Cleaved surface of a reference calcite crystal in the virgin state. Note the smoothness of the surfaces and the trace of a single cleavage step. (b) Pits developed on the cleaved surface of a reference crystal added to sample M2. Experimental conditions: $\sigma_c = 35$ MPa, $T = 150$ °C, $P_f = 20$ MPa. Such pits are not seen in dry-compacted samples and are interpreted to be dissolution pits developed through IPS at the contact with grains in the powdered sample. The thin arrow indicates deformation twins cut by the later dissolution pits. (c) Details of dissolution pits developed on the surface of a reference crystal added to wet-compacted sample M2. (d) Growth layers developed on the surface of a reference crystal added to wet-compacted sample M2. The thin arrows indicate precipitated layers, while the thick arrow indicates dissolution pitting.

5.4 Discussion

5.4.1 Deformation mechanisms

As described in section 3.1, precompaction under dry conditions, at a stress of 50 MPa, resulted in 10–15% of instantaneous or time-independent compaction strain. Given the microstructure of the dry control sample Mdry, this strain was presumably caused by time-independent, intergranular sliding, contact cataclasis, and/or crystal plastic deformation (twinning) as well as minor elastic strain contribution. The minor amount of compaction

creep (strain < 0.6%) shown by the control samples that were reloaded dry or with silicone oil as pore fluid (Figure 5.2a) suggests a rapidly decelerating transient creep mechanism, perhaps involving subcritical cracking or work-hardening plasticity. The behavior of the oil-flooded samples further suggests that the precompacted or locked aggregates cannot be “unlocked” by purely physical effects such as fluid “lubrication” or surface wetting. As the samples tested wet (i.e., reloaded with CaCO₃-saturated solution at 20 MPa) showed much more time-dependent compaction than the dry or oil-flooded samples (Figures 5.2a–2c, Table 5.1), additional fluid-enhanced deformation mechanisms must have operated in wet samples. The microstructures seen only in the wet-compacted samples, namely the indented, sutured, and interlocking grain contacts, as well as the dissolution pits and growth layers developed on the reference crystal surfaces, provide strong evidence that the main deformation mechanism in these samples was intergranular pressure solution.

5.4.2 Comparison of IPS theory and experimental results

In the following section, we compare the trends seen in the creep data derived from our wet experiments with those predicted by conventional intergranular pressure solution theory, focusing on the effects of strain, effective stress, grain size, and temperature on strain rate. Note that by conventional IPS, we mean IPS dominated by internal grain boundary dissolution and diffusion in an adsorbed fluid film or dynamically island-channel structure (Rutter, 1976, 1983; Lehner, 1990, 1995; Paterson, 1995; de Meer & Spiers, 1999; Spiers et al. 2004).

5.4.2.1 Theoretical rate equations for compaction by IPS

In the conventional theory, IPS is a coupled mechanical-chemical process driven by non-hydrostatic stress and achieved, in a chemically closed system (i. e. without significant removal or addition of solid mass), through the three serial processes of dissolution with highly stressed grain contacts, diffusion of material along the grain contacts through a solution film (Rutter 1976, 1983) or a microscale channel network (Lehner 1990, 1995), and precipitation on pore walls. Under steady state conditions, the slowest of these three processes controls the strain rate (Raj 1982; Lehner 1990; Renard et al., 2000; Spiers et al., 2004). Following DeMeer & Spiers (1999), Niemeijer et al. (2002) or Spiers et al. (2004), and assuming linear kinetic relations for the dissolution and precipitation relations (i. e. linear relation between under/super saturation and dissolution and precipitation rate), the theoretical IPS creep equations for uniaxial compaction of a simply packed array of spherical solid grains can be written in the form:

$$\dot{\epsilon}_s = k_s \frac{\left[\exp\left(\frac{B\sigma_e\Omega}{RT}\right) - 1 \right]}{d} f_s(\phi_0, e_v) \quad \text{for dissolution control} \quad (5.1)$$

$$\dot{\varepsilon}_d = DCS \frac{\left[\exp\left(\frac{B\sigma_e\Omega}{RT}\right) - 1 \right]}{d^3} f_d(\phi_0, e_v) \quad \text{for diffusion control} \quad (5.2)$$

$$\dot{\varepsilon}_p = k_p \frac{\left[\exp\left(\frac{B\sigma_e\Omega}{RT}\right) - 1 \right]}{d} f_p(\phi_0, e_v) \quad \text{for precipitation control} \quad (5.3)$$

Here $\dot{\varepsilon}_x$ represents the volumetric strain rate for each rate controlling process ($x=s, d, p$), k_s and k_p represent the temperature-dependent rate coefficients for the dissolution and precipitation reaction ($\text{m}\cdot\text{s}^{-1}$), D is the diffusivity of ions within the grain boundary fluid, C is the solubility of the solid, S is the mean thickness of the grain boundary fluid phase and d is grain or particle size. The term $B(\phi_0, e_v)$ is a strain or porosity dependent measure of stress concentration at grain contacts compared with the applied stress. Similarly, $f_x(\phi_0, e_v)$ is a geometric function of initial porosity and compaction strain which accounts for evolving aggregate structure, but which is mechanism specific ($x=s, d, p$). These geometric terms are defined explicitly in Appendix A (see also Spiers et al., 2004). Finally, Ω represents the molar volume of the granular solid phase (m^3/mol), while R and T represent the gas constant and absolute temperature, respectively.

Note that equations (5.1), (5.2) and (5.3) predict different dependence on aggregate grain size (d) and on aggregate structure $f_x(\phi_0, e_v)$ (see Appendix A). This gives a potential means of determining rate-controlling mechanism from experiments, notably by varying d to distinguish diffusion from reaction control. Equations (5.1), (5.2) and (5.3) further predict that the absolute rate of compaction by IPS in a granular solid, such as our calcite samples, will be determined by the magnitude of the kinetic parameter term k_s , DCS and k_p . For the diffusion controlled case (equation 2), the magnitude of DCS and hence the IPS rate are directly related to the solubility (C) of the solid phase. Mineral solubility is temperature and pressure dependent. Unlike most other minerals, the solubility of calcite decreases with increasing temperature at constant pressure (Ellis, 1959, 1963). Plummer and Busenberg (1982) studied the temperature dependence of the solubility of calcite at temperature 0-90 °C. They found the following temperature-dependence for the solubility product at atmosphere pressure

$$\text{Log}K_{sp} = -171.9065 - 0.077993T + 2839.319/T + 71.595\text{Log}T \quad (5.4)$$

where K_{sp} is the molal solubility product of calcite defined for the reaction $\text{CaCO}_3 \rightleftharpoons \text{Ca}^{2+} + \text{CO}_3^{2-}$. Taking a_i to represent the activity of species i , this implies

$$K_{sp} = a_{\text{Ca}^{2+}} a_{\text{CaCO}_3} / a_{\text{CaCO}_3} = \gamma_{\text{Ca}^{2+}} C_{\text{Ca}^{2+}} \gamma_{\text{CO}_3^{2-}} C_{\text{CO}_3^{2-}} \approx C^2 \quad (5.5)$$

where γ_i , C_i are the activity coefficients and molal concentration of Ca^{2+} and CO_3^{2-} .

Since the solubility of calcite is not strongly pressure dependent, we can accordingly use (4) and (5) to quantify C for calcite. Similar relations for C are given by Duan and Li (2008). Since the values of D and S can also be estimated from the literature (see Table 5.2), the product DCS can be evaluated.

For the dissolution- and precipitation-controlled cases of IPS, values of k_s and k_p can be approximated using the rate coefficients determined from geochemical kinetic experiments on unstressed aggregates (van Noort et al., 2008) specifically from experiments where the rates of dissolution and precipitation are expressed as linear functions of the degree of undersaturation or supersaturation (e.g., Berner and Morse, 1974; Inskeep and Bloom, 1985; Gledhill and Morse, 2006). Suitable data from such experiments are listed in Table 5.2.

5.4.2.2 Comparison of experimental data with model predictions

By coupling equations (5.1) to (5.3) with the values for the dissolution and precipitation rate coefficients, calcite solubility, grain boundary diffusivity and mean grain boundary fluid film thickness given in Table 5.2, it is now possible to predict the IPS rate for the cases of dissolution, diffusion and precipitation control. To do this, we used the expression for B and f_x given in Appendix A for a simple cubic pack of grains (following the work of Renard et al., 1997), assuming that the aggregate and grain contact geometry are unaffected by elastic deformation of the aggregate. This will be a valid assumption beyond the first few tenths of a percent of compaction, during which Hertzian elastic distortion of the contacts will be relieved as grain contact stresses fall. Using this approach, reaction (dissolution and precipitation) controlled IPS creep is predicted to be 20-30 times faster than the grain boundary diffusion-controlled process at 150 °C, for the range of strains (porosities) covered in our experiments. This means that diffusion is predicted to be the rate-limiting step in a pure $\text{CaCO}_3\text{-H}_2\text{O}$ system. The predicted diffusion-controlled strain rates are compared with experimental strain rates obtained for representative wet samples tested at 150°C in Figures 3a and 3b. The low strain data ($e_v < 4\%$) fall close to the model predictions made assuming grain boundary diffusion-controlled pressure solution using the diffusion product $DS = 5.98 \times 10^{-19} \text{ m}^3 \text{ s}^{-1}$. At higher strains (>4–6%), agreement is poor, as the experimental data show a sharp drop or z-shaped kink (e.g., Figure 5.3b). This suggests a change of deformation mechanism or rate-controlling process or perhaps a change in grain boundary structure (Dysthe et al., 2002, 2003). A further possibility is a change in grain contact geometry as strain increases, caused by the fact that the grains in our samples are irregular rather than perfect spheres (Schutjens, 1991).

Items	Formula/value	Sources
Dissolution in pure system	$R_s = k_s(1 - Q_s)$ $k_s = k_s^0 \exp(-Q_s/RT)$ $k_s = 8.49 \times 10^{-10} \text{ m} \cdot \text{s}^{-1}$ at $T = 150^\circ \text{C}$ $Q_s = 33 \text{ kJ/mol}$	Reddy & Wang, 1980 Inskeep and Bloom, 1985 Busenberg & Plummer 1986
Precipitation in pure system	$R_p = k_p(Q_p - 1)$ $k_p = k_p^0 \exp(-Q_p/RT)$ $k_p = 1.61 \times 10^{-11} \text{ m} \cdot \text{s}^{-1}$ at $T = 25^\circ \text{C}$ $Q_s = 46 \text{ kJ/mol}$ $k_p = 3.89 \times 10^{-9} \text{ m} \cdot \text{s}^{-1}$ at $T = 150^\circ \text{C}$	Reddy & Wang, 1980 Inskeep and Bloom, 1985
Diffusion coefficient	$D = 1 \times 10^{-10}$ at $T = 25^\circ \text{C}$ $D = D_0 \exp(-Q_d/RT)$ $Q_s = 15 \text{ kJ/mol}$ $D = 5.98 \times 10^{-10}$ at $T = 150^\circ \text{C}$	Nakashima, 1995
Grain boundary thickness	$S = 1 \times 10^{-9}$	Renard et al. 1997
Solubility product	$\text{Log} K_{sp} = -171.9065 - 0.077993T + 2839.319/T + 71.595 \text{Log} T$	Plummer and Busenberg 1982
Molar volume of calcite	3.692×10^{-5} at 25°C	

Table 5.2. Kinetic data used for modeling of intergranular pressure solution. DS represents the diffusion product (diffusion coefficient times the thickness of water film along grain boundary).

To gain further insight into the mechanism(s) controlling compaction in our experiments, we now explicitly compare the effects of grain size, stress, and temperature on strain rate predicted by equations (5.1), (5.2), and (5.3), with the effects of these variables as observed in our experiments. To compare the effects of these variables, we have to compare the rate data of different samples at the same microstructures. For unconsolidated materials such as used in our tests, it is not possible to achieve the same microstructures for different samples, even if they have the same initial porosity. For samples with same initial porosity, microstructures at fixed strain can be taken as owing the same structures. For samples with different initial porosity, neither strains nor absolute porosity can be taken as same microstructures. A better way to represent the “same microstructure” is to use the normalized porosity (ϕ/ϕ_0) (Niemeijer et al., 2002). The rate data in Figure 5.3 are replotted against normalized porosity and shown in Figure 5.6.

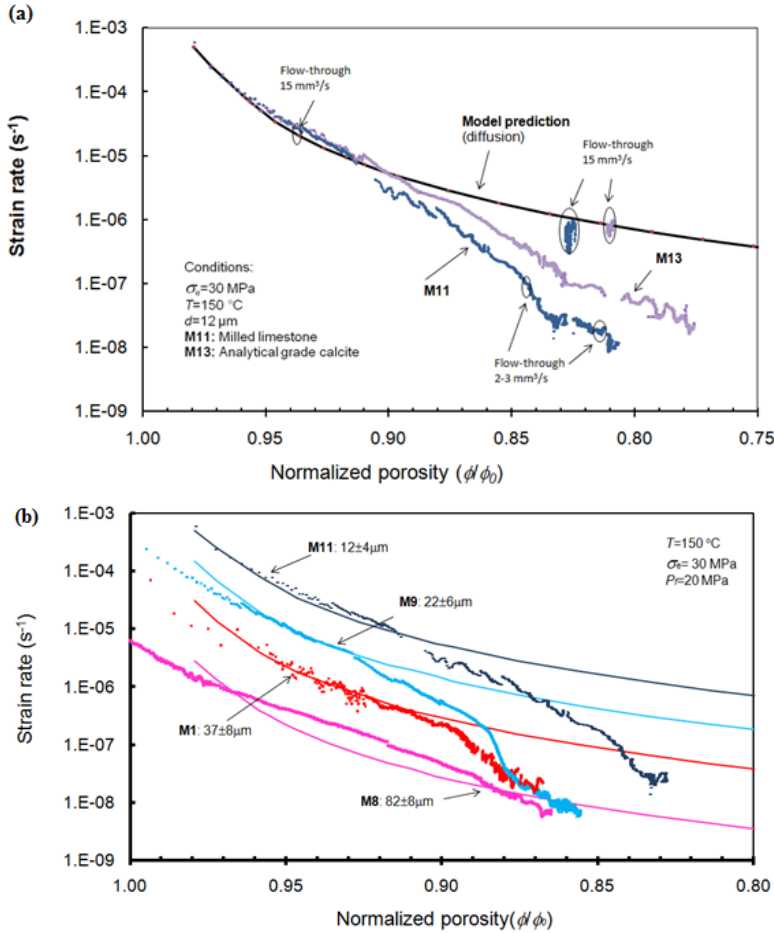


Figure 5.6. Strain rates versus normalized porosity for data shown in Figure 5.3. (a) Flow-through test of M11 and M13. (b) Tests for samples M1, M8, M9, and M11 with different grain size, compacted at 30 MPa effective stress and 150°C. Solid lines represent the model for DS in Table 5.2 ($DS = 5.98 \times 10^{-19}\ m^3\ s^{-1}$ at 150°C and with initial porosity $\phi_0 = 30\%$).

Our experimental data for crushed limestone ($\phi_0 = 27.8 \pm 2.1\%$) presented in Figures 5.3b and 5.6b show clear effects of grain size on creep rate. Fine-grained samples achieved larger strains and crept at faster rates than coarser samples under otherwise identical experimental conditions. From the agreement between experimental and theoretical curves plotted in Figure 5.6b, it is clear that the dependence of strain rate on grain size at fixed normalized porosity is consistent with that predicted by the diffusion-controlled IPS model at low volumetric strains. This is confirmed in the log-log plot of compaction strain rate versus grain size shown in Figure 5.7, which is derived from the data of Figure 5.6b. The

data presented in Figure 5.7 show a slope close to 3 (individual best fits give 2.6 ± 0.5) for normalized porosity >0.89 (strains $\leq 4\%$, i.e., before the kinks seen in Figure 5.3b). These results support the hypothesis that compaction occurs by diffusion-controlled pressure solution at small strains ($\leq 4\%$).

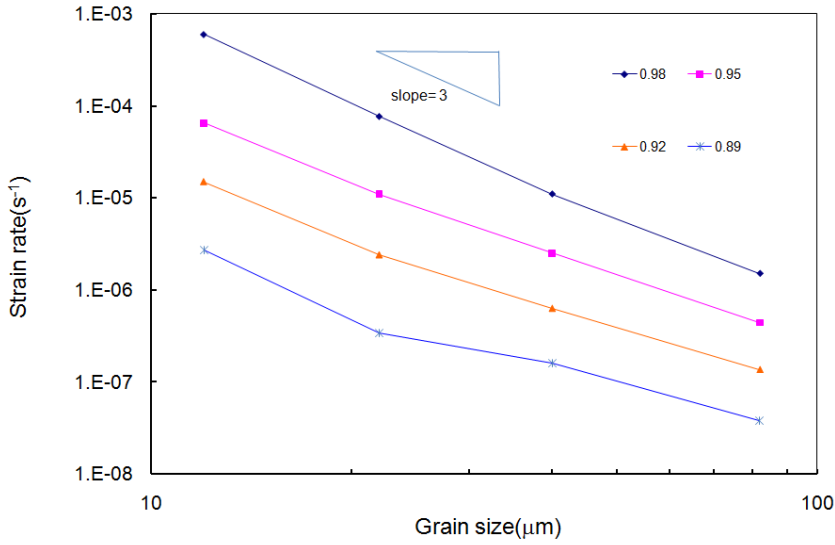


Figure 5.7. Grain size dependence of compaction strain rates for crushed limestone samples (M1, M8, M9, and M11) at fixed normalized porosity (ϕ/ϕ_0) shown in Figure 5.6b. Experimental conditions: $\sigma_e = 30$ MPa, $P_f = 20$ MPa, $T = 150$ °C. Note the grain size dependence shows a slope close to 3, consistent with diffusion-controlled IPS.

5.4.2.4 Strain rate response to changes in effective stress

In accordance with the model predictions (equations (5.1) to (5.3)), our experiments on wet, crushed limestone samples show an increase in compaction rate with increasing effective stress (see Figure 5.2a). Our data on the effect of effective stress (σ_e) on strain rate ($\dot{\epsilon}$) at fixed normalized porosity (ϕ/ϕ_0) are sparse (Figure 5.8) as a result of the stress-stepping method used in our experiments. Indeed, such data are available only for stresses of 20–30 MPa, a grain size of 37 μm , and strains up to 2% (M1, M3). Nevertheless, the data for these low strains do indicate a positive dependence of strain rate on stress with an empirical power law n value (in $\dot{\epsilon} = A\sigma_e^n$) of 1.98 ± 0.9 . This is much lower than could be expected for a dislocation creep or glide mechanism in calcite ($n > 7$ at 150°C, De Bresser et al., 2002), which can be excluded anyway because almost no creep occurred in our dry and oil-flooded samples. The observed n value is, however, more consistent with expectations for IPS; the exponential dependence embodied in equations (1) to (3) predicts an apparent n value of ~ 2 for calcite under the present conditions, assuming a stress concentration factor (B – value) at grain contacts of 10–20 appropriate for strains of a few

percent. However, the observed stress dependence of $\dot{\epsilon}$ gives no indication of the possible rate-controlling mechanism of IPS.

Let us now examine the transient response expected upon stress stepping. In theory, in a chemically closed system undergoing steady state IPS with precipitation as the rate-limiting step, the pore fluid is supersaturated with respect to the unstressed pore walls and the chemical potential of dissolved solid approaches that of the solid phase at the grain contacts (De Meer and Spiers, 1997). If the stress is stepped down at this moment, the chemical potential at the grain contacts will drop to a lower value than the one in the pore fluid. In other words, the pore fluid becomes supersaturated with respect to the stressed grain contacts. As a result, compaction will transiently stop due to lack of driving force for dissolution and diffusion at grain contacts. Compaction can only resume when the supersaturation with respect to the stressed particle contacts has been removed by precipitation. On the other hand, if the stress is stepped up, the chemical potential at particle contacts will exceed that in the bulk pore fluid, so that creep will become transiently dissolution- or diffusion-controlled until a new, higher supersaturation is built up with respect to unstressed pore walls. In this case, the switch in rate-limiting step due to the stress increment will cause a transient increase of strain rate in excess of the expected steady state rate. Such transient effects are not expected when dissolution or diffusion are rate controlling (De Meer and Spiers, 1997).

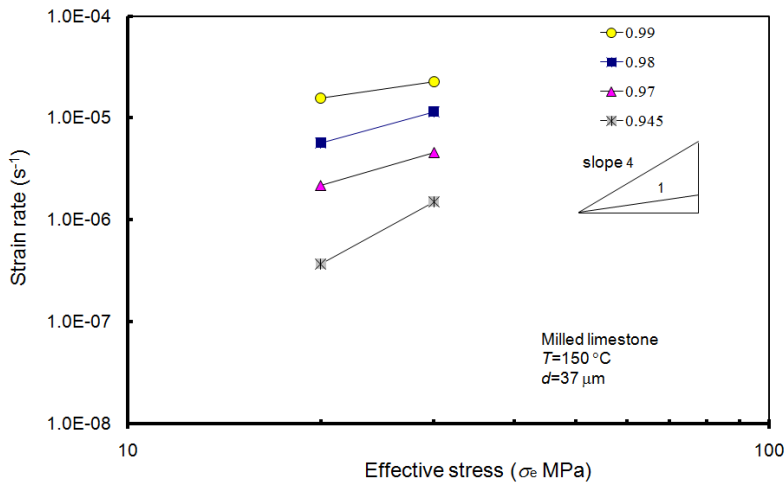


Figure 5.8. Dependence of compaction strain rate ($\dot{\epsilon}$) on effective stress (σ_e) as far as can be derived from our experimental data (Figure 5.2a).

Through our stress-stepping experiment M1, we tested the strain rate response to stress by downstepping from 30 to 20 MPa at strain of 5% (i.e., beyond the z-shaped kink seen in the log strain rate versus strain data for M1 (Figure 5.3b)). This shows a complete halt in creep from around 220 to 370 h in the strain-time curve (Figure 5.2a), followed by creep at very low rates from 370 to 400 h. Reapplication of 30 MPa effective stress at 400 h resulted

in a clear increase of creep rate, at a rate slightly higher than observed before the stress downstep from 30 to 20 MPa. From the theoretical argument given above, this behavior suggests the possibility of precipitation-controlled IPS in experiment M1 beyond the z-shaped kink in Figure 5.3b, while diffusion-controlled IPS is ruled out. All of our other stress-stepping experiments show an acceleration of creep upon increasing the applied stress. However, without an intervening downstep, it is impossible to assess if the observed rates are faster than expected.

5.4.2.5 Effects of temperature and the apparent activation energy for creep

In an attempt to assess the effect of temperature on strain rate in our crushed limestone samples, we carried out upward steps in temperature in experiment M5 (100 °C, 130 °C, and 150 °C) and downward steps in test M9 (150 °C and 28 °C). To gain further insight, the data from these experiments can be combined with those from individual tests carried out at different temperatures (100 °C versus 150 °C) under otherwise identical experimental conditions (Figure 5.2b).

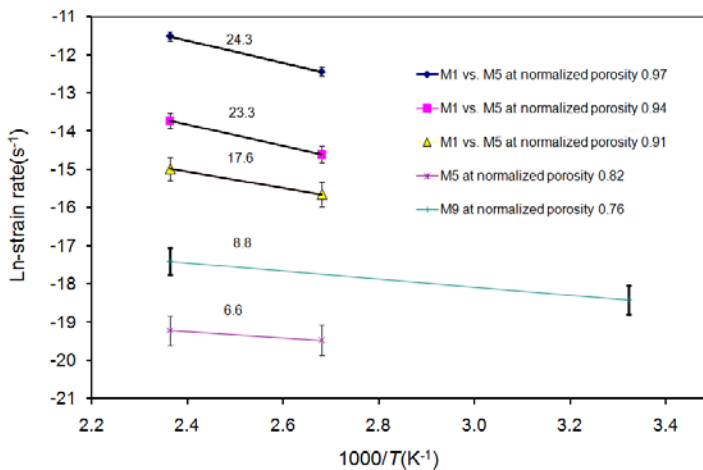


Figure 5.9. Apparent activation energy obtained from different experiments. The activation energy was obtained from the slope of the plot of natural logarithm strain rate versus $1000/T$ (in K) times R .

Although our data are few, the effect of temperature on compaction rate was clearly rather minor within our experimental range of 28 °C–150 °C. Apparent activation energies were crudely estimated from the experimental data by plotting the Arrhenius diagram shown in Figure 5.9. Values of 17.6–24.3 kJ/mol were obtained from data for the first 4% strain in tests M1 and M5, conducted at 150°C and 100°C, respectively (Figure 5.2b). These values are close to the activation energy of 15–20 kJ/mol expected for nano-pore or thin film (grain boundary) diffusion, as obtained by Nakashima (1995). However, Nakashima's estimates of the temperature dependence of D are for undersaturated solutions and, as such, do not account for the temperature dependence of C in the product DC , which

determines the rate of diffusive transport in saturated solutions (and thus during diffusion-controlled IPS). Taking into account the temperature dependence of C embedded in equation (5.4) and using Nakashima's estimate of the activation energy for diffusion shows that the product DC is expected to be virtually independent of temperature in the range 100 °C–150 °C. This suggests that diffusion-controlled IPS alone cannot explain the temperature dependence of creep seen at strain below 4–5% ($\phi/\phi_0 = 0.86$ –0.9) in our wet limestone samples unless the grain boundary structure is also dependent on temperature in an appropriate way.

Turning to higher strains, beyond the z-shaped kink in our data (e.g., Figures 2b and 3b), activation energy values of 8.8 and 6.6 kJ/mol were obtained from experiments M9 and M5 at strains of 9.7% ($\phi/\phi_0 = 0.76$) and 6.3% ($\phi/\phi_0 = 0.82$), respectively. Although lower than seen at small strains, these values are not in agreement with expectations for a diffusion-controlled process or typical activation energies for calcite dissolution or precipitation in pure systems far from equilibrium. The generally accepted activation energy for dissolution of calcite is 33 kJ/mol versus 46 kJ/mol for precipitation (Wiechers et al., 1975; Nancollas and Reddy, 1971; Inskeep and Bloom, 1985; Plummer et al., 1978; Stumm, 1992). Note, however, that these literature values were all obtained for high-purity systems at low temperatures (<70 °C).

On this basis, it is difficult to reach any firm inferences regarding the processes controlling the temperature sensitivity of creep in our tests. However, the fact that the activation energies obtained from the low strain portion of M1 and M5 are different from those obtained from temperature-stepping experiments at larger strains, beyond the z-shaped kink in our strain rate versus strain data, does suggest some switch in deformation mechanism during compaction. In conclusion to this section, we note that low values of apparent activation energy were also obtained by Hellmann et al. (2002) in their compaction experiments on chalk at temperatures of 20 °C–80 °C. Their values are ~1 kJ/mol, close to that expected for a diffusion-controlled process as explained previously.

5.4.2.6 Effects of intermittent flow-through

Our intermittent flow-through tests performed during experiments M11 (limestone) and M13 (analytical grade calcite) showed little or no effect of flow-through on strain rate at low volumetric strains or at low flow-through rates (i.e., before the z-shaped kink in the strain rate versus strain data), but a large, accelerating effect at high strains (beyond the z-shaped kink; Figure 5.3a) when the flow-through rates were high. At low strains, the diffusion-controlled model for IPS, plotted taking $DS = 5.98 \times 10^{-19} \text{ m}^3 \text{ s}^{-1}$ (at 150 °C), agrees favorably with our experimental data for samples M11 and M13 (Figures 5.3a and 5.6a). Using detailed theoretical arguments, de Meer and Spiers (1997) have shown that diffusion-controlled IPS is not accelerated by flushing a compacting material with fluid that is saturated with respect to unstressed solid (which is the case for our flow-through tests) because the pore fluid composition during diffusion-controlled IPS is almost identical to that of the newly introduced fluid. The absence of an effect of flow-through at low strains in experiments M11 and M13 is therefore consistent with compaction by diffusion-controlled IPS.

De Meer and Spiers (1997) have also shown that intermittent flow-through can only speed up IPS when the process is precipitation controlled before flow-through starts. This is because when precipitation is rate controlling the pore fluid is supersaturated with respect to the (unstressed) pore walls within the compacting material due to the slow precipitation step. Flushing under these conditions, with fluid that is saturated with respect to unstressed solid, removes the need for the precipitation step so that deformation will proceed at a faster rate determined by dissolution or diffusion control. It is clear from Figures 5.3a and 5.6a that at strains above 4–5% (i.e., beyond the z-shaped kink) our measured creep rates slow down to values below those predicted by the diffusion-controlled IPS model. However, flow-through at these high strains speeds up compaction to strain rates that closely approach those predicted by the diffusion-controlled model (Figures 5.3a and 5.6a). On this basis, we argue that compaction most likely occurs by diffusion-controlled IPS at low strains, giving way in the absence of flow-through to precipitation control at high strains (i.e., beyond the z-shaped kink in our strain rate versus strain curves (Figures 5.3 and 5.6)).

Why such a transition from diffusion- to precipitation-controlled IPS should occur is more difficult to explain. Evidence for the z-shaped kink in our data is seen in virtually all our experiments. Given that the maximum strains achieved are around 10%, changes in pore wall area available for precipitation will be small during our experiments. This rules out marked deceleration of precipitation, and an associated switch to precipitation-controlled IPS, as a result of a reduction in pore wall area as compaction proceeds. Other possibilities for the decrease in strain rates observed at the z-shaped kink in our data include a decrease in the grain boundary diffusion product DCS , for example, through changes in grain boundary structure or a rapid increase in grain contact area and hence grain boundary diffusion path length. These changes could lead to a significant slowing of diffusion-controlled IPS toward high strains, but diffusion would then remain rate controlling, which is inconsistent with the results of our flow-through tests. The possibility that the Z-shaped kink in our strain rate versus strain data (Figures 5.3 and 5.6) might reflect a machine-related artifact can also be rejected as it occurs at different strains and different piston positions in different experiments. Moreover, we have seen no such kink in similar experiments on other materials or on wet calcite aggregate with injected CO_2 (Liteanu and Spiers, 2009). A remaining possibility that cannot be eliminated is that there may be a buildup of impurity ions in the pore fluid during our experiments derived either from the sample or from the apparatus. It is well documented in the literature that small quantities of dissolved impurity ions can dramatically slow down the kinetics of precipitation of calcite due to surface site contamination, thus leading to precipitation-controlled mass transfer (Zhang and Spiers, 2005a, 2005b).

M11				M13			
Ca ppm	Mg ppm	S ppm	Notation	Ca ppm	Mg ppm	S ppm	Notation
44.9	3.8	10.6	Start saturated solution	27.4	0	0	Start saturated solution
55.1	3.3	11.0	First flow through at strain 1.5%	45.7	0.5	1.8	First flow through at strain of 1.5%
53.1	3.9	9.8	Send flow through at strain 5.7%	43.7	0.2	1.1	Second flow through at strain 5.9%
63.2	5.7	12.6	Beginning of third flow through at strain 6.1%	65.8	1.2	0	Third flow through at strain of 8.7%
46.3	4.5	8.1	End of third flow through at strain 6.3%	102.2	5.1	5.1	End of test at strain of 9.2%

Table 5.3. Pore fluid analysis from Transmittent flow-through tests of M11 and M13. Units are in mg/kg (ppm).

5.4.2.7 Effects of sample impurities

Our measurements of pore fluid composition, made by collecting the fluid released during our flow-through tests on samples M11 and M13, provide a firm basis for testing the possibility advanced in the previous section that the z-shaped kink in our data of Figures 5.3a and 5.6a might be due to the buildup of impurity ions in the pore fluid. Our fluid composition data shown in Table 5.3 indeed show that there is a significant increase in the concentrations of Ca, Mg, and S in the pore fluid during the progress of our compaction experiments. These species cannot be derived from our setup as the Monel alloy from which it is made contains very little Ca, Mg, and S but a great deal of Fe, Ni, and Cu, which are not found in the pore fluid. We infer that the observed contamination of the pore fluid by Mg, Ca, and S is caused by liberation of these species from the solid samples. Of these contaminants, Mg^{2+} is known to drastically inhibit precipitation of calcite and thus to decelerate IPS in calcite (Reddy and Wang, 1980; Zhang and Spiers, 2005a, 2005b). We accordingly infer that the z-shaped kink seen in the present strain rate versus strain data is caused by a buildup of sample-derived Mg^{2+} in the pore fluid and that this most likely caused a switch from diffusion-controlled IPS at low strains to precipitation-controlled IPS creep at higher strains. It is also possible that the observed change in S concentration played a similar role.

To examine the effects of sample impurity content further, we now compare our results for crushed limestone, analytical grade calcite (99% pure), and superpure calcite (99.95%) as seen in experiments M11, M13, and M18 (Figures 2c and 10). Samples M11, M13, and

M18 are of the same grain size fraction ($12 \pm 4 \mu\text{m}$) and were tested under identical conditions. From the creep curves presented in Figure 5.2c, it is clear that the superpure calcite sample achieved larger strains at any given time than the analytical grade or crushed limestone samples (Figure 5.2c). Note, however, that the starting porosity of M11 ($\phi_0 = 27.6\%$) was significantly lower than for M13 and M18 (both $\phi_0 = 34\%$). To take into account the effect of initial porosity, normalized porosity (ϕ/ϕ_0) was used in Figure 5.10. Comparing Figures 3a and 10, it is clear that M11 and M13 become closer in plot of strain rate versus normalized porosity (ϕ/ϕ_0). At small strains (or large ϕ/ϕ_0), all three samples showed similar compaction rates (Figure 5.10) and good agreement with the diffusion-controlled model for IPS taking $DS = 5.98 \times 10^{-19} \text{ m}^3 \text{ s}^{-1}$ at 150°C and an initial porosity of 30%. However, the kink in the strain rate versus strain curve occurs at larger strains in M18 (superpure) than in M13 (analytical grade) and at larger strains in M13 than in M11 (crushed limestone; Figure 5.10). This is consistent with a higher level of impurities in the pore fluid in impure samples, leading to an earlier retarding effect of species such as Mg^{2+} as they are liberated by ongoing dissolution of the sample.

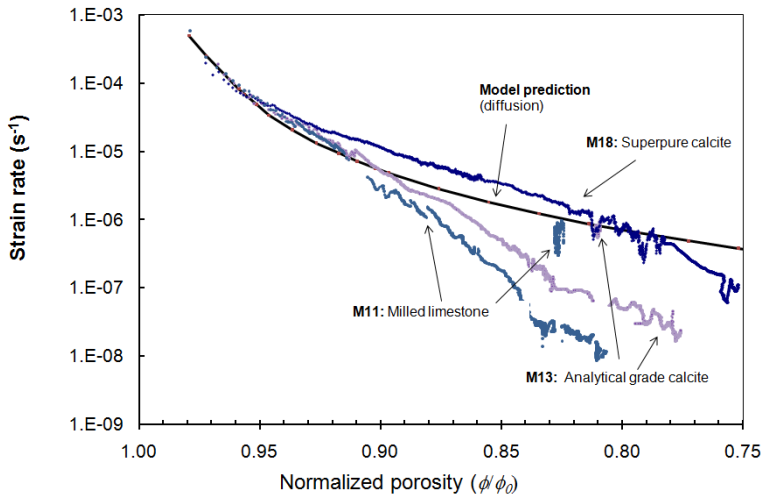


Figure 5.10. Effect of impurities on the compaction rates. The strain rate drop occurs earlier (at smaller strains or larger normalized porosity) in crushed natural limestone than in analytical grade and superpure calcite sample. Conditions: $\sigma_e = 30 \text{ MPa}$, $T = 150^\circ\text{C}$, and $d = 12 \mu\text{m}$.

This interpretation remains consistent with the notion that creep in our experiments is controlled by diffusion-limited IPS at low strains, giving way to precipitation control at high strains as a result of the retardation of precipitation by the growing impurity content of the pore fluid. Making use of the data presented by Zhong and Mucci (1989), we further note that the retardation of calcite precipitation by impurities is most significant at relatively low driving forces for precipitation (saturation ratio < 2.6). In our experiments, the driving force for IPS is related to the effective stress and the compaction strain. At small strains, the stress concentration is large at the grain contact, so the local chemical

potentials and hence the driving force for dissolution and precipitation are high. In this case, the effects of impurities on precipitation are thus expected to be relatively unimportant. However, at larger strains, the driving force for IPS is lower, so that precipitation inhibitors in the pore fluid are likely to have a larger effect, promoting a change from diffusion- to precipitation-controlled IPS further.

5.4.3 Synthesis: deriving creep parameters for diffusion-controlled IPS in calcite

Taken together, our microstructural, mechanical, flow-though, and chemical data, plus our consideration of theoretical models for IPS, all point strongly to creep of our wet calcite samples being dominated by diffusion-controlled IPS at low strains (<4–5%) with precipitation-controlled IPS taking over at higher strains. This transition seems to be associated with a buildup of Mg^{2+} and perhaps other ions in solution, which slow down the calcite precipitation reaction. We cannot explain the effect of temperature on creep well, but the data are few and still broadly consistent with IPS in that the observed values are unusually low.

Assuming now that diffusion-controlled IPS is indeed the main mechanism controlling creep in our experiments at low strains, we now try to evaluate the relevant constitutive parameter DCS (i.e., to obtain a flow law for compaction of (pure) granular calcite by this mechanism). We have already shown that putting $DS = 5.98 \times 10^{-19} \text{ m}^3 \text{ s}^{-1}$ gives reasonable agreement with our low strain data. We now refine this estimate. We follow the work of Spiers and Brzesowsky (1993) by deriving DCS values from our experiments carried out under different conditions, and then isolate DS from C using the experimental data on calcite solubility given via equation (5.4) by Plummer and Busenberg (1982) (see also Duan and Li, 2008). The DCS values derived by fitting equation (5.2) to our experimental rate data at 150°C for strains up to 4% lie between 9.25×10^{-25} and $1.85 \times 10^{-25} \text{ m}^3 \text{ s}^{-1}$. The DS values isolated for calcite then fall between 2.98×10^{-18} and $3.73 \times 10^{-19} \text{ m}^3 \text{ s}^{-1}$ at 150 °C. If we assume a grain boundary thickness of 1 nm, the D values obtained for calcite at 150 °C are then 2.98×10^{-9} to $3.73 \times 10^{-10} \text{ m}^2 \text{ s}^{-1}$. Extrapolating the D and DS values to room temperature using an activation energy of 15 kJ/mole (Nakashima, 1995), we obtain D values of 4.59×10^{-10} to $5.74 \times 10^{-11} \text{ m}^2 \text{ s}^{-1}$ and DS values of 4.59×10^{-19} to $5.74 \times 10^{-20} \text{ m}^3 \text{ s}^{-1}$, which are remarkably close to those obtained by Spiers et al. (2004) for diffusion-controlled IPS in halite at room temperature. To model compaction of pure calcite aggregates by diffusion-controlled IPS, these values can be inserted into equation (5.2), using (5.4) to provide C , an activation energy of 15 kJ/mole to describe the temperature dependence of D , and the functions for $B = B(\phi_0, e_v)$ and $f_d(\phi_0, e_v)$ given in Appendix A.

5.5 Conclusions

Uniaxial compaction creep experiments have been carried out on granular calcite samples consisting of crushed/crushed limestone, analytical grade calcite, and superpure calcite. Samples with mean grain size fractions varying from 12 to 86 μm were tested at 28°C to 150°C, applied effective stresses of 20 to 47 MPa, and a pore fluid pressure of 20 MPa. The pore fluid used consisted of a CaCO_3 solution that was presaturated with respect

to unstressed sample material. Most experiments were done on the crushed limestone samples at 150 °C. Control experiments were carried out on lab-dry samples and samples flooded with (chemically inert) silicone oil. Intermittent flow-through experiments were also performed to assess the effect of flushing the samples with the pore fluid. The main findings are summarized below.

1. Wet samples (i.e., samples tested with the pore fluid solution phase) showed easily measurable compaction creep, while the dry and oil-flooded samples showed little or no creep, demonstrating that compaction was due to a water-enhanced deformation mechanism.

2. The microstructures developed in the wet samples showed grain-to-grain indentations, sutured grain contacts, and overgrowths as well as dissolution pits and growth layers developed on reference crystal surfaces added to the samples. The implication is that the dominate deformation mechanism during wet compaction was intergranular pressure solution or IPS.

3. The creep rates measured at low strains (<4 or 5%) in wet samples were found to be consistent with rate predictions made using a standard model for diffusion-controlled pressure solution, inserting parameter estimates from the literature. The data on creep rate at these low strains showed a roughly inverse cube dependence on grain size, a low sensitivity to effective stress (mean apparent n value around 2), and a low sensitivity to temperature (apparent activation energy of 6–24 kJ/mole), also broadly consistent with diffusion-controlled IPS. Creep rate predictions made using models assuming dissolution- or precipitation-controlled IPS resulted in rates more than one order of magnitude faster than observed and predicted an inverse linear dependence of strain rate on grain size. We infer that creep in the low strain regime was dominated by diffusion-controlled IPS.

4. Creep rates obtained at the higher strains investigated (5–10%) showed a marked decrease to rates well below those predicted by the diffusion-controlled IPS model. In this higher strain regime, transient flushing of the sample (i.e., transient flow-through) with “fresh” pore fluid led to an acceleration of creep by around one order of magnitude to rates expected for diffusion control. This type of behavior is predicted by theoretical models for creep by precipitation-controlled IPS only. No such effect was seen at low strains. At the high strains, we also found that through-flushed pore fluid became enriched in magnesium and other sample-derived contaminant ions compared with the low strain regime. Contaminant ions such as magnesium are known to decelerate the precipitation reaction in calcite and slow pressure solution by promoting precipitation control. On this basis, we infer that the reduction in creep rates observed at strains beyond 4–5% is probably caused by a transition from diffusion- to precipitation-controlled IPS, as the concentration of sample-derived contaminants builds up with progressive dissolution of the sample material. This interpretation is supported by the fact that superpure samples compacted more and faster than analytical grade material, which in turn compacted faster than the crushed limestone.

5. Fitting of the theoretical model for diffusion-controlled IPS to our low strain creep data for wet, crushed limestone allowed an estimate to be made of the diffusion products DCS and DS that determine the absolute rate of pressure solution by IPS in calcite. The experimentally derived values of the diffusion product DS (grain boundary diffusion coefficient times mean thickness of the grain boundary fluid film) for calcite is between

2.98×10^{-18} to 3.73×10^{-19} m³/s at 150 °C and between 4.59×10^{-19} to 5.74×10^{-20} m³ s⁻¹ at room temperature, assuming an activation energy for diffusion of 15 kJ/mole from the literature. These values of DS at room temperature are remarkably close to the DS values obtained for diffusion-controlled IPS in halite at room temperature.

Appendix A: Explicit Expressions for the Functions $B(\phi_0, e_v)$ and $f_x(\phi_0, e_v)$

In deriving expressions for the stress intensification factor $B(\phi_0, e_v)$ and the porosity functions $f_x(\phi_0, e_v)$ in equations (5.1) to (5.3), we follow previous workers (Renard et al., 1999) in assuming that the grains are spheres with diameter d and have a simple cubic packing. At zero strain, the grains thus have point contacts of zero area. In practice, however, a small elastic distortion (Hertian distortion) will ensure a finite contact. At a strain e_v , accumulated by postelastic creep, the grain-to-grain contacts become a circle and the material removed from the truncated spheres is redistributed to the free pore walls.

From the geometry thus defined, it is easily shown that the stress intensification factor at grain contacts is:

$$B = \frac{6d^2(1 - e_v)^{2/3}}{A_c} \quad (5.A1)$$

where A_c is the contact areas of per grain at strain e_v , given by:

$$A_c = 6\pi(r^2 - x^2) \quad (5.A2)$$

where x is the distance from grain center to grain contact center at strain e_v and r is the grain radius measured from grain center to pore wall. In turn, x is given by:

$$x = \frac{d}{2}(1 - e_v)^{1/3} \quad (5.A3)$$

and r can be obtained by solving the cubic equation:

$$-2r^3 + 4.5r^2x - 1.5x - \frac{d}{2} = 0 \quad (5.A4)$$

The porosity functions $f_x(\phi_0, e_v)$ given in equations (5.1) to (5.3) are geometric functions given by:

$$f_s(\phi_0, e_v) = \frac{6}{(1 - e_v)^{1/3}} \quad (5.A5)$$

$$f_d(\phi_0, e_v) = \frac{144\pi d^2}{A_c(1 - e_v)^{1/3}} \quad (5.A6)$$

$$f_p(\phi_0, e_v) = \frac{A_c}{A_p} \frac{6}{(1 - e_v)^{1/3}} \quad (5.A7)$$

where A_p is the pore area per grain at strain e_v given by:

$$A_p = 4\pi r^2 - 6(2\pi r(r - x)) \quad (5.A8)$$

5.6 References

- Bathurst, R. G. C. (1958), Diagenetic fabrics in some British Dinantian limestones, *Liverpool and Manchester Geology*, 2, 11-36.
- Berner, R. A., and J. W. Morse (1974), Dissolution kinetics of calcium carbonate in sea water IV, Theory of calcite dissolution, *Am. J. Sci.*, 274, 108-134.
- Bos, B., and C. J. Spiers (2002), Frictional-viscous flow phyllosilicate-bearing fault rock: Microphysical model and implication for crustal strength profiles, *J. Geophys. Res.* 107, (132), doi: 10.1029/2001JB000301.
- Busenberg, E., and L. N. Plummer (1986), A comparative study of dissolution and crystal growth kinetics of calcite and aragonite. *U.S Geol. Surv. Bull.* 1578. 139-168.
- Caine, J. S., J. P. Evans, and C.B. Forster (1996), Fault zone architecture and permeability structure, *Geology* 24, 1025–1028.
- De Bresser, J. H. P., B. Evans and J. Renner (2002). On estimating the strength of calcite rocks under natural conditions. *Geological Society, London, Special Publications* 200. 309-329, doi: 10.1144/GSL.SP.2001.200.01.18.
- De Meer, S., and C. J. Spiers (1997), Uniaxial compaction creep of wet gypsum aggregates, *J. Geophys. Res.* 102, 875-891.
- De Meer, S., and C. J. Spiers (1999), Mechanisms and kinetics of creep by intergranular pressure solution. in: *Growth, Dissolution and Pattern Formation in Geosystems*, edited by B. Jamtveit and P. Meakin, Kluwer Academic Publishers, Dordrecht, 345-363.
- Duan, Z. and D. Li (2008), Coupled phase and aqueous species equilibrium of the $\text{H}_2\text{O}-\text{CO}_2-\text{NaCl}-\text{CaCO}_3$ system from 0 to 250 °C, 1 to 1000 bar with NaCl concentrations up to saturation of halite. *Geochim. Cosmochim. Acta*, 72, 5128-5145, doi: 10.1016/j.gca.2008.07.025.
- Durney, D. W. (1972), Solution transfer, an important geological deformation mechanism, *Nature*, 235, 315-317.
- Dysthe, D. K., Y. Podladchikov, F. Renard, J. Feder, and B. Jamtveit (2002), Universal Scaling in transient creep, *Phys. Rev. Lett.*, 89, 246102-1-246102-4.
- Dysthe, D. K., F. Renard, J. Feder, B. Jamtveit, P. Meakin, and T. Jøssang (2003), High resolution measurement of pressure solution creep, *Phys. Rev. E.*, 68, 011603(1-13).

- Ellis, A. (1959), The solubility of calcite in carbon dioxide solutions, *Am. J. Sci.* 257, 354-365.
- Ellis, A.J. (1963), The solubility of calcite in sodium chloride solutions at high temperatures, *Am. J. Sci.* 261, 259-267.
- Gledhill, D and J. W. Morse (2006), Calcite dissolution kinetics in Na-Ca-Mg-Cl brines, *Geochim. Cosmochim. Acta.* 70, 5802-5813, doi: 10.1016/j.gca.2006.03.024.
- Gratier J.P., P. Favreau., F. Renard and E. Pili (2002), Fluid pressure evolution during the earthquake cycle controlled by fluid flow and pressure solution crack sealing, *Earth Planets Space* 54, 1139-1146.
- Gratier J. P., P. Favreau and F. Renard (2003), Modeling fluid transfer along californian faults when integrating pressure solution crack sealing and compaction process, *J. Geophys. Res.*, 108 (B2) 28-52.
- Hellmann, R., P. J. N. Renders, J. P. Gratier, and R. Guiguet (2002), Experimental pressure solution compaction of chalk in aqueous solutions Part 1, Deformation behavior and chemistry, in: *Water-Rock Interaction, Ore Deposits, and Environmental Geochemistry: A Tribute to David A. Crerar*, edited by R. Hellmann and S. A. Wood, The Geochemical Society, Special Publication 7, 129-152.
- Inskip, W. P., and P. R. Bloom (1985), An evaluation of rate equations for calcite precipitation kinetics at pCO₂ less than 0.01 atm and pH greater than 8, *Geochim. Cosmochim. Acta*, 9, 2165-2180
- Lehner, F. K. (1990), Thermal dynamics of rock deformation by pressure solution, in: *Deformation Processes in Minerals, Ceramics and Rocks*, edited by D. Barber and P. Meredith, Unwin Hyman, London, pp. 296-33
- Lehner, F. K. (1995), A model for intergranular pressure solution in open systems, *Tectonophysics* 245, 153-170.
- Liteanu, E. and C. J. Spiers (2009), Influence of pore fluid salt content on compaction creep of calcite aggregates in the presence of supercritical CO₂. *Chem. Geol.* 265, 134-147. doi:10.1016/i.chemgeo.2008.12.010.
- Miller, S. A., Y. BenZion, J. P. Burg (1999), A three dimensional fluid-controlled earthquake model: Behavior and implications, *J. Geophys. Res.* 104, 10621-10638.
- Nakashima, S. (1995), Diffusivity of ions in pore water as a quantitative basis for rock deformation rate estimates, *Tectonophysics* 245, 185-203.
- Nancollas, G. H., and M. M. Reddy (1971), The crystallization of calcium carbonate II: Calcite growth mechanism, *J. Colloid Interface Sci.* 37, 843-830.
- Niemeijer, A. R., C. J. Spiers, and B. Bos (2002), Compaction creep of quartz sand at 400-600 °C: Experimental evidence for dissolution-controlled pressure solution, *Earth Planet. Sci. Lett.* 195: 261-275.
- Paterson, M. S. (1995), A theory for granular flow accommodated by material transfer via an intergranular fluid, *Tectonophysics* 245, 135-152.
- Plummer, L. N., and E. Busenberg (1982), The solubilities of calcite, aragonite and vaterite in CO₂-H₂O solutions between 0 and 900 °C, and an evaluation of the aqueous model for the system CaCO₃-CO₂-H₂O, *Geochim. Cosmochim. Acta* 46, 1011-1040.
- Plummer, L. N., T. M. L. Wigley, and D. L. Parkhurst (1978), The kinetics of calcite dissolution in CO₂-water systems at 50 to 600 °C and 0.0 to 1.0 atm CO₂, *Am. J. Sci.* 278, 179-216.

- Pokrovsky, O.S., and J. Schott (2002), Surface chemistry and dissolution kinetics of divalent metal carbonates. *Environ. Sci. Technol.* 36, 426–432.
- Reddy, M. M. and K. K. Wang (1980), Crystallization of calcium carbonate in the presence of metal ions. I. Inhibition of magnesium ion at pH 8.8 and 250 °C, *J. Cryst. Growth* 50, 470-480.
- Renard F., P. Ortoleva, and J. P. Gratier (1997), Pressure solution in sandstones: influence of clays and dependence on temperature and stress, *Tectonophysics* 280, 257-266.
- Renard F., Park A., P. Ortoleva, and J. P. Gratier (1999), A transitional pressure solution model. *Tectonophysics* 312, 97-115.
- Renard, F., J. P. Gratier, and B. Jamtveit (2000), Kinetics of crack-sealing, intergranular pressure solution, and compaction around active faults, *J. Struct. Geol.* 22, 1395-1407.
- Renard, F., J. Schmittbuhl, J. P. Gratier, P. Meakin, E. Merino (2004), The three-dimensional morphology of stylolites: roughness analysis and possible genetic implications, *J. Geophys. Res.* 108, B03209, doi:10.1029/2003JB002555.
- Renard, F., E. Gundersen, R. Hellemann, M. Collombet, and Y. LeGuen (2005), Numerical modeling of the effect of carbon dioxide sequestration on the rate of pressure solution creep in limestone: Preliminary results, *Oil & Gas Science and Technology-Rev. IFP* 60, 381-399.
- Rutter, E. H. (1976), The kinetics of rock deformation by pressure solution, *Philos. Trans. R. Soc. London* A283, 203-219.
- Rutter, E. H. (1983), Pressure solution in nature, theory and experiment, *J. Geol. Soc. Lond.* 140, 725-740.
- Schutjens, P. M. T. M. (1991), Experimental compaction of quartz sand at low effective stress and temperature conditions, *J. Geol. Soc. Lond.* 148, 527–539.
- Sjöberg, E.L. and D. T. Rickard (1984), Temperature dependence of calcite dissolution kinetics between 1 and 62 °C at pH 2.7 to 8.4 in aqueous solutions. *Geochim. Cosmochim. Acta* 48, 485–493.
- Schlumberger, (2007), Schlumberger Market Analysis, http://www.slb.com/services/industry_challenges/carbonates.aspx
- Spiers, C. J., P. M. T. M. Schutjens, R. H. Brzesowsky, C. J. Peach, J. L. Liezenberg & H. J. Zwart, Eds. (1990), "Experimental determination of constitutive parameters governing creep of rocksalt by pressure solution. *Deformation Mechanisms, Rheology and Tectonics*, The Geology Society, London.
- Spiers, C. J., and R. H. Brzesowsky (1993), Densification behaviour of wet granular salt: theory vs. experiment, in *Seventh Symp. On Salt*, edited by Kakihana, H., Hardy, H.R. Jr., Hoshi, T., Toyokura, K., vol I, 83-92.
- Spiers, C. J., S. DeMeer, A. R. Niemeijer, and X. Zhang (2004), Kinetics of rock deformation by pressure solution and the role of thin aqueous films. In *Physiochemistry of water in Geological and Biological Systems* (ed. S. Nakashima et al.). pp. 129-158, Universal Academy Press, Inc.
- Stumm, W. (1992), *Chemistry of the solid-water interface*, John Wiley & Sons, USA, 428 pp.
- Tada, R., and R. Siever (1989), Intergranular pressure solution during diagenesis, *Annu. Rev. Earth. Planet. Sci.* 17, 89-118.

- Tuncay, K., and P. Ortoleva (2004), Quantitative basin modeling: present state and future developments towards predictability, *Geofluids* 4, 23-39.
- Van Noort, R., H. J. M. Visser, and C. J. Spiers (2008), Influence of grain boundary structure on dissolution controlled pressure solution and retarding effects of grain boundary healing, *J. Geophys. Res.* 113, B03201, doi:10.1029/2007JB005223.
- Weyl, P. K. (1959), Pressure solution and the force of crystallization – a phenomenological theory, *J. Geophys. Res.* 64, 2001-2025.
- Wiechers, H. N. S., P. Sturrock, and G. V. R. Marais (1975), Calcium carbonate crystallization kinetics, *Water Res.* 9, 835-845.
- Yang, X. S. (2000), Pressure solution in sedimentary basins: effect of temperature gradient, *Earth Planet. Sci. Lett.* 176, 233-243.
- Zhang, X., J. Salemans, C. J. Peach, and C. J. Spiers (2002), Compaction experiments on wet calcite powder at room temperature: evidence for operation of intergranular pressure solution, in *Deformation Mechanisms, Rheology and Tectonics: Current Status and Future Perspectives*, edited by S. de Meer, M. R. Drury, J. H. de Bresser, G. M. Pennock, Geological Society, London, Special Publications, 200, 29-39.
- Zhang, X., and C. J. Spiers (2005a), Compaction of granular calcite by pressure solution at room temperature and effects of pore fluid chemistry, *Int. J. Rock. Mech. Min. Sci.* 42, (7-8), 950-960, doi:10.1016/j.ijrmms.2005.05.017.
- Zhang, X., and C. J. Spiers (2005b), Effects of phosphate ions on intergranular pressure solution in calcite – an experimental study, *Geochim. Cosmochim. Acta* 69, (24), 5681-5691, doi: 10.1016/j.gca.2005.08.006.
- Zhang, X., Putnis, A., Putnis, C and C. J. Spiers (2009), Effects of salinity on the morphology of dissolution pits in calcite -implication for CO₂ sequestration in carbonate rocks, *International Symposium of the Society of Core Analysts*, The Netherlands 27-30 September, 2009, SCA2009-39.
- Zhong, S., and A. Mucci (1989), Calcite and aragonite precipitation from sea water solutions of various salinities: Precipitation rates and overgrowth compositions, *Chem. Geol.* 78, 283-299.
- Zubtsov, S., F. Renard, J. P. Gratier, D. K. Dyshe, and V. Traskine (2005), Single-contact pressure solution creep on calcite monocrystals, *Geological Society, London, Special Publications* 243, 81-95.

6. Effects of pore fluid flow and chemistry on compaction creep of calcite by pressure solution at 150 °C

This chapter is accepted for publication as: Zhang, X., C. J. Spiers and C. J. Peach (2010), Effects of pore fluid flow and chemistry on compaction creep of calcite by pressure solution at 150 °C, accepted, Geofluids.

Abstract

Uni-axial compaction creep experiments were performed on crushed limestone and analytical grade calcite powders at 150 °C, a pore fluid pressure of 20 MPa and 30 MPa effective axial stress. Previous experiments have shown that compaction under these conditions is dominated by intergranular pressure solution. The aim of the present tests was to determine the inter-relationship between pore fluid chemistry, compaction rate and rate controlling process. Intermittent flow-through runs conducted using CaCO₃ solution in chemical equilibrium with unstressed sample material showed no effect on creep rate at low strains (<4-5%) but a major acceleration at high strains (5-10%). Measurements of the Ca²⁺ concentration present in the fluid samples collected from compacting samples during periods of flow-through revealed the build-up of a high super-saturation of CaCO₃ during compaction under zero flow conditions, especially at high strains. Active flow-through led to a drop in Ca²⁺ concentration, which corresponded with creep acceleration at high strains. Addition of NaCl to the pore fluid at a concentration of 0.5 M increased the creep rate of the analytical grade calcite sample roughly in proportion to the enhancement of calcite solubility. Addition of Mg²⁺ and HPO₄²⁻ to the pore fluid, in concentrations of 0.05 M and 0.001 M respectively, caused major retardation of compaction creep of the analytical grade samples. Integrating our mechanical, flow-through and chemical data, points strongly to diffusion controlled IPS being the dominant deformation mechanism under closed system (zero flow) conditions at lower strains, giving way to precipitation control at higher strains. The fluid composition data collected suggest that this transition is due to accumulation of impurities in the pore fluid, derived either from the sample or the apparatus. Mg²⁺ and phosphate ions are common in natural pore fluids, it is likely that retarded precipitation will be the rate limiting step in IPS of carbonates in nature. To qualify diagenetic compaction and porosity and permeability reduction rate in carbonates need to account for this.

6.1 Introduction

Intergranular pressure solution (IPS) is an efficient deformation and compaction mechanism under upper and mid crustal conditions and is an important process of porosity and permeability reduction both in bulk rock and in fault zones (Durney, 1972; Elliot, 1976; Rutter, 1983; Tada and Siever, 1989; Graham et al., 2003; Renard et al., 2004; Yashuhara et al., 2005; Tondi et al., 2006). It is of particular importance in the diagenetic compaction, in fault sealing and healing and in the development of stylolite solution seams in carbonate

reservoir rocks (Bathurst, 1958, 1975; Wanless, 1979; Buxton and Sibley, 1981; Peacock et al., 1998; Ehrenberg et al., 2006). Compaction by IPS involves dissolution of mineral grains at stressed grain contacts, diffusion of the dissolved material along grain boundary fluid films or channels, followed by precipitation on free pore walls (e.g. Tada & Siever, 1989) or removal of mass by long range advection in the pore fluid (Lehner, 1990, 1995; Renard & Ortoleva, 1997; Spiers et al., 2004; Gundersen et al., 2002; Zubtsov et al., 2005). The grain boundary and pore fluid phase forms the medium for each of the serial kinetic processes involved in IPS. Previous work on the kinetics of intergranular pressure solution (see Lehner, 1990, 1995; Dewers & Hajash, 1995; Bathurst, 1996; DeMeer & Spiers, 1997, 1999; Ngwenya et al., 2000) has shown that the concentration of dissolved solute present in the pore fluid during deformation by IPS offers a chemical signature which can be used to investigate the rate limiting step of IPS in experiments or to distinguish IPS from other deformation mechanisms (Elias & Hajash, 1992; He et al., 2003). In addition, pore fluid composition can be manipulated to accelerate or retard the elementary kinetic processes of dissolution and/or precipitation and to change mineral solubility, thus influencing the rate of IPS and providing insight into the rate limiting step (Zhang & Spiers, 2005a, 2005b; DeMeer & Spiers, 1997; Traskine et al., 2008; Zhang et al., 2010). Indeed impurity ions commonly seen in natural pore fluids may significantly reduce the IPS rates and change the rate limiting step of IPS in nature (Zhang and Spiers, 2005a, 2005b; Liteanu & Spiers, 2009).

In a previous study of the compaction behaviour of wet granular calcite (crushed limestone and analytical grade calcite powders) at 150 °C, we reported mechanical, microstructural and limited chemical evidence for IPS being the dominant deformation mechanism (Zhang et al., 2010). However, we were unable to unambiguously identify the rate controlling processes. Here, we extend those compaction experiments, at the same temperature and stress conditions (i.e. at 150 °C, at effective stresses of 30 and 40 MPa, and at a pore fluid pressure of 20 MPa), focusing on pore fluid chemical signatures and the effects of pore fluid composition on deformation mechanism and rate limiting step. Our specific aims are: 1) to determine the effects of flow-through of fresh pore fluid on the rates of IPS, simulating an open system; 2) to investigate chemical signatures present in the pore fluid as potential indicators of rate limiting mechanism; and 3) to investigate the effects of adding known dissolution/precipitation inhibitors and NaCl to the pore fluid. Our results confirm that chemical conditions in the pore fluid have a strong influence on the rate and the rate limiting mechanism of IPS in calcite and need to be taken into account in any attempts to predict IPS rates in nature (Liteanu & Spiers, 2009).

6.2 Experimental method

The experiments consisted of uniaxial or 1-dimensional compaction creep tests conducted in a high temperature oedometer at applied effective stresses (σ_e) of mostly 30 or 40 MPa, a pore fluid pressure (P_f) of 20 MPa and a temperature (T) of 150 °C. Flow-through tests were carried out during compaction. Pore fluids sampled during flow-through tests were analyzed using Inductively Coupled Plasma mass spectrometry (ICP-MS) to investigate chemical signatures for deformation mechanisms. The effects of pore fluid

additives such as Mg^{2+} , HPO_4^{-2} and NaCl on the mechanical behaviour were also investigated.

6.2.1 Starting materials and pore fluids

Hydrocarbon-free, oil field limestone samples, provided by Shell Research, and analytical grade calcite powder (Merck 99% pure) were used as the starting materials in this study (see also Zhang et al., 2010). The limestone was crushed, ball-milled and sieved. It was then gravity settled into grain size fractions of 12 ± 4 and 22 ± 6 μm , using a deionised water column. A fraction with grain size of $37 \pm 9 \mu\text{m}$ was prepared by crushing, milling and sieving only. The grain size distributions of the various fractions were measured using a Malvern particle size analyser. For all samples, more than 80wt% of the grains fell in the stated ranges. XRF and XRD analysis recently re-measured at lab of the crushed and sieved material showed that the limestone consisted of mainly calcite (>96%) with impurities of SiO_2 , MgO and Al_2O_3 etc (Table 6.1). The Merck analytical grade calcite powder has a purity of 99% calcium carbonate, the main impurities being Sr, Na and Mg according to the manufactory specification. The grain size of the Merck calcite samples was determined using Scanning Electron Microscope (SEM) observations, plus linear intercept analysis, and fell between 1 and 40 μm with an average value of 14 μm . A 12 ± 4 μm fraction of Merck material was made for use in the experiments, by gravity settling.

Pre-saturated pore fluid solutions were made for individual calcite samples by adding excess sample powder to deionized water and stirring for at least 48 hours at room temperature. On the basis of the data presented by Rickard and Sjöberg (1983), Sjöberg and Rickard (1984) and Pokrovsky and Schott (2002), 48 hours are expected to be sufficient to obtain a saturated solution at atmospheric conditions. Since the solubility of calcite decrease with increasing temperature, the pore fluid solution used in this study would have been slightly super-saturated with calcite when brought to the experimental conditions (150 °C and 20 MPa). Magnesium, phosphate and NaCl bearing solutions were made by adding a fixed mass of $\text{MgCl}_2 \cdot 6\text{H}_2\text{O}$, Na_2HPO_4 or NaCl respectively to the pre-saturated calcite solution, again in the presence of excess sample powder. These additives were used only in experiments reported on the Merck calcite powder.

SiO_2 (%)	Al_2O_3 (%)	Fe_2O_3 (ppm)	MnO (ppm)	MgO (%)	CaO (%)	Na_2O (%)	K_2O (ppm)	TiO_2 (ppm)	P_2O_5 (ppm)	Sum (%)
0.99	0.26	0.0	40.5	0.79	97.7	0.13	359.9	154.9	674.6	99.94

Table 6.1. XRF analysis of the hydrocarbon-free, oil field limestone used as a starting material. XRD analysis showed calcite only, with other phases below reliable detection.

6.2.2 Experimental apparatus

A schematic overview of the experimental apparatus used is presented in Figure 6.1 (see Zhang et al., 2010 for detailed description). The equipment consists of an externally heated, 1-D compaction apparatus loaded using an Instron 8562 materials testing machine, a pore fluid flow-through and pressure control system, a temperature control system and a

computer control and data acquisition system. The Instron 8562 machine was equipped with a 100 kN load cell employed to measure the external stress applied to the loading piston. The compaction vessel has an inner diameter of 20 mm and is sealed against the upper and lower loading pistons using viton O-rings. The pistons are tipped with porous stainless steel plates to allow easy fluid access to the sample through the piston bores. The pore fluid system consists of a 13 ml fluid-filled hand-driven syringe pump, an 11 ml gas-backed pressure separator, and an argon gas reservoir maintained at 20 MPa pressure in all tests. The upstream pore fluid pressure was trimmed via the hand pump and measured using a 50 MPa pressure transducer located in the two pore fluid inlet line. Experiments with pore fluid at a pressure of 20 MPa were performed with the downstream needle valve closed. The down-stream pore fluid pressure was measured using a 50 MPa pressure transducer installed between the needle valve and the sample. To enable flow-through experiments and fluid sampling, the down-stream needle valve was opened to obtain a fixed flow rate. Flow-through rates were measured by monitoring the collected fluid volume versus time. Sample temperature was measured via a K-type thermocouple placed in the vessel wall. The displacement of upper piston relative to pressure vessel, hence sample shortening, was measured using an external LVDT with accuracy of 0.5 μm (Figure 6.1). The externally applied stress, temperature and pore fluid pressures were measured with an accuracy of 0.001 MPa, 0.1 $^{\circ}\text{C}$ and 0.01 MPa respectively.

6.2.3 Calibration and data acquisition

Calibration of seal friction showed this was generally small at the test conditions so no attempt was made to correct for this. The stiffness of the testing machine and effects of room temperature fluctuations on apparatus expansion/contraction, and hence on measured displacement, were pre-calibrated using a dummy steel sample (see Zhang et al., 2010). This provided a basis for accurately correcting our measured displacement (LVDT) data for loading-related distortion and thermal expansion of the testing machine. Additional calibration experiments were carried out in flow-through mode using a dummy sample with reduced cross-section under typical experimental conditions, i. e. at $T=150\text{ }^{\circ}\text{C}$, $\sigma_e=30\text{ MPa}$, $P_f=20\text{ MPa}$ and at flow rates in the range of 0-15 mm^3/s . The aim of these runs was to check for any temperature-induced contraction of the sample or pistons during flow-through tests. However, no such thermal expansion and contraction effects could be measured in the range of flow rates adopted. During the tests, the experimental data, i. e. the loaded cell, LVDT, sample temperature and the up- and down-stream pore fluid pressure signals, were logged every 100 seconds, or in case of flow-through tests, every 5 seconds. The raw data were processed to yield effective axial stress (σ_e), sample compaction strain (e_v) and compaction strain rate ($\dot{\epsilon}$) vs. time, as described by Zhang et al. (2010). Note that compaction strain is defined here as $e_v=\Delta V/V_0=\Delta L/L_0$ where ΔV is volumetric compaction measured with respect to the sample volume (V_0) after pre-compaction, and L is the sample shortening measured with respect to the sample length (L_0) after pre-compaction. The compaction strain rate, on the other hand is defined as $\dot{\epsilon} = -\dot{L}/L$ here L is the instantaneous sample length.

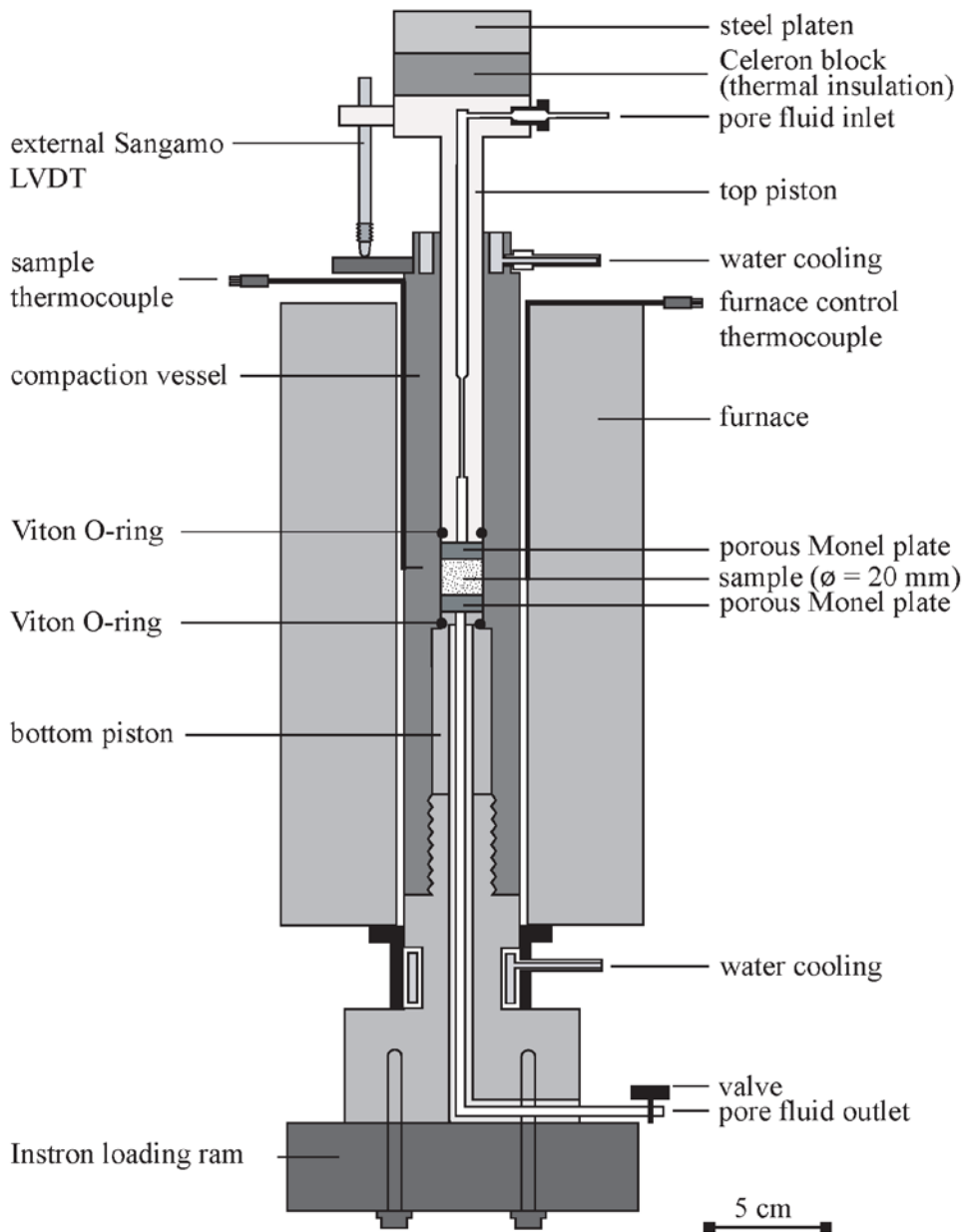


Figure 6.1. Semi-schematic diagram of the experimental apparatus.

6.2.4 Testing procedure

In performing each experiment, 6 grams of powdered sample material was first pre-compacted under lab-dry conditions for 30 minutes at room temperature to achieve a porosity of $29 \pm 2\%$ for the crushed limestone and $34 \pm 1\%$ for the analytical grade calcite, using an applied stress of 50 MPa. This was done with the aim of generating a stable, interlocked aggregate structure, thus eliminating any strains caused purely by straightforward grain rotation or intergranular sliding in subsequent creep testing at lower effective stress (30 MPa). After dry compaction, the applied stress (σ) was reduced to 20 MPa and pore fluid was injected at this pressure, leading to a state of zero effective stress ($\sigma_e = \sigma - P_f = 0$). The pressure vessel was then heated to achieve a sample temperature of 150 °C. During heating, the pore fluid pressure of 20 MPa, the applied stress, and hence the state of zero effective stress was maintained, and the system allowed to settle for about 15 hours to allow chemical equilibration of the pore fluid (Zhang et al., 2010). In experiments at fixed pore fluid pressure, without flow-through, the axial load was then instantaneously stepped up to achieve an effective axial stress of 30 MPa, and the resulting compaction was monitored as a function of time. Flow-through tests of typically 30 minutes duration were initiated shortly before or at varying intervals during compaction of sealed samples. This was done by carefully opening the needle valve at the down- stream end of the vessel, to create a pressure drop across the sample of 0.1 to 1 MPa. Up-stream, the fluid pressure was maintained at 20 MPa by the gas-backed pore fluid system. The remaining experimental variables were kept the same as in the tests performed without flow-through. The pore fluid expelled from the sample during flow-through was collected to measure not only the flow rates but also for chemical analysis using ICP mass spectrometry. Note that in a few tests. The applied axial load was increased during the run to values of 20 and/or 40 MPa.

Experiments were terminated by closing the down-stream flow-through valve (when open), by reducing the applied stress to 20 MPa (zero effective stress), and allowing the sample to cool to room temperature. The pore fluid pressure and remaining applied stress were then reduced to zero simultaneously. Compressed air was then used to blow through and to dry the sample in the vessel. After removing the vessel from the setup, the pistons were extracted and the sample was carefully pressed out from the vessel using a hydraulic hand pump plus a dummy piston.

6.3 Experimental results

The experiments carried out in this study are listed in Table 6.2. Initial pre-compaction under dry conditions and at 50 MPa applied stress, created a well defined initial porosity. The pre-compacted samples showed instantaneous elastic strain but little or no creep when reloaded dry, or in the presence of an inert silicone oil, at an effective axial stress of 30 MPa (Figure 6.2). However, all samples, when compacted wet (i.e. in the presence of aqueous pore fluid), showed time-dependent creep (Figure 6.2). The creep strain, and strain rate measured at fixed strain (hence roughly fixed porosity), increased strongly with decreasing grain size and increasing applied stress (Figure 6.2), see also Zhang et al., 2010).

Exp.	Mater.	d (μm)	Pore fluid	T (°C)	P_f (MPa)	σ_e (MPa)	Final e_v (%)	Exp. time (hour)	ϕ_0 (%)	Dry - compaction stress/time (MPa/h)
Md	Dummy sample (hard metal)		Solution (flow through)	150	20	30	0	50		50 /0.5
Mdry	Lst	37±8	Lab air	150	0	30	0.5	100	27.0	50 /0.5
M0	Lst	37±8	Silicone oil	150	20	30	0.6	400	28.0	50 /0.5
M1	Lst	37±8	Solution	150	20	30, 20, 30,40	5.2	224	26.8	50 /0.5
M9	Lst	22±6	Solution (flow- through 9.3 &9.5% strain)	150	20	30 & 40	9.7	460	31.5	50/0.5
M10	Lst	22±6	Solution (flow through)	150	20	30	4.1	213	28.9	50 /0.5
M11	Lst	12±4	Solution (flow through)	150	20	30	6.9	192	27.6	50 /0.5
M13	AlgCal.	12±4	Solution (flow through)	150	20	30	9.7	160	34.5	50 /0.5
M14	AlgCal.	12±4	Solution +Mg ²⁺ -0.05	150	20	30	2.4	139	35.9	50 /0.5
M15	AlgCal.	12±4	Solution +HPO ₄ ⁻ 0.001	150	20	30	6.7	148	35.0	50 /0.5
M16	AlgCal.	12±4	Solution+Na Cl(0.5M)	150	20	30	9.6	194	35.6	50 /0.5

Table 6.2. List of experiments carried out in this study. Lst=crushed limestone; AlgCal=analytical grade calcite. T denotes the temperature, P_f the pore fluid pressure, σ_e the effective axial stress, ϕ_0 the porosity after pre-compaction (here referred to as the initial porosity). The solution used as pore fluid was de-ionized water pre-saturated with CaCO_3 . Pore fluid additive concentrations are indicated in molarities where used.

Flow-through runs were carried out at varying intervals in four compaction experiments (M9, M10, M11 and M13). Their details are given in Table 6.3. Detailed chemical data on the fluids sampled during the flow-through tests (M10, M11 and M13 only) are given in Table 6.4. The flow-through events or runs conducted within individual experiments had little influence on the creep curves obtained for the representative samples, at least at strains below typically 5-6% (see Figure 6.2). At higher strains, however, effects of flow-through were visible, especially where flow rates were high. Figure 6.3 shows an expanded scale view of a typical example of the creep curves obtained during flow-through tests at large strains (in this case, experiment M9 performed without pore fluid additives). A low flow rate of 0.5 mm³/s applied to this sample (0.4 times of the pore volume replaced) at a strain of 9.3%, led to little immediate change in strain or strain rates. However, after flow-

through, the creep rate increased in the subsequently closed system. By contrast, flow-through at high flow rates ($10 \text{ mm}^3/\text{s}$) (about 5 times pore volume replaced) increased the compaction creep rate significantly, at a strain of 9.5% (See Figure 6.3).

The effects of flow-through on the strain rate at different stages of compaction in the three remaining flow-through experiments on crushed limestone and analytical grade calcite (samples M10, M11 and M13) are shown in Figures 6.4a, 6.5a and 6.6a. At the lower strains (1-5% - see Figures 6.4a-6.6a), flow-through had no influence on the creep rate. At larger strains ($>2\text{-}5\%$), flow-through promoted the creep rates in all samples, provided the flow rate was larger than $5 \text{ mm}^3/\text{s}$.

The results of the chemical analysis done on the fluids collected during the flow-through stages of experiments M10, M11 and M13 are shown in Tables 3 and 4 but also in Figure 6.4b, 6.5b and 6.6b. Special attention was paid to the Ca^{2+} content as a measure of the degree of saturation of the pore fluid with respect to calcite during compaction. From Table 6.3, Table 6.4 and Figures 6.4b-6.6b, it is clear that all solutions sampled during active compaction creep were super-saturated with respect to the initial Ca^{2+} concentration, namely to fm10, fm11 and to fm13 for samples of M10, M11 and M13 respectively. Particularly high Ca^{2+} concentrations, or high degrees of super-saturation of the pore fluid occurred in two cases. First, high concentrations were measured in the fluid samples collected at the very beginning of the compaction (at small strains of 0.5-1%), just after the samples were loaded. For example, the concentrations measured for fluid samples of f1 in experiment M10, f10 in M11 and f30 in experiment M13 are all high. Second, high concentrations were generally obtained in the first sample taken during an individual flow-through run, following long term compaction without flow-through. Examples here include f2 in M10, f13 and f15 in M11 and f34 in M13. These data show that high Ca^{2+} concentrations generally built up during compaction under closed-system (Figure 6.4b, 6.5b, 6.6b). Conversely, the low Ca^{2+} concentration values were obtained from fluid samples collected at the end of individual flow-through runs, i. e. after a relatively large fluid volume had been flushed through the sample (Figure 6.4b, 6.5b, 6.6b). Consider, for instance, the values of f7 in experiment M10, f14 and f16 in experiment M11, and f33 in experiment M13. These all correspond to the last sample taken during individual flow-through run. As a matter of fact, Ca^{2+} concentrations decreased steadily in pore fluids sampled continuously during individual flow-through runs. This can be clearly seen in Figure 6.4 from the Ca^{2+} content measured in fluid samples f2 to f7 and in Figure 6.6 from fluid samples f31 to f33. The decrease of Ca^{2+} concentration reduced in samples from f34 to f35 in M13 was less significant due to the short sampling interval (Table 6.4, Figure 6.6b). From Table 6.4, it is clear that aside from these changes in Ca^{2+} concentration, before, during and after flow-through events, there is correlation between Ca^{2+} concentration and that of several impurity ions. For instance, in samples M11 and M13, higher Ca^{2+} concentrations clearly correspond to higher Mg, Sr, and S concentrations.

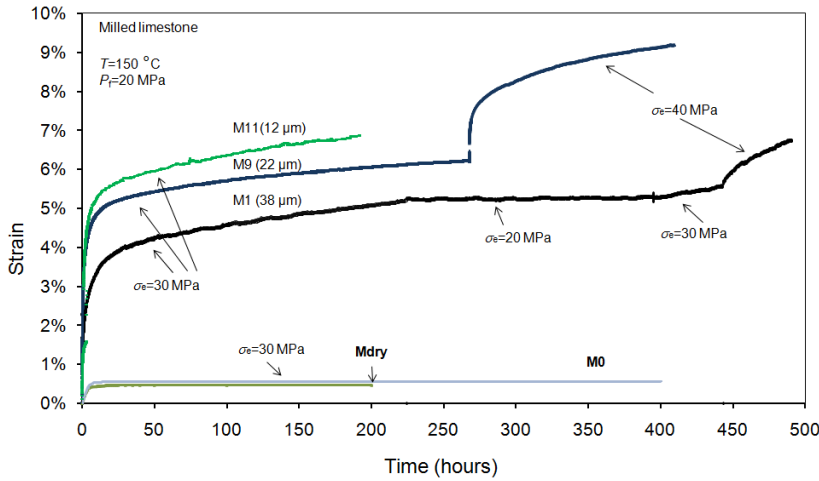


Figure 6.2. Typical compaction creep curves obtained for (crushed limestone) samples tested using carbonate-saturated solution as pore fluid, without additives. Curves obtained for lab-dry (Mdry) and silicone –oil-saturated material (M0) are shown for comparison. Experimental conditions: $P_f = 20$ MPa; $\sigma_e = 30$ MPa, $T = 150$ °C. Note that flow-through runs conducted in experiments M9 and M11 had seemingly little influence on the creep curves except towards the high strains.

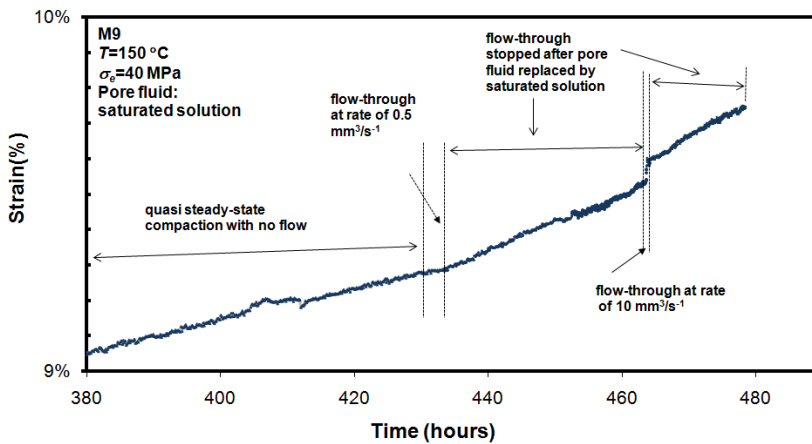


Figure 6.3. Flow-through tests conducted in the late stages of experiment M9 (i.e. at large strains of 9.3 and 9.5%). Compaction curves show a clear increase in compaction rate after the pore fluid was replaced at low flow rate (~ 0.5 mm³/s, 0.4 times of pore fluid volume replaced). Flow-through at high flow rate (10 mm³/s, about 5 times of pore fluid volume replaced) produced an immediate increase in strain and strain rate followed by a return to the pre-flow strain rate after flow-through was terminated.

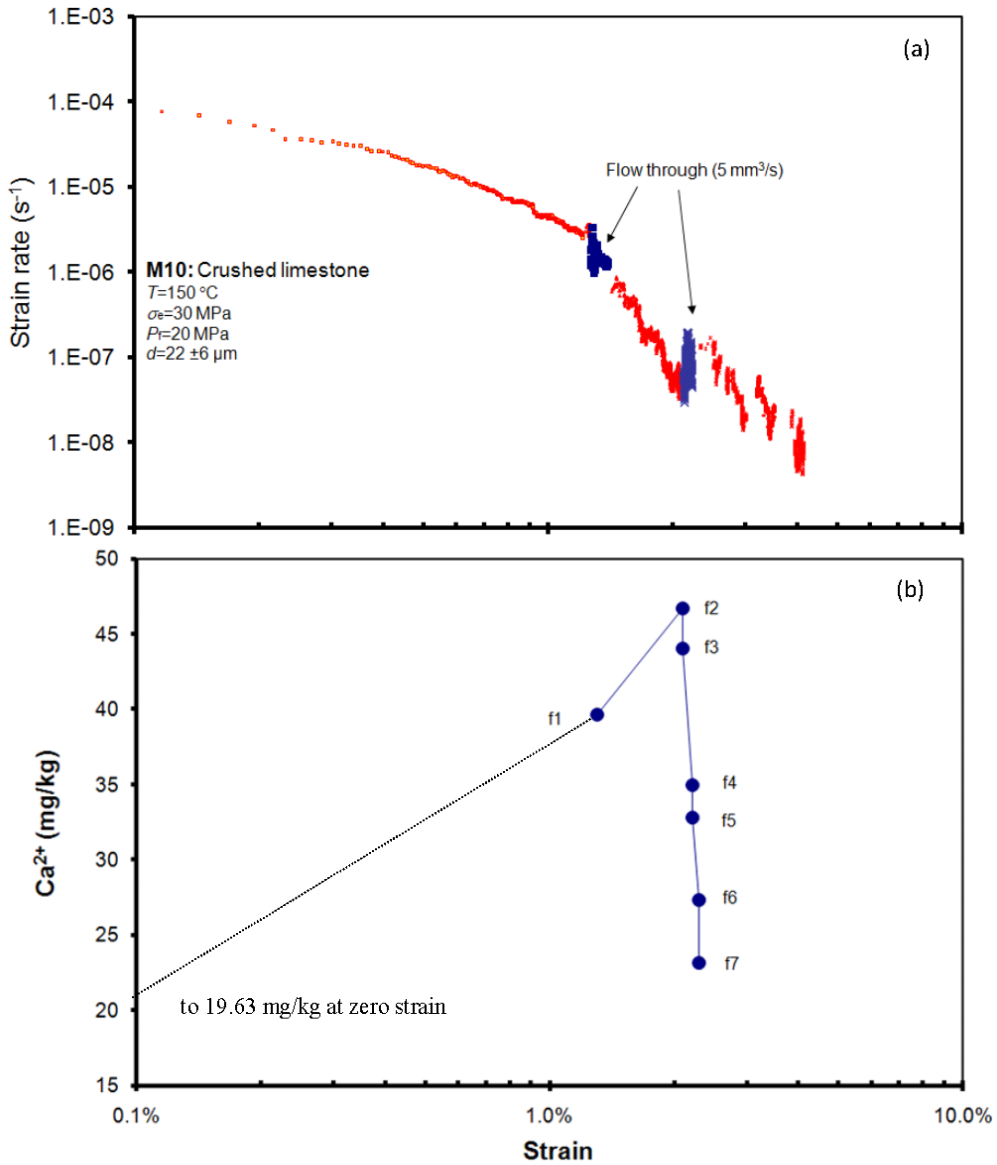


Figure 6.4. Effects of flow-through on a) the creep rate and b) the Ca^{2+} concentration in the pore fluids for M10. Note compaction creep rates increase during flow-through at large strains ($>2\%$), provided the flow rates are sufficiently high i. e. $> 5 \text{ mm}^3/\text{s}$. No increase in creep rate is observed at low strains. Ca^{2+} concentrations decrease (supersaturated) during flow-through.

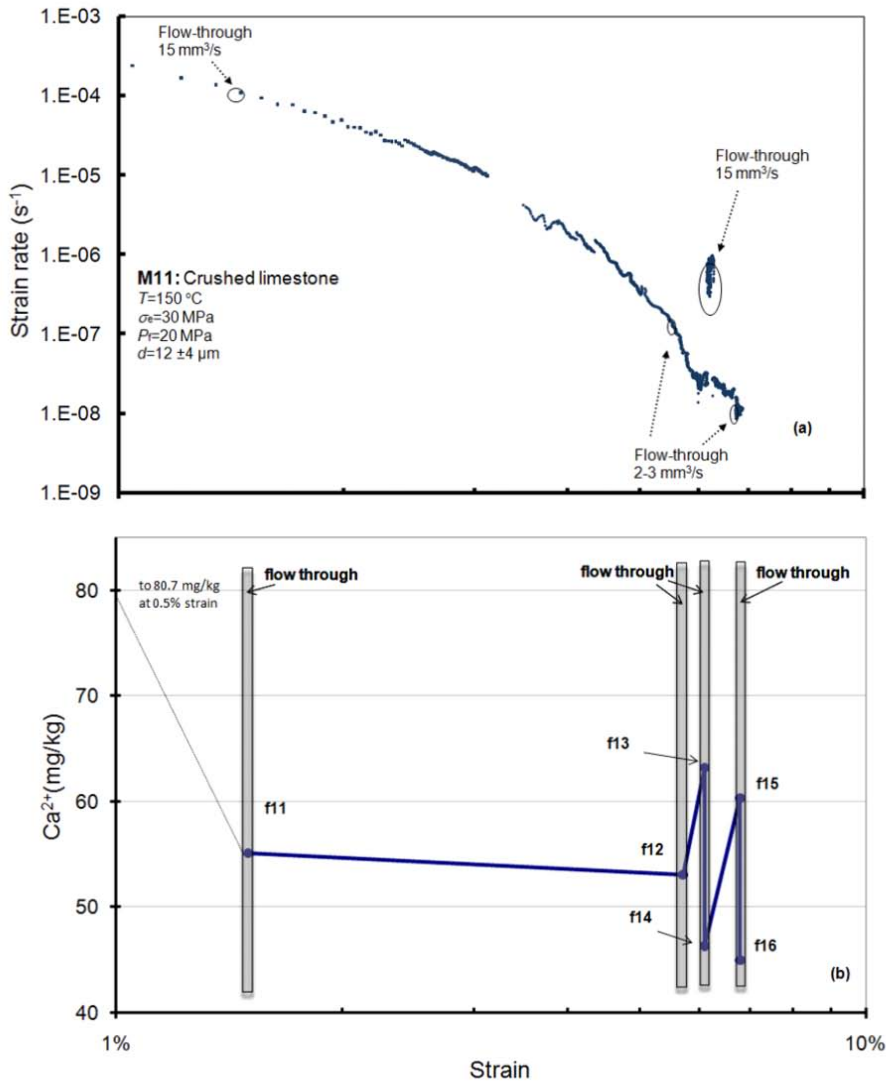


Figure 6.5. Effects of flow-through on a) the creep rate and b) the Ca^{2+} concentrations in the pore fluids for M11 increase (supersaturated) in a close system after each flow through tests. Note compaction creep rates increase during flow-through at large strains ($>5\%$), provided the flow rates are sufficiently high i. e. $> 5 \text{ mm}^3/\text{s}$. No increase in creep rate is observed at low strains. Ca^{2+} concentrations decrease (supersaturated) during flow-through.

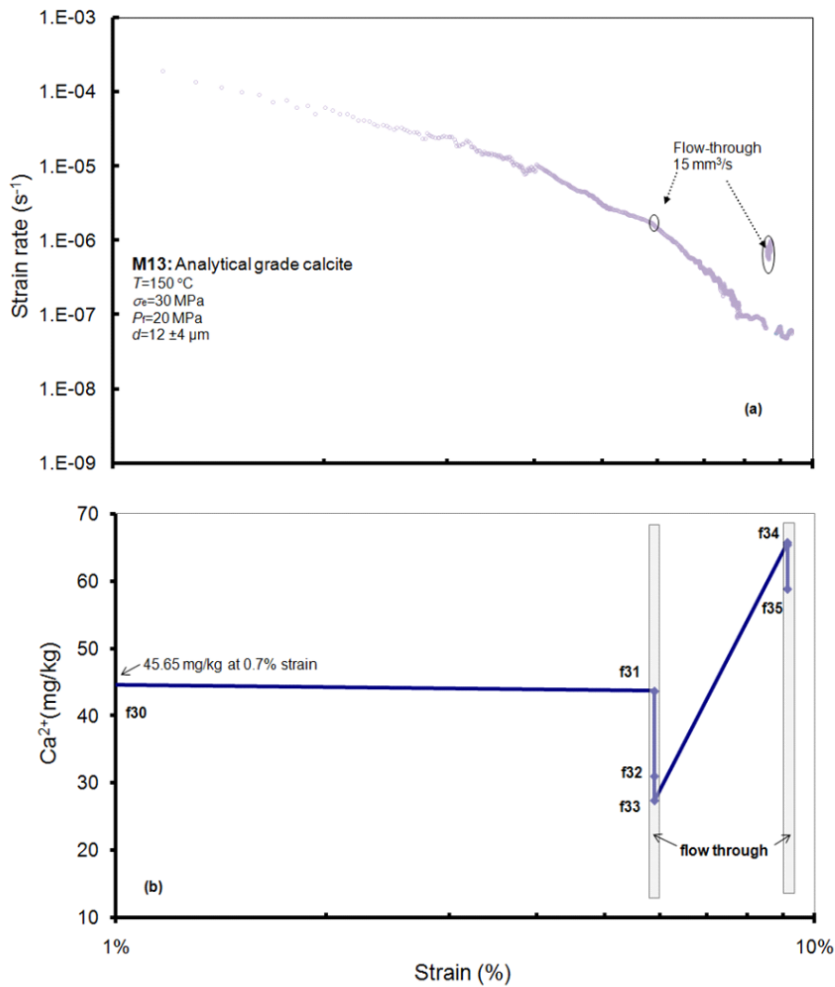


Figure 6.6. Effects of flow-through on a) the creep rate and b) the Ca^{2+} concentrations in the pore fluids for M13 increase (supersaturated) in a close system after each flow through tests. Note compaction creep rates increase during flow-through at large strains ($>7\%$), provided the flow rates are sufficiently high i. e. $> 5 \text{ mm}^3/\text{s}$. No increase in creep rate is observed at low strains. Ca^{2+} concentrations decrease (supersaturated) during flow-through.

Exp. No.	Pore fluid	Ca ²⁺ content (mg/kg)	Fluid sampling time from start of compaction (hours)	Sampling strain (%)	Rate of flow-through (mm ³ /s)	Volume Pore fluid replaced (%)	Flow-through Run and associated start/stop time
M9 (Lst)	n/a	n/a	358 and 542	9.3 and 9.5	0-15	n/a	No sampling, low and high flow-rates applied
M10 (Lst)	fm10	19.83	0	0	n/a	n/a	pre-saturated solution (room temperature)
	f1	39.60	0.5	1.3	~5	~60	collected at half hour experimental time (I)
	f2	46.70	17	2.1	~5	~10	collected at time 17 hours, at the beginning of flow through(II)
	f3	44.06	17.2	2.1	~5	~30	collected at time 17.2 hours, at the beginning of flow through (II)
	f4	34.94	21	2.2	~5	240	collected at the end of fluid through experiment(II)
	f5	32.79	21.2	2.2	~5	~30	collected at the end of fluid through experiment (II)
	f6	27	21.4	2.2	~5	~30	collected at the end of fluid through experiment(III)
	f7	23.13	21.6	2.2	~5	~30	collected at the end of fluid through experiment(IV)
M11 (Lst)	fm11	37.65	0	0	n/a	n/a	pre-saturated solution (room temperature)
	f10	80.70	0.05	0.5			start of experiment
	f11	55.11	1.5	1.5	15	~60	at the beginning of experiment (I)
	f12	53.06	27	5.7	2-3	~150	25-30 hours after experiment start (II)
	f13	63.23	74	6.1	15	60	after 3 days compaction (III)
	f14	46.32	74.5	6.1	15	120	end of flow through(III)
	f15	60.32	191	6.8	2-3	10	flow through after 2 weeks (IV) compaction in close system
	f16	44.99	191.5	6.8	2-3	120	end of flow through (IV)
M13 (algCal)	fm13	22.57	0	0	n/a	n/a	pre-saturated solution (room temperature)
	f30	45.65	0.7	0.7	15	30	start of experiment (I)
	f31	43.68	18	5.9	15	30	after a day compaction (II)
	f32	31.03	18.1	5.9	15	30	middle of flow through (II)
	f33	27.41	18.2	5.9	15	120	end of flow through (II)
	f34	65.81	44	8.6	15	30	after compaction in closed system(III)
	f35	58.89	44.5	8.7	15	120	end of flow-through (III)

Table 6.3. Details of flow-through tests and Ca²⁺ concentrations measured in the fluid samples collected. Note that flow-through was conducted at discrete intervals in each experiment. Experimental conditions per sample are shown in Table 6.2.

Exp.	Samp.	Stra (%)	B	Ba	Ca	K	Mg	Mn	Mo	Na	Ni	S	Sr
M10	fm10	0*	0.14		19.83			0.07		0.93			
	f1	1.3	1.08	0.15	39.6	10.89	0.12		0.45	35.64	0.21	11.4	0.39
	f2	2.1			46.7	3.62			0.57	4.81		10.9	0.58
	f3	2.1	0.35		44.06	5.81			0.68	11.86		11.2	0.86
	f4	2.2	0.12	0.12	34.94	2.37	0.18		0.5	2.44	0.08	11.1	0.73
	f5	2.2	0.13	0.11	32.79	1.35			0.39	1.21		9.6	0.73
	f6	2.3			27.29				0.32	1.56		2.8	0.71
	f7	2.3		0.14	23.13				0.5	0.99		2.1	0.59
M11	fm11	0**			37.65	1.76	4.20			19.90		6.8	0.12
	f10	0.5	1.55	0.27	80.7	13.72	6.99		0.45	61.78	0.24	22.9	1.43
	f11	1.5	0.5	0.22	55.11	6.05	3.3		0.42	29.26		11.0	1.01
	f12	5.7	0.35	0.27	53.06	3.36	3.91		0.22	22.96		9.8	1.04
	f13	6.1	0.57	0.47	63.23	6.13	5.71		0.91	25.57		12.6	1.87
	f14	6.1	0.49	0.12	46.32	3.56	4.52			22.72		8.1	0.18
	f15	6.8	0.6	0.19	60.32	5.42	5.45		0.46	22.79		9.3	0.84
	f16	6.8	0.51	0.12	44.99	4.17	3.84		0.37	23.21		10.6	0.77
M13	fm13	0**			22.57	7.50				16.12			
	f30	0.7	1.24		45.65	6.13	0.5		0.61	6.3	0.43	1.8	0.32
	f31	5.9	0.42		43.68	3	0.24	0.25	0.75	2.65	0.55	1.1	0.29
	f32	5.9	0.16		31.03				0.25	0.64			
	f33	5.9	0.14		27.41				0.23	0.5			
	f34	8.6	0.51		65.81	4.06	1.2	0.33	0.34	1.85	1.41		0.33
	f35	8.7	0.26		58.89		0.71		0.58	1.16		0.7	0.34

Table 6.4. Pore fluid compositions measured for fluid samples collected during flow-through tests M10, M11 and M13. Units in mg/kg. Blank cells correspond to concentrations that were too low to be detected. Note that the high Ca concentrations correlate with high Mg and S concentrations. No sampling for sample 9. *pore fluid pressure 0 MPa, **pore fluid pressure 20 MPa.

Moving now to the effects of pore fluid additives, there had a major influence on total compaction creep strains and creep rates in the experiments on Merck analytical grade where they were used. These effects of Mg^{2+} , HPO_4^{2-} and NaCl additives on compaction creep by Merck samples (M14-16) are presented in Figure 6.7. Compared with Merck material flooded with pure carbonate solution (M13), samples tested with Mg^{2+} (0.05 M) and phosphate ions (0.001M) in the pore fluid attained much lower strains (25-70% lower), while the single sample tested with saline solution (0.5 M NaCl with flow-through at 4-7% strain)) attained somewhat larger strains (~ 10% higher see Figure 6.7a). Strain rates measured in the sample with added Mg^{2+} (M14) were significantly slowed down i.e. by 6.3 to 85 times at strains of 1 and 2% respectively (Figure 6.7b). Phosphate also reduced the compaction strain rate, by 2.6 and 10 times at strains of 1% and 6% (sample M15 Figure

6.7b). In contrast, sodium chloride in the pore fluid at a concentration of 0.5 M (sample M16) increased the compaction creep rates by 2-4 times at strains of 1-3% (Figure 6.7b). At higher strains (4-7%), flow-through of the saline pore fluid in sample M16 resulted in the opposite effect to that seen in flow-through experiments performed without additives i.e. the creep rate decreased significantly after flow-through (Figure 6.7b).

6.4 Discussion

In our previous study on calcite at similar condition (150 °C, 30-40 MPa effective applied stress and 20 MPa pore fluid pressure) (Zhang et al., 2010), we showed that intergranular pressure solution (IPS) was the dominant deformation mechanism, both in crushed limestone and in calcite powders compacted in the presence of saturated calcium carbonate solution. The evidence for IPS being the dominant deformation mechanism included grain-to-grain indentation microstructures as well as a direct dependence of strain rate on applied stress and an inverse the inverse dependence of strain rate on grain size, qualitatively in line with the predictions of theoretical models for IPS (Spiers et al., 2004). Additional observations included an acceleration of creep seen in a single flow-through test at high but not at low strains, plus a transient strain rate response to changes in applied stress, seen at high strains (see Zhang et al., 2010). These observations, are consistent with theoretical models that assume a transition from diffusion to precipitation controlled IPS during the progress of compaction (DeMeer & Spiers, 1997; Zhang et al., 2010). On this basis, our previous experiments suggested that diffusion along wetted grain boundaries was the rate limiting step at low strains and that precipitation on pore walls controlled the IPS rate at higher strains. Limited chemical data further suggested that impurity accumulation from the samples might be the cause of the change in rate-limiting mechanism (Zhang et al., 2010).

The mechanical behaviour observed in the present experiments (i. e. the direct dependence of creep rate on applied effective stress, the strong inverse dependence on grain size, and the inverse dependence compaction strain) is closely similar to that reported in our previous work (Zhang et al., 2010), but extends our data on flow-through and introduce new data on pore fluid chemistry and on the influence of pore fluid additives. In the following, we make use of the effects of flow-through and additives observed in the present tests to gain greater insight into the mechanism controlling the rate of IPS in granular calcite at 150 °C. We also make use of our new, much more extensive chemical data on the evolving composition of the pore fluid in our experiments.

6.4.1 Effects of flow- through on IPS strain rates: theoretical aspects

As a first step, it is useful to review the theoretical background needed to interpret our flow-through results. It is well established (Lehner, 1991, 1995; Spiers et al., 2004) that the driving force for compaction by intergranular pressure solution in calcite, under “closed system” steady-state conditions (i. e. where there is no flow-through or long range diffusion) can be expressed as

$$\Delta\mu \approx \Delta\sigma_n \Omega \quad (6.1)$$

where $\Delta\mu$ and $\Delta\sigma_n$ are the differences in the surface chemical potential of the solid and the interfacial normal stress which exist between grain contacts (dissolution or source sites) and pore walls (precipitation or sink sites), and where Ω is the molar volume of the solid. For small driving forces, this can be alternatively written in terms of a normalized solubility difference

$$\frac{\Delta C}{C_{pw}} \approx \frac{\Delta\sigma_n \Omega}{RT} \quad (6.2)$$

developed between stressed grain contacts and pore walls (Spiers, et al., 2004). Here C_{pw} is the solubility of the stressed solid at pore walls, which is approximately equal to the solubility (C_0) of the unstressed granular solid provided the applied stresses (hence changes in the Helmholtz free energy f^s and the molar volume Ω within the grains) are not too high, T is the temperature (in K) and R is the gas constant (in J/mol·K).

Following the reasoning adopted by DeMeer & Spiers (1997), we now consider the simplified grain-to-grain contact geometry illustrated in Figure 6.8. This grain-to-grain contact with surface area A_{gc} is assumed to possess an interconnected fluid phase in either thin film or micro-channel form and to remain flat at the scale of the grain contact. During intergranular pressure solution creep, under steady-state, closed-system conditions, the potential drop $\Delta\mu$ or equivalent solubility difference ΔC between contacts and pores will be taken up driving the serial processes of dissolution from A to B, grain boundary diffusion from B to C, pore diffusion from C to D and precipitation at D (Figure 6.8). This is easily appreciated from the fact that each serial process (x) typically obeys a flux (J_x) vs. driving force ($\Delta\mu_x$) relation of the form $J_x = k_x \Delta\mu_x$, where k_x is a reaction rate or diffusion coefficient. Thus, by analogy with an electrical circuit, a flux of matter is transferred from dissolving contacts to be precipitated on pore walls, with each kinetic step consuming part ($\Delta\mu_x$) of the available driving force ($\Delta\mu$). Because the diffusivity of solute through the pore fluid is much larger than the effective grain boundary diffusivity ($D_{pore} \gg D_{gb}$), the pore fluid solution is assumed to be in equilibrium, and the potential drop for pore fluid diffusion from C to D is neglected in relation to the other potential drops. In the limiting cases of dissolution, grain boundary diffusion and precipitation control, this means that the entire potential drop $\Delta\mu$ or solubility difference ΔC will appear across whichever of the processes of dissolution, grain boundary diffusion and precipitation is the slowest, thus leading to the potential and concentration distributions depicted in Figure 6.8 (See also Schutjens, 1991; DeMeer and Spiers, 1997).

We now, with the help of Figure 6.8, assess the effect of open-system conditions, i. e. of flushing the pores with a solution maintained at or near the concentration C_0 corresponding to the solubility of loose, unstressed calcite. Since $C_0 \approx C_{pw}$ at relatively low pore pressure, it is clear from Figure 6.8 that, when creep under closed system conditions is controlled by grain boundary dissolution or diffusion, rapid flushing of the pores with a solution of input concentration C_0 will cause little change compared with closed system. In this situation, dissolution or grain boundary diffusion will remain rate limiting for deformation, with a more or less unchanged driving force and unchanged rate of transport from grain-to-grain contacts to pores. The dissolved mass will, of course, be removed by the through-flowing fluid, or in part precipitated on pore walls (if flushing is relatively slow). By contrast, when precipitation is rate controlling under closed-system conditions

(Figure 6.8), rapid flushing with a solution with a solute concentration $C_0 \approx C_{pw}$ can be expected have much bigger effects. In essence, the super-saturation $\Delta C/C_0$ tending to develop in the pore fluid will be flushed away by the moving fluid ($C_{pw} + \Delta C \rightarrow C_0 \approx C_{pw}$), so that precipitation will be prevented and the driving forces $\Delta\mu$ and ΔC for compaction will appear across the easier dissolution and/or grain boundary diffusion steps. One of these relatively easy processes will then become rate controlling and a drastic increase in creep rate can be expected. Alternatively, if the flushing rate is slow enough, the rate of deformation will become controlled not by dissolution or diffusion but by the rate of advective rates removal by the flowing fluid.

This analysis demonstrates that flow-through experiments offer a means of discriminating between precipitation controlled IPS and dissolution or diffusion controlled IPS. If precipitation is rate controlling under closed system conditions, then flow-through will accelerate compaction by IPS. The magnitude of this effect will large at rapid flow rate, and will decrease at low flow rates. On the other hand, compaction by dissolution –or diffusion-controlled IPS is expected to be more or less unaffected by flow-through of the pore fluid.

Effects of flow-through on observed compaction creep

In order to make use of flow-through experiments in the manner described above, selection of the flow rate is important to avoid effects other than changing the solute concentration in the pore fluid. On the one hand, if the flow-through rate is too high, the sample and apparatus could become cooled and apparent compaction caused by thermal contraction could be introduced. On the other hand, if the flow-through rate is too low, the pore fluid will not be effectively replaced, i. e. the fluid composition close to the pore walls may not be influenced. As described under our methodology, to rule out possible ‘cooling’ effect, a control experiment (Md) was carried out using an incompressible steel dummy sample. This showed that at flow rates ranging from 0.5-15 mm³/s, no thermal contraction effects could be measured. This implies that temperature effects induced during flow-through were negligible for the flow rates used in our compaction tests. Our results can therefore be interpreted in terms of changing pore fluid saturation alone.

In our previous study of calcite compaction at 150 °C, we proposed that deformation was dominated by grain boundary diffusion controlled IPS at low strains, giving way to precipitation controlled at higher strains, where creep rates showed a sharp drop (Zhang et al., 2010). The strain rate drop and inferred mechanism transition were attributed to retardation of the precipitation reaction due to the accumulation of impurities progressively dissolving from the sample. A similar drop in strain rate at strains above 4-6% was also observed in the present experiments, namely in M10, M11 and M13 (see Figures 4a, 5a, 6a). Since these experiments involved intermittent flow-through, the data obtained can be used to test further the hypothesis of a switch in rate controlling process from grain boundary diffusion at low strain to precipitation at high strains.

Our data from samples M10, M11 and M13 showed that flow-through had no effect on compaction strain rate when carried out at small strains (<2-3% for crushed limestone and <6% for analytical grade calcite) or at the beginning of the experiments (first few hours). This was observed for all flow rates used (<0-15 mm³/s). In contrast, flow-through

increased the compaction strain rates measured at larger strains (Figures 6.4a, 6.5a, 6.6a), at least when the flow rate was higher than 5 mm³/s. Significantly, the strain rates measured during rapid flow-through (15 mm³/s) in M11 and M13 reached the trend line exhibited by the low strain part of the corresponding compaction rate versus strain curve (Figure 6.5 and Figure 6.6). While dissolution control cannot be completely eliminated at low strains on the basis of the present experiments, these results along with high sensitivity of creep rate to grain size seen at low strains (Figure 6.2), strongly support our previous interpretation that the rate limiting step under closed system conditions is diffusion at small strains, with a transition to precipitation control at large strains. Experiment M9 also supports the interpretation of precipitation control at high strain (9.3-9.5%), as the response to flow-through depend on the flow-through rate.

The observation of a significant decrease in creep rate after flow-through in saline sample M16 at 4-8% strain is difficult to explain (Figure 6.7). A possible explanation might be that a NaCl concentration gradient developed in the upstream part of the fluid system due to temperature gradients, gravity induced stratification of NaCl concentration or corrosion, though we have no independent evidence to verify this.

6.4.2 Ca²⁺ content of the pore fluid

The results of our fluid analysis for compaction experiments M10, M11 and M13 show substantial variation in Ca²⁺ concentration during the individual experiments and from experiment to experiment (Table 6.3). The values of Ca²⁺ concentration measured in M10, M11 and M13 (fm0, fm11 and fm13) before the compaction creep was initiated were taken as the initial saturation values. These measured values are higher than the theoretical solubility of calcite i. e. the solubility of pure calcite based on thermodynamic modelling results (Duan & Li, 2008). At room temperature, 1 bar pressure and $pCO_2 \approx 3 \times 10^{-5}$ MPa, Duan & Li's model gives a Ca²⁺ concentration at equilibrium of 12.24-16 mg/kg for pure calcite in water. At 150 °C, 20 MPa pore fluid pressure and $pCO_2 \approx 3 \times 10^{-5}$ MPa the solubility given by the Duan & Li's model is 18.9 mg/kg. The higher starting values of 20-38 mg/kg seen in our samples are probably due to the effects of dry pre-compaction of our samples (cataclastic grain size reduction, plastic strain) and/or to impurities present in the starting materials.

Our data on the evolution of the Ca²⁺ concentration during our creep experiments show that high concentrations well above the starting values developed in two cases. In the first case, high concentrations were measured at the very beginning of the compaction. This may reflect grain scale brittle or plastic deformation during initial loading, as previously inferred in relation to compaction experiments on quartz (Elias & Hajash, 1992). Secondly, high Ca²⁺ concentrations were observed to build up in samples compacted to large strains, over long times, under closed system conditions (Figure 6.4b-6.6b). Flushing with fresh pore fluid reduced the Ca²⁺ concentration and accelerated creep in most of the high strain flow-through tests shown Figure 6.4, 6.5 and 6.6. After flow-through, a high super-saturation was generally re-established. These changes in Ca²⁺ concentration are consistent with IPS compaction being controlled by precipitation at pore walls between flow-through periods at high strain, as discussed above (Figure 6.8). On the other hand, at lower strains where flow-through did not accelerate creep, Ca²⁺ concentration also fell, in some flow-through

runs (Figure 6.4-6.6). This is not consistent with our inference that grain boundary diffusion controlled IPS at low strains, but may indicate that flow-through removed Ca^{2+} derived from both IPS and Ca^{2+} bearing impurities in the samples.

6.4.3 Effects of the pore fluid salinity (NaCl)

From the geochemistry literature, it is known that salinity (NaCl) increases the solubility of the calcite (Ellis, 1959, 1963; Wolf et al., 1989; Mucci, 1983; Duan & Li, 2008). According to conventional intergranular pressure solution theory, the rate of IPS is directly proportional to mineral solubility, when grain boundary diffusion is the rate-limiting step (Rutter, 1983; Lehner, 1995; Renard & Ortoleva, 1997; Spiers et al., 2004). Hence, increasing solution salinity should increase compaction strain rate if diffusion is the rate controlling step. Our experimental results for Merck sample M16 show that a pore fluid NaCl concentration of 0.5 M increased compaction creep rates in calcite. Compared to the NaCl-free Merck sample M13, the strain rates measured for sample M16 are 2.2, 3.0 and 4.4 times faster at strains of 1%, 2% and 3% respectively (Figure 6.7b). The experimental results of Ellis (1963) and thermodynamic modelling results by Duan and Li (2008) have shown that the solubility of calcite in a solution of 0.5 M NaCl increases by about 3 times compared to NaCl-free solution at a temperature of 150 °C and a pressure of 20 MPa. The increase of compaction strain rate seen in experiment M16 was thus roughly in proportion to the increase in solubility of calcite expected for a pore fluid phase containing 0.5 M NaCl. This suggests that IPS in NaCl free and NaCl-bearing experiments might have been grain boundary diffusion controlled, at least at low strains before the first flow-through tests (see Figures 6.6, 6.7). At high strains, such as 8%-9%, the creep rate of saline sample M16 was only slightly higher (1.7-1.5 times) than in the NaCl free sample M13, perhaps suggesting a different rate controlling process, such as precipitation.

A number of laboratory investigations have been done on the influence of salinity (ionic strength) on the rates of calcite dissolution and precipitation. Gledhill and Morse (2006) found that salinity had no effect on the dissolution rate of calcite in the low $p\text{CO}_2$ region (< 0.01 MPa) at temperatures of 20-80 °C. Several studies have also been conducted on the effects of salinity on calcite precipitation rates. However, the results remain inconclusive and controversial (Zhong & Mucci, 1989). For example, Chen et al. (1979), Kazmlerczak et al. (1982) and Walter (1986) infer that salinity and ionic strength have no effect on the rate of calcite precipitation. On the other hand, Zuddas and Mucci (1989) argue that salinity has a large accelerating effect on the rate of calcite precipitation at room temperature and CO_2 partial pressure of 10^{-4} MPa. We can therefore draw no further conclusions on the effects of pore fluid salinity in our experiments, except to say that the observed fluid acceleration of creep is consistent with a mechanism of grain boundary diffusion controlled intergranular pressure solution at small strains ($< 6\%$ in M16).

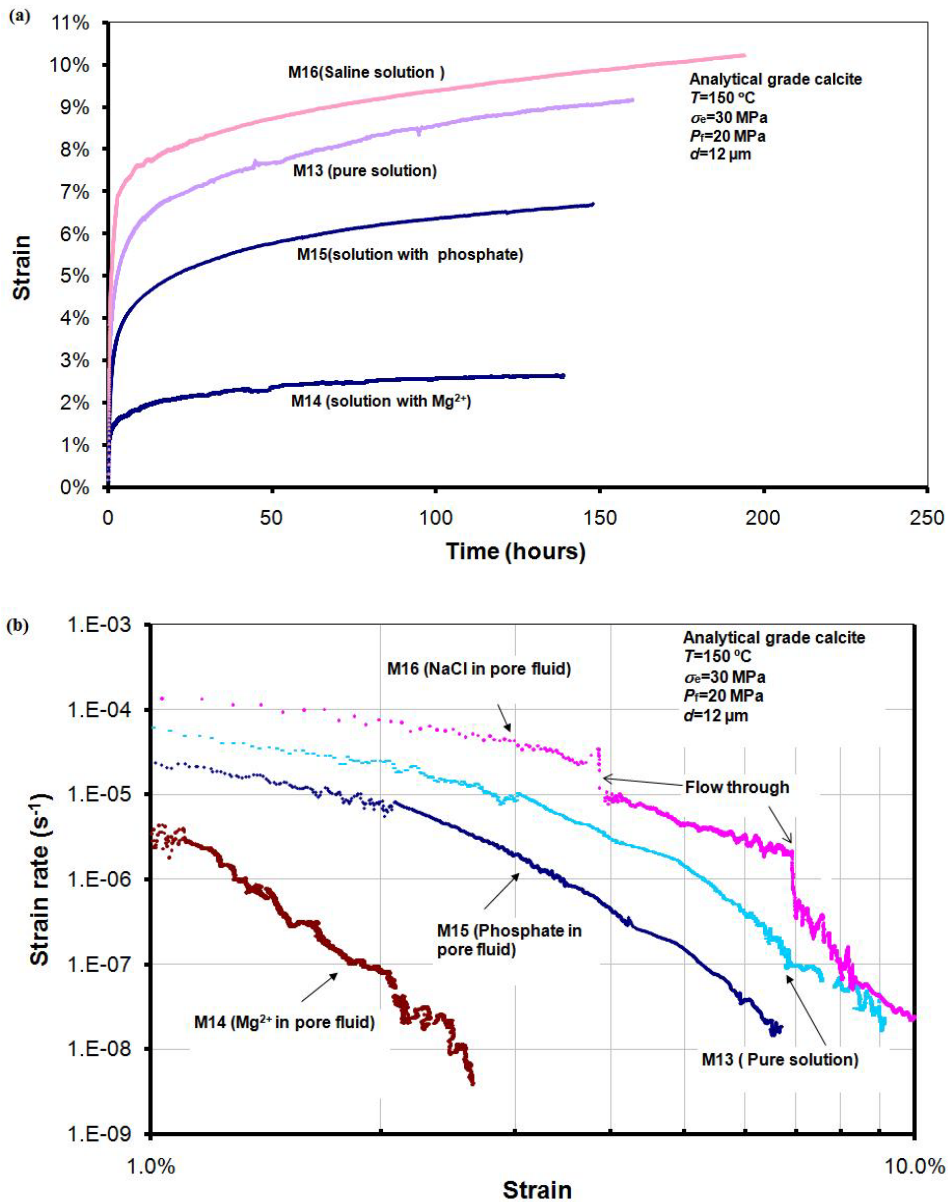


Figure 6.7. Effects of pore fluid additives on the compaction creep strains and creep strain rates obtained in experiments on analytical grade calcite. a) Creep curves compared to the additive free sample. The sample tested using a solution containing NaCl (0.5 M, sample M16) attained larger strains despite creep deceleration during flow-through at 4-7% strain), while samples tested using solutions containing 0.05 M Mg^{2+} and phosphate ions (0.001 M) attained much lower strains. b) Compaction creep rates vs. volumetric strain plots.

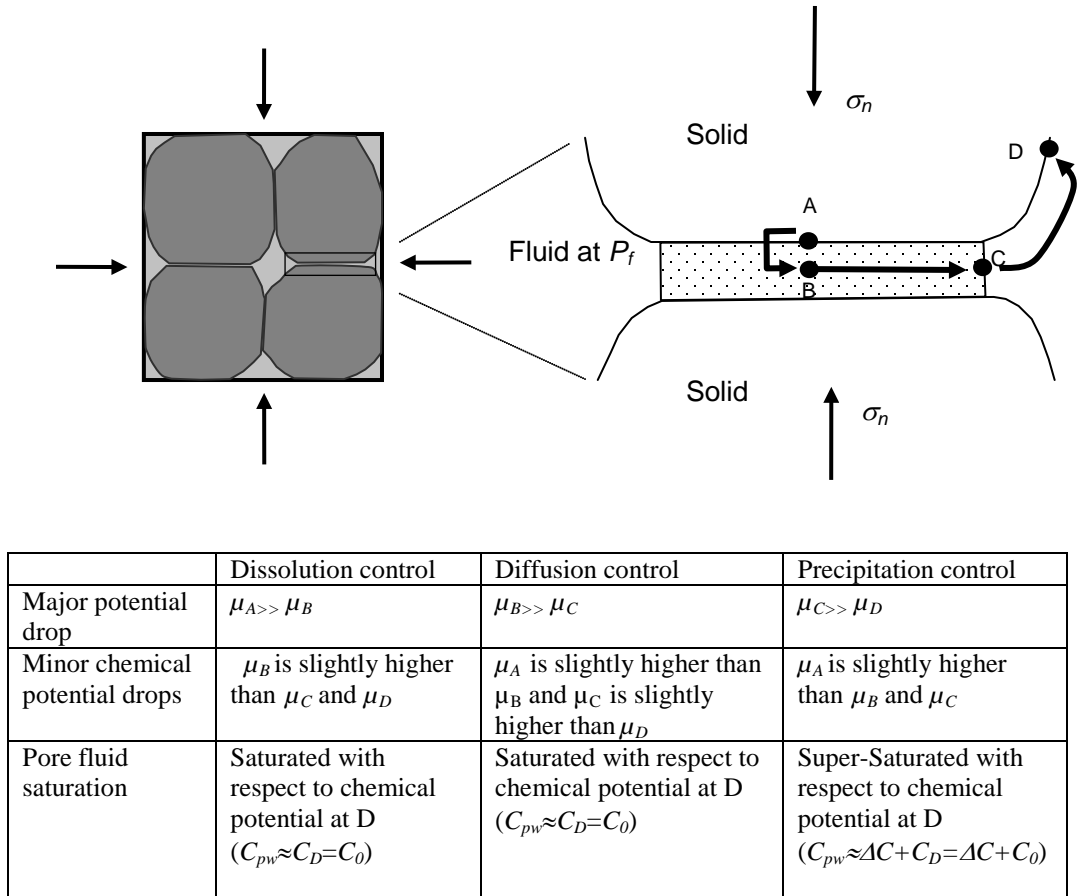


Figure 6.8. The chemical potentials developed within grain contacts, in the pore fluid phase and at pore walls in a granular aggregate undergoing steady-state IPS, assuming rate control by dissolution, diffusion along grain boundaries, or precipitation at free pore walls as the rate limiting steps. Table shows values of the different potential and concentration distributions for each rate controlling process.

Zhang et al. (2009) investigated the effects of salinity on intergranular pressure solution by carrying out comparison experiments between compaction tests on fine grained calcite and dissolution experiments on cleaved calcite surfaces performed using an Atomic Force Microscope (AFM) plus in-situ dissolution cell. Their compaction tests were carried out at room temperature and low stress (4 MPa). AFM observations showed that salinity controlled the morphology of the dissolving calcite surface. During dissolution at low salinity (i.e. in 0.1-0.5 M NaCl solution), dissolution pits associated with dislocations progressively deepened and thus roughened the dissolving calcite surface. However, at high salinity (>0.8-1 M), the dissolution pits assumed shallow, regular, rhombohedral shape and the surface greatly flattened. The compaction experiments showed an increase in creep rate

with pore fluid salinity at NaCl concentrations in the range 0.1-0.5 M, but no effect of any increase in higher salinity (>0.8-1 M). The direct correlation between the effects of salinity on dissolution morphology and creep rate led the authors to conclude that the salinity might control the grain boundary structures for ongoing intergranular pressure solution in calcite. Although the experimental conditions were different from the present study, the effects of salinity (at 0.5 M NaCl) on creep rate were consistent with the present study. Following Zhang et al. (2009), we therefore suggest that the effect of pore fluid NaCl content in the present experiments might be related to an acceleration of grain boundary diffusion due to roughening of dissolving grain boundaries- rather than to an effect of NaCl on calcite solubility alone.

Finally, it is important to note that the effects of salinity on compaction of crushed Carrara marble were investigated by Liteanu & Spiers (2009) at a temperature of 80 °C, an effective stress of 30 MPa and at 10 MPa pore fluid pressure. They found that a NaCl concentration in the pore fluid of 1 M slowed down creep rates in their CO₂ free tests. However, the grain sizes were larger in their experiments and, on the basis of a positive dependence of creep rate on grain size, subcritical micro-cracking was inferred to be the main grain-scale deformation mechanism (Liteanu & Spiers 2009).

6.4.4 Effects of Mg²⁺ and HPO₄²⁻

Impurity ions dissolved in the fluid phase can substantially inhibit precipitation and dissolution of calcite (Berner & Morse, 1974; Reddy, 1977; Meyer, 1984; Reddy & Wang, 1980; Dove & Hochella, 1993; Takasaki et al., 1994). Among such inhibitors, magnesium and phosphate ions are the most well-studied due to their importance in sea water and in formation water (Reddy, 1977; Reddy & Wong, 1980; Warren & Smalley, 1994; Jonasson et al., 1996; Alkattan et al., 2002). In previous studies, we tested the effects of dissolved magnesium and phosphate in the pore fluid on the compaction behaviour of granular calcite at room temperature and low stresses (<8 MPa) and showed that both greatly reduced compaction creep rates (Zhang et al., 2002; Spiers et al., 2004; Zhang & Spiers, 2005a, 2005b). The present study has shown that both magnesium and phosphate ions also retard compaction creep significantly at 150 °C and 30 MPa effective stress. Compared to samples flooded with pure CaCO₃-saturated solution (Merck sample M13), the creep rate in Merck sample M14, flooded with solution containing 0.05 M Mg²⁺ ions, was slowed down by about 1 to 2.5 orders magnitudes at strains of 1 to 2.5% while is similar to the retardation observed at room temperature. Phosphate ions at a concentration of 0.001 M in the pore fluid slowed down compaction strain rates by 3-10 times (M15 vs. M13), which is 10-40 times less than the effect seen at room temperature and at lower stress (Zhang et al., 2005b).

These effects of magnesium and phosphate ions on the creep rates of calcite prove that the compaction mechanism in calcite under our experimental conditions must have involved calcite dissolution or precipitation reactions i.e. IPS. The fact that phosphate had less influence on compaction strain rate at 150 °C than at room temperature is also in agreement with the results by Jonnase et al. (1996) who showed that the phosphate inhibition of calcite precipitation becomes less efficient at temperatures above 100 °C.

Our few results on Mg^{2+} and HPO_4^{2-} are consistent with the results of Helleman et al (2002) on these ions on creep of wet chalk but differ from the results of Liteanu and Spiers (2009) who found that added Mg^{2+} (1-3 M) increased the creep rates. In impure systems such as those with additives of Mg^{2+} , HPO_4^{2-} , the significantly inhibited reaction of calcite precipitation or dissolution should control the intergranular pressure solution rate. Carbonate precipitation reactions are found much more readily inhibited by various chemical species, such as Mg^{2+} , HPO_4^{2-} and SO_4^{2-} than are dissolution reactions (Walter, 1986). Retarded precipitation is therefore more likely the rate limiting step in intergranular pressure solution of carbonate rocks in nature.

6.5 Conclusions

Compaction creep experiments have been performed on crushed limestone and analytical grade calcite powders under conditions where previous work has shown compaction to be dominated by intergranular pressure solution, i. e. At a temperature of 150 °C, a pore fluid pressure of 20 MPa, and applied effective stresses of 30-40 MPa. The aim was to investigate the inter-relationship between pore fluid chemistry, compaction rate and rate controlling process, in an attempt to elucidate the last. The problem was approached by manipulate pore fluid composition using flow-through tests performed with fresh, calcite saturated solution, and by adding NaCl, Mg^{2+} or phosphate ions to the pore fluid mainly without flow-through. The main findings and conclusion were as follows:

1). Compaction experiments performed using a stationary pore fluid and no additives showed mechanical behaviour that was closely similar to that obtained in previous work reported by us (Zhang et al., 2010) implying that intergranular pressure solution (IPS) was the dominant deformation mechanism as inferred in our previous study.

2). Intermittent flow-through runs conducted using CaCO_3 solution in chemical equilibrium with unstressed sample material showed no effect on creep rate at low strain (<2-5%) but a major acceleration at high strains. Comparison with IPS theory supports the conclusion that deformation was dominated by IPS and implies that the process was grain boundary diffusion controlled at low strains and precipitation controlled at high strains, under zero flow conditions. At high flow rates, diffusion probably became rate controlling at high strain also.

3). Measurements of the Ca^{2+} concentration present in fluid samples collected from compacting samples in intermittent flow-through runs revealed a build up to high supersaturation of CaCO_3 during compaction under zero flow conditions, specially at high strains. Flow-through led to a drop in Ca^{2+} concentration, which corrected with creep acceleration at high strains. These data further support the inference that precipitation controlled the rate of IPS at high strains, as IPS theory predicts a significant supersaturation build up only for precipitation control.

4). The build up of Ca^{2+} in the pore fluid during creep without flow-through especially at high strains was accompanied by an increase in Mg^{2+} and S. This is believed to reflect progressive dissolution of impurities in the natural samples (and/or contamination of the apparatus).

5). Addition of NaCl to the pore fluid in a concentration of 0.5 M increased the creep rate of analytical grade calcite roughly in proportion to the enhancement of NaCl on calcite solubility –from IPS theory, this may reflect an acceleration of IPS via acceleration of grain boundary diffusion control, at least at lower strains. The presence of NaCl may also have promoted grain boundary roughening and hence diffusion.

6). Addition of Mg^{2+} (in the form of $\text{MgCl}_2 \cdot 6\text{H}_2\text{O}$) and HPO_4^{2-} (in the form of Na_2HPO_4) to the pore fluid, in concentration of 0.05 M and 0.001 M respectively, caused major retardation of compaction creep of analytical grade samples. Since the ions are known to retard dissolution and precipitation of calcite, their effects provide strong support for compaction being controlled by a dissolution-precipitation process such as IPS.

7). Integrating our mechanical, flow-through and chemical data, and taking into account our previous mechanical data for its present system and conditions (Zhang et al., 2010), points strongly to diffusion controlled IPS being the dominant deformation mechanism under closed system (zero flow) conditions at strains up to few percents, giving way to precipitation control at higher strains. Our (chemical) data suggest that this transition is due to accumulation of impurity in the pore fluids from samples or apparatus.

8). Since Mg^{2+} and phosphate ions are common in natural pore fluids, since they are known to retard dissolution and especially precipitation of calcite, it is likely that retarded precipitation will be the rate limiting step in IPS of carbonates in nature. Further, to qualify diagenetic compaction and porosity and permeability reduction rate in carbonates need to account for this.

6.6 References

- Alkattan M, E. H Oelkers, J. L. Dandurand and J. Schott (2002), An experimental study of calcite dissolution rates at acidic conditions and 25 °C in the presence of Na_3PO_3 and MgCl_2 , *Chem. Geol.* 190, 291-302.
- Bathurst R. G. C. (1958), Diagenetic fabrics in some British Dinantian limestones, *Liverpool and Manchester Geology* 2, 11-36.
- Bathurst R. G. C. (1975), Carbonate sediments and their diagenesis, *Development in Sedimentary* 12, 2nd edition, Elsevier, Amsterdam, New York, 658 pp.
- Berner R. A. and J. W. Morse (1974), Dissolution kinetics of calcium carbonate in sea water IV, Theory of calcite dissolution, *Am. J. Sci.* 274, 108-134.
- Buxton T. M. and D. F. Sibley (1981), Pressure solution in a shallow buried limestone, *J. Sediment. Res.* 51, 19-26.
- Chen Y, X. Wang, Q. Sha and N. Zhang (1979), Experimental studies on the system of Ca^{2+} - Mg^{2+} - HCO_3 - H_2O at room temperature and pressure, *Science of Geology China* 1: 22-36 (In Chinese, with English Abstract).
- DeMeer S. and C. J. Spiers (1997), Pressure solution creep in Gypsum: evidence for precipitation reaction control, *Physics and Chemistry of Earth* 22, 33-37.
- DeMeer S. and C. J. Spiers (1999), Mechanisms and kinetics of creep by intergranular pressure solution, in: B. Jamtveit, P. Meakin (Eds.), *Growth, Dissolution and Pattern Formation in Geosystems*, Kluwer Academic Publishers, Dordrecht, 345-363.

- Dewers T. and A. Hajash (1995), Rate law for water-assisted compaction and stress-induced water-rock interaction in sandstones, *J. Geophys. Res.* 100, 13,093-13,112.
- Dove P. M. and M. F. Hochella (1993), Calcite precipitation mechanisms and inhibition by orthophosphate: In situ observations by Scanning Force Microscopy, *Geochim. Cosmochim. Acta* 57, 705-714.
- Duan Z. and D. Li (2008), Coupled phase and aqueous species equilibrium of the H₂O-CO₂-NaCl-CaCO₃ system from 0 to 250 C, 1 to 1000 bar with NaCl concentrations up to saturation of halite, *Geochim. Cosmochim. Acta*, doi: 10.1016/j.gca.2008.07.025.
- Durney D. W. (1972), Solution-transfer- an important geological deformation mechanism, *Nature* 235, 315-317.
- Ehrenberg S. N., G. P. Eberli, M. Keramati and S. A. Moallemi (2006), Porosity-permeability relationships in interlayered limestone-dolostone reservoirs, *AAPG Bulletin* 90, 91-114; doi: 10.1306/08100505087
- Elias B. P. and A. Hajash (1992), Changes in quartz solubility and porosity due to effective stress: An experimental investigation of pressure solution, *Geology* 20, 451-454.
- Elliot D. (1976), The energy balance and deformation mechanisms of thrust sheets, *Phil. Trans. R. Soc. Lond. A* 283, 289-312.
- Ellis A. J. (1959), The solubility of calcite in carbon dioxide solutions, *Am. J. Sci.* 257, 354-365.
- Ellis, A. J. (1963), The solubility of calcite in sodium chloride solutions at high temperatures, *Am. J. Sci.* 261, 259-267.
- Gledhill D. and J. W. Morse (2006), Calcite dissolution kinetics in Na-Ca-Mg-Cl brines, *Geochim. Cosmochim. Acta*, 70, 5802-5813, doi: 10.1016/j.gca.2006.03.024.
- Graham B., M. A. Antonellini and A. Aydin (2003), Formation and growth of normal faults in carbonates within a compressive environment, *Geology* 31, 11-14.
- Gundersen E, F. Renard, D. K. Dysthe, K. Bjorlykke and B. R. Jamtveit (2002), Coupling between pressure solution creep and diffusive mass transport in porous rocks, *J. Geophys. Res.* 107. doi:10.1029/2001JB000287.
- He W., A. Hajash and D. Sparks (2003), Creep compaction of quartz aggregates: effects of pore fluid flow- a combined experimental and theoretical study, *Am. J. Sci.* 303, 73-93.
- Jonasson R. G., K. Rispler, B. Wiwchar and W. D. Gunter (1996), Effect of phosphate inhibitors on calcite nucleation kinetics as a function of temperature using light scattering in an autoclave, *Chem. Geol.* 132, 215-225.
- Kazmierzczak T. F., M. B. Tomson and G. M. Nancollas (1982), Crystal growth of calcium carbonate – a controlled composition kinetic study, *Journal of Physical Chemistry* 86, 103-107.
- Lehner F. K. (1990), Thermal dynamics of rock deformation by pressure solution, in: *Deformation Processes in Minerals, Ceramics and Rocks*, edited by D. Barber and P. Meredith, Unwin Hyman, London, pp. 296-33
- Lehner F. K. (1995), A model for intergranular pressure solution in open systems, *Tectonophysics* 245, 153-170.
- Meyer H. J. (1984), The influence of impurities on the growth rate of calcite, *J. Cryst. Growth* 66, 639-646.
- Mucci A. (1983), The solubility of calcite and aragonite in seawater at various salinities, temperatures, and one atmosphere total pressure, *Am. J. Sci.* 283, 780-799.

- Ngwenya B. T., S. C. Elphick, I. G. Main, G. B. Shimmield (2000), Experimental constraints on the diagenetic self-sealing capacity of faults in high porosity rocks, *Earth and Planet. Sci. Lett.* 183, 187-199, doi:10.1016/S0012-821X(00)00261-2.
- Peacock D. C. P., Q. J. Fisher, E. J. M. Willemse and A. Aydin (1998), The relationship between faults and pressure solution seams in carbonate rocks and the implications for fluid flow, *Geological Society, London, Special Publications* 147, 105-115.
- Pokrovsky O. S. and J. Schott (2002), Surface chemistry and dissolution kinetics of divalent metal carbonates. *Environnemental Science and Technology* 36, 426-432.
- Reddy M. M. (1977), Crystallization of calcium carbonate in the presence of trace concentrations of phosphorous –containing anions. I inhibition by phosphate and glycerophosphate ions at pH 8.8 and 25 C, *J. Cryst. Growth* 41, 287-295.
- Reddy M. M. and K. K. Wang (1980), Crystallization of calcium carbonate in the presence of metal ions. I. Inhibition of magnesium ion at pH 8.8 and 250C, *J. Cryst. Growth* 50, 470-480.
- Renard F. and P. Ortoleva (1997), Water films at grain contacts: Debye-Hückel, osmotic model of stress, salinity, and mineralogy dependence, *Geochim. Cosmochim. Acta* 61, 1963-1970.
- Renard F, J. Schmittbuhl, J. P. Gratier, P. Meakin and E. Merino (2004), Three-dimensional roughness of stylolites in limestones, *J. Geophys. Res.* 109, B03209, doi:10.1029/2003JB002555
- Rickard D. and E. L. Sjöberg (1983), Mixed kinetic control of calcite dissolution rates, *Am. J. Sci.* 283, 815-830.
- Rutter E. H. (1983), Pressure solution in nature, theory and experiment, *J. Geol. Soc. Lond.* 140, 725-740.
- Sjöberg E. L. and D. T. Rickard (1984), Temperature Dependence of Calcite Dissolution Kinetics between 1 and 62°C at pH 2.7 to 8.4 in Aqueous Solutions. *Geochim. Cosmochim. Acta* 48, 485-493.
- Spiers C. J., S. DeMeer, A. R. Niemeijer and X. Zhang (2004), Kinetics of rock deformation by pressure solution and the role of thin aqueous films. In *Physiochemistry of water in Geological and Biological Systems* (ed. S. Nakashima et al.). pp. 129-158, Universal Academy Press, Inc.
- Tada R. and R. Siever (1989), Pressure solution during diagenesis, *Annual Review of Earth and Planetary Sciences*, 89-118.
- Takasaki S., K. I. Parsieglia and J. L. Katz (1994), Calcite growth and the inhibiting effects of iron, *J. Cryst. Growth* 143, 261-268.
- Tondi E., M. Antonellini, A. Aydin, L. Marchegiani, and G. Cello (2006), The role of deformation bands, stylolites and sheared stylolites in fault development in carbonate grainstones of the Majella Mountain, Italy *J. Struct. Geol.* 28, 376-391.
- Traskine V., Z. Skvortsova, and A. Muralev (2008), Intergranular pressure solution in internally wetted polycrystals: Effect of additives, *Materials Science and Engineering*, 495(1-2), 132-137.
- Walter L. M. (1986), Relative efficiency of carbonate dissolution and precipitation during diagenesis: a progress report on the role of solution chemistry. In: D. L. Gautier (Editor), Roles of organic matter in sediment diagenesis, *Soc. Econ. Paleontol. Mineral., Spec. Publ.* 38, 1-11.

- Wanless H. R. (1979), Limestone response to stress; pressure solution and dolomitization, *J. Sediment. Res.* 9, 437-462.
- Warren E. A. and P. C. Smalley (1994), *North Sea Formation Waters Atlas*, The Geological Society of London.
- Wolf M, O. Bretkopf and R. Puk (1989), Solubility of calcite in different electrolytes at temperature between 10 to 60 °C and at CO₂ partial pressure of about 1 kPa, *Chem. Geol.* 76, 291-301.
- Yashuhara H., C. Marone and D. Elsworth (2005), Fault zone restrengthening and frictional healing: The role of pressure solution, *J. Geophys. Res.* 110, B06310, doi:10.1029/2004JB003327.
- Zhang X., J. Salemans, C. J. Peach and C. J. Spiers (2002), Compaction experiments on wet calcite powder at room temperature: evidence for operation of intergranular pressure solution, in *Deformation Mechanisms, Rheology and Tectonics: Current Status and Future Perspectives*, edited by S. de Meer, M. R. Drury, J. H. de Bresser, G. M. Pennock, Geological Society, London, Special Publications, 200, 29-39.
- Zhang X. and C. J. Spiers (2005a), Compaction of granular calcite by pressure solution at room temperature and effects of pore fluid chemistry, *Int. J. Rock. Mech. Min. Sci.* 42, 950-960, doi:10.1016/j.ijrmms.2005.05.017.
- Zhang X. and C. J. Spiers (2005b), Effects of phosphate ions on intergranular pressure solution in calcite: an experimental study, *Geochim. Cosmochim. Acta.* 69, 5681-5691, doi:10.1016/j.gca.2005.08.006 .
- Zhang X, A. Putnis, C. Putnis and C. J. Spiers (2009), Dissolution pits in calcite-implication for CO₂ sequestration in carbonate rocks, *International Symposium of the Society of Core Analysts*, Noordwijk, The Netherlands, 27-30 September, 2009, SCA2009-39.
- Zhang X, C. J. Spiers and C. J. Peach (2010), Compaction of wet calcite at 150 °C, *J. Geophys. Res.* doi:10.1029/2008JB005853.
- Zhong S. and A. Mucci (1989), Calcite and aragonite precipitation from sea water solutions of various salinities: Precipitation rates and overgrowth compositions, *Chemical Geology* 78, 283-299.
- Zubrtsov S., F. Renard, J. P. Gratier, D. K. Dysthe and V. Traskine (2005), Single-contact pressure solution creep on calcite monocrystals, *Geological Society, London, Special Publications* 243(1), 81-95.
- Zuddas P. and A. Mucci (1998), Kinetics of calcite precipitation from seawater: II. The influence of the ionic strength, *Geochim. Cosmochim. Acta* 62, 757-766.

7. Conclusions and suggestions for future research

In this thesis, the process of compaction of (simulated) carbonate rocks by Intergranular Pressure Solution (IPS) was investigated. This was done by carrying out a variety of 1-D compaction experiments on wet granular calcite aggregates and on crushed limestone, under conditions ranging from surface (i. e. temperature and stress of 100 m) to reservoir (hydrothermal) conditions. The present section provides an overview of the principal conclusions of the work and identifies unsolved problems and new questions arising.

7.1 Conclusions

The general conclusions drawn, in relation to the research aims specified in the introduction, are as follows:

Development of test procedure for compaction by IPS

1). Benefitting from previous work by Spiers, Litean and De Meers, a general procedure was developed to verify the operation of pressure solution during compaction of carbonate aggregates. The procedure includes: a) Pre-compaction of dry sample at a stress higher than the intended testing stress to form a well-controlled initial porosity; b) Dry reloading of the pre-compacted samples. This should show no creep at effective stresses lower than the pre-compaction stress; c) Oil-flooding and reloading of pre-compacted samples at stresses below the pre-compaction stress. Again, samples should show no creep or very minor creep; d) Flooding with saturated carbonate solution followed by reloading, the pre-compacted samples will show significant creep if IPS is important. e) Addition of dissolution or precipitation inhibitors to wet sample, the rate of IPS creep of wet samples can be slowed down or accelerated by such additives; f) Micro-structural observation of wet compacted compared with dry samples. If intergranular pressure solution is dominant then indentations and overgrowth, should dominate over other features, such as micro-cracking, provided strains are high enough.

Verification of the operation of pressure solution in carbonate rocks in experiments

2). Pressure solution was shown to be the dominant compaction mechanism in experiments on relatively pure calcite aggregates (crushed limestone and analytical grade sample) and crushed limestones. The experiments were performed using fined grained sample materials (2-90 μm) at conditions of room temperature, and 1-4 MPa applied effective stress and at temperatures up of 150 $^{\circ}\text{C}$, using effective stresses 20-47 MPa. We note that Liteanu and Spiers (2009) found evidence at intermediate temperature (80 $^{\circ}\text{C}$) and stress of 20-40 MPa for creep controlled by subcritical brittle processes under otherwise similar conditions.

3). Creep strains obtained in short term experiments at room temperature achieved insufficient strain to develop unambiguous microstructural evidence for the active

deformation mechanisms. However, microstructures typical of intergranular pressure solution were reproduced in samples compacted for long times at 150 °C and 30-35 MPa effective stress. These consisted of indented and sutured grain contacts, overgrowths, and dissolution pits and precipitated layers developed on reference crystal surfaces inserted into the granular samples.

The effects of key variables on intergranular pressure solution in carbonates

4). The dependence of the pressure solution dominated compaction strain rates ($\dot{\epsilon}$) on applied effective stress (σ) can be described by a power law of the form $\dot{\epsilon} \propto \sigma^n$ with $n=1-2$ in the present experiments on samples compacted at 1-4 MPa, at room temperature. A similar stress sensitivity of strain rate was seen in samples compacted at 20 and 30 MPa at 150 °C.

5). Compaction creep rates were found to be always inversely proportional to grain size to the power of ~ 3 , at least at the small strains i. e. up to 3-5%, achieved in most experiments. This suggests diffusion controlled IPS. In addition, samples with a wider grain size distribution compact faster than those with same mean grain size but with a narrower distribution, as shown in samples tested at 2 MPa applied effective stress and room temperature.

6). Temperature had only a minor positive effect on compaction rates in the temperature range up to 150 °C. The apparent activation energy for creep estimated crudely from the compaction of samples at small strains ($<3\%$) at different temperatures was 19-21 kJ/mol. The activation energy estimated from temperature-stepping experiments at larger strains was 6-9 kJ/mol. These low values, though very rough, are consistent with expectations for a diffusion controlled pressure solution process.

Effects of pore fluid chemistry and flow-through on the rate of intergranular pressure solution and final implication for rate limiting mechanism

7). Salinity ranging from 0.1-0.5 M NaCl concentration increased the pressure solution compaction rate by 3 times compared to NaCl free pore fluid at room temperature and at applied effective stress of 4 MPa. Similar acceleration of compaction by salinity of 0.5 M was obtained in experiments carried out at 150 °C and 30 MPa effective stress.

8). In experiments carried out at room temperature and at 4 MPa, an increase in phosphate ion concentration in the pore fluid from 0 to 10^{-6} M decreased pressure-solution-dominated strain rates by a factor of ~ 2 . Further increase in concentration from 10^{-6} to 10^{-3} M decreased pressure solution strain rates by an additional 2 orders of magnitude. This reduction in strain rate is similar to the reduction in the calcite precipitation reaction rate caused by adding phosphate ions, suggesting that precipitation on pore walls is the rate limiting step in samples tested using a phosphate-bearing pore fluid. A phosphate concentration of 10^{-3} M, also slowed down compaction in samples tested at 150 °C and 30 MPa by a factor of 3-10.

9). Addition of Mg^{2+} ions to the pore fluid, in the form of 0.05 M $\text{MgCl}_2 \cdot 6\text{H}_2\text{O}$ caused major retardation (2.5 orders magnitude) of compaction creep of analytical grade calcite

powder tested at 150 °C and 30 MPa. Without Mg^{2+} , clear evidence for IPS was found in under these conditions. Major slowing down of compaction was also measured in samples tested at room temperature and 4 MPa, by Mg^{2+} in concentrations of 0.001 to 1 M in the pore fluid.

10). No pressure solution compaction can be measured in samples flooded with the hydrocarbons decane, toluene, cyclohexane or hexane at room temperature and applied effective stresses 4 MPa. However, if the sample was first water-wet, flushing with decane only slowed down compaction creep moderately. In contrast, in samples initially wetted with decane oil, flushing with brine promoted very little creep. The conclusion drawn is that hydrocarbons that wet calcite better than aqueous solution can stop IPS, unless dissolving grain boundaries are already water wet.

11). Purer calcite samples (Merck 99% and 99.95%) achieved much larger strains than impure samples (crushed limestone) notably in long duration tests at 150 °C and effective stresses of 30 MPa. Compaction in samples of crushed, oil-contaminated limestone was much less than in samples of oil-free limestone at room temperature and 4 MPa. This supports the idea that hydrocarbon inhibits intergranular pressure solution, though other difference in impurity content may also have played a role.

12). In experiments carried out at 150 °C and 30 MPa, flow-through promoted creep rates at larger strains ($> 5\%$) while no effects on strain rates occurred at lower strains. Comparison of these results with IPS theory provides strong evidence for a transition from diffusion-controlled IPS at small strains to precipitation controlled IPS at larger strains. This supports the grain size dependence data obtained at lower temperatures and stresses which point to diffusion control at low strains.

13). Measurements of the Ca^{2+} concentration present in fluid samples collected from compacting samples in intermittent flow-through runs revealed a build up to high supersaturations of CaCO_3 during compaction under zero flow conditions, notably at high strains. Flow-through led to a drop in Ca^{2+} concentration, which corresponded with creep acceleration at high strains. These data further support the inference that precipitation controlled the rate of IPS at high strains, as IPS theory predicts a significant supersaturation build up only for precipitation control. The buildup of Ca^{2+} in the pore fluid during creep without flow-through especially at high strains was accompanied by an increase in Mg^{2+} , SO_4^{2-} . This is believed to reflect progressive dissolution of impurities in the natural samples which may have caused the switch to precipitation controlled.

Deriving constitutive parameters for intergranular pressure solution in carbonate rocks

14). The weight of evidence obtained in this thesis strongly indicates that IPS in calcite under the conditions investigated is diffusion controlled at low strains becoming precipitation controlled at higher strains ($>5\text{-}7\%$), especially at higher temperature (150 °C). The experimentally derived values of the diffusion product DS (diffusion coefficient times effective thickness of water film) for IPS in calcite at low strain is between 2.98×10^{-18} to $3.73 \times 10^{-19} \text{ m}^3/\text{s}$ at 150 °C. As impurity ions like Mg^{2+} and HPO_4^{2-} can drastically slow down IPS due to the effect on the precipitation reaction, it is likely that IPS in calcite in nature is much slower than seen in Lab experiments on pure systems.

7.2 Future research

- I. In addition to pressure solution, stress corrosion induced micro-cracking might be also important in calcite compaction. The process was not dominant in the present experiments, as is expected to lead to a direct dependence of strain rate on grain size- opposite to the observation here (Liteanu et al., 2009). However, grain scale cracking or grain contact crushing may have accelerated grain boundary diffusion in the present experiments, in the manner described by Gratiers, Renard and co-workers. This cannot be ruled out. The conditions where pressure solution and stress corrosion cracking dominate needed to be experimentally investigated in more detail with respect to grain size and applied stress.
- II. In this study, the weight of the evidence points strongly to the IPS in granular calcite being controlled by grain boundary diffusion and/or precipitation on pore walls, depending on strains and other conditions. In flow-through experiments with no additives, flow can apparently be used to switch between diffusion and precipitation controlled IPS. The strain rate dependence on grain size, stress and temperature can best be determined under these conditions in future, specifically to each mechanism.
- III. Effects of hydrocarbons on pressure solution to the wettability of carbonate rocks are important. Wettability of carbonate rocks (water-wet vs. oil-wet) are extensively studied in the oil industry, combination of these data with petrographic pressure solution especially from the transition zone will advance the knowledge of pressure solution in reservoir characterization.
- IV. In comparing experimental data on compaction creep with microphysical models of IPS, uncertainties arise from differences between the actual and modeled grain contacts and pore surface areas etc. Direct measurement of micro-structural parameters such as porosity, pore size, pore volume and pore wall plus grain contact surface areas, in lab samples, will significantly improve the basis for comparison and will better constrain experimentally derived kinetic parameters. These micro-structural parameters can be measured by Mercury injection porometry or Nuclear Magnetic Resonance. In addition, the porosity, as well as the pore structure evolution during compaction can be monitored by NMR. The evolution of pore and pore throat evolution is of great importance in controlling the capillary pressure of reservoir rocks, for hydrocarbon development and production.
- V. The present experiments have shown that pore fluid composition, for example Mg^{2+} contents, can strongly influence the kinetics of compaction

Conclusions and future research

of calcite aggregates undergoing IPS. Sample composition also has a major effect. This means that site-specific experiments are needed to understand and quantify IPS in natural situations. Using the formation brine composition and carbonate material from well, oil field or basin for experiments, should yield better site specific pressure solution parameters which can be used to aid reservoir quality prediction. This approach will give more accurate parameters for modeling of specific regions.

- VI. Clay minerals are known play a major role in forming pressure solution features such as stylolites. The present results have shown that flow-through tests can promote pressure solution and may point the way to producing stylolites in the lab. By conducting flow-through tests on pre-compacted clay + carbonate mixtures, stylolite microstructures can be expected to develop as flow and dissolution become localized and the process of stylolite development can perhaps be quantified. A large fluid volume would be needed to for this, hence , a syringe pump is needed in addition to the present compaction setup.
- VII. Pressure solution compaction during burial diagenesis of carbonates can cause reservoir heterogeneity. Sedimentary or stratigraphically induced heterogeneities can be enhanced by the processes of pressure solution compaction. Experiments on the effects of heterogeneity of start material properties on pressure solution are needed.
- VIII. Carbonate cementation is common in sandstone reservoirs. Pressure solution in nearby carbonate rocks can provide sources for calcite cementation. Open system theory and open system experiments are needed to quantify these important effects.
- IX. The behaviors observed in the present experiments should also occur in cataclastically deformed calcite fault gouge. More work is needed to assess the effects of IPS in calcite on fault rock compaction and strength recovery, versus fault creep behaviour and the transition from stable to unstable slip.

Samenvatting

Veel van de grootste olie en gas velden in de wereld bevinden zich in carbonaatgesteentes. Carbonaat reservoirgesteentes bevatten meer dan 60% van de wereld's olievoorraden en 40% van de gasvoorraden. De ontwikkeling van de kwaliteit van zulke reservoirgesteentes, d.w.z. hun porositeit en permeabiliteit, wordt voor een belangrijk deel bepaald door compactie als gevolg van drukoplossing. Naast het bepalen van de kwaliteit van het reservoir kan compactie door drukoplossing ook leiden tot migratie van vloeistoffen in carbonaatgesteentes over de geologische tijdschaal. Samen met processen als het smeren van klei en korrelgrootte-verkleining door breken en verpulveren is drukoplossing een effectief mechanisme voor het afdichten van breuken in carbonaatgesteentes. Bovendien kan drukoplossing, tijdens de productie van koolwaterstoffen en na de injectie van CO₂ in carbonaat reservoirs voor geologische opslagdoeleinden, leiden tot tijdafhankelijke verticale compactie en verzakking aan de oppervlakte. Het kwantificeren van compactie door drukoplossing in carbonaatgesteentes is dus een onderwerp van wezenlijk praktisch en economisch belang, met name voor de exploratie en productie van koolwaterstoffen en voor het beoordelen van de veiligheid van geologische opslag van CO₂ in uitgeputte carbonaat reservoirs.

Dit proefschrift beschrijft de resultaten van een experimentele studie van compactie door drukoplossing in korrelige calciëte aggregaten, d.w.z. nagebootste carbonaat reservoirgesteentes, onder de omstandigheden die heersen in koolwaterstofreservoirs. Focus is op zogenaamde Intergranular Pressure Solution of IPS, d.w.z. oplossing en neerslag op korrelgrootte schaal als gevolg van spanning in het materiaal. De doelen waren te verifiëren of drukoplossing inderdaad actief was door het reproduceren van microstructuren die karakteristiek zijn voor drukoplossing, te bepalen wat de effecten zijn van variabelen zoals spanning, temperatuur, korrelgrootte, chemie van de poriënvloeistof en vloeistofstroom op de snelheid van het proces, en door middel van vergelijking met theoretische modellen vast te stellen en te kwantificeren wat het snelheidslimiterende mechanisme is.

In **Hoofdstuk 1** wordt achtergrond informatie gegeven over drukoplossing als een belangrijk proces van diagenese tijdens het begraven van carbonaatgesteentes. Een overzicht wordt gegeven van de wijdverspreide kenmerken van drukoplossing zoals gezien in de natuur, van de effecten van drukoplossing op de eigenschappen van carbonaatgesteente, zoals porositeit, en van de invloed van geologische variabelen op drukoplossing. Eerder experimenteel werk aan drukoplossing in carbonaten wordt ook besproken en de belangrijkste openstaande vragen worden vastgesteld. De doelen van het huidige onderzoek worden dus gemotiveerd in dit hoofdstuk.

Hoofdstuk 2 beschrijft 1-dimensionale compactie-experimenten, uitgevoerd met fijnkorrelige pure aggregaten van calciëte, bij lage spanningen (1-4 MPa) en op kamertemperatuur. Een algemene procedure is ontwikkeld die geschikt is voor compactie-experimenten gericht op het onderzoeken van drukoplossing in carbonaat. Door allereerst onder droge condities een spanning van 8 MPa aan te brengen verkregen we een reproduceerbare startporositeit en konden we deformatiemechanismen zoals korrelherschikking, -verschuiving en -breking, voor een groot deel uitsluiten voor de latere

kruip compactie-testen onder natte condities. Na de droge voor-compactie bij 8 MPa werden de monsters nat gecompacteerd onder “afgewaterde” condities. Daarbij werd gebruikgemaakt van een vantevoren verzadigde oplossing als poriënvloeistof. Controle-experimenten, gedaan onder droge omstandigheden of met chemisch inerte poriënvloeistof, lieten verwaarloosbare compactie zien in deze fase. Echter, monsters getest met een verzadigde oplossing als poriënvloeistof lieten gemakkelijk te meten kruip-compactie zien. De compactiesnelheid nam af met toenemende compactie en korrelgrootte, en nam toe met toenemende spanning. Het toevoegen van Mg^{2+} ionen aan de verzadigde poriënvloeistof verminderde de compactiesnelheid drastisch. Door het waargenomen compactiegedrag te vergelijken met een theoretisch model voor IPS in calciëten en in aanmerking nemend dat het bekend is dat de aanwezigheid van Mg^{2+} ionen in oplossing het oplossen en neerslaan van calciëten verhindert, verifieerden we dat IPS het dominante compactiemechanisme was onder onze experimentele condities. De resultaten demonstreerden ook dat drukoplossing al kan leiden tot compactie op relatief kleine dieptes (slechts enkele tientallen meter) als andere variabelen, vooral de chemie van de poriënvloeistof, gunstig zijn.

Hoofdstuk 3 rapporteert de resultaten van 1-D compactie-experimenten gedaan op verpulverde kalksteen en korrelige pure calciëten op kamertemperatuur, bij 1-4 MPa effectieve spanning en met poriënvloeistoffen variërend van verzadigde carbonaatoplossing met en zonder bevuilende ionen, tot aan een verscheidenheid van koolwaterstoffen. Wederom werden alle monsters eerst gecompacteerd onder droge condities op 8 MPa om een goed gecontroleerde beginporositeit te verkrijgen en pure mechanische compactieprocessen te elimineren tijdens testen onder lagere spanningen. Compactie-kruip vond alleen plaats in monsters gevuld met waterige oplossing, bij deformatie snelheden van 10^{-6} tot 10^{-9} s^{-1} . De gemeten deformatiesnelheden nemen toe met afnemende korrelgrootte en toenemende effectieve spanning, volgens machtsvergelijkingen met exponenten van ongeveer -3 en 1 tot 2, respectievelijk. Bovendien werd de compactie-snelheid van natte monsters significant verlaagd door de toevoeging van oplossing- en neerslagremmers (bv. magnesium) aan de poriënvloeistof. Dit wijst erop dat calciëtoplossing en -neerslag een rol speelden bij de kruip. Poriënvloeistof met een zoutgehalte (NaCl) van 0.1 – 0.5 M vergrootte de compactie-deformatie snelheid in vergelijking met niet zoute oplossingen. Van groot belang is dat aggregaten van calciëten die eerst gevuld waren met een zoutoplossing en vervolgens gespoeld werden met koolwaterstoffen veel meer compacteerden dan monsters die eerst bevochtigd waren met koolwaterstoffen en dan gespoeld in omgekeerde volgorde. In vergelijking met de theorie, suggeren de experimentele resultaten dat het belangrijkste deformatie mechanisme drukoplossing was en dat diffusie waarschijnlijk het snelheidsbeperkende proces is in pure calciëten systemen. Verder impliceren de resultaten dat compactie en de ontwikkeling van porositeit en permeabiliteit in natuurlijke carboneetgesteentes erg afhankelijk zal zijn van de chemie van de poriënvloeistof, alsmede de mechanische condities. Poriënvloeistoffen met ionen die optreden als oplossing- en neerslag remmers voor calciëten kunnen er bijvoorbeeld voor zorgen dat de porositeit in carbonaatgesteentes behouden blijft. Bovendien kan de vroege insluiting van koolwaterstoffen de compactie door drukoplossing in carbonaatgesteentes sterk vertragen of zelfs stoppen.

Nadat we de werking van IPS in natte calcië-aggregaten gedemonstreerd hebben in de vorige hoofdstukken, richt **Hoofdstuk 4** zich op de effecten van fosfaat-ionconcentratie in de poriënvloeistof op de 1-D compactie van fijn-korrelige calcië poeders. Hierbij gaat het om IPS op kamer temperatuur en bij toegepaste axiale spanningen van 1-4 MPa. Fosfaat werd bestudeerd omdat het een belangrijke biologische component is in zee- en poriënwater. Door de fosfaatconcentratie in de poriënvloeistof te verhogen van 0 tot 10^{-3} mol/l werden de compactie-deformatiesnelheden systematisch tot wel 2 orders van grootte verlaagd. De gevoeligheid van de compactie-deformatiesnelheid met betrekking tot de fosfaatconcentratie was gelijk aan de gevoeligheid van calcië neerslagsnelheden die in de literatuur worden gerapporteerd met betrekking tot de toevoeging van fosfaat-ionen. Dit suggereert dat de snelheid van IPS in monsters met fosfaat gecontroleerd werd door de neerslag van calcië op de wanden van de poriën. De resultaten impliceren dat de snelheden van IPS en daarmee gepaard gaande porositeits/permeabiliteit vermindering in calcië sedimenten sterk verlaagd kunnen worden als de poriënvloeistof verrijkt is in fosfaat, bijvoorbeeld door hoge biologische productiviteit of door een zeewater origine. In het modelleren van IPS gerelateerde processen moet dus rekening worden gehouden met de effecten van de chemie van de poriënvloeistof, met name met het beperken van oppervlaktereacties door de aanwezigheid van fosfaat alsook door kation-onzuiverheden.

Terwijl hoofdstukken 2,3 en 4 IPS behandelen onder de lage spanningen en temperaturen die overeenkomen met een relatief kleine diepte, beschouwen hoofdstukken 5 en 6 compactie onder omstandigheden van verhoogde spanning en temperatuur – daarbij diepe diagenetische of rijpe reservoir condities simulerend. **Hoofdstuk 5** documenteert 1-D compactie-experimenten uitgevoerd met verpulverde kalksteen, analytische kwaliteit calciëpoeder en bijzonder pure calciëpoeder op temperaturen tot 150 °C, bij 20 – 47 MPa effectieve spanning, onder droge en natte condities. Scanning Electron Microscopy (SEM) onthulde microstructuren typisch voor drukoplossing in de natte gecompacteerd monsters, zoals gehechte korrelcontacten, inkepingen en overgroeistrukturen. Oplossingsgroeven en lagen van neergeslagen calcië waren ook ontwikkeld op oppervlaktes van gespleten kristallen die waren toegevoegd aan de gepoederde monsters als referentie kristallen voor de microstructuur. Deze groeven en neerslagen zijn duidelijke aanwijzingen dat drukoplossing actief was in onze experimenten. Aanzienlijke kruip-compactiedeformatie werd bereikt in de nat gecompacteerd monsters, terwijl droge monsters weinig of geen kruip en geen van de massa-overdracht microstructuren lieten zien. De compactie-deformatiesnelheden gemeten tijdens natte testen namen systematisch toe met toenemende effectieve spanning en afnemende korrelgrootte. Temperatuur had bijna geen effect op de compactie-deformatiesnelheid tussen 28 en 150 °C. De effecten van korrelgrootte, effectieve spanning (veranderingen) en de samenstelling van het beginmateriaal, in combinatie met een vergelijking van de experimentele data met modellen van drukoplossing, suggereren dat de snelheid-beperkende mechanismes uit een overgangsgebied kwamen van diffusie-gecontroleerde drukoplossing bij weinig vervorming en neerslag gecontroleerde drukoplossing bij veel vervorming. De waarde voor het korrelgrensdiffusie produkt $D \cdot S$ (diffusiecoëfficiënt maal de effectieve dikte van de korrelgrens water film) zoals bepaald met experimenten ligt tussen 2.98×10^{-18} en 3.73×10^{-19}

m³/s voor calciet tijdens diffusiegecontroleerde drukoplossing bij 150 °C, wat vergelijkbaar is met de waarde voor veel ionische zouten onder vergelijkbare condities.

In **Hoofdstuk 6**, worden de compactie-experimenten op natte verpulverde kalksteen en analytische kwaliteit calciet, uitgevoerd bij 150 °C en bij effectieve spanningen van 30 en 40 MPa, opnieuw bekeken, nu met de nadruk op de chemische signatuur van de poriënvloeistof met betrekking tot het overheersende deformatiemechanisme. Het probleem is aangepakt door de samenstelling van de poriënvloeistof te manipuleren met behulp van doorstroomtesten met verse, calciet verzadigde oplossing en door het toevoegen van NaCl, Mg²⁺ of fosfaat-ionen aan de poriënvloeistof voornamelijk zonder doorstroming. Zoals geconcludeerd in hoofdstuk 5 was IPS het overheersende deformatiemechanisme onder deze condities. Onderbroken doorstromingstesten gedaan met CaCO₃ verzadigde oplossingen lieten geen effect op de kruipsnelheid zien bij lage vervorming (< 4-6 %), maar juist een grote versnelling bij hoge vervorming. Metingen van de Ca²⁺ concentratie in de vloeistofmonsters die werden verzameld van gecompacteerd aggregaten uit onderbroken doorstromingstesten onthulden een opbouw naar hoge oververzadiging van CaCO₃ tijdens compactie zonder doorstroming, vooral bij hoge vervorming. Als er wel doorstroming was leidde dit tot verval in de Ca²⁺ concentratie. Deze waarnemingen zorgen voor verdere ondersteuning van de gevolgtrekking dat neerslag de snelheid van IPS bij hoge vervorming controleert, omdat theorie voorspelt dat alleen neerslag gecontroleerde IPS voor een significante opbouw van oververzadiging zorgt.

Toevoeging van NaCl aan de poriënvloeistof in een concentratie van 0.5 M verhoogde de kruipsnelheid van analytische kwaliteit calciet ruwweg in verhouding tot de verhoging van de oplosbaarheid van calciet veroorzaakt door aanwezigheid van NaCl – beschouwd vanuit de theorie kan dit een versnelling van IPS via een versnelling van de korrelgrens diffusie weerspiegelen, tenminste bij lage vervorming. Toevoeging van Mg²⁺ en HPO₄⁻ aan de poriënvloeistof, in concentraties van 0.05 M en 0.001 M respectievelijk, veroorzaakte een behoorlijke vertraging van de compactie-kruip. Omdat het bekend is dat de ionen de oplossing en neerslag van calciet vertragen, bieden hun effecten verdere ondersteuning aan de conclusie dat compactie gecontroleerd wordt door een oplossing-neerslag proces zoals IPS.

Wanneer we onze mechanische, doorstromings- en chemische data combineren, en we daarbij de mechanische data gerapporteerd in hoofdstuk 5 meenemen, wijst alles er op dat diffusie gecontroleerde IPS het overheersende deformatie mechanisme is bij lage vervorming (tot aan een paar procent), maar dit plaatsmaakt voor neerslaggecontroleerde IPS bij hogere vervorming. Onze (chemische) gegevens suggereren dat deze overgang het gevolg is van de opeenhoping van onzuiverheden in de poriënvloeistof vanuit de monsters of het apparaat.

Omdat Mg²⁺ en fosfaat-ionen gewoon zijn in natuurlijke poriënvloeistoffen en omdat het bekend is dat ze de oplossing en vooral de neerslag van calciet vertragen, is het aannemelijk dat vertraagde neerslag de snelheidsbepalende stap is in IPS van carbonaten in de natuur. Deze studie impliceert dat porositeit in carbonaat behouden kan worden in diepe reservoirs, d.w.z. > 4-5 km als de poriënvloeistof rijk zijn in remmers van de calciereactie, zoals Mg²⁺ en fosfaat-ionen. De stroming van vloeistoffen kan drukoplossing versnellen

Samenvatting

door het veranderen van het snelheidsbepalende mechanisme, dit zou kunnen gebeuren in de natuur bij de formatie van stylolieten en oplossingsaders.

Hoofdstuk 7 resumeert de voornaamste conclusies van dit proefschrift en documenteert suggesties voor toekomstig werk dat nodig is.

Samenvatting

Acknowledgements

Many people have supported me for many years and they helped me to make this thesis into what it is now. I am indebted to all of them and I want to thank a number of them in particular.

Firstly, I would like to thank my supervisor, Professor Chris Spiers for giving me the opportunity to work in the HPT lab. His constant enthusiasms and interest for me and my research were enlightening and very important. I benefited from his guidance, creativity, clear scientific thinking and lab experience. He was always there for me when I needed him. Our good and close cooperation formed a firm basis for this successful thesis. It was a privilege and pleasure to work with him. I appreciate our friendship.

Secondly, I would like to thank Dr. Colin. Peach. Colin was very supportive and friendly and has given many help and advice in getting the experimental equipments and methods up and running. I benefited from his knowledge and experience of lab petrophysics. Thanks also goes to your help with any computer-related issues I had in the lab.

I would also like to thank the rest of the HPT team: Dr. Hans de Bresser, Gert Kastelein, Peter van Krieken, Eimert de Graaf and Magda Marthot-Martens. Thank you all for creating a friendly and supportive environment. Gert, Peter and Eimert are thanked for all technical supports. Particularly, Peter is thanked for taking the SEM and pore fluid analysis. Gert and Peter are thanked for helping the sample preparations and apparatus operation. Magda is thanked for taking care of me in management and organizing so many things, many times beyond her job responsibilities. Furthermore, I would like to thank my colleagues in the faulty, Marten, Gill, Siese, Robert, Jan, Bart, Sasiak, Andre, Arthur, Reinier, Sander, Emilia, Susan and Esther for the good working atmosphere and nice time when I was there from 1999 to 2006. Special thanks to Hans and Andre for translating the English summary into Dutch.

Thanks to Jan Constants, Fred Dula, Paul Wagner from Shell Rijswijk for sponsoring this research on carbonate rocks. Thanks to Ajar Poly and Jarques Grupa from NRC for sponsoring other projects on similar topics - intergranular pressure solution in rocksalt. I am grateful to Prof. Andrew Putnis from University of Muenster for giving me opportunity to work with him during 2006-2008 on the topic of calcite dissolution and precipitation using AFM. Prof. J. Gratier is thanked for the fruitful discussion on intergraular pressure solution in carbonate rocks in the AGU conference.

I would like to thank journal reviewers, Brian Evans, François Renard, Eric Oelkers, Jean Gratier, Daniel Koehn and Roland Hellmann and several anonymous reviewers for their constructive comments.

Acknowledgements

Finally I am grateful to my friends and family. Thanks to my son, Wenzhi whose love helps me to get through the difficult time of my life. Special thanks to my brothers and sisters for their love and for taking care of my parents. This thesis is hence dedicated to my two brothers (Xianggou, Jianmin) and two sisters (Xiangjiu, Sujiu).

Curriculum Vitae

Xiangmin Zhang was born on 30 November, 1965 at Yuanshi, China. He received a Bachelor Degree of Engineering in Geology from the HeBei Institute of Geology, HeBei, China in 1986. From 1986 to 1989 he studied Structural Geology at Changan University and earned his MSc in 1989. He worked at ARSC, China Coal Geology, Xian from 1989 to 1998 as an assistant Engineer, Engineer and senior Engineer. He studied remote sensing geology at International Institute of Geoinformatics and Earth Sciences (ITC), Enschede and earned an advanced degree in remote sensing geology from Delft University of Technology. He carried out researches at Utrecht University from 1999 to 2006 and at University of Münster from 2006 to 2008. He is working for PanTerra Geoconsultants since 2008.